Modelling of Infectious Animal Viral Disease Transmission by Aerosols

by

AMY LA

A Thesis submitted to the Faculty of Graduate Studies of

The University of Manitoba

in partial fulfillment of the requirement for the degree of

DOCTOR OF PHILOSOPHY

Department of Biosystems Engineering

University of Manitoba

Winnipeg, Manitoba

Abstract

An integrated model was developed to simulate airborne transmission of infectious animal viral diseases. Computational fluid dynamics (CFD), viral infectivity decay, and dose-response models were integrated to simulate physical and biological processes in the aerosol transmission pathway of animal disease. In the first part of this study, a CFD model was developed and validated for simulating movement of bioaerosols of porcine reproductive and respiratory syndrome virus (PRRSV) in laboratory conditions where air flowed from a source to a recipient chamber. The model performed well (normalized mean square error NMSE <0.25) at simulating steady-state PRRSV bioaerosol concentrations, but differences were greater (NMSE >0.25) during the transient stage of airflow. In the second part of this study, a series of dose-response models were performed for five infectious animal viruses on various transmission routes. The transmissibility of animal viruses varied with the transmission route, and aerosol transmission required lower doses to cause infection than intranasal and oral transmission for PRRSV. The CFD model was coupled with aerosol transmission dose-response models for PRRSV. The coupled models predicted probability of infection (82% to 100%), which was in good agreement with observed rates in two experimental studies (84% and 90%). In the third part of this study, an integrated model consisting of CFD, infectivity decay, and dose-response was developed to simulate the aerosol transmission of PRRSV between a source and a recipient building in field conditions, based on an experimental study reported in the literature. CFD was used to model the PRRSV aerosol movement towards and within the recipient building, and the infectivity decay and dose-response models were used to predict the probability of infection upon exposure to the calculated aerosol dose of PRRSV. The integrated model predicted that the aerosol transmission event occurred in the recipient building on a day when the environmental conditions (wind, temperature, etc.) were favorable for aerosol transmission, and this model prediction was in agreement with the experimental observation. The integrated modeling approach developed in this work provided novel ways of improving the understanding of airborne animal viral disease transmission and modelling specific components of the aerosol transmission pathway.

Acknowledgements

I would like to thank my co-advisors and the members of my Ph.D. committee, Dr. Zhang, Dr. Cicek, Dr. Levin, and Dr. Coombs. Thank you for your support and kindness.

Thank you to the Department of Biosystems Engineering.

Thank you to all my lab-mates: Rong (Daisy) Yue, Charles Nwaizu, Tony De Luca, Desmond Essien, Xiaojie (Emily) Yan, Xinyi Wu, Chenchen Sun, Trina Semenchuk.

Dedication

I am dedicating my thesis to my mom and dad as well as to my husband, Leno.

Table of Contents

Abstract i

Acknowledgements ii

Dedication iii

List of Tables viii

List of Figures xi

Nomenclature list (by chapter) xvi

Chapter 1. Introduction 1

1.1. General introduction 1

1.2. Research gaps and objectives 2

1.3. Significance of research contributions 3

1.4. Thesis structure 5

1.5. Contribution of authors 6

Chapter 2. General literature review 7

2.1. Infectious animal diseases 7

2.2. Factors affecting transmission of infectious animal diseases 10

2.3. Modelling aerosol and airborne transmission 12

2.4. Computational fluid dynamics (CFD) 13

2.5. Dose-response modelling 15

2.6. Modelling survival of viruses in environmental conditions 17

Chapter 3. Current understanding of airborne transmission of important viral animal pathogens in disease spread 19

3.1. Abstract 19

3.2. Introduction 20

3.3. Focus of review 21

3.4. Laboratory studies of short distance transmission by aerosol 21

3.4.1. Controlled exposure of individual animals to aerosols 22

3.4.2. Two-chamber tests for assessing aerosol transmission 22

3.4.3. Multiple cage experiments 23

3.5. Field studies of long-distance transmission by aerosols 28

3.5.1. Airborne transmission from buildings with inoculated animals 28
3.5.2. Long distance transport from naturally infected buildings or animals 31
3.6. Modelling airborne transmission based on data of past outbreaks 39
3.7. Factors that affect aerosol transmission 47
3.7.1. Aerosol type 47
3.7.2. Shedding of viruses from infected animals 47
3.7.3. Temperature and relative humidity effect on virus survival 53
3.7.4. Aerosol infectious dose 54
3.8. Conclusions of the journal paper 55
Chapter 4. Experimental validation of CFD simulations of bioaerosol movement in a mechanically ventilated airspace 56
4.1. Abstract 56
4.2. Introduction 57
4.3. Methodology 57
4.3.1. Experimental bioaerosol chamber system 57
4.3.2. Smoke test 59
4.3.3. CFD simulation of continuous phase (air) 60
4.3.4. Discrete phase modeling of bioaerosols 62
4.3.5. Mesh refinement test 65
4.3.6. Data analysis 66
4.3.7. Normalized mean square error and fractional bias 67
4.4. Results 68
4.4.1. Mesh refinement test 68
4.4.2. Model validation 69
4.5. Conclusions of journal paper 77
4.6. Acknowledgements 77
Chapter 5. Dose-response modelling of infectious animal diseases coupled with computational fluid dynamics: A simulation of airborne porcine reproductive and respiratory syndrome virus 78
5.1. Abstract 78

5.2. Introduction 79
5.3. Materials and Methods 79
5.3.1. Compilation of data from literature 79
5.3.2. Stochastic dose-response modelling 80
5.3.3. CFD simulation of a case study 82
5.4. Results and Discussion 88
5.4.1. Comparison of three dose-response models 88
5.4.2. Dose-response modelling by exact Beta-Poisson model 92
5.5. Case study of coupling CFD simulation with dose-response modelling 106
5.6. Conclusion of journal paper 108
5.7. Acknowledgements 109
Chapter 6. Modelling aerosol transmission of porcine reproductive and respiratory syndrome virus between buildings using computational fluid dynamics 110
6.1. Abstract 110
6.2. Introduction 111
6.3. Methodology 111
6.3.1. Field simulation (CFD Model 1) 112
6.3.2. Recipient building simulations (CFD Model 2) 124
6.3.3. Predicting pig infection (virus decay and dose-response models) 129
6.4. Results and Discussion 135
6.4.1. Mesh refinement 135
6.4.2. Aerosol concentration in building 139
6.4.3. Airborne PRRSV concentration in building 145
6.4.4. Exposure dose and probability of infection 149
6.5. Conclusions 152
Chapter 7. Overall Discussion, Conclusions and Recommendations 154
7.1. Knowledge gaps in modelling airborne transmission of viral pathogens 154
7.2. Modelling approaches to foster understanding of aerosol transmission pathway 155
7.2.1. CFD modelling of aerosol transport 155
7.2.2. Dose-response modelling 156

7.2.3. Modelling survival of infectious animal viruses in atmosphere 157
7.3. Importance of air sampling measurements in computer modelling..... 158
7.4. Limitations of research 161
7.4.1. Chapter 3 161
7.4.2. Chapter 4 162
7.4.3. Chapter 5 163
7.4.4. Chapter 6 164
7.5. Conclusions..... 166
7.6. Recommendations..... 167
Appendix A. Fundamental equations for CFD 172
References 175

List of Tables

Table 3.1. Experiment type and strain of ASFV, PEDV, and PRRSV tested for airborne transmissibility (AT) over short distances 25

Table 3.2. Experiment type, strain of FMDV, and animal type tested for airborne transmissibility (AT) over short distances 27

Table 3.3. Ranges and average PRRSV concentrations of air samples collected from the exhaust of a mechanically ventilated finisher facility with 25 to 120 kg infected pigs. 29

Table 3.4. Downwind distance and infectious PRRSV concentration collected in air samples 30

Table 3.5. Air sample collection from animal facilities naturally infected with PEDV, AIV, or PRRSV. 35

Table 3.6. Models assessing AT in previous outbreaks of PEDV, AIV, and PRRSV 39

Table 3.7. Analytical methods and models used to study contribution of airborne transmission in various historical cases of FMDV 43

Table 3.8. Study, virus, strain, days post-inoculation of air sampling monitoring, and significant findings on shedding of virus into air. 50

Table 4.1. Boundary conditions of CFD simulation 61

Table 4.2. DPM parameters for particle injection in CFD simulation 63

Table 4.3. DPM injection parameters for treatments 1 to 4 63

Table 4.4. Mesh characteristics, number of nodes, combined volume of cells, and coordinate range of nodes used to determine mean aerosol concentration in mesh refinement tests 65

Table 4.5. Mean, standard deviation, and range of simulated aerosol concentration in nodes surrounding measurement point in mesh refinement tests 69

Table 4.6. Comparison of measured and simulated aerosol concentrations (mg m^{-3}) at steady-state using Normalized Mean Square Error (NMSE), Fractional Bias (FB), and relative difference. 75

Table 4.7. Average and range of simulated aerosol concentrations (mg m^{-3}) in the first chamber. 76

Table 5.1. Summary of datasets compiled from literature for dose-response modelling. 80

Table 5.2. CFD input parameters 86

Table 5.3. Parameter values for dose-response models developed for aerosol exposure of PRRSV 88

Table 5.4. Comparison of the predicted probability of infection using exponential, exact beta-Poisson, and approximate beta-Poisson models (maximum likelihood estimate; MLE) to observed rates of infection for PRRSV on aerosol (dataset from Hermann et al. 2009), intra-nasal, and oral (datasets from Hermann et al. 2005) transmission routes. 90

Table 5.5. Maximum likelihood estimate (MLE), 2.5-percentile estimate and 97.5-percentile estimate for parameters α and β in the exact beta-Poisson models of PRRSV, AIV, FMDV, ASFV, and PEDV on various transmission routes. 93

Table 5.6. Predicted probabilities of infection by exponential, approximate beta-Poisson, and exact beta-Poisson models based on exposure doses from CFD simulations. 108

Table 6.1.Wind speeds and wind directions simulated in CFD (10 m from ground) 117

Table 6.2. Velocity (U), pressure (p), turbulent viscosity (μ_t), turbulent kinetic energy (k), and rate of dissipation of turbulent energy (ε) boundary conditions for field simulations 120

Table 6.3. Air properties, k-epsilon parameters, windbreak parameters, and numerical schemes for field CFD simulations 121

Table 6.4. Injection rate of parcels (P_d) generated from north ($P_{d,north}$) and south ($P_{d,south}$) exhaust fans of the source building according to equivalent diameter (d_{eq}) and aerodynamic diameter (d_a). 124

Table 6.5.Properties of three meshes generated for the recipient building 127

Table 6.6. Velocity (U), pressure (p), turbulent viscosity (μ_t), turbulent kinetic energy (k), and rate of dissipation of turbulent energy (ε) boundary conditions for recipient building simulation 128

Table 6.7. The PRRSV conversion factor (R_{VP}) used to convert aerosols to infectious airborne PRRSV particles for each aerodynamic diameter (d_a) used in the CFD simulations. 131

Table 6.8. Parameter θ for calculating the fraction of infectious PRRSV remaining after field exposure (F_{field}) and building exposure ($F_{building}$) to different relative humidity (RH) and temperature (T) conditions in the simulations 134

Table 6.9. Values of parameters α and β used to calculate probability of infection due to PRRSV exposure by aerosol 135

Table 6.10. Predicted probabilities of infection of pigs within recipient building according to pig weight, pen location, PRRSV concentration in source building exhaust air on June 6. MLE was the probability of infection based on the maximum likelihood estimation of parameters α and β in the exact Beta-Poisson dose-response model for aerosol transmission of PRRSV. The 95% confidence interval (CI) was the range of probability of infection values predicted with the 2.5%-percentile and 97.5-percentile estimates for α and β were used in the exact Beta-Poisson dose-response model for aerosol transmission of PRRSV. 151

Table 6.11. Predicted probabilities of infection of pigs within recipient building according to pig weight, pen location, PRRSV concentration in source building exhaust air on June 7. MLE was the probability of infection based on the maximum likelihood estimation of parameters α and β in the exact Beta-Poisson dose-response model for aerosol transmission of PRRSV. The 95% confidence interval (CI) was the range of probability of infection values predicted with the 2.5%-percentile and 97.5-percentile estimates for α and β were used in the exact Beta-Poisson dose-response model for aerosol transmission of PRRSV. 152

List of Figures

Figure 3.1. PRRSV concentration in exhaust air from mechanically-ventilated finisher building containing infected pigs (Otake et al., 2010) 29

Figure 4.1. (a) Sketch of the aerosol experiment system, (b) schematic diagram of the IRIS damper, digital manometer, bypass damper to control airflow rate in chambers (dimensions are in meters). 58

Figure 4.2. (a) Geometry of chambers and (b) Mesh with 0.05 m size cells in chambers and baffles 60

Figure 4.3. Distribution of smoke (grey / white cloud) in chambers (black background) during smoke test at ventilation rate of 34.0 $m^3 h^{-1}$ at (a) 3 s, (b) 30 s, (c) 50 s, and (d) 60 s. White orb seen in pictures is a light source that was used to make smoke visible in video recording. 70

Figure 4.4. Volume rendering of particle concentration in first chamber during treatment one at (a) 10.67 s, (b) 32.01 s, (c) 53.35 s, (d) 64.02 s 70

Figure 4.5. Velocity profiles at centerline of flow for (a) treatments 1 and 2, (b) treatments 3 and 4. 71

Figure 4.6. Velocity streamlines of (a) treatment 1 and (b) treatment 3 simulations. 72

Figure 4.7. Change in aerosol concentration with time during experiments and CFD simulation for (a) treatment 1, (b) treatment 2, (c) treatment 3, and (d) treatment 4. The dashed line indicates the time in the simulation and experiments at which the steady-state concentration was reached. 73

Figure 4.8. Parameters for evaluating the performance of CFD simulations at predicting experimental aerosol concentrations: (a) NMSE for treatments 1 and 2, (b) NMSE for treatments 3 and 4, (c) FB for treatments 1 and 2, and (d) FB for treatments 3 and 4. Values lower than the dashed line in (a) and (b), and the area between the dashed lines in (c) and (d) indicate the NMSE and FB values, respectively, that show that model is not biased and performed adequately according to ASTM standards. 74

Figure 4.9. Aerosol concentration in chamber 1 at centerline of flow during steady-state in (a) treatment 1, (b), treatment 2, (c) treatment 3, and (d) treatment 4. 77

Figure 5.1. Geometry of the two-chamber system used in the CFD simulation. The green area indicates where aerosols were generated at the beginning of the CFD simulation and the blue area indicates where the aerosol concentration was calculated every 0.5s timestep. The fogger and the pigs (not simulated) were placed in the first and second chamber, respectively Dee, Batista, et al. (2006) and Dee, Deen, et al. (2006). Each chamber had a height, width, and depth of 1.8 m, 1.3 m, and 1.3 m, respectively. The duct height, width, and depth were 0.65 m, 1.3 m, and 0.65 m, respectively. The outlet diameter was 0.3 m, and the inlet area was 0.4 m^2. 83

Figure 5.2. Comparison of the dose-response models of PRRSV for aerosol, intranasal, and oral transmission routes, with the theoretical maximum (TM), 2.5-percentile (2.5%-tile), 97.5-percentile (97.5%-tile), and maximum likelihood estimates (MLE): (a) exponential model, (b) exact beta-Poisson models, (c) approximate beta-Poisson models. The literature data for aerosol are from Hermann et al. (2009), while the intra-nasal and oral datasets are from Hermann et al. (2005). 90

Figure 5.3. The exact beta-Poisson dose response models for PRRSV, with the theoretical maximum (TM), 2.5-percentile (2.5%-tile), 97.5-percentile (97.5%-tile), and maximum likelihood estimates (MLE): (a) aerosol transmission route (based on dataset of Hermann et al. (2009), (b) intranasal transmission route (based on dataset of Hermann et al. 2005), and (c) oral transmission route (based on dataset of Hermann et al. 2005). 94

Figure 5.4. The predicted infectious dose at 50% probability of infection (maximum likelihood estimate; MLE): (a) PRRSV on aerosol, intra-nasal, and oral transmission routes; (b) AIV H9N2 on aerosol, intra-nasal, and oral transmission routes; (c) PEDV in terms of feed per gram, orogastrically, and oral (50% diarrhoea dose) transmission routes. 96

Figure 5.5. The exact beta-Poisson dose response models for AIV H9N2 (based on datasets of Guan et al. 2013), with the theoretical maximum (TM), 2.5-percentile (2.5%-tile), 97.5-percentile (97.5%-tile), and maximum likelihood estimates (MLE): (a) aerosol, (b) intra-nasal, and (c) oral transmission routes. 97

Figure 5.6. The exact Beta-poisson dose response models for AIV H5N1, with the theoretical maximum (TM), 2.5-percentile (2.5%-tile), 97.5-percentile (97.5%-tile), and maximum likelihood estimates (MLE): (a) aerosol transmission route (lethal dose; based on dataset of Agranovski et al. 2010), (b) intra-nasal and intratracheal transmission routes (based on datasets of Spekreijse et al. 2011). 98

Figure 5.7. The exact beta-Poisson dose response models for FMDV, with the theoretical maximum (TM), 2.5-percentile (2.5%-tile), 97.5-percentile (97.5%-tile), and maximum likelihood estimates (MLE): (a) intra-nasal transmission route on sheep (based on dataset of Hughes et al. 2002), (b) aerosol transmission route on sheep (based on dataset of Gibson & Donaldson 1986), (c) natural aerosol transmission route on cows (based on dataset of Donaldson et al. 1987), (d) artificial aerosol transmission route on cows (based on dataset of Donaldson et al. 1987). 100

Figure 5.8. The exact beta-Poisson dose-response modelling results for ASFV, with the theoretical maximum (TM), 2.5-percentile (2.5%-tile), 97.5-percentile (97.5%-tile), and maximum likelihood estimates (MLE): (a) feed ingestion, (b) liquid ingestion (based on dataset of Niederwerder et al. 2019), (c) nasopharyngeal inoculation, and (d) oropharyngeal inoculation (based on dataset of Howey et al. 2013). 102

Figure 5.9. The exact beta-Poisson dose-response models for PEDV, with the theoretical maximum (TM), 2.5-percentile (2.5%-tile), 97.5-percentile (97.5%-tile), and maximum likelihood estimates (MLE): (a) oral transmission route, measuring probability of diarrhoea (based on dataset of Liu et al. 2015), (b) feed, in grams feed (based on dataset of Schumacher et al. 2016), (c) orogastric transmission route (based on dataset of Thomas et al. 2015). 104

Figure 5.10. (a) Simulated aerosol concentration in second chamber over 200-second simulation, (b) cumulative aerosol dose of PRRSV for 12-kg and 25-kg pigs over the 200-second simulation. 107

Figure 6.1. Integrated model used to simulate the aerosol transmission of PRRSV from source to recipient buildings 112

Figure 6.2. Illustration of the CFD simulation steps for the field study 113

Figure 6.3. Illustration of simulation domain: (a) modelled site with source and recipient buildings identified (b) modelled site in domain with inlet, outlet, sides, top, ground, and windbreak identified 115
Figure 6.4. Summary of the CFD simulations and data analysis used to predict PRRSV exposure doses and probability of infection in pig pens in the recipient building 125
Figure 6.5. Geometry used for recipient building simulations, with arrows dictating the direction of airflow into and out of the building. (a) locations of vent (inlet) and exhaust fans, (b) top view of the geometry with location of pens A-F 126
Figure 6.6. Cumulative fraction of aerosol (airborne particle) sizes measured in Alonso et al. (2017) 130
Figure 6.7. Fraction of PRRSV infectivity remaining after exposure time in field conditions in (a) the June 6 simulation and (b) the June 7 simulation. The hour of the day (time) is associated with specific temperature and relative humidity conditions indicated in Table 6.8 that affected the survival of PRRSV. 133
Figure 6.8. Mesh refinement results for field domain simulation, showing velocity variation between coarse, moderate, and fine meshes at (a) inlet, (b) within windbreak, (c) through source building, (d) before inlet of recipient building, (e) near outlet of the domain. 137
Figure 6.9. Average percent difference in the aerosol count (with aerodynamic diameters of 1.44×10^{-6} m and 3.60×10^{-6} m) in each pen (a) between the coarse and moderate meshes and (b) between the moderate and fine meshes. 138
Figure 6.10. Frequency of aerosol entry rates into recipient building, according to wind speed for aerosol with aerodynamic diameters of (a) 1.44 μm, (b) 3.60 μm, and (c) 8.88 μm 140
Figure 6.11. Aerosol concentration (# m^{-3}) during June 6 simulation in each pen in terms of time (s) since aerosol entry into building began, for aerodynamic diameter (a) 1.44 μm, (b) 3.60 μm, (c) 8.88 μm, (d) all particles 143
Figure 6.12. Aerosol concentration (# m^{-3}) during June 7 simulation in each pen in terms of time (s) since aerosol entry into building began, for aerodynamic diameter (a) 1.44 μm, (b) 3.60 μm, (c) 8.88 μm, (d) all particles 145

Figure 6.13. For June 6 simulation, the airborne PRRSV concentration ($TCID_{50}$ per m^3) in pens when different PRRSV concentrations were exhausted from source building, with PRRSV entry occurring during 0 to 25200s for different PRRSV concentrations released from the source building. (a) minimum release concentration of 4.2 $TCID_{50}$ m^{-3}, (b) mean release concentration of 500 $TCID_{50}$ m^{-3}, (c) maximum release concentration of 125,000 $TCID_{50}$ m^{-3}. 147

Figure 6.14. For June 7 simulation, the airborne PRRSV concentration ($TCID_{50}$ per m^3) in the pens when different PRRSV concentrations were exhausted from source building, with PRRSV entry occurring during 0 to 21600s for different PRRSV concentrations released from the source building. (a) minimum release concentration of 4.2 $TCID_{50}$ m^{-3}, (b) mean release concentration of 500 $TCID_{50}$ m^{-3}, (c) maximum release concentration of 125,000 $TCID_{50}$ m^{-3}. 148

Nomenclature list (by chapter)

Chapter 2 and 7

ABPM	Approximate beta-Poisson model
ADM	Air dispersion modelling
AIV	Avian influenza virus
ASF	African swine fever
ASFV	African swine fever virus
ASTM	American Society of Testing and Materials
CFD	Computational fluid dynamics
DNA	Deoxyribonucleic acid
EBPM	Exact beta-Poisson model
EM	Exponential model
FB	Fractional bias
FMD	Foot and mouth disease
FMDV	Foot and mouth disease virus
HPAIV	Highly pathogenic avian influenza virus
IAV	Influenza A virus
LPAIV	Lowly pathogenic avian influenza virus
LPM	Live poultry market
NMSE	Normalized mean square error
PCR	Polymerase chain reaction
PED	Porcine epidemic diarrhea
PEDV	Porcine epidemic diarrhea virus
PRRS	Porcine reproductive and respiratory syndrome
PRRSV	Porcine reproductive and respiratory syndrome virus
RANS	Reynolds-averaged Navier Stokes model
RNA	Ribonucleic acid
SARS-CoV	Severe acute respiratory syndrome coronavirus
UV	Ultraviolet irradiation

Chapter 3

ADM	Air dispersion modelling
AI	Avian influenza
AIV	Avian influenza virus
ASF	African swine fever
ASFV	African swine fever virus
AT	Airborne transmission
BSL	Biosafety level
CFD	Computational fluid dynamics
DNA	Deoxyribonucleic acid
EID_{50}	50% embryo infectious dose
FMD	Foot and mouth disease
FMDV	Foot and mouth disease virus
H	Haemagglutinin
HPAIV	Highly pathogenic avian influenza virus
IAV	Influenza A virus
ID_{50}	Infectious dose 50%
LD_{50}	Lethal dose that kills 50% of test subjects
LPAIV	Lowly pathogenic avian influenza virus
LPM	Live poultry market
MCMC	Monte Carlo Markov chain
N	Neuraminidase
PED	Porcine epidemic diarrhoea
PEDV	Porcine epidemic diarrhoea virus
PFU	Plaque forming unit
PRRS	Porcine reproductive and respiratory syndrome
PRRSV	Porcine reproductive and respiratory syndrome virus
qRT-PCR	Quantitative reverse-transcription polymerase chain reaction

RIMPUFF	Risø-Mesoscale-Puff model
RNA	ribonucleic acid
RT-PCR	Reverse-transcription polymerase chain reaction
$TCID_{50}$	50% Tissue Culture Infectious Dose
$TCID_{eq}$	Equivalent $TCID_{50}$
UV_{254}	Ultraviolet irradiation with wavelength of 254 nm

Chapter 4

λ	Molecular mean free path (6.691×10^{-8} m)
ρ_{air}	Density of air (1.19 kg m^{-3}).
ρ_f	Density of air (kg m^{-3})
ρ_p	Density of bioaerosol (kg m^{-3})
μ	Dynamic viscosity of air (1.845×10^{-5} kg m^{-1} s^{-1})
A	Area of the inlet (m^2)
AIV	Avian influenza virus
APSS	Aerosol particle size spectrometer
ASTM	American Society of Testing and Materials
C_C	Cunningham correction factor
$C_{chamber}$	Bioaerosol concentration in the chamber (mg m^{-3})
CFD	Computational Fluid Dynamics
$C_{measured}$	Bioaerosol concentration measured in chamber experiments (mg m^{-3}).
C_{node}	Bioaerosol concentration at node (mg m^{-3})
$C_{o,average}$	Average measurement bioaerosol concentration (mg m^{-3})
C_{oi}	Measured bioaerosol concentrations at replicate *i* of treatment test (mg m^{-3})
C_p	Simulated bioaerosol concentration (mg m^{-3})
$C_{surround}$	Bioaerosol concentration in cells surrounding measurement point (mg m^{-3})
d_p	Mean diameter (m)
DPM	Discrete phase modelling
FB	Fractional bias

FMDV	Foot and mouth disease virus
g	Gravitational constant (m s^{-2})
HEPA	High efficiency particulate air
$M_{aerosol}$	Modified bioaerosol generation rate (bioaerosol mass flow rate) (kg s^{-1})
M_{air}	Mass flow rate of air exiting chambers (kg m^{-3})
MWPS	Midwest plan service
N	Total number of time steps for treatment
n	Number of replicates per treatment
NMSE	Normalized mean square error
n_{node}	Number of nodes surrounding the measurement point
$n_{node,\ chamber}$	Number of cells in a chamber
PBS	Phosphate-buffered saline
PRRSV	Porcine reproductive and respiratory syndrome virus
Q	Ventilation rate of the chambers (m^3 h^{-1}) (measured values were used in simulations).
R_p	Reynolds number of the bioaerosol
t	Length of time step (s)
T	Simulation time, or time to steady-state (s)
v	Velocity of airflow during treatment (m s^{-1})
V_{node}	Volume of cells adjacent to nodes (m^3)
V_t	Stokes settling velocity (m s^{-1})
x_{min}	Minimum mesh size (m)

Chapter 5

Δt	Time step size (0.5 s)
${}_1F_1$	Kummer confluent hypergeometric function
2.5%-tile	2.5 percentile curve
97.5%-tile	97.5 percentile curve
α, β	Parameters for the exact and approximate beta-Poisson dose-response models

$\alpha_{P,}$ β_p	Parameters for the PRRSV exact beta-Poisson model for aerosol transmission
$\alpha_{P,approx.}$, $\beta_{P,approx}$	Parameters for the PRRSV approximate beta-Poisson model for aerosol transmission
θ	Model parameter(s) in the dose-response model (*r, α, β*)
ρ_s	Density of stock solution (998.2 kg m^{-3})
ΣD_p	Cumulative PRRSV exposure dose ($TCID_{50}$) over 200-s simulation
ABPM	Approximate beta-Poisson model
AIV	Avian influenza virus
ASFV	African swine fever virus
C_a	Average aerosol concentration in the chamber at a time step (kg m^{-3})
cf	Conversion factor
CFD	Computational fluid dynamics
CI	Confidence interval
C_{node}	Aerosol concentration at a node at a time step (kg m^{-3})
C_{stock}	PRRSV concentration in the stock solution ($TCID_{50}$ m^{-3})
D	Dose of infectious pathogen
DD_{50}	Diarrhoea dose at 50% probability
D_P	PRRSV dose at a time step ($TCID_{50}$)
EBPM	Exact beta-Poisson model
EID_{50}	50% embryo infectious dose
EM	Exponential model
FFU	Focus forming units
FMDV	Foot and mouth disease virus
f_X	Fraction of aerosols with aerodynamic diameter *X*
H5N1	Highly pathogenic subtype of AIV
H9N2	Low pathogenic subtype of AIV
HAD_{50}	50% hemadsorbing dose
i	Dose of infectious pathogen (units vary)

ID_{50}	Infectious dose at 50% probability
k_i	Number of infected pigs at dose level *i*
$k_{infected}$	Number of infected animals in case study
$L(\theta)$	Likelihood as a function of parameters θ
LD_{50}	Lethal dose at 50% probability
MCMC	Markov chain Monte Carlo simulations
MLE	Maximum likelihood estimate
MLE	Maximum likelihood estimation
M_X	Mass injection rate of aerosols with aerodynamic diameter *X* (kg 0.002 s^{-1} $node^{-1}$)
N	Number of nodes in the mesh
$n_{exposed}$	Number of exposed animals in case study
n_i	Number of exposed pigs at dose level *i*
$P(D, \theta)$	Probability of infection as a function of dose and parameter(s) θ.
PEDV	Porcine epidemic diarrhoea Virus
PFU	Plaque forming units
$P_{infected}$	Observed rate of infection in case study
p_{max}	Maximum particle size (50 μm)
p_{mean}	Mean of the normal distribution of the logarithmic particle sizes
p_{min}	Minimum particle size (5 μm)
PRRSV	Porcine reproductive and respiratory syndrome virus
r	Probability of a single virus particle causing an infection and the model parameter in the exponential dose-response model
R	Respiration rate of pigs (m^3 s^{-1})
r_p	Parameter for the PRRSV exponential model for aerosol transmission
SD	Standard deviation of the normal distribution of the logarithmic particle sizes
$TCID_{50}$	50% tissue culture infectious dose
TM	Theoretical maximum (Probability of infection exponential model when *r* = 1)

V_{node}	Volume of cell (m^3)
V_s	Volume of stock solution of PRRSV aerosolised in experiment (0.001 m^3)
X	Aerodynamic diameter of aerosols (μm)

Chapter 6

$\|U\|$	Modulus of wind speed (m s^{-1}),
${}_1F_1$	Kummer confluent hypergeometric function
α, β	Parameters for the dose-response function
β_p, β_d, $C_{\varepsilon 4}$, $C_{\varepsilon 5}$	Windbreak modelling constants
Δd	Size range between particle diameters d_1 and d_2 (μm)
θ	Parameter used to describe shape of PRRSV decay in decay model
κ	von Karman's constant
λ	Mean free path of air
ρ	Density of air (kg m^{-3})
ρ_o	Unit density (kg m^{-3})
ρ_p	Density of aerosols (kg m^{-3})
A_{cool}	Minimum cool pad area (m^2)
C_1, C_2, σ_k, σ_ε	k-ε turbulence model constants
C_C	Slip correction factor
C_d	Drag coefficient
C_{dust}	Concentration of particulate matter in finisher building (mg m^{-3})
$C_{inf}(t)$	Concentration of infectious PRRSV in pen at time t ($TCID_{50}$ m^{-3})
$C_{M\mu}$	Turbulence viscosity coefficient
$C_{N,m}$	Measured aerosol (count) concentrations (# m^{-3}),
$C_{N,\Delta d}$	Aerosol (count) concentration in size range Δd (# m^{-3})
$C_{P,fan}$	Concentration of PRRSV at source building exhaust ($TCID_{50}$ m^{-3})
$C_{P,m\Delta d}$	PRRSV RNA concentration within size range Δd (RNA m^{-3})

$D(t)$	PRRSV aerosol dose at time t ($TCID_{50}$)
d_a	Aerodynamic diameter (µm)
d_{eq}	Equivalent diameters of aerosols (µm)
d_{fan}	Diameter of the fan (m)
d_{vent}	Equivalent diameter of vent (m)
ε	Rate of dissipation of turbulent energy ($m^2\ s^{-3}$)
$\varepsilon(z)$	Rate of dissipation of turbulent energy profile at the inlet as a function of height z ($m^2\ s^{-3}$)
$F_{building}$	Fraction of infectious PRRSV remaining after time in building
f_d	Fraction of aerosols of diameter d_a
F_{field}	Fraction of infectious PRRSV remaining after time in field
f_{mod}	Modification factor
$F_{N,\Delta d}$	Fraction of particles within size range Δd
GSD	Geometric standard deviation
h	Height of the vent (m)
I	Turbulence intensity of fans (%)
icoUKPF	icoUncoupledKinematicParcelFOAM solver in OpenFOAM
ID_{50}	Infectious dose at 50% probability
k	Turbulent kinetic energy ($m^2\ s^{-2}$)
k(z)	Turbulent kinetic energy profile at the inlet as a function of height z ($m^2\ s^{-2}$)
l	Length scale (m)
LAD	Leaf area density (m^{-1})
M	Mass flow rate of aerosols ($kg\ s^{-1}$)
M_d	Fractional mass flow rate for aerosols of diameter d_a ($kg\ s^{-1}$)
MLE	Maximum likelihood estimate
MMD_{eq}	Equivalent spherical mass median diameter (µm)
M_{pig}	Mass of pig (kg)

$n_{aerosol}$	Number of aerosols per parcel (aerosols parcel^{-1})
n_{fan}	Number of exhaust fans
N_{inf}	Number of infectious PRRSV particles in a parcel ($TCID_{50}$)
n_n	Number of nursery pigs (head)
n_{pig}	Number of pigs in the building
P_d	Injection rate of aerosols of diameter d_a generated by source building (parcels s^{-1}),
$P_{d,north}$, $P_{d,south}$	Injection rate of aerosols of diameter d_a generated from fans on north and south sides of source building, respectively (parcels s^{-1})
p_{fan}	kinematic pressure at fan (m^2 s^{-2})
P_{inf}	Probability of infection (%)
p_T	Total pressure (Pa)
$Q_{building}$	Ventilation rate of the building (m^3 s^{-1})
Q_{head}	Summer ventilation rate per head (cfm head^{-1})
$Q_{n,h}$	Ventilation rate for nursery pigs per head (cfm head^{-1})
R_{pig}	Respiration rate of pigs (m^3 s^{-1} kg^{-1})
R_{VP}	Ratio of PRRSV virus particles to airborne particles (i.e., the PRRSV conversion factor) for aerosol diameter d_a
$S\varepsilon$	Source term for rate of dissipation of turbulent energy from windbreak effect
S_k	Source term for turbulent kinetic energy from windbreak effect
S_U	Source term for momentum equations from windbreak effect
t	Building simulation time (s)
$T_{age,building}$	Time that aerosols were inside of the building at time t (s)
$T_{age,field}$	Time that airborne particles were in the field (s)
T_{enter}	Time that aerosols entered building (s)
U	Wind speed in the i-direction (m s^{-1})
U(z)	Velocity profile at the inlet as a function of height z (m s^{-1})
U^*	friction velocity (m s^{-1})
u_{fan}	Velocity of the exhaust fan of source building (m s^{-1})

U_{ref}	Velocity at z_{ref} (m s^{-1})
u_{vent}	Velocity at the vent (m s^{-1})
V_{eq}	Volume of a single aerosol of diameter d_a (m^3 $aerosol^{-1}$)
v_{fan}	Velocity at fan of the recipient building (m s^{-1})
V_{pen}	Volume of a pen (m^3)
w	Width of the vent (m)
z_0	Surface roughness height (m)
z_g	Minimum z-coordinate (m)
z_{ref}	Reference height (m)

Chapter 1. Introduction

1.1. General introduction

Infectious animal diseases are a significant problem to livestock producers and the livestock industry. The outcomes of a disease outbreak can vary from reduced herd size and growth of infected animals to the culling of all infected or susceptible herds or flocks to prevent continued spread of disease in a region. An example of the former occurs in pig herds when infected with porcine reproductive and respiratory syndrome (PRRS) virus; while this disease does not normally lead to the loss of entire herds, the overall annual productivity cost due to PRRS is $664 million in the United States (Holtkamp et al., 2013). An example of the latter is the culling of more than 17 million birds in 2004 to control the spread of highly pathogenic avian influenza virus in Fraser Valley, British Columbia, Canada; the outbreak resulted in losses greater than $380 million (Bowes, 2007). These examples show that it is pertinent for preventative measures to be established to reduce outbreaks and the spread of infectious animal diseases. However, the prevention and control of infectious animal disease outbreaks is optimised when there is a clear understanding of disease transmission, including thorough knowledge about the factors that affect transmission of infectious animal diseases on different transmission routes. Airborne transmission of diseases is still elusive.

Airborne transmission is a mode of transmission for some infectious animal viruses. The contribution of airborne transmission in spreading disease is well understood for some viruses, such as foot and mouth disease virus (Donaldson, Alexandersen, Sørensen, & Mikkelsen, 2001a), but there are some infectious animal viruses such as African swine fever virus (Olesen et al., 2017) and porcine epidemic diarrhoea virus (Gallien et al., 2018; Niederwerder et al., 2016) in which there is not enough research knowledge to understand how airborne transmission contributes to the spread of infectious disease. A better understanding of the factors that affect airborne transmission can help animal producers make informed decisions to reduce the spread of infectious animal viruses.

Airborne transmission of animal diseases involves several complicated physical and biological processes, including transport of aerosols in the air currents, decay of pathogens in the environment, and the critical dose to cause infections (dose-response). There has been a research

history of using computer models to better understand the transmission of infectious animal diseases, such as research about the spread of foot and mouth disease virus by airborne transmission (Gloster et al., 2010). With recent technology advancements, computer modelling has become more powerful and capable of simulating complex processes and systems. Additionally, many software packages that can be utilised to perform computer modelling are now open source, providing researchers with affordable, well-documented software packages that allow for customisation of the computer models. However, there are many applications of computer modelling that have been minimally explored in regards to understanding infectious animal disease transmission. The overall goal of this thesis was to demonstrate and discuss how specific computer modelling tools can be used and/or combined to gain knowledge about infectious animal disease transmission. Specifically, this thesis focusses on using computational fluid dynamics for aerosol transport in the air currents, virus survival, dose-response modelling to simulate the aerosol transmission pathway and probability of infection of other transmission routes.

1.2. Research gaps and objectives

Aerosol and airborne transmission of different infectious animal viruses are understood to different degrees, in terms of the factors affecting transmission as well as the computer modelling knowledge. Understanding the various factors affecting aerosol transmission is important to accurately model aerosol transmission of disease pathogens. Therefore, it is beneficial to compile the current scientific knowledge on these factors and computer modelling of aerosol and airborne transmission of important animal viruses to identify specific knowledge gaps and future research opportunities.

It is also evident that computer models could be used to improve the understanding of aerosol and airborne transmission of infectious animal viruses in the livestock industry. Specifically, CFD could be used to study specific scenarios of aerosol transport and transmission. Half-life models of virus survival in aerosols can provide a better estimation of the quantity of infectious virus remaining in the air that is received by susceptible animals. Lastly, dose-response modelling can estimate the probability of infection based on the infectious virus dosage. However, these models are currently studied separately by researchers in different disciplines.

Specifically, CFD modelling of aerosol transport is pursued in engineering, while virus decay and dose-response are studied in the realm of biological sciences. For example, there is an abundance of literature information on PRRSV about factors affecting aerosol transmission, but there are currently no CFD studies about aerosol transport or transmission of PRRSV. Therefore PRRSV modelling was selected as the focus of this thesis. The research objectives of this thesis were to:

1) review the scientific knowledge and existing computer models of aerosol and airborne transmission of the infectious animal viruses. Specifically, identify research gaps in understanding factors that affect airborne transmission of specific infectious animal viruses and research gaps in computer modelling of aerosol and airborne transmission,

2) develop a CFD model to simulate the movement and concentration of PRRSV-laden aerosols in an experimental chamber system and compare the model predictions with experimental data (aerosol concentration),

3) perform dose-response modelling using literature data available for the infectious animal viruses to improve understanding of exposure dose and infectious dose on transmission of infectious disease,

4) demonstrate the combined use of dose-response modelling and CFD to estimate the probability of aerosol transmission of PRRSV within a confined space and compare with observed results in a case study, and

5) develop an integrated model (CFD, half-life, and dose-response models) to predict aerosol transport and aerosol transmission of PRRSV between buildings in the field conditions.

1.3. Significance of research contributions

Chapter 3 identified current knowledge of airborne transmission of five infectious animal diseases based on an extensive literature review. The review also identifies research gaps and provides recommendations for future research. The information in this chapter may also help the animal industry to better understand airborne transmission of infectious animal diseases, and thus to improve the biosecurity measures to minimize disease spread.

Chapter 4 described CFD simulations of transport of PRRSV aerosols from a source chamber to a recipient chamber. The results indicated that the CFD was proficient in modelling the transport of PRRSV aerosols under the steady-state conditions. However, there were some discrepancies between the CFD predicted PRRSV concentrations and the experimental data during the transient stage (prior to steady-state being reached). Ultimately, the study showed that CFD was capable of simulating PRRSV transport and performing air sampling of airborne viruses is important to validate the CFD modelling.

Chapter 5 described dose-response modelling of five infectious animal viruses on various transmission routes. Additionally, a CFD simulation of the PRRSV concentration in a confined space was coupled with a dose-response model to predict the probability of infection by aerosol transmission. The study showed that infectious dose of animal disease viruses was highly affected by the transmission route. For example, aerosol transmission required less virus to cause infection in susceptible animals compared to intranasal transmission for FMDV and intranasal and oral transmission for PRRSV and AIV. The coupled CFD and dose-response modelling predictions corresponded well with the observed rates of infection in the two case studies. Overall, the study demonstrated the importance of transmission route in understanding the spread of infectious animal disease. The study also demonstrated how CFD and dose-response models could be combined to simulate the aerosol transport and predict the probability of infection by aerosol transmission.

Chapter 6 described the use of an integrated model to predict the probability of infection of PRRSV via aerosol transmission between buildings in the field conditions. The model predictions were compared to a case study where building to building airborne transmission of PRRSV was observed. This study was the first in: i) using CFD to simulate building to building transmission of PRRSV; and ii) integrating CFD, a half-life model, and dose-response modelling to study the spread of an infectious animal virus by aerosol transmission. The study showed that the concentration of PRRSV exhausted from an infected pig facility highly affected the downwind concentration of PRRSV and subsequently the probability of infection due to aerosol dose of PRRSV in nearby facilities. This showed the importance of air sampling at the exhaust

of infected facilities and at the inlet of susceptible buildings in model development and validation.

Overall, the work in this thesis provided modelling approaches that can be used to enhance the research community's understanding of airborne transmission of infectious animal diseases. The work in this thesis, particularly the coupled dose-response and CFD models in chapter 5 and the integrated model in chapter 6, provided research methods of simulating the airborne transmission process of animal diseases within a building (chapter 5) and from an infected to susceptible building (chapter 6). These computer models can be customized to simulate specific airborne transmission scenarios by changing the setting, farm dimensions and locations, virus type and strain, shedding and survival of virus, and other factors. This can allow for researchers to assess the contribution of airborne transmission in past outbreaks, predict spread by airborne transmission in future outbreaks, and evaluate control or prevention mechanisms to reduce spread by airborne transmission.

1.4. Thesis structure

This thesis has a traditional/sandwich hybrid structure, consisting of a general introduction, a general literature review, four journal papers, an overall discussion, and a conclusion. A complete list of references used in this thesis will be located at the end of the thesis in the format of the Biosystems Engineering Journal.

Chapter 2 consists of a general literature review to describe the problems and knowledge gaps addressed in this thesis. The literature review is in the Biosystems Engineering Journal format.

Chapters 3 to 6 describe the research contributions of specific journal papers. Each chapter includes: the journal paper abstract, a brief introduction, the journal paper objectives, the methodology of the research, the results of the research, the discussion specific to the results of the research, and a conclusion to the journal paper. The journal papers in chapter 3 and 4 have been published in refereed journals, while the journal paper in chapter 2 is currently under review and the paper in chapter 5 is at the final stage of preparation for submission. The introduction (literature review) portion of the journal papers have been moved to the general literature review in chapter 1 or removed entirely to reduce repetitious information in this thesis.

Chapter 7 provides a discussion of the overall contributions of the research conducted in the thesis; common elements between specific chapters are identified and discussed in this chapter. The discussion also identifies remaining research gaps and general recommendations for future work.

1.5. Contribution of authors

The work and first draft of journal paper described in chapter three was written by myself, Amy La. It was co-authored by Dr. Qiang Zhang in the Department of Biosystems Engineering at the University of Manitoba, for providing research guidance and reviewing the research paper for publication. Dr. Nazim Cicek and Dr. Kevin Coombs were also co-authors as they reviewed the research paper and provided feedback for improvement prior to submission to the journal.

The work and first draft of the journal paper descried in chapter four was written by myself, Amy La. It was co-authored by Dr. Qiang Zhang in the Department of Biosystems Engineering at the University of Manitoba, for providing research guidance and reviewing the research paper for publication.

The modelling work, data analysis, and writing of the first draft of the journal paper described in chapter five was performed by Amy La. Dr. Zhang provided guidance during the research and reviewed the research paper for publication. Dr. Cicek, Dr. Levin, and Dr. Coombs were also co-authors as they also reviewed and provided comments to the paper prior to submission to the journal.

The modelling work, data analysis, and writing of the first draft of the journal paper described in chapter six was performed by Amy La. Dr. Zhang provided guidance during the research as well as reviewed and provided feedback on the research paper for publication. The paper has not yet been submitted to a journal.

Chapter 2. General literature review

2.1. Infectious animal diseases

There are numerous infectious viral animal diseases that impact the livestock production globally. The five infectious animal viruses are discussed in detail in this work are: African swine fever virus (ASFV), porcine epidemic diarrhoea virus (PEDV), avian influenza virus (AIV), porcine reproductive and respiratory syndrome virus (PRRSV), and foot and mouth disease virus (FMDV). These five animal viruses have caused significant financial costs to the livestock industry during past outbreaks, and the literature currently has varying amounts of evidence supporting airborne transmissibility of these viruses.

African swine fever (ASF) is caused by the African swine fever virus(ASFV). ASFV is a large, enveloped double-stranded DNA virus that belongs to the family *Asfarviridae* and genus *Asfivirus* (Beltrán-Alcrudo, Arias, Gallardo, Kramer, & Penrith, 2017; Galindo & Alonso, 2017; Pikalo, Zani, Hühr, Beer, & Blome, 2019). It has an average diameter of 200 nm (Galindo & Alonso, 2017). There are 24 genotypes of ASFV (Zhou et al., 2018). Clinical signs of ASFV depends on the virulence and lethality of the ASFV isolates, which are categorised as peracute, acute, subacute, chronic, and asymptomatic (Beltrán-Alcrudo et al., 2017). A general sign of ASFV is "sudden death of pigs", which occurs in peracute cases; however, death occurs 90 to 100% in acute cases, 30 to 70% of the time in subacute cases, and less than 30% in chronic cases (Beltrán-Alcrudo et al., 2017). The first documented case occurred in Kenya in 1909 (Montgomery, 1921). The spread of ASFV outside of Africa began in 2007, with spread to Georgia, Caucasus, and the Russian Federation in 2007. ASFV has been introduced to Ukraine, Belarus, the European Union, and Moldova (Beltrán-Alcrudo et al., 2017). In 2018, the first case of ASF in China was reported (Zhou et al., 2018). ASF was reported in Mongolia, Vietnam, Cambodia, North Korea, Laos, Philippines, Myanmar, Timor-Leste, South Korea (Mason-D'Croz et al., 2020), and Indonesia in 2019, as well as Papua New Guinea and India in 2020 (Woonwong, Tien, & Thanawongnuwech, 2020). The recent spread of ASFV in China and Vietnam significantly affected pork prices and local supply of pork (Woonwong et al., 2020).

Porcine epidemic diarrhoea (PED) is caused by the porcine epidemic diarrhoea virus (PEDV). It is an enveloped, single-stranded RNA virus and its order, family, and genus are

Nidovirales, *Coronaviridae*, and *Alphacoronavirus*, respectively (Kocherhans, Bridgen, Ackermann, & Tobler, 2001). PED is characterised by vomiting, watery diarrhoea, dehydration, and reduction in growth performance (Lin, Saif, Marthaler, & Wang, 2016). It causes high mortality in nursing pigs and low mortality in finisher and farrowing herds (Kochhar, 2017). PEDV was first reported in 1978 in the United Kingdom (Chasey & Cartwright, 1978). Since then, there were numerous outbreaks across Europe and Asia (Kochhar, 2017). PEDV was introduced to the United States in 2013 (Kochhar, 2017; Lin et al., 2016). As of February 2018, there were more than 3855 confirmed positive premises infected with PEDV in the United States (USDA, 2018). Introduction of PEDV in Canada occurred in 2014 and mostly affected farms in Ontario (Kochhar, 2017). Manitoba experienced PEDV outbreaks in 2017 and 2019, affecting 90 and 82 premises, respectively (Manitoba Agriculture, 2020).

Avian influenza is caused by avian influenza virus (AIV). AIV are influenza A viruses, which belong to the family *Orthomyxoviridae* (Webster, Bean, Gorman, Chambers, & Kawaoka, 1992) . In general, influenza A viruses (IAV), are single-stranded RNA viruses with a diameter of 80 to 120 nm and whose RNA is divided into eight segments (Webster et al., 1992). IAV have two important envelope proteins; hemagglutinin (H), of which there are currently 18 known subtypes and neuraminidase (N), of which there are currently 11 known subtypes (Lycett, Duchatel, & Digard, 2019). AIV is often identified as lowly pathogenic (LPAIV) or highly pathogenic (HPAIV) in the literature, depending on the disease severity in the infected birds (Alexander, 2000). HPAIV causes "systemic disease characterised by mortality rates that can reach 100%" (Pasick et al., 2005). Comparatively, LPAIV causes respiratory disease with mild symptoms, unless there are other factors that causes it to worsen, such as other infections (Alexander, 2000). AIV is normally carried by wild birds in North America and their appearance in domestic flocks are usually due to a rare transmission event caused by a mutation of a wild strain (Berhane et al., 2009; Pasick et al., 2014; Pasick et al., 2005). H5 and H7 subtypes of AIV have a history of causing HPAIV outbreaks and LPAIV strains of H5 and H7 subtypes have the potential to mutate into HPAIV strains (Pasick et al., 2005). The 2004 and 2014 Canada HPAIV outbreaks affected 42 commercial poultry facilities (17 million animals; Bowes, 2007) and 11 commercial poultry facilities (240,000 animals; Xu et al., 2016), respectively.

Porcine reproductive and respiratory syndrome (PRRS) is caused by porcine reproductive and respiratory syndrome virus (PRRSV). PRRSV is an enveloped RNA virus with a diameter of 50 to 65 nm. Its order, family, and genus are *Nidovirales*, *Arteriviridae*, and *Arterivirus*, respectively (Cho & Dee, 2006). PRRS causes respiratory disease in pigs of all ages, but it can cause more severe outcomes in younger pigs, such as respiratory failure and death (Egli, Thür, Liu, & Hofmann, 2001). The first report of type 2 PRRSV (North American; PRRSV VR 2332) was in 1987, while the first reports of type 1 PRRSV (European; Lelystad virus) were in 1990 (Egli et al., 2001). Since then, PRRSV outbreaks in Canada and the U.S. occur frequently. In a 2011 study of the economic impacts of PRRS on the U.S. pig industry, it was estimated that the annual productivity losses in breeding and growing herds was $664 million (Holtkamp et al., 2013). A pilot study found that there was an annual PRRSV epidemic in the U.S. from mid-October to mid-March over a three-year-period (Tousignant & Morrison, 2012).

Foot and mouth disease (FMD) is caused by foot and mouth disease virus (FMDV). FMDV is a single-stranded, non-enveloped RNA virus that is 25 to 30 nm in diameter; it belongs to the family *Picornaviridae* and genus *aphthovirus* (Belsham, 1993; Malik et al., 2017). It has seven serotypes: A, O, C, SAT1, SAT2, SAT3, and Asia 1, but this system of organising the virus is considered obsolete (CFIA, 2013). Clinical signs of the disease include "fluid-filled blisters" called vesicles and "erosions in the mouth, nostrils, teats, and on the skin between and above the hoofs" (CFIA, 2013). It causes mortality more frequently in young animals than adult animals (Alexandersen, Zhang, Donaldson, & Garland, 2003). FMDV infects cloven-hoofed animals (Donaldson & Alexandersen, 2002). Some examples of susceptible domestic animals are, but not limited to, pigs (Alexandersen & Donaldson, 2002), sheep (Gibson & Donaldson, 1986), and cattle (Donaldson, Gibson, & Oliver, 1987). FMD has a significant effect on the livestock industry globally, as it has direct and indirect costs on farmers (Rushton & Knight-Jones, 2012). As of 2011, FMD was "endemic in almost all developing countries" and farmers from these countries were likely the most affected by the costs associated with FMD (Rushton & Knight-Jones, 2012).

2.2. Factors affecting transmission of infectious animal diseases

Infectious disease transmission is related to a complex combination of factors, including: the virus strain or pathogenicity (Cho et al., 2006; Cho, Deen, & Dee, 2007); the transmission route (Guan, Fu, Chan, & Spencer, 2013; Hermann, Muñoz-Zanzi, Roof, Burkhart, & Zimmerman, 2005); the amount of pathogen exposure (i.e., the dose); the dose required to cause infection (Hermann et al., 2005; Hermann, Muñoz-Zanzi, & Zimmerman, 2009; Niederwerder et al., 2019); the shedding of virus from infected animals into the environment (Cho et al., 2006; Howey, Donnell, Carvalho, Borca, & Arzt, 2013); and its persistence in the environment with exposure to various temperature and relative humidity conditions (Hermann et al., 2007). These factors are often inter-related. For example, the pathogenicity and strain of a virus may affect the amount of virus that is shed into the environment, and more shed virus may increase the ability to transmit.

The transmission routes primarily discussed in this thesis are aerosol transmission and airborne transmission. Aerosol transmission occurs when an animal becomes infected with a virus after inhaling aerosols containing infectious virus. Airborne transmission occurs when viruses become airborne and infect an animal either due to inhalation or due to settling on an object that came in contact with an animal (i.e., by aerosol or fomite; Arruda et al. 2019). An example of airborne transmission is the long distance transmission of FMDV from Brittany, France to Jersey and Isle of Wight, UK in 1981 (Donaldson, Gloster, Harvey, & Deans, 1982; Sørensen, Jensen, Mikkelsen, Mackay, & Donaldson, 2001). Other transmission routes that are discussed to some degree in this thesis are fomite transmission, oral transmission, and intranasal transmission. Fomite transmission occurs when an animal becomes infected after coming into contact with an object that is contaminated with infectious virus. An example is a pig herd becoming infected with PRRSV due to the contaminated workers' clothing or boots (Otake et al., 2002). Oral transmission occurs when animal becomes infected from eating or drinking items contaminated with infectious viruses. An example is the introduction of ASFV into a country due to pigs eating table scraps contaminated with ASFV, which is what introduced ASFV into China in 2018 (Zhou et al., 2018). Intranasal transmission occurs when infectious viruses enter an animal's nasal cavity and causes infection. This mode of transmission is often used to inoculate

animals with an infectious virus in an experimental study, as was done for AIV (Guan et al., 2013), ASFV (Olesen et al., 2017), and PRRSV (Pitkin, Deen, & Dee, 2009).

The infectious dose of a virus is the amount of virus that is required to cause infection in a susceptible animal. In animal research, the infectious dose 50 (ID_{50}) or the amount of infectious required to cause infection in 50% of exposed animals is often quantified using experiments. In these experiments, groups of susceptible animals are exposed to different doses of an infectious virus and the proportion of animals infected in each dosage group is quantified (Cutler, Wang, Hoff, Kittawornrat, & Zimmerman, 2011; Donaldson et al., 1987; Gibson & Donaldson, 1986; Guan et al., 2013; Hermann, Muñoz-Zanzi, & Zimmerman, 2009; Sergeev et al., 2013). The infectious dose of an infectious virus is not uniform across all transmission routes, as seen in infectious dose studies for PRRSV (Hermann, Muñoz-Zanzi, Roof, Burkhart, & Zimmerman, 2005; Hermann et al., 2009), AIV (Guan et al., 2013; Sergeev et al., 2013), and ASFV (Howey et al., 2013). By oral transmission, the infectious dose of ASFV differed depending on if contaminated liquid or feed was ingested (Niederwerder et al., 2019). The infectious dose for FMDV depends on the susceptible animal; for example, cattle and sheep required less virus to be infected than pigs by aerosol transmission (Donaldson et al., 2001a). The age of the susceptible animal may also affect the infectious dose, as 5-day-old pigs required less virus than 3-week-old pigs to become infected (Thomas et al., 2015). The virus strain may also have an effect on the infectious dose. For example, different strains of H5N1 AIV (Sergeev et al., 2013), PRRSV (Cutler et al., 2011; Hermann et al., 2009), and FMDV (Donaldson et al., 1987) have different ID_{50} values by aerosol route.

Infectious viruses may be found in the different excretions and secretions of infected animals. PRRSV is shed in the exhaled breath (Cho et al., 2006), urine, serum, saliva (Wills, Zimmerman, Yoon, et al., 1997), nasal fluids, and faeces (Yoon, Joo, Christianson, Morrison, & Dial, 1993) of infected pigs. Buccal, choanal, cloacal, feathers, faecal, laryngopharyngeal, nasal, oral, oropharyngeal, and tracheal samples have been collected in experimental studies to detect AIV; the most common samples collected were oropharyngeal and cloacal swabs (Germeraad, Sanders, Hagenaars, de Jong, & Gonzales, 2019). FMDV is shed in the saliva, nasal secretions, milk, breath, urine, blood, and faeces of infected animals (Alexandersen, Zhang, et al., 2003).

Pigs shed higher amounts of FMDV than cattle or sheep (Donaldson, Herniman, Parker, & Sellers, 1970; Sellers & Parker, 1969). High shedding virus from infected pigs contributed to the introduction of FMDV into the United Kingdom in the 1981 outbreak (Donaldson et al., 1982). PEDV shedding has been documented in the faeces, nasal secretions, saliva, and sera of infected pigs (Niederwerder et al., 2016). ASFV is shed within the saliva, tears, nasal secretions, urine, faeces, blood, and genital secretions of infected animals (Beltrán-Alcrudo et al., 2017; McVicar, 1984). ASFV can be present in the raw meat of slaughtered infected pigs and ASFV can be transmitted to pigs fed with swill feed contaminated with ASFV (Mazur-Panasiuk, Żmudzki, & Woźniakowski, 2019; Olesen et al., 2020).

The survival of a virus, or the ability of a virus to remain infectious is dependent on the environmental conditions. Temperature and relative humidity can affect the length of time that viruses remain infectious. In general, for aerosolised viruses: increased temperature conditions have a negative effect on viruses, non-enveloped viruses survive better at higher relative humidity conditions, and enveloped viruses survive better in lower relative humidity conditions (Sobsey & Meschke, 2003). Viruses can have different survivability on different materials. FMDV survival in aerosols was affected by the aerosolised liquid, such as cell culture fluid compared to salivary fluid (Barlow & Donaldson, 1973). FMDV also survives better on vegetation than on inanimate surfaces (Mielke & Garabed, 2020). PEDV survival on different animal feed ingredients was ingredient dependent (Dee et al., 2016), and this was also observed for ASFV and PRRSV survival on different feed ingredients (Dee et al., 2018).

2.3. Modelling aerosol and airborne transmission

Aerosol transmission of infectious diseases is a complicated process, involving both the physical process of aerosol transport in the atmosphere, as well as the biological behaviour of pathogens during transport. Aliabadi, Rogak, Bartlett, & Green (2011) described the key elements of aerosol transmission of infectious pathogens (i.e., the aerosol infection pathway) as: (i) the source of infection; (ii) the aerosolisation of pathogens; (iii) the dispersion of pathogens nearby (i.e., near-field dispersion) and drying of aerosols; (iv) the deactivation of airborne pathogens and the dispersion of pathogens to farther distances (i.e., far-field dispersion); (v)

exposure of individuals to airborne pathogens via deposition of aerosols during inhalation and exposure at the cellular level; and (vi) infection with symptoms.

Computer models can be used to model specific aspects of the aerosol transmission pathway of infectious animal diseases. For example, computer models that can simulate the trajectory of airborne particles or the dispersion of airborne contaminants can be used to study the transport of airborne viruses over short or long distances. Modelling of long distance airborne transmission is important because it can be used to predict outbreaks of infectious disease in susceptible farms at a distance from a source farm (Donaldson, Alexandersen, Sørensen, & Mikkelsen, 2001b; Seo, Lee, Hong, Noh, & Park, 2015). The accuracy of these computer models can depend on the available research data about factors affecting aerosol or airborne transmission. Specifically, the amount of airborne virus shed from an infected animal, the survival of viruses in the air at different environmental conditions, and the infectious dose provide clarity on specific aspects of the aerosol transmission pathway. This information could improve the accuracy of computer models during model development and/or during the post-model analysis of outputted results.

2.4. Computational fluid dynamics (CFD)

Computational Fluid Dynamics (CFD) is modelling method that can predict airflow behaviour and the trajectory of airborne particles based on user input parameters. CFD is highly customisable, allowing for users to model specific scenarios. Examples of input parameters include the velocity, air pressure, and air turbulence at inlets, walls, and outlets of a domain. The geometry of simulations can be created specifically to match the scenario by including the atmospheric boundary layer airflow behaviour (Richards & Hoxey, 1993), buildings (Franke et al., 2006; Tominaga et al., 2008), complex topography (Hong et al., 2011; Seo et al., 2010; Seo et al., 2014; Seo et al., 2015), windbreaks (Dalpé & Masson, 2009; Desmond, Watson, & Hancock, 2017; Desmond et al., 2014; Endalew, Hertog, Delele, et al., 2009; Endalew, Hertog, Gebrehiwot, et al., 2009; Segersson, 2017) and other obstacles or attributes that would affect airflow behaviour. The customisation of CFD to unique scenarios makes CFD a powerful tool that can be used to assess countless airborne transmission scenarios. The disadvantage of CFD is that these models can be computationally expensive, but this becomes less of a problem as

computer hardware becomes more affordable and users learn to make assumptions about a scenario that can decrease computational requirements.

The fundamental equations that are used in CFD are the continuity equation and the Navier-Stokes equations. The continuity equation ensures the conservation of mass. The Navier-Stokes equations are derived from Newton's second law and are applicable for Newtonian Fluids (Versteeg & Malalasekera, 2007). The Reynolds-averaged Navier Stokes (RANS) turbulence models are a popular way of introducing air turbulence; these models focus on turbulence effects on the mean air flow and use modified Navier-Stokes equations (Versteeg & Malalasekera, 2007). The standard k-ε turbulence model is a well-known RANS turbulence model that calculates the turbulent kinetic energy (k) and the rate of dissipation of turbulent kinetic energy (ε). The continuity equation, RANS, and standard k-ε equations are shown in Appendix A.

CFD was previously applied in the field of infectious human disease transmission to assess the contribution of aerosol transmission in spreading disease in previous outbreaks. A CFD simulation showed that imbalanced airflow within the three-bay hospital ward led to patients and students that stayed in or visited a bay with a patient infected with severe acute respiratory coronavirus (SARS-CoV) were exposed to higher concentrations of SARS-CoV than patients or visitors in adjacent and distant bays (Li, Huang, Yu, Wong, & Qian, 2004; Wong et al., 2004; Yu et al., 2004). In a similar study by the same research group, a CFD simulation showed that the airflow pattern generated by an air purifier transported airborne influenza A virus from the index patient to an adjacent bay, likely leading to infection of patients in this bay (Wong et al., 2010). In another study, a CFD simulation predicted that a north-easterly wind blew SARS-CoV bioaerosols from one building to three other buildings in an apartment complex that experienced an outbreak of SARS-CoV (Yu et al., 2004).

In terms of livestock building applications, Norton, Sun, Grant, Fallon, & Dodd (2007) reviewed CFD applications in the livestock industry and the best guidelines for performing and validating CFD simulations within livestock buildings were provided by Rong, Nielsen, Bjerg, & Zhang (2016). A comparison of turbulence models in livestock buildings was performed by Li, Rong, & Zhang (2017).

There are some studies that have used CFD to study aerosol or airborne transmission of infectious animal viruses, but it is still under-utilised in this research area. Seo et al. (2014) studied the 2008 HPAIV outbreak in Korea. The authors ran 960 CFD simulations of aerosol transport of HPAIV to develop a large matrix describing the probability of farms spreading HPAIV to other farms by aerosol spread. The probability matrix was used within a HPAIV spread network model that considered fomite transmission (via delivery of feed or medicine) and aerosol transmission as possible transmission routes during the outbreak (Lee et al., 2014). Using the network model, the authors found that 10 out of 13 farms were infected by fomite transmission, 2 out of 13 farms were infected by aerosol transmission, and the transmission of the last farm could not be determined. Seo et al. (2015) created a web-based forecasting tool to predict the airborne spread of FMDV in the Anseong region in Korea, using real-time weather data and a database of CFD-simulated airflow behaviour within a CFD simulation to predict the transport of the emitted virus in the region on three-hour-intervals. Wei et al. (2018) is an example of a CFD study that compares simulation results with collected air samples of airborne infectious animal virus. The authors used CFD to simulate the potential spread of AIV aerosols in a live poultry market and compared the results to air sample concentrations of AIV RNA.

2.5. Dose-response modelling

Dose-response modelling is a mathematical method used to generate equations that describe probability of infection (response) as a function of exposure dose. Dose-response models can be utilised to predict the probability of infection in an individual upon exposure to different doses of infectious pathogen. Modelling utilises experimental data in which groups are infected with different doses of infectious pathogens (e.g., viruses) and monitored to determine the fraction of infection within each dose group. The modelling is used to determine the values of parameters that are specific to different dose-response model equations. Brouwer, Weir, Eisenberg, Meza, & Eisenberg (2017) previously described a list of some well-known dose-response models, as well as the model parameters and properties. For example, the exponential model (EM) is described by the equation Probability = $1 - \exp(-r \times \text{dose})$; modelling would be used to determine the best estimate for the value "r" for a specific set of experimental data and each set of experimental data would produce a different set of parameters.

There are various dose-response model types, and these models can be generally categorised as deterministic or stochastic models (Sze To & Chao, 2010). Deterministic models assume that pathogens act "cooperatively" and that an individual becomes infected after the pathogen dose exceeds that individual's infection tolerance threshold (Sze To & Chao, 2010). Examples of deterministic models include the log-logistic, lognormal, and Weibull models. Stochastic dose-response models are a type of dose-response modelling technique that is based on the assumption that there is a probability of the host becoming infected at any dose, with the probability increasing as the dose increases (Sze To & Chao, 2010). The most basic form of a stochastic model is the EM, as previously described, where the parameter "r" is the infectivity of a single pathogen particle (Schmidt, Pintar, Fazil, & Topp, 2013); EM has been used to model the human dose-response of viruses such as Echovirus 12 and Poliovirus (Haas, 1983). More sophisticated stochastic dose-response models include the exact beta-Poisson (EBPM) and approximate beta-Poisson models (ABPM). The EBPM was used in human dose-response modelling of various pathogens, including Norovirus (Teunis et al., 2008), Influenza A virus (Teunis, Brienen, & Kretzschmar, 2010), and Rotavirus (Teunis & Havelaar, 2000). The ABPM model was used in the human dose-response modelling of such pathogens as Echovirus, Poliovirus (Haas, 1983) and Rotavirus (Teunis & Havelaar, 2000).

Dose-response modelling has been performed on many different human infectious diseases, both viral and bacterial (Brouwer et al., 2017; Haas, 1983; Holcomb et al., 1999; Teunis, Nagelkerke, & Haas, 1999; Teunis & Havelaar, 2000; Teunis, Brienen, & Kretzschmar, 2010; Teunis et al., 2008). Dose-response modelling has been limitedly applied to some infectious animal viruses, such as PRRSV (Brookes, Hernández-Jover, Holyoake, & Ward, 2014; Cutler et al., 2011; Hermann et al., 2005, 2009), FMDV (Colenutt et al., 2020), and ASFV (Niederwerder et al., 2019). Each of these animal studies investigated a single type of infectious animal virus and some investigated multiple transmission routes. The understanding of disease transmission, such as the effect of transmission route, could be improved by compiling existing datasets in literature that have sufficient information and using these datasets to perform dose-response modelling. However, at this point, this has not been reported in literature.

Dose-response models can also be coupled with other research methods, such as Brookes et al. (2014) modelling the dose-response of PRRSV by oral transmission using experimental data from Hermann et al. (2005). The authors integrated the dose-response model into their risk assessment to estimate the risk of PRRSV entering Australia via contaminated meat products. Ssematimba et al. (2012) paired a Gaussian plume dispersion model and a dose-response model to estimate the proportion of farms that became infected with AIV due to aerosol transmission during an epidemic of AIV in the Netherlands.

As of writing this thesis, dose-response modelling has not used with CFD modelling to simulate the aerosol transmission of infectious animal viruses. However, CFD and dose-response modelling were performed to assess an outbreak of COVID-19 in a restaurant (Ho, 2021); the probability of infection due to aerosol transmission amongst restaurant patrons was estimated using a dose-response model that was developed using a surrogate virus of SARS-COV (Watanabe et al. 2010).

2.6. Modelling survival of viruses in environmental conditions

Several studies modelled the decay of infectious virus in different environmental conditions using experimental data. The decay of ASFV within different animal feed ingredients and the half-life of ASFV within the feed ingredients was modelled (Stoian et al., 2019), as well as the survival of PEDV on feed ingredients and surfaces at different temperature conditions (Trudeau, Verma, Urriola, et al., 2017). The half-life of PRRSV in liquid form was modelled at different pH or temperature conditions (Bloemraad, de Kluijver, Petersen, Burkhardt, & Wensvoort, 1994) and different temperature conditions (Jacobs et al., 2010). Kurmi et al. (2013) modelled the survival of H5N1 AIV in wet and dried manure at different temperature conditions. Quist-Rybachuk et al. (2015) modelled the survival of PEDV and the half-life of PEDV in minimum essential medium and porcine plasma at different pH and temperature conditions.

In terms of virus survival in aerosols, there are not many models describing different temperature and relative humidity effects on the survival of airborne infectious viruses. The half-life of PRRSV in aerosol form at different temperature and relative humidity conditions was modelled (Hermann et al., 2007). The half-life equations changed depending on the temperature and relative humidity of the room and the survival of PRRSV in aerosols decreased at higher

temperatures and relative humidity conditions. Use of this half-life model has not been applied with other models, such as CFD and dose-response modelling, although it could provide a researcher with an estimation of virus quantity after exposure to environmental conditions.

Chapter 3. Current understanding of airborne transmission of important viral animal pathogens in disease spread

Chapter 3 is based on the journal paper titled "Current understanding of airborne transmission of animal viral pathogens in disease spread". It is formatted according to Biosystems Engineering Journal. The version of the journal paper included in this thesis was submitted to Biosystems Engineering Journal in July 2022. The final version of that journal paper was accepted in September 2022. The citation for the final version is: La, A., Zhang, Q., Cicek, N., & Coombs, K. M. (2022). Current understanding of the airborne transmission of important viral animal pathogens in spreading disease. *Biosystems Engineering*, *224*, 92–117. https://doi.org/10.1016/j.biosystemseng.2022.09.013

Portions of the original published paper, specifically in the introduction, have been removed from this thesis to reduce repeated information. The discussion and recommendations were moved to the general discussion in Chapter Six.

3.1. Abstract

Current research about airborne transmission of African swine fever virus (ASFV), porcine epidemic diarrhoea virus (PEDV), avian influenza virus (AIV), porcine reproductive and respiratory syndrome virus (PRRSV), and foot and mouth disease virus (FMDV) was reviewed to evaluate commonalities, knowledge gaps, and methodologies in studying airborne transmission of animal diseases. The studies are categorized as short-distance transmission (within a single airspace/facility) and long-distance transmission (beyond a single facility/site). Short-distance airborne transmission was demonstrated for at least 1 strain of the above-mentioned viral pathogens in experimental settings. Most studies reported are on FMDV, whereas limited information is available for ASFV and PEDV to assess their short-distance airborne transmissibility. Air sampling upwind, downwind, and within naturally infected facilities is used to provide evidence of long-distance airborne transmissibility. There were mixed amounts of air sampling evidence for each of the reviewed viruses, varying from no evidence (ASFV) to evidence in multiple settings (AIV). Computer modelling was used to study the past outbreaks of infectious diseases to assess the contribution of airborne transmission. There was a multitude of computer models, reported in the literature on long-distance airborne

transmission of FMDV in past outbreaks and as a predictive tool for assessing future risk of airborne transmission. Some examples of important computer models are epidemiology analysis, weather analysis, and air dispersion models. Few models are reported for ASFV, PEDV, and PRRSV. Studies in literature indicate that airborne transmission is generally affected by the virus strain, aerosol type, shedding duration and concentration, environmental conditions, and aerosol infectious dose.

3.2. Introduction

The role and mechanisms of airborne transmission in spreading infectious viral diseases in the livestock industry are not well understood, with the level of scientific information available about the airborne transmission differing substantially for each specific virus. Arruda et al. (2019) recently performed a detailed review describing the research community's knowledge on airborne transmission of Porcine Reproductive and Respiratory Syndrome Virus (PRRSV), as well as the knowledge gaps for airborne transmission of PRRSV. The authors reported that more research on airborne transmission of PRRSV is required, including genetic sequencing of PRRSV strains; field research of airborne transmission of European PRRSV; field research in more diverse environmental conditions; improvement in air sampling methodology and technology; air sampling of PRRSV under field conditions; and contribution of the deposition of aerosols towards environmental contamination. Thus, although it is one of the most researched infectious animal diseases in the context of airborne transmission, the review indicated that there was still more to learn about airborne transmission of PRRSV. It is inevitable that research gaps also exist for other infectious animal disease pathogens, such as African Swine Fever Virus (ASFV), Porcine Epidemic Diarrhoea Virus (PEDV), Avian Influenza Virus (AIV), and Foot and Mouth Disease Virus (FMDV). A critical review of the knowledge of airborne transmission of important infectious animal viruses will help researchers and producers to understand commonalities, and identify overall knowledge gaps in airborne transmission of viruses, as well as knowledge gaps specific to an animal virus.

The objectives of this review were to: (1) review experimental studies of short-distance airborne transmission of infectious animal viruses; (2) review field research about long-distance airborne transmission of infectious animal viruses; (3) review modelling strategies that have been

used to simulate or estimate airborne transmission in past outbreaks of infectious animal disease; (4) identify important factors that affect airborne transmission of infectious animal viruses; and (5) identify commonalities and knowledge gaps in understanding airborne transmission of the infectious animal viruses.

3.3. Focus of review

In this review, we focused on four important swine diseases with viral causative agents that have some evidence that they are airborne transmissible and have had significant economic impact on livestock industries globally. These four diseases are: African Swine Fever (ASF); Porcine Epidemic Diarrhoea (PED); Porcine Reproductive and Respiratory Syndrome (PRRS); and Foot and Mouth Disease (FMD). Also a significant animal disease, avian influenza (AI), which is also a significant animal disease and has been proven to be airborne transmissible and well-studied, is included in this review as a reference.

3.4. Laboratory studies of short distance transmission by aerosol

A fundamental question that often does not have an easy answer is: what diseases are airborne transmissible? The contribution of airborne transmission towards spreading infectious disease is often elusive and debated in the literature. Many experimental studies of short distance transmission of animal diseases have evaluated the airborne transmissibility of an infectious animal virus and are described in further detail in Chapters 3.4.1, 3.4.2, and 3.4.3. Short distance aerosol transmission here refers to transmission of disease pathogens within a single airspace (a chamber, room, or building). In studies reported in the literature, viral aerosols were generated naturally (shed) from animals that were either inoculated with the infectious virus or naturally infected, or generated artificially with aerosol generating devices filled with a stock solution of infectious virus; shedding is described in further detail in Chapter 3.7.2.

A summary of short distance airborne transmission experiments in terms of the virus strain, experiment type, and whether or not airborne transmission was demonstrated is shown in Table 3.1 and Table 3.2. Overall, airborne transmission over a short distance was demonstrated for at least 1 strain of ASFV, PEDV, H9N2 AIV, H5N1 AIV, and PRRSV (Table 3.1) and several strains of FMDV (Table 3.2). Short distance airborne transmission of AIV, PRRSV, and

FMDV is well demonstrated, while more work is required to assess for airborne transmission of ASFV and PEDV.

3.4.1. Controlled exposure of individual animals to aerosols

In controlled exposure experiments, animals were directly exposed to aerosols of infectious virus by placing their head (Agranovski et al., 2010; John W. McVicar & Eisner, 1983; Sergeev et al., 2013) or entire body (Guan et al., 2013; Guan, Fu, & Shayan, 2015; Yao, Lv, Huang, Yang, & Chai, 2014) within a chamber filled with artificially generated virus aerosols at certain concentrations. Another approach was using masks or placing animal faces in exposure ports that directed air containing aerosols of infectious virus towards their faces (Alexandersen, Brotherhood, & Donaldson, 2002; Alexandersen & Donaldson, 2002; Cutler, Wang, Hoff, Kittawornrat, & Zimmerman, 2011; Dee, Deen, Rossow, Mahlum, & Pijian, 2005; Donaldson et al., 1987; Gibson & Donaldson, 1986; Hermann, Muñoz-Zanzi, & Zimmerman, 2009). This methodology was used at various doses of naturally generated (Alexandersen, Brotherhood, et al., 2002; Alexandersen & Donaldson, 2002; Donaldson et al., 1987; Gibson & Donaldson, 1986) or artificially generated aerosols to estimate the infectious dose of the viruses (Agranovski et al., 2010; Cutler et al., 2011; Donaldson et al., 1987; Guan et al., 2013; Hermann et al., 2009; Sergeev et al., 2013; Yao et al., 2014). Air sample collection and laboratory analyses were used to determine the aerosol dose of infectious viruses in these studies.

3.4.2. Two-chamber tests for assessing aerosol transmission

Many studies used a two-unit (chamber) approach in which the first unit contained the source of the virus aerosols (either infected animals or aerosol generating devices) and the air from that unit was partially or completely directed into a second unit containing a single or group of susceptible recipient animals. A few researchers used a mechanically-ventilated swine facility as the source unit, while the second unit was a separate facility located a short distance away (Fano, Pijoan, & Dee, 2005; Otake, Dee, Jacobson, Torremorell, & Pijoan, 2002; Trincado et al., 2004). In these studies, the second facility was sometimes connected to the exhaust fans of the first facility through a duct to artificially create airborne transmission opportunities.

The success or failure to demonstrate airborne transmission is a good first step in understanding airborne transmission (Tables 3.1 and 3.2). Successful demonstrations of airborne

transmission in these studies provided evidence that airborne transmission is a possible mode of transmission for the infectious animal virus. It should be cautioned that failure to demonstrate airborne transmission could mean that the pathogen was not airborne transmissible, but it could also be due to insufficient levels of airborne virus to cause infection in the experiment. There were numerous studies in which air samples were collected (Cho, Deen, & Dee, 2007; Colenutt et al., 2016; Spekreijse, Bouma, Koch, & Stegeman, 2013; Torremorell, Pijoan, Janni, Walker, & Joo, 1997; Wilkinson, Donaldson, Greig, & Bruce, 1977; Yao et al., 2011), but airborne virus was only successfully detected in some air samples (Cho et al., 2007; Colenutt et al., 2016; Spekreijse et al., 2013; Yao et al., 2011). Failure to demonstrate transmission may also be due to the specific strain having a low chance of efficiently transmitting by the airborne route. For example, PRRSV MN-30100 did not transmit in some studies (Fano et al., 2005; Otake et al., 2002; Trincado et al., 2004), but transmitted in another study due to a high concentration of artificially-generated PRRSV aerosols in a controlled exposure experiment (Dee, Deen, et al., 2005).

It must be noted that because the experimental conditions were inflated to artificially increase the probability of airborne transmission in two-chamber tests, it is difficult to ascertain the likelihood of airborne transmission occurring in a typical farm setting. Additionally, airborne transmission occurring over a short distance in an experiment does not necessarily mean that long distance transmission (from facility to facility) is possible.

3.4.3. Multiple cage experiments

Studies were also reported to determine the possibility of airborne transmission in an environment without artificial control of aerosol dose or airflow (Table 3.1 and 3.2). In these studies, animals were placed in cages or pens in a room and the source animals were physically distanced from recipient animals to ensure that airborne transmission was the only mode of transmission between source and physically-distanced animals. Several researchers also performed such experiments for PRRSV in a mechanically-ventilated facility, but were unable to conclude airborne transmission due to not ruling out other modes of indirect transmission, such a faecal and urine contamination or vector (insect) transmission (Fano et al., 2005; Otake et al., 2002; Trincado et al., 2004; Wills, Zimmerman, Swenson, et al., 1997). Quantification of the

airborne virus concentrations was generally accomplished by taking air samples, which were then analysed for DNA or RNA concentrations or the airborne infectious virus concentrations. Airborne virus was quantified for ASFV (Olesen et al., 2017; Wilkinson et al., 1977), PEDV (Gallien et al., 2018), AIV (Guan et al., 2013; Spekreijse, Bouma, Koch, & Stegeman, 2011), and FMDV (Alexandersen & Donaldson, 2002; Alexandersen, Quan, Murphy, Knight, & Zhang, 2003; Esteves, Gloster, Ryan, Durand, & Alexandersen, 2004; Valarcher, Gloster, Doel, Bankowski, & Gibson, 2008).

These studies showed that airborne transmission depended on several factors such as the number of source animals, the ventilation rate, and virus strain, with these factors dictating the concentration of infectious virus in the air. Some important observations include: i) an insufficient number of infected animals would result in airborne virus doses that were too low to cause infection; ii) high ventilation could reduce the viral aerosol concentration, which was hypothesized as the reason that airborne transmission did not occur in (Niederwerder et al., 2016); (iii) virus strain could affect the probability for airborne transmission to occur, as seen in Gallien et al. (2018), when airborne transmission did not occur for strain PEDV/FR/001/2014 (an INDEL strain that had insertions and deletions in the S gene; Vlasova et al. 2014) but occurred for strain PEDV/USA/2014/IOWA (a non-INDEL strain). It should be noted that these experiments were usually performed within biosafety level (BSL) facilities with ventilation rates and animal density/distribution that are not typical of an animal farm. While these experiments are useful in demonstrating airborne transmission over short distances, they do not necessarily translate to a farm setting or to long distance transmission.

Another drawback of multiple cage experiments is that the exposure dose of airborne pathogens is not controlled. While the number of source animals was usually described in reported studies, the ventilation (airflow) was described in some studies only (Aggarwal et al., 2002; Alexandersen & Donaldson, 2002; Bouma, Dekker, & De Jong, 2004; Esteves et al., 2004; Guan et al., 2013; Niederwerder et al., 2016; Olesen et al., 2017; Spekreijse, Bouma, Koch, et al., 2011; Valarcher et al., 2008).

Table 3.1. Experiment type and strain of ASFV, PEDV, and PRRSV tested for airborne transmissibility (AT) over short distances

Virus	Strain	Exp. type	AT?	Studies
ASFV	POL/2015/Podlaskie/ Lindholm	Multiple cage	Yes	(Olesen et al., 2017)
	Kirawira (KWH/12)	Two chamber & Multiple cage	Yes	(Wilkinson & Donaldson, 1977; Wilkinson et al., 1977)
PEDV	USA/KS/2013	Multiple cage	No	(Niederwerder et al., 2016)[c]
	USA/2014/IOWA	Multiple cage	Yes	(Gallien et al., 2018)
	FR/001/2014		No	
H9N2 AIV	Ck/SH/F/98	Multiple cage	Yes	(Shi, Ashraf, Gao, Lu, & Liu, 2010)
	Ck/GD/SS/94	Multiple cage	No	(Shi et al., 2010)
	A/Chicken/Shandong/1/08	Two chamber & Controlled exposure	Yes	(Yao et al., 2011), (Yao et al., 2014)[a],
	A/Ck/HN/98	Controlled exposure[a] & Multiple cage	Yes	(Guan et al., 2013)
H9N2 AIV	A/Chicken/Henan/1/1998	Controlled exposure	Yes	(Guan et al., 2015)[a]
	A/environment/Bangladesh/10306/2011	Multiple cage	Yes	(Seiler et al., 2018)
	A/chicken/Bangladesh/10450/2011		Yes	
	A/quail/Bangladesh/19462/2013		Yes	
	A/chicken/Shandong/C9QH/2011	Multiple cage	Yes	(Zhu et al., 2018)[d]
	A/chicken/Jiangsu/JT12/2011		Yes	
	A/chicken/Jiangsu/TM71/2014		Yes	
	A/chicken/Jiangsu/TM58/2013		Yes	
	A/chicken/Jiangsu/JT95/2013		Yes	
	A/chicken/Anhui/WB/2014		Yes	
H5N1 AIV	A/turkey/Turkey/1/2005 (clade 2.2)	Two chamber & Multiple cage	Yes	(Spekreijse et al., 2013; Spekreijse, Bouma, Koch, et al., 2011)
	A/Ck/Yama/7/04	Multiple cage	Yes	(Tsukamoto et al., 2007)

Virus	Strain	Exp. type	AT?	Studies
H5N1 AIV	A/Chicken/Suzdalka/Nov-11/2005	Controlled exposure	Yes	(Agranovski et al., 2010)[a],(Sergeev et al., 2013)[a]
	A/Turkey/Suzdalka/Nov-1/2005	Controlled exposure	Yes	(Sergeev et al., 2013)[a]
	A/Chicken/Kurgan/05/2005		Yes	
	A/Duck/Kurgan/08/2005		Yes	
	A/Chicken/Crimea/04/2005		Yes	
	A/Chicken/Omsk/06		Yes	
	A/Chicken/Krasnodar/02/06		Yes	
	A/Chicken/Dagestan/06		Yes	
PRRSV	VR-2332	Two chamber & Controlled exposure	Yes	(Torremorell et al., 1997) (Hermann et al., 2009)[ab]
	NADC	Two chamber	Yes	(Brockmeier & Lager, 2002)
	Lelystad (EU PRRSV)	Two chamber	Yes	(Kristensen, Bøtner, Takai, Nielsen, & Jorsal, 2004)
PRRSV	MN-184	Two chamber & Controlled exposure	Yes	(Cutler et al., 2011)[ab],(Cho et al., 2007; Dee, Batista, Deen, & Pijoan, 2005)
	Ingelvac MLV	Two chamber	Yes	(Dee, Batista, Deen, & Pijoan, 2006; Dee, Deen, Cano, Batista, & Pijoan, 2006)[a]
	MN-1b	Two chamber	No	(Torremorell et al., 1997)
	MN-30100	Two chamber (unit to unit or building to unit)	No	(Cho et al., 2007; Fano et al., 2005; Otake et al., 2002; Trincado et al., 2004)
	MN-30100	Controlled exposure	Yes	(Dee, Deen, et al., 2005)[a]

[a] artificial aerosols used, [b] exposed via face mask, [c] result possibly affected by high ventilation rate, [d] isolated in live poultry markets

Table 3.2**.** Experiment type, strain of FMDV, and animal type tested for airborne transmissibility (AT) over short distances

Strain	**Animal**	**Experiment type**	**AT?**	**Citation**
O1 BFS 1860	Sheep	Controlled exposure	Yes	(Gibson & Donaldson, 1986)[a]
	Cows	Controlled exposure	Yes	(Donaldson et al., 1987)[a]
SAT2/SAR/3/79	Cows	Controlled exposure	Yes	(Donaldson et al., 1987)[a]
O1/Lausanne/Sw/65	Pigs	Controlled exposure[a] & Multiple cage	Yes	(Alexandersen, Brotherhood, et al., 2002; Alexandersen & Donaldson, 2002)[a]
O/SKR/1/2000	Pigs	Controlled exposure[a] & multiple cage	No	(Alexandersen & Donaldson, 2002)
O/UKG/2001	Pigs	Multiple cage	No	(Alexandersen & Donaldson, 2002)
	Pigs	Multiple cage	Yes	(Aggarwal et al., 2002)
O/UKG/2001	Sheep	Multiple cage	Yes	(Aggarwal et al., 2002; Esteves et al., 2004)
	Sheep	Multiple cage	No	(Valarcher et al., 2008)
	Cows	Multiple cage	Yes	(Aggarwal et al., 2002)
C Noville (Swiss 73)	Pigs	Multiple cage	Yes	(Alexandersen, Quan, et al., 2003)
Asia 1 (HKN/05/2005)	Cows	Two chamber	Yes	(Colenutt et al., 2016)
O/TAW/1997	Pigs	Multiple cage	Yes	(Alexandersen, Quan, et al., 2003; Eblé, De Koeijer, Bouma, Stegeman, & Dekker, 2006)
NET/2001/1	Cows	Multiple cage	No	(Bouma et al., 2004)
NET/2001/3	Cows		No	

[a] faces of animals exposed to aerosols using masks or exposure ports

3.5. Field studies of long-distance transmission by aerosols

3.5.1. Airborne transmission from buildings with inoculated animals

These studies typically used a commercial livestock building to house inoculated animals for generating airborne infectious virus. The studies involved: (1) performing air sampling at the exhaust of a source building with inoculated animals to confirm shedding and release of viruses from the source building; (2) performing air sampling at downwind locations from the source building, demonstrating aerosol transport of the virus after exiting the infected facility; (3) monitor and quantify infection of susceptible recipient animals in a downwind building to demonstrate airborne transmission.

Research was conducted by a team at University of Minnesota in a mechanically-ventilated pig finisher facility that was ≈16 km far from other pig farms (Dee, Otake, & Deen, 2010; Dee, Otake, Oliveira, & Deen, 2009; Otake, Dee, Corzo, Oliveira, & Deen, 2010; Pitkin, Deen, & Dee, 2009). Table 3.3 displays the range and average of infectious PRRSV concentrations measured in the exhaust air of the source building. The results indicated that PRRSV was not constantly emitted from the exhaust of a building with infected pigs, with the frequency of positive samples less than 34%. One exception was observed by Otake et al. (2010) that had a 100% positivity rate in the air samples collected. Otake et al. (2010) had a shorter sampling period (21-days) than the other studies, and reported that the airborne concentration of infectious PRRSV at the exhaust varied with the sampling day, but was consistently ≥ 750 $TCID_{50}$ m^{-3} for MN-184 (Fig. 3.1).

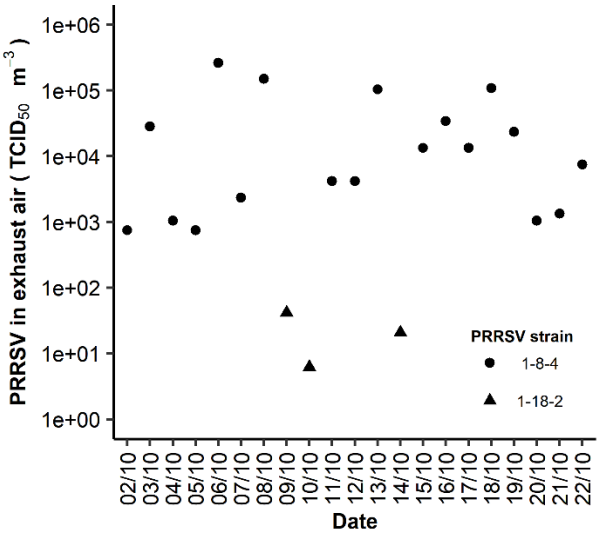

Figure 3.1. PRRSV concentration in exhaust air from mechanically-ventilated finisher building containing infected pigs (Otake et al., 2010)

Table 3.3. Ranges and average PRRSV concentrations of air samples collected from the exhaust of a mechanically ventilated finisher facility with 25 to 120 kg infected pigs.

Study	Sampling period	% positive (# positive / # sampled)	Range of concentration ($TCID_{50}$ m^{-3} air)[a]	Average concentration ($TCID_{50}$ m^{-3} air)[a]
Dee et al. (2009)	50 days	34% (17/50)	22 to 1.2×10^6	1.6×10^5
Pitkin et al. (2009)	1 year	29% (55/190)	4.2 to 1.3×10^5	5.0×10^2
Otake et al. (2010)	21 days	100% (21/21)	6.3 to 2.6×10^5	3.6×10^4
Dee et al. (2010)	1st year	12% (38/324)	4.2 to 1.8×10^4	1.7×10^3
	2nd year	22% (69/312)	4.2 to 1.3×10^5	1.0×10^4

[a] 50% Tissue Culture Infectious Dose ($TCID_{50}$) per m^3 air, calculated from the PRRSV concentration in the solution, volume of the collection fluid (5 mL), sampling rate (400 L/min), and sampling time (30 min).

Dee et al. (2009) and Otake et al. (2010) collected air samples for PRRSV at various downwind distances from the source building (Table 3.4). The transport, dilution, and downwind concentration of airborne viruses, like other air pollutants, depend on environmental/meteorological conditions (ambient temperature, relative humidity, and solar irradiation), which not only affect the aerosol dispersal but also the stability/survival of PRRSV in the atmosphere (Hermann et al., 2009). Meteorological conditions that reduce the dilution of infectious PRRSV aerosols will increase the likelihood of detecting infectious PRRSV

downwind of the virus source. In Dee et al. (2009) and Otake et al. (2010), the optimal conditions for airborne transmission, in terms of shedding of PRRSV and meteorological conditions, occurred, allowing for detection of infectious PRRSV at various long distances downwind of the source building (Table 3.4).

Table 3.4. Downwind distance and infectious PRRSV concentration collected in air samples

Study	**Downwind distance (direction)**	**Airborne concentration of PRRSV ($TCID_{50}$ m^{-3} air)[a]**
Dee et al. (2009)	4.7 km (NW)	1.25×10^{1}
	4.7 km (NW)	1.71×10^{1}
	4.7 km (NW)	2.17×10^{2}
	4.7 km (NW)	3.25×10^{2}
Otake et al. (2010)	2.3 km (NW)	4.17×10^{2}
	2.3 km (SE)	7.08×10^{2}
	4.6 km (SW)	1.29×10^{2}
	6.6 km (NW)	2.50×10^{1}
	9.1 km (SE)	1.75×10^{1}

[a] 50% Tissue Culture Infectious Dose ($TCID_{50}$), calculated from the PRRSV concentration in the solution, volume of the collection fluid (5 mL), sampling rate (400 L/min), and sampling time (30 min).

Pitkin et al. (2009) performed 26 two-week replicates to test for airborne transmission from a source finisher facility to a recipient building containing 20 nursery pigs. Out of the 26 replicates, there were 8 replicates in which airborne transmission to the recipient building occurred. Additionally, 20 of 190 air samples collected at the inlet of the recipient building contained infectious PRRSV. In the same setting, Dee et al. (2010) performed 26 four-week replicates of airborne transmission to a recipient building housing 10 nursery pigs. There were 12/26 replicates that demonstrated airborne transmission of PRRSV to the recipient building. At the inlet of the recipient building, 11/324 (3%) and 33/312 (11%) of air samples collected during the first and second year, respectively, contained infectious PRRSV.

It should be noted that the conditions of these studies were purposely optimized to increase the likelihood of aerosol transport and transmission of PRRSV. Specifically, PRRSV was allowed to spread in the source building from animal to animal, increasing the amount of airborne PRRSV within the building and emission from the building. Thus, the frequency of

airborne transmission that occurred in these studies was higher than normal. However, these studies ultimately demonstrated that airborne transmission from building to building was possible under the right conditions and the process involved three steps: (1) animals infected with the PRRSV strain shed the virus into the air; (2) after the PRRSV was exhausted from the building, there was little dilution and loss of infectivity, resulting in a concentrated infectious PRRSV plume; and (3) in the recipient building downwind to the source building, the exposure doses of the animals were high enough to result in at least 1 infection.

3.5.2. Long distance transport from naturally infected buildings or animals

Studies included in this category investigated aerosol transport and airborne transmission occurring naturally without human (scientific) interference (i.e., without experimental inoculation of animals and adjusting management of a facility to exacerbate transmission in a building to increase airborne shedding). Air sampling inside, outside, and downwind of naturally infected farms for PEDV, AIV, and PRRSV were reported in these studies (Table 3.5). Air samples were usually analysed for viral RNA with reverse-transcription polymerase chain reaction (RT-PCR). Non-quantitative RT-PCR tested for the presence of virus in air samples, while were quantitative RT-PCR (qRT-PCR) was used to quantify the amount of viral RNA in the air in units of RNA copies per m^3 air.

3.5.2.1. PEDV

In a study reported by Alonso et al. (2017), air samples collected inside and at the exhaust of two nursery farms were all qRT-PCR positive and contained high concentrations of PEDV RNA. Downwind of infected facilities, high airborne concentrations of PEDV RNA were detected at various distances, with the concentration decreasing with distance (Alonso et al., 2014). The measurement results clearly showed that PEDV could readily become airborne after shedding from infected animals and travel downwind from infected facilities in high concentrations. The likelihood of the airborne PEDV causing infection (i.e., airborne transmission) after PEDV is transported downwind is unclear as the amount of infectious airborne virus inside and outside of the facilities was not quantified in these studies. However, Alonso et al. (2014) tested the air samples for infectivity by orally inoculating 10-day-old pigs with the air sample collection fluid (i.e., a bioassay test). The air samples collected downwind

did not cause infection, showing that the downwind air samples did not have sufficient infectious PEDV to cause infection.

3.5.2.2. AIV

A study was performed by Chen et al. (2010) to investigate airborne transport of IAV and H5-subtype IAV during Asian dust storms in Taiwan. The researchers concluded that IAV could be transported long distances during Asian dust storms. Several studies were performed to investigate the pandemic potential of AIV originated in live poultry markets (LPM), with positive samples sequenced to determine the isolate type and/or lineage (Bui et al., 2019; Chen et al., 2009; Wu et al., 2017; Zeng et al., 2017; Zhou et al., 2016). Chen et al. (2009) detected varying airborne IAV RNA concentrations in positive air samples, from below a detection limit of 8.86×10^2 RNA copies $m^{-3}$to 3.7×10^4 RNA copies m^{-3}. Wu et al. (2017) and Zeng et al. (2017) detected one infectious virus strain within the air samples and sequencing identified the strains as H5N6 and H9N2 strains, respectively. Zhou et al. (2016) performed air sampling within 4 LPM and identified 58 isolates that were either H9, H9/H7, or H9/H5 subtypes, with H9N2 being the most common isolate. Wei et al. (2018) performed air sampling in one LPM and quantified the IAV RNA copies per m^3 as well as the 18S ribosomal RNA per m^3, which is a housekeeping gene used to quantify avian cells infected with influenza A viruses (Kuchipudi et al., 2012). In general, these studies provided evidence that many different subtypes of AIV could be shed from infected poultry and into the air in LPM. It is important to continue surveillance of these LPM to track for the development of highly pathogenic strains.

More detailed studies were conducted by several researchers to sample air inside, upwind, downwind, and at the exhaust of infected poultry facilities, including turkey, chicken, and duck flocks (Alonso, Raynor, et al., 2017; Jonges, Leuken, Wouters, Koch, & Meijer, 2015; Li, Zhou, Gao, Pang, & Miao, 2017; Power, 2005; Schofield, Ho, Kournikakis, & Booth, 2005; Scoizec et al., 2018; Torremorell et al., 2016). These studies have shown that air samples collected inside and at the exhaust of infected farms were RT-PCR positive and the mean airborne RNA concentrations inside the buildings were usually at least 10^5 RNA copies m^{-3}. Power (2005) detected infectious AIV in two indoor air samples with a concentration of 292 $TCID_{50}$ m^{-3}. Torremorell et al. (2016) detected infectious virus in 14/48 air samples inside the building. Li et

al. (2017) detected infectious virus in 6/18 air samples collected from three farms. The airborne RNA concentration of AIV at the exhaust of buildings was also high, with values $>10^2$ RNA copies m^{-3} per particle size range (Alonso, Raynor, et al., 2017) and $>10^4$ RNA copies m^{-3} (Scoizec et al., 2018; Torremorell et al., 2016). The airborne RNA concentration generally decreased with distance from the infected facilities (Li et al., 2017; Scoizec et al., 2018; Torremorell et al., 2016). Overall, these studies showed that AIV can become airborne within farms with infected animals, released from infected buildings into the atmosphere, and travel downwind from an infected facility. However, the likelihood of this resulting in long distance airborne transmission is unclear as the quantity of infectious AIV within downwind samples was often not quantified or not quantifiable.

3.5.2.3. PRRSV

Kauffold et al. (2005) indirectly sampled air by swabbing the inside of ultrasound machines used within pig farms. In their dust swabs, both EU and US PRRSV were detected. Other studies performed air sampling either inside of infected facilities (Alonso, Raynor, et al., 2017; Stein et al., 2018), at the exhaust of an infected facilities (Alonso, Raynor, et al., 2017), or outside facilities with air samplers orientated to receive air from incoming wind (Brito, Dee, Wayne, Alvarez, & Perez, 2014; Spronk, Otake, & Dee, 2010).

Air samples for PRRSV RNA inside naturally infected farms and at the exhaust of these farms (Table 3.5) were significantly less frequently positive compared to air samples collected at the exhaust of buildings containing pigs inoculated with PRRSV (Table 3.3). There are many factors that could have contributed to the difference in frequency. The number of samples collected may be a factor, as the studies with inoculated animals collected more air samples over a longer time frame than the studies with naturally infected animals. Another factor is the timing of sample collection, i.e., if the sampling occurred during the stage of infection that corresponded to shedding of the virus into the air. The strain of the PRRSV is also important, as the inoculation studies used a highly pathogenic strain MN-184, which sheds frequently into the air (Cho et al., 2006). Lastly, the differences in air sampling methodology in terms of equipment, sampling rate, sampling time, and sampling medium also may affect the results. The studies in which pigs were inoculated with PRRSV used a liquid cyclonic collector to perform air sampling

at a high sampling rate (400 L/min) for 30 minutes into minimum essential medium (Dee et al., 2010; Dee et al., 2009; Otake et al., 2010; Pitkin et al., 2009). Alonso et al. (2017), who collected 2/16 positive air samples, used two types of cascade impactors (Andersen and Tisch) to perform size-differentiating sampling, while Stein et al. (2018) used three different air samplers (Coriolis® μ, MD8 Airscan, IOM Multidust Sampler) but did not capture any positive air samples inside the infected facility. The sampling time, sampling rate, and sampling medium used in Alonso et al. (2017) and Stein et al. (2018) varied depending on the instrument used to perform air sample collection.

The numerous infectious PRRSV air samples collected towards the prevailing wind directions provide evidence that airborne transmission is important in areas where the farm density is high. Brito et al. (2014) noted that the amount of viable PRRSV in air samples was significantly higher around a farm that was in an area with a denser population of pig farms. Additionally, 14 different isolates of PRRSV were collected in air samples around this specific farm.

3.5.2.4. FMDV

There were not many studies in which air samples were collected from naturally infected animal facilities. Colenutt et al. (2018) sampled air close to infected cows in five small backyard farms in Nepal and was able to detect FMDV RNA in 7/13 samples belonging to the O/ME-SA/Ind-2001 lineage.

Table 3.5. Air sample collection from animal facilities naturally infected with PEDV, AIV, or PRRSV.

Study	Infected herd/flock	Strain / subtype	Inside / Exhaust/ Downwind	RT-PCR positive (infectious) / Samples collected	Mean airborne concentration (RNA copies m^{-3}) or other units
PEDV					
Alonso et al. (2014)	8 finishing / breeding herds	Not identified	**Downwind**	11/62	Range (note: not infectious by bioassay)
			0.01 mi		1.81×10^5 - 4.99×10^5
			0.5 m		4.04×10^4
			1 mi		$4.21 \times 10^3 – 2.65 \times 10^4$
			3 mi		$1.73 \times 10^4 – 3.50 \times 10^4$
			10 mi		7.98×10^3
Alonso et al. (2017)	2 nursery farms	Not identified		Positive + suspect	
			Inside	12/12	$>10^4$ per size range (<1, 1-3, >3 µm)
			At exhaust (~5 m away)	4/4	$>10^4$ per size range (<1, 1-3, >3 µm)
AIV					
Chen et al. (2010)	2 monitoring stations	IAV, H5 subtypes	**During Dust storms**	IAV / H5	IAV (H5)
			Rural station	14/24 / 3/24	268 (1.8)
			Urban station	11/24 / 0/24	276 (None)
Power (2005); Schofield et al. (2005)	3 chicken farms	H7N3	Upwind/downwind	0/240	N/A
			Inside	2/2	292 $TCID_{50}\ m^{-3}$
			800 m downwind	1/9	Not quantifiable
Jonges et al. (2015)	5 infected farms	H7N7, H9N2, H5N2, H10N09	Inside (Farm 5)	1/2	Not quantifiable
			Downwind 7-54 m		
			Farm 1 (chicken; H7N7)	0/4	
			Farm 2 (turkey; H9N2)	3/4	
			Farm 3 (swans; H5N2)	0/5	
			Farm 4 and 5 (turkeys; H10N9)	3/4 and 6/7	

Study	Infected herd/flock	Strain / subtype	Inside / Exhaust/ Downwind	RT-PCR positive (infectious) / Samples collected	Mean airborne concentration (RNA copies m^{-3}) or other units
Torremorell et al. (2016)	3 turkey, 3 chicken flocks	H5N2			Turkey / Layers
			Inside	18(14)/48	1.2×10^5 / 2.8×10^4
			Exhaust (~5m)	14(10)/27	5.1×10^4 / 3.2×10^4
			Downwind (70 m-150 m)	1(1)/4	5.3×10^3 / 8.8×10^3
			Downwind (500 – 1000 m)	?	Not tested / 3.4×10^3
Alonso et al. (2017)	3 turkey, 1 layer flock	HPAIV		Positive + suspect	Depending sampler and size range:
			Inside	14/16	10^2 to 10^5
			Exhaust (~5 m away)	10/12	10^2 to $>10^4$
Scoizec et al. (2018)	3 duck, 2 chicken flocks	H5N8			Chicken / Duck
			Inside	5/5	1.15×10^5 / 1.76×10^5
			Exhaust (~5m)	4/4	1.24×10^5 / 2.27×10^5
			Downwind (50m – 110 m)	3/5	5.73×10^4 / 8.72×10^4
Li et al. (2017)	3 chicken farms	H9N2	**Inside**		
			Farm A	6(3)/6	4.36×10^5
			Farm B	6(2)/6	5.29×10^5
			Farm C	6(1)/6	6.72×10^5
			Downwind (100 m – 1.5 km)		100 m, 1.0 km, 1.5 km:
			Farm A	9/18	4.32×10^3, 2.88×10^3, 0
			Farm B	16/18	4.73×10^3, 3.89×10^3, 2.62×10^3
			Farm C	15/18	5.21×10^3, 3.93×10^3, 2.72×10^3
Chen et al. (2009)	LPM	IAV	In market	55.5%	Range: below detection (8.86×10^2) to 3.7×10^4; None contained H5 gene

Study	Infected herd/flock	Strain / subtype	Inside / Exhaust/ Downwind	RT-PCR positive (infectious) / Samples collected	Mean airborne concentration (RNA copies m^{-3}) or other units
Zhou et al. (2016)	4 LPM	IAV	In market	Varied by market, particle size	58 isolates of H9, H9/H7, and H9/H5 detected, H9N2 most frequent isolate
Wu et al. (2017)	3 LPM	IAV	In market	19/243	1 sample infectious → H5N6 strain
Zeng et al. (2017)	10 LPM	IAV	In market	275/807	1 sample infectious → H9N2 strain
Wei et al. (2018)	1 LPM	IAV	In market	<1 μm 3/21 1-4 μm 12/21 >4 μm 19/21	1.8×10^2 to 5.9×10^3 2.6×10^2 to 1.1×10^5 6.4×10^2 to 3.2×10^5
		18S (Avian rRNA)	In market	<1 μm 21/21 1-4 μm 21/21 >4 μm 21/21	2.0×10^3 to 5.9×10^5 1.3×10^4 to 3.0×10^7 9.7×10^4 to 2.2×10^8
Bui et al. (2019)	1 LPM	IAV H5/H7	In market	27/30 0/30	Not tested
PRRSV					
Kauffold et al. (2005)	18 ultrasound machines	EU, US	**Dust swabs of machines**		Not tested
			PRRSV	9/18	
			EU PRRSV	8/18	
			US and EU PRRSV	1/18	
Spronk et al. (2010)	1 sow herd	Not identified	Towards prevailing wind	2/73	Not tested

Study	**Infected herd/flock**	**Strain / subtype**	**Inside / Exhaust/ Downwind**	**RT-PCR positive (infectious) / Samples collected**	**Mean or range of airborne concentration (RNA copies m^{-3}) or other units**
Brito et al. (2014)	4 sow herds	8-14 strains per location	Towards prevailing wind		Mean viable virus ($TCID_{50}$ mL^{-1} solution)
			Farm A	15/51	4.1 log_{10}
			Farm B	22/53	4.4 log_{10}
			Farm C	18/54	3.8 log_{10}
			Farm D	25/59	5.3 log_{10}
Stein et al. (2018)	3 farms	PRRSV1	Inside	None positive	N/A
Alonso et al. (2017)	2 nursery farms	Not identified	Inside	2/16	10^2 to 10^5 depending on particle size
			Exhaust (~5 m)	0/8	

3.6. Modelling airborne transmission based on data of past outbreaks

Many previous outbreaks of infectious animal diseases were analysed or modelled to determine the contribution of airborne transmission towards infectious disease spread. Airborne transmission modelling is limited for PEDV and PRRSV (Table 3.6) and non-existent for ASFV, while there is some computational fluid dynamics modelling (CFD), air dispersion modelling (ADM), and transmission network modelling on HPAIV. Comparatively, there was extensive modelling performed to study airborne transmission of FMDV (Table 3.7). Modelling provided evidence that airborne transmission contributed in a number of historical FMDV outbreaks to varying degrees, including: Northumberland, U.K., 1966; Bryn Farm to surrounding farms, U.K., 1967; Hampshire, U.K., 1967; Worcestershire, U.K.,1967; Isle of Wight and Jersey, U.K. from Brittany, France, 1981; Denmark, 1982-1983; U.K., 2001; and Korea, 2010-2011.

Table 3.6. Models assessing AT in previous outbreaks of PEDV, AIV, and PRRSV

Study / Virus	Models and findings
Beam et al. (2015) / PEDV	HotSpot and Directional analysis of PEDV outbreaks in 4 U.S. states in 2013. Qualitative but not definitive evidence of airborne transmission from index farm.
Ypma et al. (2012); Ypma et al. (2013) / HPAIV	Monte Carlo Markov Chain (MCMC) simulations applied to transmission trees of genetic and temporal data of Netherlands 2003 HPAIV outbreak. 18% of infected farms estimated due to wind-related transmission
Ssematimba, Hagenaars, & de Jong (2012) / HPAIV	Gaussian ADM and other mathematical probability models. 24% of outbreaks within a 25-km width area during the Netherlands HPAIV outbreak were estimated to be due to airborne transmission.
Lee et al. (2014); Seo et al. (2014) / HPAIV	960 CFD simulations to model airborne transmission during 2008 Korean outbreak of HPAIV. Integrated into network model with medical and feed transmission. Estimated 10/13 farms infected by fomite transmission, 2/13 infected by airborne transmission, 1/13 not determined
Zhao et al. (2019) / HPAIV	HYSPLIT ADM of HPAIV outbreak in Iowa, U.S. in 2015. The results were dependent on values of assumed parameters, such as shedding rate, emission rate, and half-life of the virus. Worst-case assumptions estimated that there were 33 facilities that had >10% probability of being infected by airborne transmission.

Study / Virus	Models and findings
Xu et al. (2016) / HPAIV	Epidemiology investigation of the 2014 H5N2 HPAIV outbreak in Canada, as well as phylogenetic analysis and development of transmission network using MCMC simulations. The authors suspected that one of the farms may have been infected due to airborne transmission.
Mortensen et al. (2002) / PRRSV	Statistical analysis of U.S. PRRSV outbreaks in Denmark between June 1996 and October 1997. Herd size and distance from neighbouring herd were significant factors. Authors concluded airborne transmission contributed to spread of PRRSV.
Rosendal et al. (2014) / PRRSV	Data analysis of spatial and temporal outbreaks of PRRSV in Ontario farms from September 2004 to August 2007. Did not find strong evidence of airborne transmission

Modelling is based on three approaches: epidemiology, weather data, and air dispersion. Epidemiology analysis of outbreaks in farms both spatially and temporally was often performed to determine transmission links between herds and the likely transmission routes that caused infection in herds. Analysis of weather or meteorological data was often used to determine if outbreaks could be due to dispersion of airborne infectious virus from a source facility to downwind facilities, typically by examining wind speeds, wind directions, precipitation, atmospheric stability, temperature and relative humidity. ADM was considered to be an important tool to simulate the movement of infectious FMDV aerosols from source facilities. A variety of ADM were used, many of which were based on Gaussian Plume and Gaussian Puff models. ADM allowed for the estimation of downwind airborne concentrations of infectious virus from an infectious source. Results were used to support previous meteorological and epidemiological analyses of outbreaks. CFD modelling is an alternative to ADM that can also provide estimates of downwind infectious virus from the infectious sources; while CFD was not used for past outbreaks of FMDV, it was used to study a past outbreak of HPAIV (Seo et al., 2014).

In ADM, shedding of virus from infected animals was an important input parameter. Some researchers programmed virus production models that calculated the total amount of virus produced per 24 hours; these values were inputted into the ADM during model development (Gloster, Freshwater, Sellers, & Alexandersen, 2005; Sørensen, Jensen, Mikkelsen, Mackay, & Donaldson, 2001; Sørensen, Mackay, Jensen, & Donaldson, 2000). The virus survival due to the

effect of relative humidity was considered in some simulations (Gloster, Blackall, Sellers, & Donaldson, 1981; Gloster et al., 2010; Sørensen et al., 2001) or considered in the meteorological analyses. The downwind airborne virus concentrations averaged over 24 hours was compared to the infectious dose in several studies, but was often below the infectious dose (Gloster, Champion, et al., 2005; Gloster et al., 2003; Mikkelsen et al., 2003; Sørensen et al., 2000); in some cases, the maximum hourly concentrations were also below the infectious dose (Gloster, Freshwater, et al., 2005), while in other cases, the peak concentration was close to the infectious dose (Gloster, Champion, et al., 2005). As a result of this, the NAME ADM was modified to show only the level of risk of airborne transmission, with risk categorized as low, medium, or high (Gloster et al., 2010). Some studies used equations describing the probability of infection in individual animals or in herds with ADM to ascertain the likelihood of airborne transmission (Jones et al., 2004; Sanson, Gloster, & Burgin, 2011).

There were also a number of studies that used modelling methods that were not connected to a specific past outbreak, but were used as predictive tools for airborne transmission. Cannon & Garner (1999) used a Gaussian Plume model to predict risk of airborne transmission in six scenarios in Australia. Donaldson, Alexandersen, Sørensen, & Mikkelsen (2001) used RIMPUFF to show the difference in airborne spread when cattle, sheep, and pigs were infected. Interspread, which runs MCMC simulations of outbreaks including airborne transmission, was used to assess control strategies (Morris, Wilesmith, Stern, Sanson, & Stevenson, 2001) and used to assess the success of vaccination at controlling FMDV in New Zealand (Sanson et al., 2017). Different Lagrangian ADM, such as HYSPLIT, were used to assess the risk of FMDV spreading by airborne transmission (Coffman, Sanderson, Dodd, Arzt, & Renter, 2021; Garner, Hess, & Yang, 2006; Klausner, Klement, & Fattal, 2015; Lambkin, Hamilton, McGrath, Dando, & Draxler, 2019; Mayer, Reiczigel, & Rubel, 2008). Traulsen, Rave, & Krieter (2010) used stochastic modelling and Gaussian plume dispersion to study parameters that affected the duration, number of infected pigs, and number of culled farms during outbreaks. Traulsen & Krieter (2012) developed a fuzzy logic model to predict airborne transmission, and it had good agreement with the results of a Gaussian Plume model. CFD was used to develop of a web-forecasting model that showed the risk of FMDV spread in Korea (Seo, Lee, Hong, Noh, & Park, 2015). A weather analysis of the U.S. was performed to identify locations that would provide

favourable conditions for airborne transmission of FMDV to occur (Hagerman et al., 2018). Recently, a number of modelling techniques, including stochastic modelling, dose-response modelling, and a Lagrangian particle model were used to assess the risk of airborne transmission of FMDV in Sweden (Björnham, Sigg, & Burman, 2020).

Table 3.7**.** Analytical methods and models used to study contribution of airborne transmission in various historical cases of FMDV

Citation - Model or Analysis	**Findings**
Saskatchewan, Canada 1950	
Sellers & Daggupaty (1990) Epidemiological and weather analysis	Airborne transmission was suspected to have caused an FMDV outbreak in 6-12 farms.
Daggupaty & Sellers (1990) Short range Gaussian Plume	The authors listed possible sources of FMDV aerosols and alternative transmission routes for some farms. A feedlot of pigs was the source of FMDV aerosols for many affected farms, but it was not clear from historical records if the feedlot had infected pigs at the time.
Northumberland, U.K. 1966	
Smith & Hugh-Jones (1969) Weather analysis	Analysis showed some evidence that outbreaks occurred downwind of infected sites
Sellers & Gloster (1980) Epidemiological and weather analysis	Out of 32 farms in the area, airborne transmission was suspected to be the cause of farms becoming infected in 26 farms.
Gloster et al. (1981) Gaussian Plume model	Agreed with findings of Sellers & Gloster (1980)
Bryn Farm (first case) in U.K. 1967 outbreak	
Hugh-Jones & Wright (1970) Weather analysis	It was concluded that most of the cases during the initial spread were due to windborne transmission.
Gloster, Freshwater, et al. (2005) Virus production model, UK short-range ADM, analysis of meteorological data	The source farm could have infected 12 farms NE of it within 5 km and 16 farms 16-54 km NE by airborne transmission, but there were potentially other sources for some farms. Six farms within 5 km NE of the source farm and 12 farms that were 16-54 km NE of the source farm had no other potential sources. The estimated concentrations were less than the infectious dose.
Sanson et al. (2011) NAME model, epidemiology analysis, probit dose-response model	Two emission rate profiles, based on number of infected pigs in source farm, were used as inputs to NAME model. The number of farms under the virus plume, the daily concentration of virus, and the number of farms infected by airborne transmission were estimated. Probit analysis showed that exposure dose was significantly associated with probability of infection. Overall, strong evidence of airborne transmission.

Citation - Model or Analysis	Findings
Hampshire, U.K., 1967	
Smith & Hugh-Jones (1969) Weather analysis	There was some evidence that outbreaks occurred downwind of infected sites.
Sellers & Forman (1973) Epidemiological and weather analysis	The authors discussed likely transmission routes of FMDV to farms. The abattoir played a large role in disseminating airborne FMDV to farms in the area.
Gloster et al. (1981) Gaussian Plume model	Agreed with findings of Sellers & Forman (1973)
Casal, Moreso, Planas-Cuchí, & Casal (1997); Casal, Planas-Cuchí, Moreso, & Casal (1995) Areal Location of Hazardous Atmosphere (ALOHA) 5.05, Gaussian Plume model	The model predicted that farms 5 and 11 were infected by airborne transmission. The model also predicted farms 2 and 12 could have been infected by airborne transmission, using a higher shedding rate of FMDV from infected pigs in the model.
Gloster et al. (2010) Six ADMs: NAME (U.K.), VetMet (Danish), PDEMS (New Zealand), AIWM (Australia), MLCD (Canada), NARAC (USA)	Similar risk was seen for all models at shorter distances from the source of FMDV aerosols. As distance increased, the risk predicted by the six models began to differ. The authors discussed that this was due to differences in weather information with some models using observation data and some models using numerically derived weather data.
Worcestershire, U.K. 1967	
Hendersen (1969) Epidemiology and weather analysis	The evidence indicated that FMDV carried in the wind contributed to the spread of FMDV in the area.
Casal et al. (1997); Casal et al. (1995) Areal Location of Hazardous Atmosphere (ALOHA) 5.05 Gaussian Plume model	The model predicted that farms 4, 6, 10, 11, and maybe 16 were infected by airborne transmission. The other farms received airborne doses that were too low to cause infections.

Citation - Model or Analysis	Findings
Isle of Wight and Jersey, U.K. and Brittany and Normandy, France, 1981	
Donaldson, Gloster, Harvey, & Deans (1982) Gaussian Plume model and long distance numerical model	The short distance models predicted low secondary spread due to airborne transmission. A long distance model provided evidence of two time periods in which all conditions for airborne transmission from Brittany to Jersey and Isle of Wight were met.
Moutou & Durand (1994) ICAIR 3V - Gaussian Puff and Gaussian Plume equations	The model showed that 10/13 outbreaks in Brittany may have been caused by airborne transmission.
Sørensen et al. (2000) RIMPUFF ADM, virus production model	The airborne FMDV concentration in Jersey and Isle of Wight was 500-fold less than the minimum concentration required to infect cattle but the Jersey and Isle of Wight outbreaks were likely due to airborne transmission. The number of inputted infected pigs in Brittany was likely under-reported originally and virus shed from piglets were not accounted for in the model.
Sørensen et al. (2001) RIMPUFF ADM, LINCOM (local-scale atmospheric flow model), DMI-HIRLAM to predict weather.	There were several days of high stability over the English Channel that provides evidence of airborne transmission during the 1981 France / U.K. outbreaks in Jersey and Isle of Wight.
Denmark 1982-1983	
Sørensen et al. (2000) RIMPUFF ADM, virus production model	The model agreed with unpublished results that airborne transmission spread FMDV to Denmark.
Christensen et al. (2005) Phylogenetic analysis and RIMPUFF	There were three separate introductions of FMDV into Denmark. The authors discussed that a herd in Skelskor was likely infected by airborne transmission from northern Funen.

Citation - Model or Analysis	Findings
Verona, Italy, 1993	
Moutou & Durand (1994) ICAIR 3V	The model was used to assess the potential spread in Italy, and two pig units were euthanized as a result of the model results.
Maragon et al. (1994) A puff model near source and wind speeds <2 m/s; a plume model for other conditions using simulated weather data	Pig units that were potentially infected should be euthanized to prevent them from spreading airborne FMDV. Large area would be potentially affected as pigs shed large amounts of airborne FMDV.
UK 2001	
Jones et al. (2004) NAME model, exponential dose-response model, estimated probability of infection in holding, uncertainty analysis	Burning of pyres was unlikely to have spread FMDV by airborne transmission
Gloster et al. (2003); Mikkelsen et al. (2003) Gaussian Plume; Nuclear Accident Model (NAME); Danish Emergency Response Model Atmosphere (DERMA); Local Scale Model Chain (LSMC; which incorporates RIMPUFF with LINCOM-z0 and LINCOM-T)	The risk to the main continent from the island due to airborne transmission was predicted to be negligible. The infection at Prestwick Hall farm was likely due to airborne transmission from Burnside farm. Long term averages were below infectious dose, but the authors asserted that short-term fluctuations were can affect the probability of infection.
Gloster, Champion, et al. (2005) Epidemiological and meteorological analysis. NAME ADM model with some comparisons to UK short-range ADM.	In Longtown, the peak hourly FMDV concentrations were higher than 24-hour averages of FMDV concentrations and close to the infectious dose required to cause infection, while the averages were below the infectious dose. In Penrith, the plume generated matched the observed direction of infection in the case study. The 24-hour averages and peak hourly values of FMDV concentration were below the infectious dose of FMDV. In Witton-le-Wear, a number of farms in the area were likely infected by airborne transmission.
Korea, 2010-2011	
Kritana, Taehyeung, Hyeontae, Ki Youn, & Wongeun (2014) CALPUFF non-steady-state puff ADM	In the first case study, the time period in which airborne transmission may have occurred from a farm to a second farm was narrowed down to a 12-hour period using CALPUFF results. Airborne transmission from three possible facilities was eliminated as a cause of transmission of two farms in the second case study.

3.7. Factors that affect aerosol transmission

3.7.1. Aerosol type

Experimental studies reported in the literature dealt with aerosols which were either generated artificially or produced naturally by animals (natural aerosols). The main difference between natural and artificially generated aerosols is the particle size distribution as well as the material composition of aerosols. Artificially-generated aerosols are primarily small liquid particles (Agranovski et al., 2010; La & Zhang, 2019; Pyankov, Pyankova, & Agranovski, 2012) suspended within laboratory media or agents that would boost the survival of the virus during aerosolization (Barlow & Donaldson, 1973). As aerosol size is related to the depth that aerosols can penetrate into the respiratory system (Asgharian et al., 2016), artificially-generated aerosols are likely to enter the deeper respiratory tract and cause infection. Natural viral aerosols may come from different sources, including the breath of infected animals (Cho et al., 2006; Christensen et al., 2011), animal skin cells, and dust particles that may be larger in size (Dillon, 2011). For natural aerosols, there could be a mix of deep penetration into the respiratory tract by smaller aerosols, and shallower penetration into the upper respiratory tract via larger aerosols (Asgharian et al., 2016). It must be noted that larger aerosols are more likely to settle instead of entering the respiratory tract, due to their size and higher Stokes settling velocity (de Nevers, 2017).

3.7.2. Shedding of viruses from infected animals

Shedding of viruses from infected animals into the air is an important aspect of airborne transmission. A summary of shedding observations from experimental studies is presented in Table 3.8, including: strains used in the study, duration of monitoring of airborne concentration post inoculation, units of measurement, duration of shedding post-inoculation from source animals or contact animals, and other observations of note. It should be noted that many experimental studies were performed under laboratory conditions, and the airborne virus concentrations (quantity) may not be representative of the amount of airborne virus that would be produced in naturally infected animal facilities. For example, Germeraad, Sanders, Hagenaars, de Jong, & Gonzales (2019) found an association between inoculation dose of HPAIV and the amount of shedding of HPAIV from infected animals. The herd size, animal distribution/density, ventilation rate, and management procedures are also different in laboratory studies compared to

field studies. However, shedding patterns and differences in virus shedding due to infection with different strains is information that can be gained from laboratory studies.

There were some shedding observations worth further discussion from Table 3.5 and Table 3.8. Long-term shedding of ASFV into the air (between days 7 to 23 and days 7 to 28) was reported (de Carvalho Ferreira, Weesendorp, Quak, Stegeman, & Loeffen, 2013); however, Olesen et al. (2017) did not observe the same consistency of shedding, which was possibly due to the use of different air sampling equipment, different virus strains, a shorter length of shedding monitoring, or other experimental factors, like ventilation rate. Gallien et al. (2018) performed a long-term observation of shedding of two PEDV strains and reported differences in shedding duration and airborne concentration between the two strains. Alonso et al. (2014) observed PEDV shedding from inoculated pigs from 8 hours to 63 hours after inoculation and observed concentrations $>10^7$ RNA copies per m^3. While most measurements of AIV in air samples in naturally infected facilities (Table 3.5) or experiments (Table 3.8) reported RNA copies or equivalent infectious virus quantified with qRT-PCR, Yao et al. (2011) performed a study to quantify infectious AIV in units of plaque forming units (PFU) and reported that birds inoculated with infectious H9N2 AIV shed on days 2 or 3 to day 17 after inoculation, during a 28-day experiment.

In most studies of FMDV shedding, virus in air was monitored up to four or five days after inoculation of animals (Alexandersen et al., 2003; Alexandersen, Zhang, Reid, Hutchings, & Donaldson, 2002; Amaral Doel, Gloster, & Valarcher, 2009; Colenutt et al., 2016; Donaldson, Herniman, Parker, & Sellers, 1970; Gloster, Doel, Gubbins, & Paton, 2008; Sellers & Parker, 1969; Stenfeldt et al., 2020), while longer durations was monitored in some studies (Esteves et al., 2004; Pacheco et al., 2017; Stenfeldt et al., 2018). An interesting contribution of FMDV research is how some researchers quantified shedding of virus into the air per animal over a 24-hour period (Alexandersen & Donaldson, 2002; Alexandersen et al., 2003; Alexandersen, Zhang, et al., 2002; Esteves et al., 2004; Gloster et al., 2008, 2007; Valarcher et al., 2008). Quantifying the shedding per animal allows for the estimation of shedding from a group of animals, regardless of group size. This is a useful method of quantification that should be used in future research for other infectious animal viruses.

Another critical factor in virus shedding is the sizes of aerosols that carry viruses. Alonso, Raynor, Davies, & Torremorell (2015) and Alonso et al. (2017) quantified the RNA copies per m^3 air at different aerosol size ranges for IAV, PEDV, and PRRSV. Alonso et al. (2015) used inoculated animals within a BSL facility and reported that aerosols larger than 9 μm contained the most RNA copies per m^3 for IAV, PEDV, and PRRSV, with a general trend of RNA copies per m^3 increasing as particle size increased for IAV and PEDV. Alonso et al. (2017) performed measurements inside naturally infected farms and reported that HPAIV, PEDV, and PRRSV had highest RNA copies at large (>3 μm) aerosol sizes, but that the aerosol size of 0.4 μm was also important for HPAIV and PEDV. Wei et al. (2018) performed size-differentiating air sampling in a LPM; the study reported that virus containing the 18S gene associated with AIV was present in all three size ranges (<1 μm, 1-4 μm, >4 μm) and that the highest RNA copies per m^3 was captured at an aerosol size of >4 μm. Spekreijse et al. (2013) quantified airborne AIV in non-respirable (>8 μm) and respirable (≤ 8 μm) fractions from a room containing pigs inoculated with H5N1 HPAIV. The authors reported $2.0\log_{10}$ to $3.3\log_{10}$ equivalent 50% embryo infection dose (EID_{50}) per m^3 for respirable aerosols and $1.5\log_{10}$ to $3.4\log_{10}$ equivalent EID_{50} per m^3 for non-respirable aerosols, depending on the day after inoculation and replicate. Sellers & Parker (1969) quantified FMDV shedding on three size stages, with the sizes not described in paper, while Gloster et al. (2007) quantified the shedding of FMDV per inoculated animal per 24 hours on three size ranges (>6 μm, 3 to 6 μm, <3 μm). The authors reported that the virus was "almost equally distributed" in the three sizes measured. Since the settling behaviour and the penetration of particles into the respiratory tract are dictated by particle size, the distribution of airborne virus on different particle sizes should be considered in prediction models for airborne transmission of virus pathogens.

Table 3.8. Study, virus, strain, days post-inoculation of air sampling monitoring, and significant findings on shedding of virus into air.

Study	Virus; Strain	Days monitored (time post inoculation); units	Significant findings
Olesen et al. (2017)	ASFV; Pol14/WB-17397#13	0 to 11 and 0 to 18 days; log_{10} genome copies per 5 L or 12 L of air	Quantified shedding into air from pens of inoculated, contact, and "air contact" pigs in two trials. Shedding from inoculated animals detected days 5 to 9 in trial 1, days 8 to 14 (some negative days) in trial 2. Positive air samples within air contact pig pens detected on days 7 and 8 in trial 1 and days 10, 14 to 18 in trial 2.
de Carvalho Ferreira et al. (2013)	ASFV; Brazil'78, Netherlands'86, Malta'78	0 to 9 days for Brazil'78, 0 to 70 days for Netherlands' 86 and Malta' 78; $TCID_{eq}$[a] per m^3	Quantified shedding into air from room with inoculated and contact pigs. Shedding occurred consistently at varying levels from days 4-9 (end of sampling), days 7-28, and days 7-23 for Brazil'78, Netherlands' 86, and Malta'78 strains, respectively.
Lee et al. (2021)	ASFV; VNUA/HY/Vietnam	0 to 8 days	Quantified shedding into room with inoculated animals. Shedding into the air occurred from days 5 to 8.
Gallien et al. (2018)	PEDV; non-InDel (USA/2014/IOWA, French InDel (FR/001/2014)	0 to 49 days for InDel, 0 to 72 days for non-InDel; log genome copies per L air	Quantified shedding into air between pens with inoculation, contact pigs and "air contact" pigs. Shedding for InDel started on day 2 and was higher on days 5 to 35. Shedding for non-InDel from days 1-35 and some low shedding after this period. The peak shedding was higher for the non-InDel than the InDel.
Alonso et al. (2014)	PEDV; strain not identified	8 to 63 hours; RNA copies per m^3 air	Quantified shedding from room containing inoculated animals. The shedding was $>10^7$ RNA copies /m^3
Spekreijse et al. (2013)	AIV; A/turkey /Turkey/1/2005 H5N1	1 to 14 days (varied per trial); log equivalent EID_{50} per m^3	Quantified airborne concentration of PEDV that entered the second unit where were recipient pigs held, receiving air from the first unit containing infected pigs; shedding was detected on and off, depending on the replicate. The largest shedding period was days 2 to 14 and the smallest shedding period was days 4 to 10.
Yao et al. (2011)	AIV; A/chicken/Shandong/1/8 H9N2	1 to 28 days; PFU per m^3 air	Quantified shedding in unit with inoculated and contact chickens; shedding period was days 2 or 3 to 17. Ranging from 240 to 7200 PFU per m^3.

Study	Virus; Strain	Days monitored (time post inoculation); units	Significant findings
Sellers & Parker (1969)	FMDV; O1 Lombardy, O1 Swiss 1/66, O1 BFS 1860, O2 Brescia	17 to 113 hours (for cows and sheep) and 17 to 137 (for pigs); log ID_{50}	Shedding into air from loose boxes containing inoculated animals was quantified and corresponded to clinical signs in infected animals. Shedding from cows and sheep lasted 4 days, totalling 3 $\times 10^4$ $\log_{10}$ infectious dose 50% (ID_{50}) per animal, while shedding from pigs lasted 5 days and the total titre shed was 10^6 ID_{50} per animal.
Donaldson et al. (1970)	FMDV; A22 Iraq 24/26, A5 Eystrup (Tübingen), C Lebanon 3/69, C Noville, O1 and O2	1 to 4 days for most strains and inoculation methods, 3 to 6 days for A22 intramuscularly and 3 to 8 days for animals exposed to A22 infected pigs; log ID_{50}	Shedding into air from loose boxes containing inoculated animals was quantified, when animals were infected with different strains and inoculation methods. Shedding linked to appearance of clinical signs in infected animals. Shedding quantities differed depending on strain. Pigs shed the most virus. Most strains and inoculation methods resulted in shedding of virus into air.
Alexanders en, Zhang, et al. (2002)	FMDV; O UKG 34/2001	1 to 2 days for sheep; 1 and 3 days for cattle; $\log_{10}$ $TCID_{50}$ per L air	Quantified shedding into air from infected sheep and cattle. The values were converted to airborne release per animal per 24 hour period. Virus was detected in cabinet air from inoculated sheep on day 1 only. Virus was detected in room air from infected cattle on day 3.
Alexanders en et al. (2003)	FMDV; O TAW 9/97	1 to 2 days for pigs; $TCID_{50}$ per L air	Table was displayed showing FMDV shedding into air from inoculated pigs. The values were converted into infectious virus shed per pig per 24 hours. Virus shed into air on both days.
Esteves et al. (2004)	FMDV; O UKF 34/2001	1 to 7 days for sheep and 1 to 4 for lambs; log $TCID_{50}$ and log RNA copies per 24 hours	FMDV shedding into air was quantified in a room with 1 inoculated. Infectious FMDV was detected in the cabinet with sheep for 2 days, while RNA copies were detected for 4 days.

Study	Virus; Strain	Days monitored (time post inoculation); units	Significant findings
Gloster et al. (2008)	FMDV; O/UKF/2001/34/ 2001 and C Swiss 1/73 (C Noville)	1 to 4 days; log $TCID_{50}$ per 24 hours per pig	FMDV shedding into air was quantified. Two inoculations doses were tested. Higher dosed animals emitted FMDV earlier than lower dosed animals and animals inoculated with C Noville shed more virus into air than animals inoculated with O UKG. Virus was still shed at day 4 except for pigs dosed with high amount of C Noville
Amaral Doel et al. (2009)	FMDV; O UKF 34/01	1 to 4 days; $TCID_{50}$ per L air, genome copies per L air	FMDV shedding into air was quantified in the loosebox with inoculated pigs. Infectious FMDV shedding was detected for three days and some samplers detected RNA copies on the fourth day.
Colenutt et al. (2016)	FMDV; Asia 1 virus (HKN/05/2005)	2 to 3 days; $TCID_{eq}$[a] per L air	FMDV shedding into air was quantified close to individual pigs. Shedding occurred on both days.
Pacheco et al. (2017)	FMDV A24 Cruzeiro wild type	1 to 9 days; RNA copies per 1000 L air	FMDV shedding into air was quantified close to infected pigs and contact pigs. Shedding occurred starting on day 1 to 7 for pigs inoculated with 10^4 $TCID_{50}$ and days 1 to 9 for pigs inoculated with 10^7 $TCID_{50}$.
Nelson et al. (2017)	FMDV O strain UKG/34/2001	1 to 7 or 8 days; $TCID_{eq}$[a] per m^3 air	Shedding was quantified close to infected calves and in the ambient air. FMDV RNA was detected in the air during pre-clinical, clinical, and recovery (7-8 days) phases of FMDV infection.
Stenfeldt et al. (2018)	FMDV A24 Cruzeiro	0 to 35 days;	Rooms housed infected pigs and contact cattle on day 0, before pigs were removed. FMDV was quantified in the room of vaccinated or non-vaccinated cattle. FMDV RNA was detected up to 35 days in room with non-vaccinated pigs, and up to 21 days in room with vaccinated pigs. FMDV was infectious up to day 7 in both rooms.

[a] $TCID_{eq}$ = Equivalent $TCID_{50}$, quantified using qRT-PCR but the standard curve was generated using $TCID_{50}$ measurements.

3.7.3. Temperature and relative humidity effect on virus survival

The survivability of infectious viruses in aerosols under different environmental conditions is a critical aspect of airborne transmission. Donaldson & Ferris (1976) reported that ASFV survived best at low relative humidity conditions (20-30%) immediately and 5 minutes after aerosolization. de Carvalho Ferreira et al. (2013) reported that ASFV aerosols had half-life values of 14.1 min and 19.2 min in terms of PFU and RNA, respectively, when room conditions ranged from 20.6 to 21.0°C and 61 to 81% relative humidity, and when gravity was not eliminated as a source of aerosol loss. Pyankov et al. (2012) reported the decay of artificial aerosols of H5N1 AIV in a rotating drum (to avoid gravity settling of aerosols) at 25°C and 55% relative humidity, with <20% of the virus remaining infectious at the end of the 90-minute experiments. H10N7 AIV within faecal aerosols that were collected onto filters survived longer at lower relative humidity and temperature conditions, with poor survival at 37°C and water saturated conditions (Sedlmaier et al., 2009). Belser et al. (2022) reported varying levels of stability for three IAV strains (H3N2, H7N9, H5N1) aerosolized into 20%, 50% and 70% relative humidity conditions, suggesting that there is potentially strain-specific stability of viruses in the aerosol form. Hermann et al. (2007) developed a half-life equation for PRRSV aerosols, based on the temperature and relative humidity conditions, and reported that increase in temperature and relative humidity adversely affected the survival of PRRSV. Cutler, Wang, Hoff, & Zimmerman, 2012) reported the effect of ultraviolet irradiation (UV_{254}), relative humidity, and temperature on PRRSV survival in aerosols, with UV_{254} inactivation constants varying with the temperature and relative humidity conditions; UV_{254} inactivated PRRSV best at temperatures ≤15°C and relative humidity between 25 to 79%.

Donaldson (1972) quantified the rate of decay for different strains of FMDV in aerosols at relative humidity conditions of 55% and 70%, and reported that the survival was the best at 60% relative humidity. Barlow (1972) showed that survival of FMDV in aerosols immediately after and 5 minutes after aerosolization was optimal at 60% relative humidity, with survival decreasing as the relative humidity decreased. Similarly, Barlow & Donaldson (1973) reported that FMDV in aerosols survived best immediately after aerosolization at relative humidity conditions greater than 60%. However, the survival of FMDV after five minutes was also

affected by the fluid type in which the virus was suspended, with the best survival at high relative humidity in cell culture fluid and the worst in salivary fluid.

3.7.4. Aerosol infectious dose

The minimal infectious dose is the lowest dose required to cause infection by a particular transmission route. For aerosol transmission, experimental data for determining the ID_{50} (i.e., the aerosol ID_{50}) can be gathered by exposing groups of animals to known or measured concentrations of aerosolized infectious virus at several dosage levels. The proportion of animals infected within each dosage level and the dose of infectious virus can be analysed with dose-response modelling to determine the ID_{50} (Cutler et al., 2011; Hermann et al., 2009; La, Zhang, Cicek, Levin, & Coombs, 2021).

There is generally a lack of or incomplete data for aerosol transmission infectious doses for viral swine diseases. For example, no studies were found in the literature on ASFV and PEDV. Experiments using H9N2 AIV (A/Chicken/HN/1/98) indicated that the aerosol ID_{50} was between 57 and 3.7×10^3 EID_{50} (Guan et al., 2013). Yao et al. (2014) reported an ID_{50} of 491.21 $TCID_{50}$ for H9N2 AIV (A/Chicken/Shandong/01/2008), although the authors did not perform air sampling to confirm the exposure dose of virus. Sergeev et al. (2013) reported the aerosol ID_{50} for eight strains of H5N1, with mean values ranging from $0.3\log_{10}$ to $1.2\log_{10}$ EID_{50}. The lethal aerosol dose at 50% probability (LD_{50}) for H5N1 AIV (A/Chicken/Suzdalka/Nov-11/2005) was reported as 26.5 focus forming units (Agranovski et al., 2010). The aerosol ID_{50} for PRRSV VR-2332 was $1 \times 10^{3.1}$ $TCID_{50}$ (Hermann et al., 2009). Estimates for the aerosol ID_{50} of PRRSV MN-184 varied between $1 \times 10^{-0.14}$ to $1 \times 10^{0.26}$ $TCID_{50}$, depending on the analysis method used to estimate the ID_{50}.

Many studies have been reported on infectious doses of FMDV for pigs, sheep, and cows. (Gibson & Donaldson, 1986) estimated that sheep have a minimal aerosol infectious dose of 10 $TCID_{50}$ for FMDV strain O_1 BFS 1860. Donaldson et al. (1987) reported that cows had aerosol minimal infectious doses of 12.5 $TCID_{50}$ and 25 $TCID_{50}$ for FMDV strains O_1 BFS 1860 and SAT 2, respectively. Alexandersen, Brotherhood, et al. (2002) estimated that pigs had a minimal aerosol infectious dose of 260 $TCID_{50}$ and 800 $TCID_{50}$ for FMDV O_1 Lausanne to cause sub-clinical infection and clinical disease in pigs, respectively. Alexandersen & Donaldson (2002)

revised their estimates for FMDV O_1 Lausanne, estimating a minimal aerosol infectious dose of 1500 $TCID_{50}$ and 4000-6000 $TCID_{50}$ for subclinical infection and clinical disease in pigs, respectively. Exposing pigs to aerosols of the FMDV O SKR 2000 strain did not result in infection, but authors estimated that the minimal aerosol infectious dose for pigs was greater than 1000 $TCID_{50}$. The authors also estimated that the minimal aerosol infectious dose for pigs was greater than 70,000 $TCID_{50}$ for FMDV O UKG.

3.8. Conclusions of the journal paper

The conclusion to this journal paper was relocated to the discussion of this thesis, in chapter 7.1 (knowledge gaps in modelling airborne transmission of viral pathogens) and integrated into chapter 7.6 (recommendations)

Chapter 4. Experimental validation of CFD simulations of bioaerosol movement in a mechanically ventilated airspace

Chapter 4 discusses the contribution of the journal paper titled "Experimental validation of CFD simulations of bioaerosol movement in a mechanically ventilated airspace". This journal paper was published in the Canadian Journal of Biosystems Engineering and this chapter follows the formatting of this journal publication. The citation of the published paper is: La, A., & Zhang, Q. (2019). Experimental validation of CFD simulations of bioaerosol movement in a mechanically ventilated airspace. *Canadian Biosystems Engineering / Le Genie Des Biosystems Au Canada*, 61(1), 5.01–5.14. https://doi.org/10.7451/CBE.2019.61.5.01.

Portions of the original published paper, specifically in the introduction and discussion, have been removed from this thesis to reduce repeated information.

4.1. Abstract

A CFD (computational fluid dynamics) model was developed to simulate the movement of bioaerosols in mechanically-ventilated chambers and the results were validated with experiments. Liquid aerosols containing Porcine Reproductive and Respiratory Syndrome Virus (PRRSV) were artificially generated in the chambers. Bioaerosol concentration was monitored with an optical particle counter until steady-state conditions were achieved (aerosols containing viruses are referred to as bioaerosols in this paper). Four treatments with two ventilation rates and two bioaerosol generation rates were tested. The standard k-ε turbulence model and a discrete phase model with unsteady tracking was used in an ANSYS Fluent CFD model to simulate the airflow and bioaerosol movement until steady-state was reached. A mesh refinement test was performed to select an optimal mesh size for simulations. The CFD simulations showed good agreement with the measured bioaerosol concentrations at steady-state with differences of 2% to 8%, normalized mean square error of 0.01 to 0.19, and fractional bias of 0.02 to 0.08. Simulations and validation during the transient phase could not be verified because of limited measurement locations.

4.2. Introduction

A challenge of using CFD for simulating aerosol transmission of diseases is model validation. In most studies reported in the literature, model validation is performed indirectly by correlating the model predictions to observed disease events, instead of directly comparing predicted and measured aerosol concentrations. This is because measuring aerosol concentration in the air is difficult during outbreaks. In La (2015), controlled laboratory experiments were performed, in which bioaerosols of PRRSV were generated into two connected chambers.

The purpose of the current study was to: (1) demonstrate the adequacy of CFD for simulating aerosol transmission by using the parameters measured in La (2015) to simulate bioaerosol movement in a mechanically-ventilated airspace (chambers), and (2) validate the CFD simulation by directly comparing the results to the measured bioaerosol concentrations in La (2015). Specifically, a CFD model was utilized to simulate the movement and distribution of bioaerosols containing PRRSV within two connected chambers.

4.3. Methodology

4.3.1. Experimental bioaerosol chamber system

The bioaerosol experiment system consisted of two identical chambers with dimensions of 0.99 m, 1.30 m, 1.07 m in height, width, and depth, respectively (Fig. 4.1a). The two chambers were joined together with a 0.165-m-diameter duct 0.603 m in length. The inlets of each chamber contained baffles that directed the airflow downwards to promote air circulation. A HEPA filter (model no. 01XS-24Z12Z12, Camfil Farr, Winnipeg, MB) was installed prior to the inlet of the first chamber and after the outlet of the second chamber to remove any biological organisms from the air. A 0.127-m-diameter tee-wye (Y-shaped) fitting was installed between the first chamber and the HEPA filter; the branch of the fitting was used as a port to introduce bioaerosols into the chamber system.

The airflow (ventilation) within the chambers was generated by a fan (VortexVTX800, Atmosphere, Terrebonne, QC) and controlled using an IRIS damper (IRIS-S-05, Continental Fan Manufacturing Inc., Mississauga, ON), a bypass damper, and digital manometer (475-00-FM, Dwyer, Michigan City, IN). The bypass damper was an air diffuser that was opened when a lower airflow rate was required in the chambers. These components were installed after the second HEPA filter and separated with 0.127-m-diameter duct (Fig. 4.1b). The IRIS damper

product specification guide specified that distances of ≥1d and ≥2d (where d is the diameter of the duct) for elbows and transitions, respectively, were required to obtain an airflow measurement accuracy of ±7% (Continental Fans 2012). The distance that the IRIS damper was placed from the elbow and the bypass damper was 0.6477 m and 0.7496 m, respectively, which met the requirements for accurate air flow rate measurement, as specified by the instrument supplier. It should be noted the requirements were different from the airflow measurement procedure outlined in ASHRAE (1987).

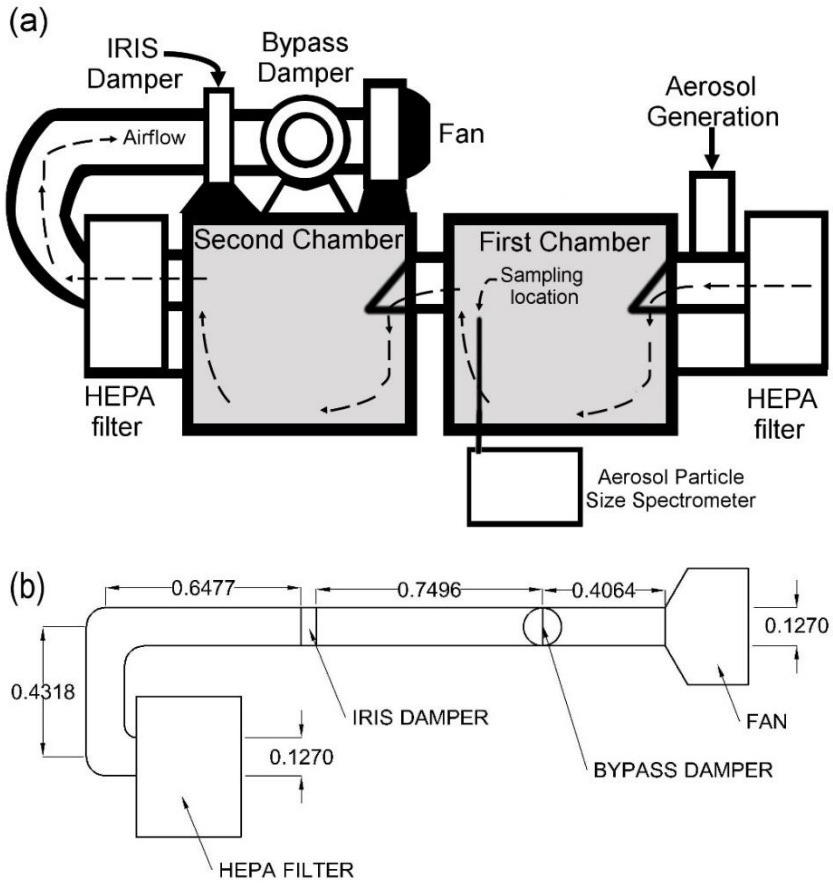

Figure 4.1. (a) Sketch of the aerosol experiment system, (b) schematic diagram of the IRIS damper, digital manometer, bypass damper to control airflow rate in chambers (dimensions are in meters).

Bioaerosols were generated using a 6-jet Collison Nebulizer (CN25, BGI Inc., Waltham, MA) driven by filtered compressed air. The nebulizer was filled with 39 ml of PBS and 1 ml of

PRRSV produced from a live vaccine (Ingelvac PRRS® MLV, Boehringer Ingelheim, St. Joseph, MO) with an initial virus concentration of 1 x 10^7 PFU $ml^{-1.}$ The final virus concentration in the aerosolized solution was 2.5×10^5 PFU ml^{-1}. The nebulizer produced a bioaerosol generation rate of 14.8 ml h^{-1} and 34.0 ml h^{-1} when supplied with compressed air at 137.9 and 413.7 kPa, respectively. The bioaerosols were monitored with an Aerosol Particle Size Spectrometer (APSS; LAP 332, Topas GmbH, Dresden, Germany) that was programmed to collect 10-s measurements for bioaerosol size and concentration repeatedly. Duration of measurements varied between 10 and 12.9 s. The APSS was connected to 6.35-mm-ID Tygon tubing that collected air in the first chamber at a location that was 0.53 m from the outlet, at a height of 0.495 m, and at a depth of 0.65 m. A Tygon tube was connected to the outlet of the APSS to return air into the chamber and prevent virus from escaping. Since the APSS had a low total volumetric flow rate of 0.18 m^3 h^{-1} (Topas 2010) relative to the airflow rates used in this study, its airflow rate effect was considered negligible and was not modelled in this study.

Two airflow (ventilation) rates of 34.0 m^3 h^{-1} and 135.9 m^3 h^{-1} and two bioaerosol generation rates of 14.8 ml h^{-1} and 33.0 ml h^{-1} were tested. These airflow rates were chosen to match the Midwest Plan Service (MWPS) recommended ventilation rates of 34.0 m^3 h^{-1} and 135.9 m^3 h^{-1} per head of sow and litter in cold and mild weather, respectively (MWPS 1983). The MWPS recommended maximum ventilation rate could not be achieved due to the limited fan capacity of the test system. The combinations of airflow rates and bioaerosol generation rates provided four treatments (Treatment 1: 34.0 m^3 h^{-1},14.8 ml h^{-1}; Treatment 2: 34.0 m^3 h^{-1}, 33.0 ml h^{-1}; Treatment 3: 135.9 m^3 h^{-1}, 14.8 ml h^{-1}; Treatment 4: 135.9 m^3 h^{-1}, 33.0 ml h^{-1}), which generated four different steady-state bioaerosol concentrations in the chambers. Each treatment was performed three times. The time required to reach steady-state was calculated to be 16 minutes and 4 minutes for airflow rates of 34.0 m^3 h^{-1} and 135.9 m^3 h^{-1}, respectively (La 2015).

4.3.2. Smoke test

A smoke test was performed for the airflow rate of 34.0 m^3 h^{-1} to qualitatively assess the movement of the airflow pattern, and specifically to confirm that: (a) the baffle installed to the inlet of the chamber was enough to direct airflow downward and allow for the bioaerosols to be well-distributed inside of the chamber, and (b) the airflow pattern demonstrated in the CFD simulation matched the airflow pattern observed in the smoke tests. Smoke cartridges (S103,

REGIN HVAC Products Inc., Oxford, CT) were lit and placed in the angled branch of the tee-wye (Y-shaped) fitting. Airflow patterns were video-recorded through an observation window made of Plexiglass.

4.3.3. CFD simulation of continuous phase (air)

Simulations were performed in ANSYS Workbench (18.1, ANSYS, Canonsburg, PA). Firstly, the geometry of the chambers was constructed in ANSYS DesignModeler. Some aspects of the chambers were simplified; most components before and after the inlet of the first chamber and outlet of the second chamber, respectively, were excluded from the geometry. In other words, the CFD simulation was focused on the chambers (Fig. 4.2). The mesh was designed in ANSYS Meshing. The mesh cell shape for the circular ducts, fittings, and baffles were unmodified from the default settings generated by ANSYS. The mesh cell shape of the chambers was modified from the default settings to tetrahedral cells (Fig. 4.2b), which increased the average mesh quality. Tetrahedral cells were chosen because they conformed better to the geometry of the chambers than hexahedral cells, especially at the entrance of the chambers where the baffles were located. The ANSYS User Guide also specifies that tetrahedral cells should be used in cases of relatively and extremely complex geometries (ANSYS 2013a). The circular faces on the circular-to-square fittings before and after the first and second chamber were set as the inlet and outlet, respectively. The remaining walls of the chambers, duct, baffles, and fittings were given a boundary condition of wall.

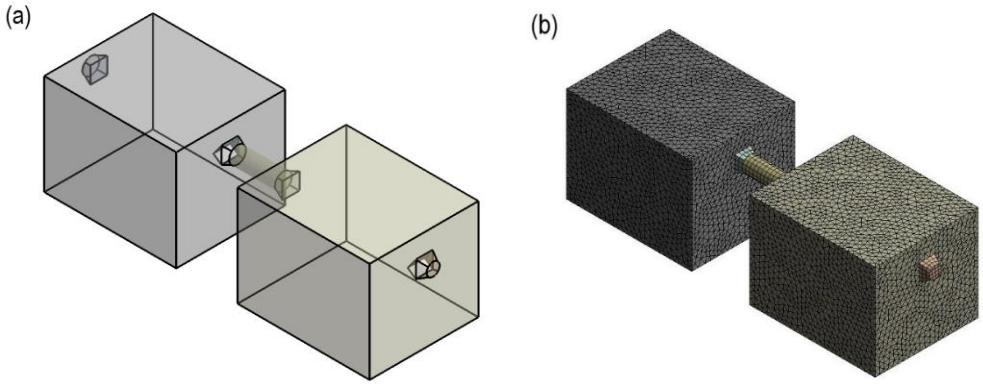

Figure 4.2. (a) Geometry of chambers and (b) Mesh with 0.05 m size cells in chambers and baffles

The boundary conditions at the inlet and outlet are indicated in Table 4.1. The velocity at the inlet and mass flow rate at the outlet were calculated from the measured airflow rate according to eqns. 4.1 and 4.2, respectively.

$$v = \frac{Q}{A} \tag{4.1}$$

$$M_{air} = Q \times \rho_{air} \tag{4.2}$$

where v = velocity (m s^{-1}),

M_{air} = mass flow rate of air exiting chambers (kg m^{-3})

Q = ventilation rate of the chambers (m^3 h^{-1}) (measured values were used in simulations).

A = area of the inlet (m^2)

ρ_{air} = density of air (1.19 kg m^{-3}).

Table 4.1. Boundary conditions of CFD simulation

Treatment	Boundary Condition	Type	Mass flow rate (kg s^{-1})	Velocity (m s^{-1})	Pressure (Pa)
1 and 2	Inlet	Velocity-inlet	N/A	0.75	-4.9768
	Outlet	Pressure-outlet	0.01124	N/A	-9.9536
3 and 4	Inlet	Velocity-inlet	N/A	2.98	-19.907
	Outlet	Pressure-outlet	0.04492	N/A	-39.814

The pressure at the inlet was set to be equal to the initial resistance due to the HEPA filter at the utilized airflow rate, which was provided by the manufacturer (Camfil 2017). The pressure at the outlet was two times the pressure at the inlet due to the presence of a second filter at the outlet.

There are several options of turbulence models in ANSYS Fluent. Given that the emphasis of this study was to validate the adequacy of CFD in simulating the discrete phase (aerosols), the standard k-ε model that was originally developed by Launder and Spalding (1972) was chosen to simulate the continuous phase (air) and avoid unnecessary convergence problems.

The pressure-velocity coupling scheme utilized was the SIMPLE-C Scheme. Momentum, turbulent kinetic energy, and rate of turbulent dissipation were solved using the

Second Order Upwind scheme. The Green-Gauss Node Based Scheme was used to solve for gradients for the Upwind scheme.

4.3.4. Discrete phase modeling of bioaerosols

Discrete phase modelling (DPM) was performed within ANSYS Fluent to solve for bioaerosol movement. It should be noted that the simulations were conducted to match the experimental conditions. Visual inspection of the chambers during experiments revealed that some bioaerosols generated by the nebulizer condensed along the tee-wye fitting before reaching the first chamber. Therefore, instead of using the bioaerosol generation rate specified for the nebulizer, the bioaerosol generation rates by the nebulizer were estimated as follows, based on the bioaerosol concentrations measured by the APSS during the experiments (La 2015).

$$M_{aerosol} = \frac{C_{measured} \times Q}{10^6 \times 3600} \tag{4.3}$$

where $M_{aerosol}$ = Modified bioaerosol generation rate (bioaerosol mass flow rate) (kg s^{-1}),

$C_{measured}$ = Bioaerosol concentration measured in chamber experiments (mg m^{-3}).

The velocity at which bioaerosols were injected into the chambers was assumed to be equal to the velocity of the continuous (air) phase at the entrance to the chamber. To simplify the simulation and reduce computational expenses, a uniform aerosol diameter was assumed in the CFD simulations. Bioaerosols usually have a size distribution that resembles a log-normal distribution (Cambra-López et al. 2010). Aerosol size variations could affect the simulation results, as aerosols of varied sizes behave differently in airflow. However, the size of droplet nuclei that are responsible for airborne disease transmission is normally in a narrow range. For example, Duguid (1946) reported that 97% of repository droplet nuclei were in a range of 0.5 to 12.0 µm. Yang et al. (2007) reported that 82% of droplet nuclei from coughing were in a narrow range of 0.74 to 2.12 µm. The size of the bioaerosols measured in this experimental study were in a range of 0.24 to 12.46 µm (as measured by the APSS). Therefore, the mass geometric mean diameters (1.15 to 1.53 µm) measured in the chamber experiment for each treatment were used as the diameters of the bioaerosols in the CFD simulations (Table 4.3) (La 2015). As discussed in the results, there was only a small relative difference in the steady-state bioaerosol

concentrations between measured and simulated values (2% to 8%); therefore, the assumption of a single uniform bioaerosol size did not drastically affect the simulation results of this study.

The general bioaerosol parameters used to perform discrete phase modelling are summarized in Tables 4.2 and 4.3. The density of the bioaerosols was assumed to be that of water at 20°C. The bioaerosols were specified to be inert, indicating that the bioaerosols would not be affected by temperature and phase change. This assumption was made as there were no reactants in the air that would cause the bioaerosols to change in size or disappear from the chamber air after the bioaerosols had reached a stable condition (i.e., no further evaporation induced shrinkage in bioaerosol size).

Table 4.2. DPM parameters for particle injection in CFD simulation

Parameter	Value
Type of injection	Surface injection (from inlet)
Particle Type	Inert
Material	Water-liquid
Density	998.2 kg m^{-3}
Drag-Law	Stokes-Cunningham
Stochastic tracking	Discrete walk model
Time constant	0.15

Table 4.3. DPM injection parameters for treatments 1 to 4

Treatment	$M_{aerosol}$ (kg s^{-1})	v (m s^{-1})	d_p (µm)	C_C	T (s)	t (s)	N
1	1.28×10^{-8}	2.98	1.508	1.11	300.608	0.05333	19200
2	1.77×10^{-8}	2.98	1.147	1.15	300.608	0.05333	19200
3	5.86×10^{-9}	0.75	1.526	1.11	1023.94	0.01342	22400
4	1.39×10^{-8}	0.75	1.416	1.12	1023.94	0.01342	22400

$M_{aerosol}$ – Aerosol mass flow rate, v – velocity of aerosols entering the chamber, d_p – diameter of aerosols, C_C – Cunningham Correction Factor, T – total simulation time, t – size of time step, N – total number of time steps

To determine which drag law to use in the simulation, the Stokes settling velocity and Reynolds number of the bioaerosols were calculated (eqn. 4.4 and 4.5, respectively). The Reynolds numbers of the bioaerosols were 6.7×10^{-6}, 5.4×10^{-6}, 6.5×10^{-6}, and 2.85×10^{-6} for

treatments 1, 2, 3, and 4, respectively. Since the Reynolds numbers were less than 10^{-4}, the Stokes-Cunningham drag law was used to compute the drag force acting on the bioaerosols (de Nevers 2017), with the Cunningham correction factors, which were calculated as per the Fluent Theory Guide (ANSYS 2013b; eqn. 4.6). The value of molecular mean free path that was utilized in eqn. 4.6 was measured at ambient pressure, a temperature of 298.15 K, and a relative humidity of 0% (Jennings 1988).

$$V_t = \frac{g d_p{}^2 (\rho_p - \rho_f)}{18\mu} \tag{4.4}$$

$$R_p = \frac{d_p V_t \rho_f}{\mu} \tag{4.5}$$

$$C_C = 1 + \frac{2\lambda}{d_p}\left(1.257 + 0.4\exp\left(\frac{-1.1 d_p}{2\lambda}\right)\right) \tag{4.6}$$

where V_t = Stokes settling velocity (m s^{-1}),

R_p = Reynolds number of the bioaerosol,

g = gravitational constant (m s^{-2}),

ρ_p = density of bioaerosol (kg m^{-3}),

ρ_f = density of air (kg m^{-3}),

μ = dynamic viscosity of air (1.845×10^{-5} kg m^{-1} s^{-1}),

C_C = Cunningham correction factor,

λ = molecular mean free path (6.691×10^{-8} m),

d_p = mean diameter (m)

Interaction of bioaerosols with the continuous phase (air) was activated to allow for unsteady tracking and injection of bioaerosols during the DPM simulation. The simulation time was subdivided into smaller time increments (steps). Parcels containing bioaerosols were generated into the chamber at the beginning of each time step and the movement of the generated bioaerosols were tracked during each time step. The simulation time chosen for the DPM was 60 s plus the time required for the bioaerosol concentration to reach steady-state within the chambers, as calculated in La (2015). The length of a time step and the total number of time

steps were calculated as indicated by the ANSYS Fluent User's Manual (eqn. 4.7 and 4.8, respectively; ANSYS 2013a).

$$t = \frac{x_{\min}}{v} \tag{4.7}$$

$$N = \frac{T}{t} \tag{4.8}$$

where t = length of time step (s),

x_{min} = minimum mesh size (m),

v = velocity of airflow during treatment (m s^{-1}),

N = total number of time steps for treatment,

T = simulation time, or time to steady-state (s).

4.3.5. Mesh refinement test

The influence of mesh size on the simulation results was tested by performing the same simulation using five meshes of different cell sizes. Firstly, the minimum cell size was set to 0.04 m for each tested mesh. The cell size of the two chambers and baffles were altered, while the cell size of the ducts and fittings were not altered. Body sizing was performed on the chambers and baffles to sizes of 0.0425 m, 0.045 m, 0.05 m, 0.0565 m, and 0.075 m. The number of cells per mesh is shown in Table 4.4.

Table 4.4. Mesh characteristics, number of nodes, combined volume of cells, and coordinate range of nodes used to determine mean aerosol concentration in mesh refinement tests

Mesh Characteristics			**Nodes surrounding measurement coordinate**			
Cell Size[A] (m)	# cells	# nodes	Combined volume of cells (m^3)	X	Y	Z
0.0425	506720	54	0.001777	0.428 - 0.529	0.434 - 0.535	0.477 - 0.578
0.045	415563	45	0.001758	0.415 - 0.522	0.452 - 0.559	0.488 - 0.573
0.05[B]	306117	35	0.001876	0.412 - 0.507	0.447 - 0.542	0.485 - 0.58
0.05625	218736	30	0.002289	0.410 - 0.516	0.442 - 0.548	0.482 - 0.589
0.075	92629	16	0.002894	0.401 - 0.507	0.459 - 0.566	0.473 - 0.58

[A] body sizing performed on mesh of the chambers and baffles

[B] 0.05 m mesh was chosen for the remaining simulations

Simulations of treatment 3 tests were then performed on each mesh. An airflow rate of 135.9 $m^3 h^{-1}$ resulted in airflow that was more turbulent than an airflow rate of 34.0 $m^3 h^{-1}$. Additionally, increasing the amount of particle generation in the CFD simulation increased the simulation time. Thus, treatment 3 was chosen to ensure that the mesh could accurately measure the airflow properties of the more turbulent airflow rate, while also decreasing the length of time required to run the multiple mesh refinement simulations.

The bioaerosol concentrations within the chambers were extracted at the final time step for each mesh. The bioaerosol concentrations measured in the experimental study were compared to the mean, standard deviation, and range of bioaerosol concentrations within the nodes surrounding the location where bioaerosol measurements were carried out. The bioaerosol concentration within the volume of cells surrounding the measurement point was calculated as per eqn. 4.9.

$$C_{surround} = \frac{\sum_{n_{node}} \left(C_{node} \times V_{node} \right)}{\sum_{n_{node}} V_{node}} \tag{4.9}$$

where $C_{surround}$ = bioaerosol concentration in cells surrounding measurement point (mg m^{-3}).

n_{node} = number of nodes surrounding the measurement point,

C_{node} = bioaerosol concentration at node (mg m^{-3}),

V_{node} = volume of cells adjacent to nodes (m^3).

4.3.6. Data analysis

4.3.6.1. Bioaerosol concentration

Results of the CFD simulation were collected from CFD-Post. For treatments 1 and 2, results were analyzed every 100 time steps, which was equivalent to every 10.667 s. For treatments 3 and 4, the results were analyzed every 400 time steps, which was equivalent to every 10.736 s. The coordinates of nodes, volume of cells, and bioaerosol concentration at nodes were exported to Excel Spreadsheets. Equation 4.9 was used to calculate the bioaerosol concentration in a zone consisting of nodes closest to where the experimental bioaerosol concentration measurements occurred. The simulated bioaerosol concentrations at steady-state

were compared to the measured bioaerosol concentrations using: (a) the six simulated bioaerosol concentration values prior to steady-state being accomplished; (b) the six simulated bioaerosol concentration values after steady-state was accomplished.

At the final time step (t=1023.936 s for treatments 1 and 2; t=300.608 s for treatments 3 and 4), the velocity and bioaerosol concentration profiles at the centerline of flow were captured by creating a plane along the XY plane at z=0.535 m and creating a contour profile on this plane. The overall bioaerosol concentration within the first chamber was also calculated (eqn. 4.10).

$$C_{chamber} = \frac{\sum_{n_{node,chamber}} \left(C_{node} \times V_{node}\right)}{\sum_{n_{node,chamber}} V_{node}} \tag{4.10}$$

where $C_{chamber}$ = bioaerosol concentration in the chamber (mg m^{-3}),

$n_{node,\ chamber}$ = number of cells in a chamber.

4.3.7. Normalized mean square error and fractional bias

ASTM specifies that indoor air quality models can be evaluated for their ability to calculate airborne pollutant concentration using the Normalized Mean Square Error (NMSE; ASTM 2008). ASTM standard D5157-97 specifies the equation and a threshold of 0.25 to indicate that the performance of the indoor air quality model is sufficient at predicting measured pollutants. Equation 4.11 was applied in this study. The NMSE was calculated for all measured bioaerosol concentrations. Because the APSS measurement durations varied from measurement to measurement, the time that bioaerosol concentration measurements occurred varied slightly between replicates. Additionally, the simulated bioaerosol concentrations occurred at slightly different times than the measured bioaerosol concentrations. To rectify the discrepancies in measurement time, the average time between replicates was compared to the CFD simulation time. Simulated bioaerosol concentrations were compared to measured bioaerosol concentrations with an average time between a range of the CFD simulation time ± 6.45 s. A value of 6.45 s was chosen as it is 0.5 times the maximum measurement duration for the APSS (12.9 s). Additionally, the NMSE was calculated at steady-state for each of the measurements.

The fractional bias (FB) was also calculated by using eqn. 4.12, according to ASTM D5157-97 (ASTM 2008). The standard recommends a threshold of ±0.25 to evaluate the

performance of the indoor air quality model. The FB was calculated during the span of the CFD simulation, comparing measured and simulated values at the time points specified for the NMSE. The FB was also calculated to compare steady-state measured and simulated bioaerosol concentrations.

$$NMSE = \frac{\sum_{i=1}^{n}\left(C_p - C_{oi}\right)^2 \Big/ n}{\left(C_p\right)\times\left(C_{o,average}\right)} \tag{4.11}$$

$$FB = 2\times\frac{\left(C_p - C_{o,average}\right)}{\left(C_p + C_{o,average}\right)} \tag{4.12}$$

where NMSE = normalized mean square error,

FB = fractional bias,

C_p = simulated bioaerosol concentration (mg m^{-3}),

C_{oi} = measured bioaerosol concentrations at replicate i of treatment test (mg m^{-3}),

$C_{o,average}$ = average measurement bioaerosol concentration (mg m^{-3}),

n = number of replicates per treatment.

4.4. Results

4.4.1. Mesh refinement test

The results of the mesh refinement tests are summarized in Table 4.5. The simulated bioaerosol concentrations calculated by eqn. 4.9 were identical to the mean simulated bioaerosol concentrations because the volumes of cells used to calculate the nodal bioaerosol concentrations did not differ much between tested meshes.

Table 4.5. Mean, standard deviation, and range of simulated aerosol concentration in nodes surrounding measurement point in mesh refinement tests

Mesh size in chambers (m)	**Aerosol concentration (mg m^{-3})**			
	Mean	SD	Range	% difference[A]
0.0425	0.35	0.06	0.23 - 0.49	2.8
0.045	0.37	0.06	0.25 - 0.49	2.8
0.05	0.36	0.06	0.22 - 0.47	--
0.5625	0.33	0.05	0.24 - 0.44	8.3
0.075	0.64	0.52	0.07 - 1.65	77.8

[A]compared to 0.05 m mesh

The mean simulated bioaerosol concentration was greater in the mesh size of 0.075 m than the other mesh sizes and there was also a greater variation in bioaerosol concentration between cells. The mean simulated bioaerosol concentration at this mesh size (0.64 mg m^{-3}) was also much greater than the experimental bioaerosol concentration (0.34 mg m^{-3}). Comparatively, utilizing mesh sizes of 0.04 m, 0.0425 m, 0.05 m, and 0.05625 m resulted in bioaerosol concentrations that were closer to the mean bioaerosol concentration. A mesh size of 0.05 m was chosen to be used for subsequent simulations as there was not a large (<3%) difference in mean bioaerosol concentration between mesh sizes of 0.05 m and 0.045 m as well as mesh sizes of 0.05 m and 0.0425 m. Also, this mesh size would require less computational resources in future simulations. Decreasing the mesh size results in an increase in the number of elements in the mesh. Because ANSYS Fluent calculates the airflow properties and tracks the particle movement within each element, increasing the number of elements requires more computer resources and more time to complete a simulation.

4.4.2. Model validation

4.4.2.1. Qualitative comparison of airflow pattern

A qualitative comparison of the experimental and simulated airflow patterns in the first chamber was accomplished using a smoke test when the fan was operating at a ventilation rate of 34.0 m^3 h^{-1}. Fig. 4.3 show the movement of smoke within the first chamber from 3 to 60 s, while the movement of bioaerosols in the CFD simulation of treatment 1 from 10 to 64 s is shown in

Fig. 4. Both the smoke images and simulations showed the air was directed downwards by the baffle. Additionally, the smoke did not initially enter the lower right corner of the chamber, which also occurred in the CFD simulation. In Fig. 4.3b-d, it can be noted that about 60 s was required for the smoke to fully distribute in the chamber. Similarly, about 60 s was required for the bioaerosols to distribute within the chamber in the CFD simulation (Fig. 4.4b-d). No further observations could be made after 60 s as the chamber was fully filled with thick smoke.

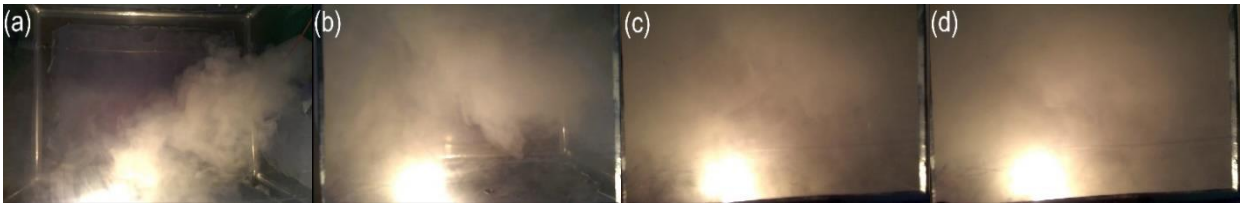

Figure 4.3. Distribution of smoke (grey / white cloud) in chambers (black background) during smoke test at ventilation rate of 34.0 m^3 h^{-1} at (a) 3 s, (b) 30 s, (c) 50 s, and (d) 60 s. White orb seen in pictures is a light source that was used to make smoke visible in video recording.

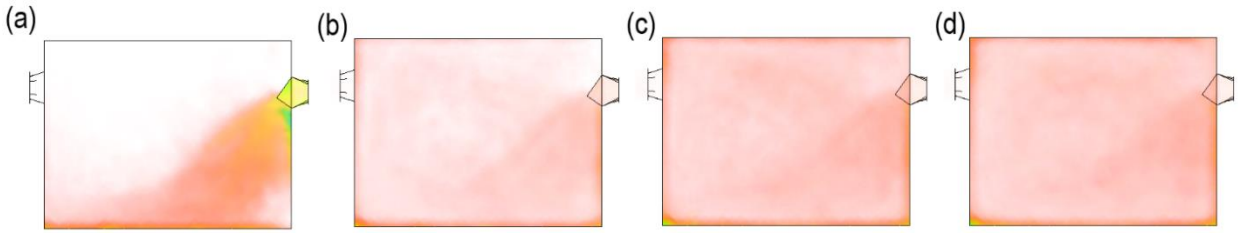

Figure 4.4. Volume rendering of particle concentration in first chamber during treatment one at (a) 10.67 s, (b) 32.01 s, (c) 53.35 s, (d) 64.02 s

The velocity profile at the centerline of the chambers is shown in Fig. 4.5. Since the boundary conditions for the continuous phase were the same for treatments 1 and 2, the velocity profiles for these two treatments were almost identical. A similar observation was made for the centerline velocity profiles of treatments 3 and 4. The velocity profiles also indicated that the airflow was directed diagonally downwards towards the floor by the baffles before the air moved up towards the outlet of the first chamber. The movement of air downwards at the entrance of the first chambers indicated that the baffles were correctly modelled, in terms of the geometry

and the boundary conditions, as this airflow pattern was also observed in the smoke test. A more detailed view of the velocity is shown in the velocity streamlines in the entire chamber system (Fig. 4.6). While the velocity streamlines of treatments 1 and 2 were not identical, the two streamlines had similar airflow patterns (only treatment 1 shown). A similar observation was made about the velocity streamlines of treatments 3 and 4 (only treatment 3 shown). Overall, the airflow moved in a clockwise direction in both the velocity streamlines, with no movement in the backwards direction.

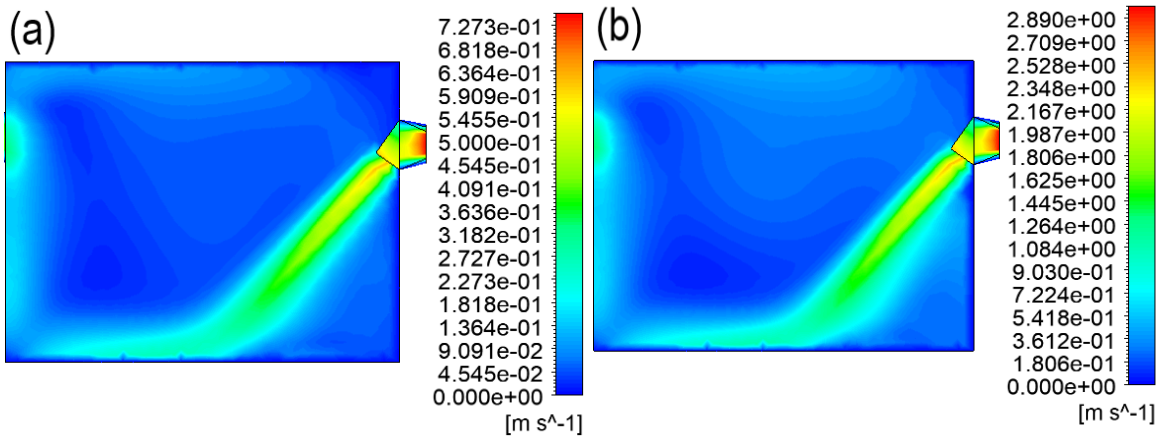

Figure 4.5. Velocity profiles at centerline of flow for (a) treatments 1 and 2, (b) treatments 3 and 4.

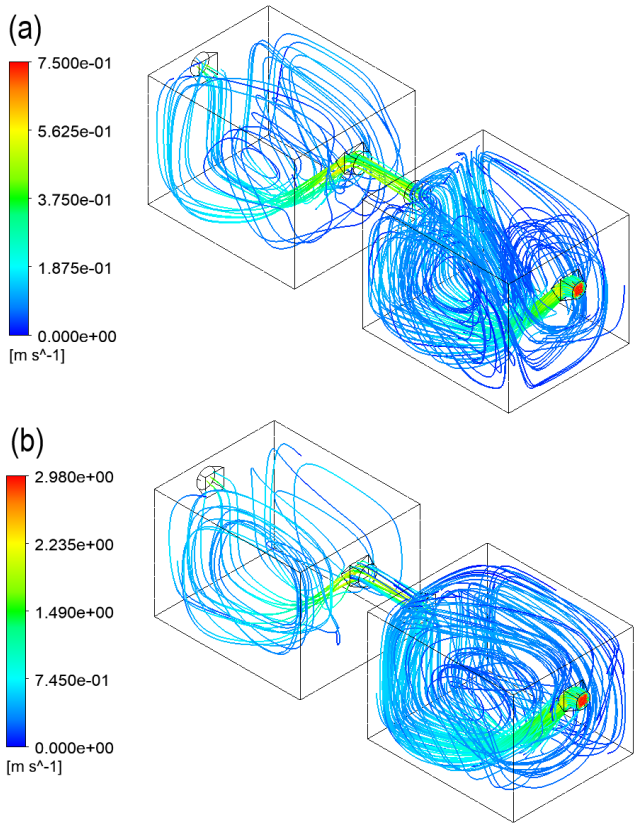

Figure 4.6. Velocity streamlines of (a) treatment 1 and (b) treatment 3 simulations.

4.4.2.2. Bioaerosol concentration

The change of bioaerosol concentration at the measurement point with time during the experiment and the CFD simulation are shown in Fig. 4.7. The NMSE and FB values used to evaluate the performance of the CFD simulation at predicting the measured bioaerosol concentration are shown in Fig. 4.8. The dashed lines in Fig. 4.8a and 4.8b indicate that the NMSE was below the good performance indicator of 0.25 and that the simulated results were acceptable. Similarly, the FB values between the two dashed lines in Fig. 4.8c and 4.8d indicate that the simulated bioaerosol concentrations were not biased and were acceptable. According to the NMSE and FB values, the majority of simulated bioaerosol concentrations after 400 s were good predictors of the measured bioaerosol concentrations for treatments 1 and 2. Similarly, for treatments 3 and 4, the majority of simulated bioaerosol concentrations predicted after 120 s were good predictors of the measured bioaerosol concentrations. In other words, the CFD simulations were adequate once the flow system reached steady-state, and the CFD simulations

could be improved for the transient state of the simulation (i.e., before steady-state was reached). In Fig. 4.7, it is evident that there was some variation in bioaerosol concentration between experimental replicates during the transient phase. This variation increases the difficulty of satisfying the NMSE and FB criteria.

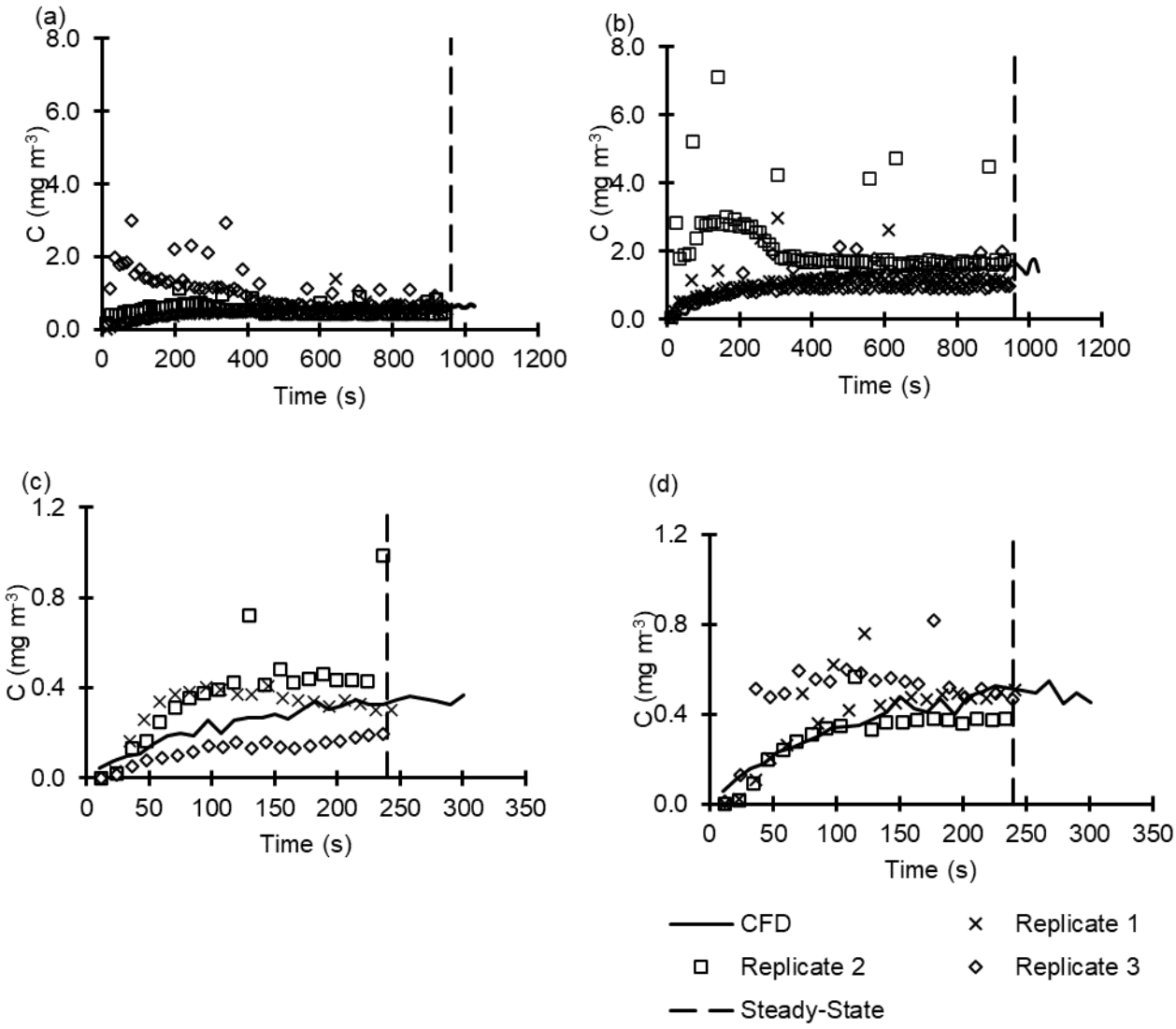

Figure 4.7. Change in aerosol concentration with time during experiments and CFD simulation for (a) treatment 1, (b) treatment 2, (c) treatment 3, and (d) treatment 4. The dashed line indicates the time in the simulation and experiments at which the steady-state concentration was reached.

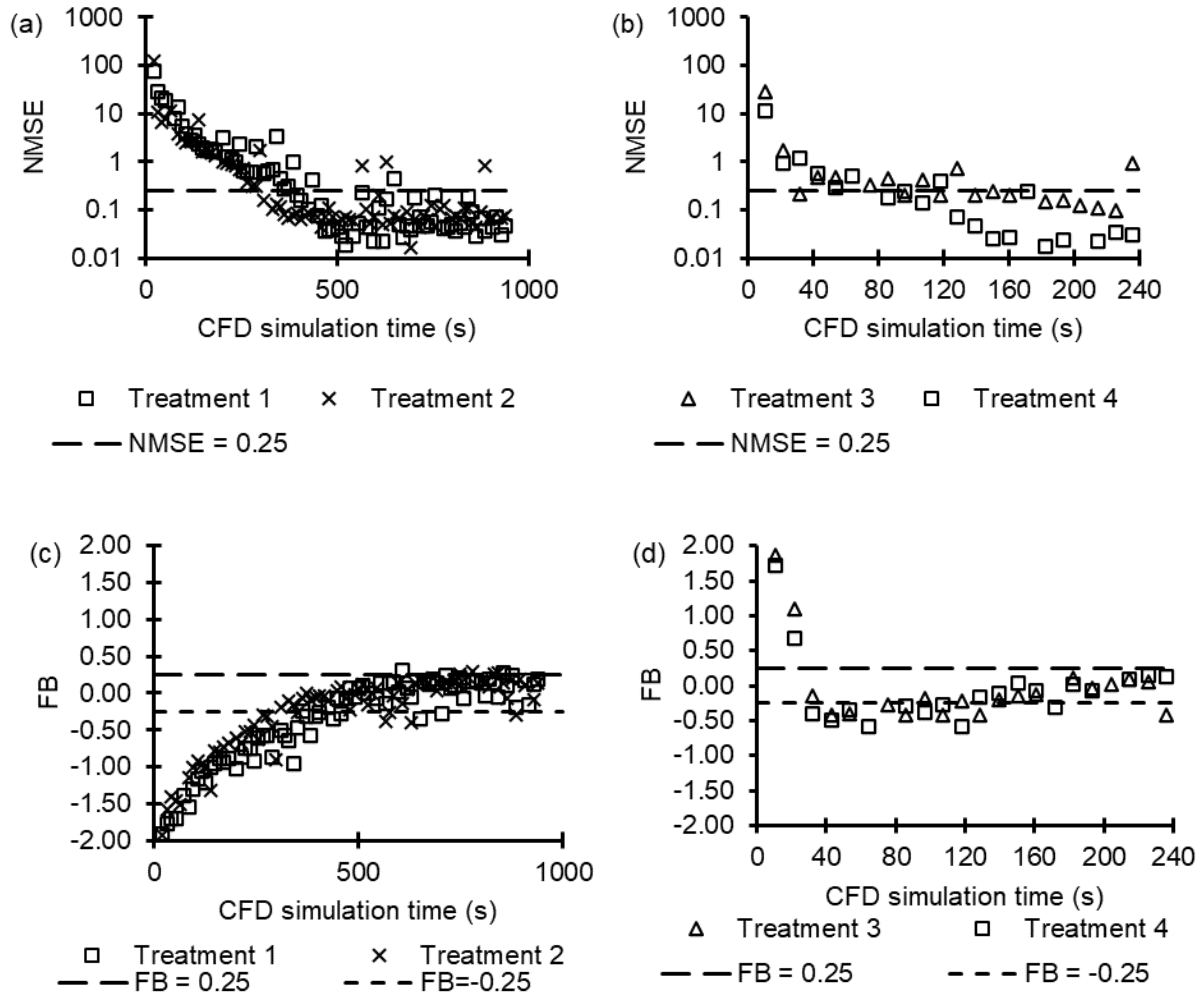

Figure 4.8. Parameters for evaluating the performance of CFD simulations at predicting experimental aerosol concentrations: (a) NMSE for treatments 1 and 2, (b) NMSE for treatments 3 and 4, (c) FB for treatments 1 and 2, and (d) FB for treatments 3 and 4. Values lower than the dashed line in (a) and (b), and the area between the dashed lines in (c) and (d) indicate the NMSE and FB values, respectively, that show that model is not biased and performed adequately according to ASTM standards.

Overall, the steady-state concentrations generated by the CFD simulations compared well with the measured bioaerosol concentrations in all treatments. A comparison of the measured and simulated bioaerosol concentrations at the measurement point and three evaluation techniques is presented in Table 4.6. The mean measured bioaerosol concentration was

calculated from the results of three replicates per treatment. For each replicate, the average of six bioaerosol concentration measurements that occurred before steady-state was calculated; the three replicate average values were calculated to obtain the steady-state measured bioaerosol concentration per treatment. Additionally, there are two mean simulated bioaerosol concentrations per treatment. The first and second CFD values are the averages of six data points before and after steady-state was reached, respectively. In terms of relative difference, the simulated bioaerosol concentrations compared well to the measured bioaerosol concentrations, with the lowest and highest differences occurring in treatment three and four (2%) and treatment 1 (8%), respectively. In terms of both NMSE and FB, the steady-state simulated bioaerosol concentrations for all treatments met the criteria provided by ASTM. The lowest and highest NMSE were 0.01 and 0.19 for treatments 1 and 3, respectively, while the lowest and highest FB were 0.02 and 0.08 for treatments 3 and 4, and 1, respectively.

Table 4.6. Comparison of measured and simulated aerosol concentrations (mg m^{-3}) at steady-state using Normalized Mean Square Error (NMSE), Fractional Bias (FB), and relative difference.

Treatment	**1**		**2**		**3**		**4**	
	Mean	SD	Mean	SD	Mean	SD	Mean	SD
Measured	0.62	0.06	1.47	0.64	0.34	0.18	0.47	0.09
CFD (before SS[A])	0.65	0.03	1.54	0.13	0.33	0.01	0.48	0.04
CFD (after SS[B])	0.67	0.03	1.54	0.17	0.35	0.01	0.49	0.04
NMSE[C] before SS	0.01		0.10		0.19		0.02	
NMSE after SS	0.01		0.10		0.18		0.02	
FB[D] before SS	0.05		0.04		-0.04		0.02	
FB after SS	0.08		0.03		0.02		0.04	
Difference before SS (%)	5		4		4		2	
Difference after SS (%)	8		4		2		5	

[A] before SS = average of six measurements before steady-state reached (960s for treatments 1 and 2; 240 s for treatments 3 and 4)
[B] after SS = average of six measurements after steady-state reached (approximately 960 s to 1024 s for treatments 1 and 2; approximately 240 s to 300 s for treatments 3 and 4).
[C] NMSE less than 0.25 shows that the CFD simulation met ASTM criterion for predicting the measured aerosol concentrations.
[D] FB between -0.25 and 0.25 shows that the CFD simulation met the ASTM criterion for predicting the measured aerosol concentration.

The average and range of simulated bioaerosol concentrations in chamber 1 are shown in Table 4.7. The non-uniform distribution of bioaerosols was evident in the profiles of simulated bioaerosol concentration at the centerline of the chambers (Fig. 4.9). The distribution of bioaerosols for treatments 1 and 2 were similar, albeit the magnitudes of bioaerosol concentration were different. Similar patterns were also observed for treatments 3 and 4. Higher concentrations of bioaerosols were visible at some locations, such as the left bottom edge of the chamber. This was probably because these areas had stagnant airflow, resulting in accumulation of bioaerosols. The stagnant zone is evident in Fig. 4.5, where the lighter colours in the corners indicate lower airflow velocity. In contrast, areas with higher velocity airflow had lower bioaerosol concentration. This can be confirmed by comparing the velocity profile (Fig. 4.5) and bioaerosol concentration profiles (Fig. 4.9). While the CFD simulations predicted the patterns of bioaerosol distribution in the chamber, the predictions could not be validated by the experimental data in this study because bioaerosols were measured at only one location. More measurements at different locations in the chamber would be required to fully validate the spatial distribution simulated by the CFD model.

Table 4.7. Average and range of simulated aerosol concentrations (mg m^{-3}) in the first chamber.

Treatment	Average	Range
1	1.13	0.2 - 70.9
2	2.68	0.5 – 177.0
3	0.78	0.1 - 120.1
4	1.08	0.1 - 164.0

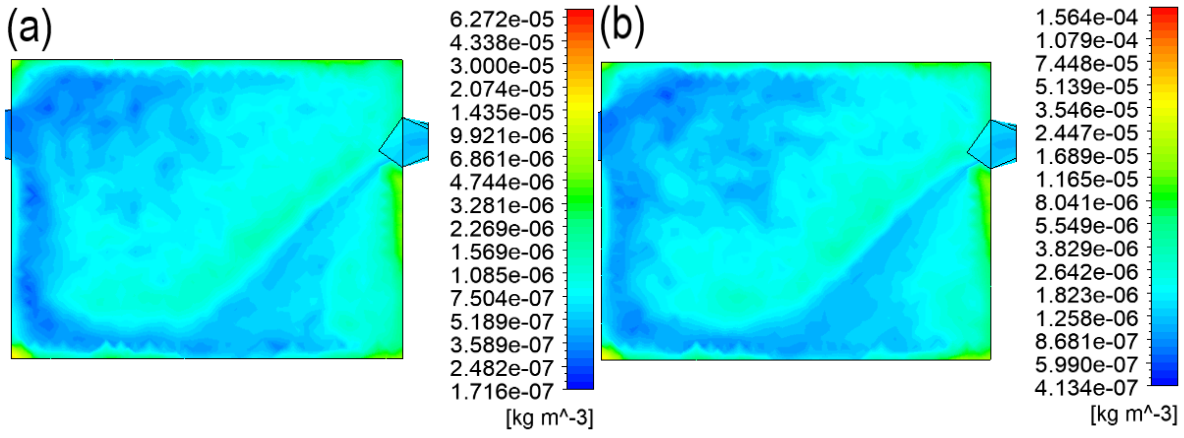

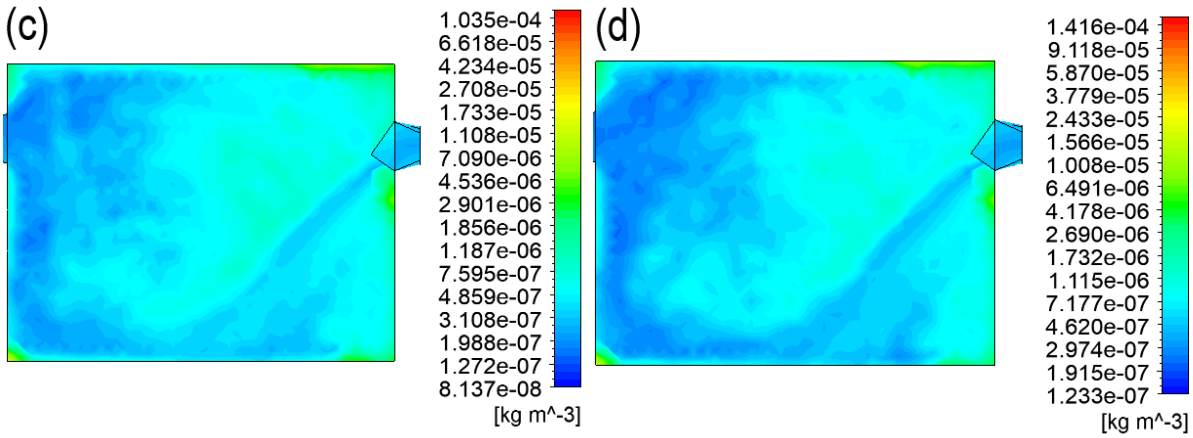

Figure 4.9. Aerosol concentration in chamber 1 at centerline of flow during steady-state in (a) treatment 1, (b), treatment 2, (c) treatment 3, and (d) treatment 4.

4.5. Conclusions of journal paper

The CFD modeling of the airflow pattern and aerosol concentration within the mechanically-ventilated chambers was successful. The CFD simulations replicated the airflow behaviour observed in the smoke test. The CFD simulations performed within the NMSE and FB guidelines for indoor air quality models as the aerosol concentration reached steady-state (i.e., after 400 s for treatments 1 and 2, and after 120 s for treatments 3 and 4). At steady-state, the lowest and highest differences occurred in treatments three and four (2%), and treatment 1 (8%), respectively, and all the treatment simulations met the NMSE and FB criteria provided by ASTM. However, the simulations were not within the NMSE and FB criteria during the transient stage of the simulation. This paper also indicated the importance of including mesh refinement tests within CFD simulations, as the mesh size can affect the accuracy of the simulated results. The mesh refinement tests indicated that a predominant cell size of 0.05 m was appropriate in this application.

4.6. Acknowledgements

We would like to thank Manitoba Pork and Manitoba Rural Adaptation Council (MRAC) for their funding support. We would also like to thank Dr. David Levin and Dr. Kevin Coombs for their technical expertise during the experimental phase of this study as well as Dr. Kevin Coombs for providing the PRRSV utilized in this study.

Chapter 5. Dose-response modelling of infectious animal diseases coupled with computational fluid dynamics: A simulation of airborne porcine reproductive and respiratory syndrome virus

Chapter Four discusses the contribution of a journal paper titled "Dose-response modelling of infectious animal diseases coupled with computational fluid dynamics: A simulation of airborne porcine reproductive and respiratory syndrome virus". Co-authors of the paper are Dr. Qiang Zhang, Dr. Nazim Cicek, Dr. David Levin, and Dr. Kevin Coombs. This journal paper was published in and follows the formatting standards of Biosystems Engineering. The citation of this paper is: La, A., Zhang, Q., Cicek, N., Levin, D. B., & Coombs, K. M. (2021). Dose–response modelling of infectious animal diseases coupled with computational fluid dynamics: A simulation of airborne porcine reproductive and respiratory syndrome virus. *Biosystems Engineering*, 208, 58–78. https://doi.org/10.1016/j.biosystemseng.2021.05.005.

Portions of the originally published paper were removed from this thesis, specifically the literature review, to reduce repeated information.

5.1. Abstract

Dose-response modelling was performed for several infectious disease viruses using the exponential, exact beta-Poisson, and approximate beta-Poisson models using existing datasets of animal infections. The exact beta-Poisson model was found to provide the best fit of the three models. The aerosol transmission route was found to require the lowest dose to cause infection compared to the intra-nasal and oral transmission routes for porcine reproductive and respiratory syndrome virus (PRRSV) and H9N2 avian influenza virus. Foot and mouth disease virus required lower doses with the aerosol transmission route than the intra-nasal transmission route. Liquid oral transmission required lower doses than feed transmission to cause infection for African swine fever virus and overall oral transmission required low doses to cause infection by porcine epidemic and diarrhoea virus. A computational fluid dynamics simulation was coupled with the dose-response modelling to simulate aerosol transmission of PRRSV in two experimental case studies. The coupled model predicted a probability of infection between 82% and 100% using the exact beta-Poisson model, which was in good agreement with the observed rate of infections in the two experimental case studies (84% and 90%).

5.2. Introduction

CFD can be coupled with dose-response models to gain a fuller picture of disease transmission, particularly aerosol transmission. Dose-response models could be used to predict the probability of infection based on the exposure to the pathogen (concentration and duration) calculated by CFD. However, limited studies combining dose-response modelling with CFD have been reported in the literature, which is an important aspect in trying to understand the overall dynamics of aerosol transmission of diseases.

The objectives of this study are to: (1) perform dose-response modelling with existing literature datasets to understand the effect of transmission route on the infectious doses of five infectious animal viruses; and (2) couple dose-response modelling with a CFD simulation to determine the probabilities of infection by aerosol transmission of PRRSV in two case studies.

5.3. Materials and Methods

5.3.1. Compilation of data from literature

A literature review was performed to compile the reported experimental data on animal exposures to different doses of viruses and the infection rates after exposure. Publications with datasets that facilitated further analysis included the exposure doses, the total inoculated animals per dose, and the number of infected animals per dose, or the publications had sufficient data to determine these parameters. The literature search focused on viruses associated with diseases that are currently significant to the livestock/poultry industry, including PRRSV, AIV, FMDV, ASFV, and PEDV. For AIV, there were two virus subtypes included in this study, which were H9N2 AIV and H5N1 AIV. The subtype H9N2 is a low pathogenic subtype of AIV, whilst H5N1 is a highly pathogenic subtype of AIV. Table 5.1 summarises the datasets that were compiled and used in this study.

Table 5.1. Summary of datasets compiled from literature for dose-response modelling.

Author	Virus (Strain)	Animal	Transmission route	Dose units[c]
Hermann et al. (2009)	PRRSV (VR-2332)	Pigs	Aerosol	$TCID_{50}$
Hermann et al. (2005)	PRRSV (VR-2332)	Pigs	Intranasal	$TCID_{50}$
Hermann et al. (2005)	PRRSV (VR-2332)	Pigs	Oral	$TCID_{50}$
Guan et al. (2013)	H9N2 AIV (A/Ck/HN/1/98)	Chickens	Aerosol	EID_{50}
Guan et al. (2013)	H9N2 AIV (A/Ck/HN/1/98)	Chickens	Intranasal	EID_{50}
Guan et al. (2013)	H9N2 AIV (A/Ck/HN/1/98)	Chickens	Oral	EID_{50}
Agranovski et al. (2010)	H5N1 (A/Chicken/Suzdalka/Nov-11/2005)	Chickens	Aerosol[a]	FFU
Spekreijse, Bouma, Stegeman, Koch, & de Jong (2011)	H5N1 AIV (A/Turkey/Turkey/1/2005 H5N1)	Chickens	Intranasal / Intratracheal	EID_{50}
Hughes, Kitching, & Woolhouse (2002)	FMDV (O/Greece/23/94)	Sheep	Intranasal	$TCID_{50}$
Gibson & Donaldson (1986)	FMDV (O1 strain BFS 1860)	Sheep	Natural Aerosol	$TCID_{50}$
Donaldson et al. (1987)	FMDV (O1 strain BFS 1860)	Cows	Artificial Aerosol	$TCID_{50}$
Donaldson et al. (1987)	FMDV (SAT 2 SAR 3/79)	Cows	Natural Aerosol	$TCID_{50}$
Niederwerder et al. (2019)	ASFV (Georgia 2007/1 isolate)	Pigs	Oral by feed	$TCID_{50}$
Niederwerder et al. (2019)	ASFV (Georgia 2007/1 isolate)	Pigs	Oral by liquid	$TCID_{50}$
Howey et al. (2013)	ASFV (Malawi Lil-20/1)	Pigs	Nasopharyngeal	HAD_{50}
Howey et al. (2013)	ASFV (Malawi Lil-20/1)	Pigs	Oropharyngeal	HAD_{50}
Liu et al. (2015)	PEDV (PC22A)	Pigs	Oral[b]	PFU
Schumacher et al. (2016)	PEDV (USA/IN19338/2013)	Pigs	Oral by feed	$TCID_{50}$ g^{-1} [feed]
Thomas et al., (2015)	PEDV (USA/IN19338/2013)	Pigs	Orogastrically	$TCID_{50}$

[a] Measured lethal aerosol dose, [b] Measured the diarrhoea oral dose, [c] Virus quantification in laboratory in terms of $TCID_{50}$ – 50% tissue culture infectious dose, EID_{50} – 50% embryo infectious dose, FFU – focus forming units, HAD_{50} - 50% hemadsorbing dose, PFU – plaque forming units

5.3.2. Stochastic dose-response modelling

Three stochastic dose-response models were used in this study to model the probability of infection upon exposure to varying levels of virus. The first model, the exponential model (EM) is defined in Eq. (5.1). It assumes that pathogens follow a Poisson distribution in the environment and all pathogens have an equal probability of surviving and infecting the host, which is defined by *r* in the model (Brouwer et al., 2017; Sze To & Chao, 2010). The second model, the exact beta-Poisson model (EBPM) is defined in Eq. (5.2) and assumes that pathogens follow a Poisson distribution in the environment, whilst the probability of individual pathogens surviving and causing infection varies on a beta distribution. Specifically, the constant parameter *r* in the exponential model is replaced with a beta function (Brouwer et al., 2017; Sze To & Chao, 2010). The third model, the approximate beta-Poisson model (ABPM) is defined in Eq. (5.3) and is a mathematically-simplified version of the exact beta-Poisson model, with an approximation probability function originally proposed by Furumoto & Mickey (1967).

$$P(D,\theta) = 1 - \exp(-rD) \tag{5.1}$$

$$P(D,\theta) = 1 - {}_1F_1(\alpha, \alpha+\beta, -D) \tag{5.2}$$

$$P(D,\theta) = 1 - \left(1 + \frac{D}{\beta}\right)^{-\alpha} \tag{5.3}$$

where $P(D, \theta)$ is the probability of infection as a function of dose and parameters θ, θ are the dose-response parameters, r is the probability of a single virus particle causing an infection (Schmidt et al., 2013). D is the dose of an infectious pathogen, ${}_1F_1$ is the Kummer confluent hypergeometric function and α, β are the parameters describing the shape of the Kummer confluent hypergeometric function.

The model parameters r, α, and β were determined by fitting compiled experimental data to the model equations using the maximum likelihood estimation (MLE) method on the binomial likelihood function (Eq. (5.4); Brouwer et al., 2017). The curve fitting processes were carried out with R programming language (R Core Team, 2017) using the software RStudio (RStudio Team, 2016). A general-purpose optimisation was performed with the Nelder-Mead algorithm on the log-likelihood equations to obtain estimates of parameters that provide the minimum log-likelihood value. In the EBPM probability equation, the Kummer confluent hypergeometric function was inputted using the GSL library in R (Hankin, 2006). Plots were constructed using the ggplot2 library in R (Wickham, 2009).

$$\log\left(L(\theta)\right) = \sum_i \left(\log \frac{k_i!}{k_i!(n_i - k_i)!} + k_i \log\left(P\left(D,\theta\right)\right) + \left(n_i - k_i\right)\log\left(1 - P\left(D,\theta\right)\right)\right) \tag{5.4}$$

where $L(\theta)$ is the likelihood as a function of parameters θ, i is the dose of infectious pathogen (various units), k_i is the number of infected pigs at dose level i, and n_i is the number of exposed pigs at dose level i.

The uncertainty of the parameters was determined with a Bayesian analysis using Markov chain Monte Carlo (MCMC) simulations, which provided posterior distributions for each parameter (Schmidt et al., 2013). The MCMC simulations were executed in RStudio using the R2OpenBUGS library (Sturtz, Ligges, & Gelman, 2005) to access the program OpenBUGS (3.2.3 rev 1012, OpenBUGS Project Management Group, UK). The OpenBUGS codes used to perform the MCMC simulations for the EM, EBPM, ABPM were obtained from Schmidt et al.

(2013). Each simulation consisted of 3 Markov chains, 10,000 burn-in iterations, 200,000 iterations after the burn-in, and a thinning interval of 10. Exceptions include the intra-nasal dataset of Hermann et al. (2005) and the aerosol dataset from Guan et al. (2013), which required 100,000 burn-in iterations and a thinning interval of 100 to converge. The initial values of r in EM for each Markov chain were randomised with values between 0 and 1. The initial values of α and β in EBPM and ABPM for each Markov chain were chosen as random values from a normal distribution with a mean of 0 and a standard deviation of 1. This was the method used in example cases to generate initial values for parameters in MCMC simulations (Su & Yajima, 2020). Post-processing of data was performed using the coda library (Plummer, Best, Cowles, & Vines, 2006), including the Gelbin-Rubin convergence analysis to check for convergence at the end of MCMC simulations. The 2.5 and 97.5 percentile (95% confidence interval) of r, α, and β was obtained from the posterior distribution of values. The maximum likelihood estimation (MLE), 2.5-percentile estimate, and 97-5 percentile estimate for the parameters were inserted into the models to obtain three probability curves per dataset and dose-response model combination. The dose that corresponded to a probability of infection of 0.5 (i.e., the infectious dose 50 or ID_{50}) was determined for each probability curve.

5.3.3. CFD simulation of a case study

A case study was carried out based on the results of experiments reported by Dee, Batista, et al. (2006) and Dee, Deen, et al. (2006). In their experiments, individual pigs placed in a two-chamber system were exposed to aerosolised PRRSV (a modified live vaccine strain was used) and infection of pigs due to aerosol transmission of PRRSV was quantified. Specifically, PRRSV aerosols were generated inside the first chamber by a fogger for 5.5 min, whilst a pig was placed in the second chamber. After aerosols of PRRSV were generated, the fan connecting the two chambers was activated, drawing air and PRRSV aerosols from the first chamber into the second chamber. The aerosol exposure in the experiments lasted 6 h. This reported experimental system was used in the current study to develop and test a CFD simulation model coupled with dose-response modelling. The CFD simulation tracked the movement and distribution of PRRSV aerosols over time, based upon which the aerosol dose was calculated and used in the aerosol transmission dose-response models for PRRSV to predict the probability of infection of pigs in the second chamber.

The CFD simulations were performed using Fluent in ANSYS Workbench (18.1, ANSYS, Canonsburg, PA, USA). The geometry of the two-chamber system used in the experiments of the case study is shown in Fig. 5.1. The chamber height, width, and depth were 1.8 m, 1.3 m, and 1.3 m, respectively, and the duct height, width, and depth were 0.65 m, 1.3 m, and 0.65 m, respectively. The diameter of the outlet was 0.2 m and the area of the inlet was 0.4 m^2. Some of the dimensions were assumed as they were not provided in the published papers, including the locations of the duct, inlet, and outlet as well as the length and width of the inlet.

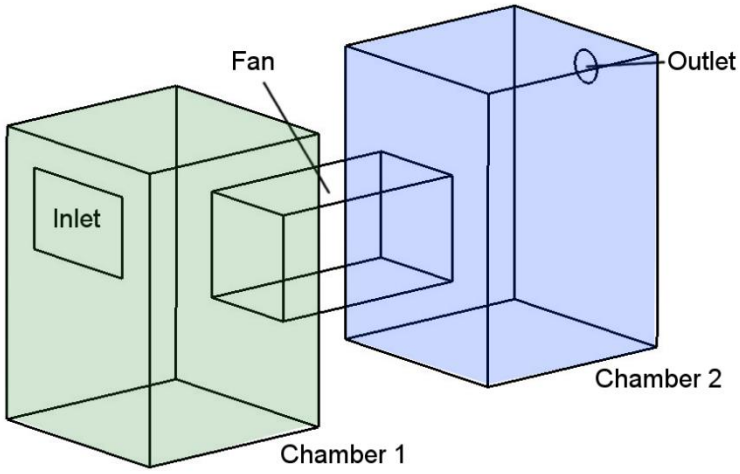

Figure 5.1. Geometry of the two-chamber system used in the CFD simulation. The green area indicates where aerosols were generated at the beginning of the CFD simulation and the blue area indicates where the aerosol concentration was calculated every 0.5s timestep. The fogger and the pigs (not simulated) were placed in the first and second chamber, respectively Dee, Batista, et al. (2006) and Dee, Deen, et al. (2006). Each chamber had a height, width, and depth of 1.8 m, 1.3 m, and 1.3 m, respectively. The duct height, width, and depth were 0.65 m, 1.3 m, and 0.65 m, respectively. The outlet diameter was 0.3 m, and the inlet area was 0.4 m^2.

Mesh selection was accomplished by comparing the aerosol concentration in the second chamber between three meshes for the first 12 s of simulation time. The coarse, moderate, and fine meshes had mesh sizes of 0.1 m, 0.075 m, and 0.0575 m, respectively, and had element counts of 98,167, 205,000, and 422,402, respectively. The aerosol concentration in the second chamber between the moderate and fine meshes, as well as the coarse and moderate meshes, were compared. Aside from the first two time steps in which aerosols were still entering the

second chamber (4.5 to 5.0s), the difference in aerosol concentration between meshes was less than ±10% during the first 12 s of simulation. After taking into consideration the computational time and resources that were required to run a discrete particle simulation, the moderate-sized mesh (0.075 m) was chosen to perform the remaining simulation. The chosen mesh was constructed out of 205,000 tetrahedral elements, with an average mesh quality of 0.8853, and an average skew of 0.14112.

The boundary conditions and discretisation schemes are shown in Table 5.2. The simplest approach in determining the inlet boundary condition was to utilise a velocity-inlet boundary condition, as the inlet velocity could be calculated from the ventilation rate (375 $m^3 h^{-1}$) and the cross-sectional area of the inlet (0.4 m^2) that were provided in the experimental studies. The mass flow rate at the outlet was calculated using the ventilation rate and density of air. The standard k-epsilon turbulence model was used (Launder & Spalding, 1972).

5.3.3.1. Aerosol properties

The size range of the aerosols produced by the fogger in the experiments of Dee, Batista, et al. (2006) and Dee, Deen, et al. (2006) was not available from the manufacturer's website at the time the simulation work was performed. Therefore, the aerosol size range was assumed to be equal to the size range produced by a similar fogger manufactured by the same company (i.e. 5 to 50 μm; Sanitizer, Curtis Dyna-fog, Jackson, GA, USA). The standard deviation and the mean of the logarithmic size range were calculated, with the assumption that the particle sizes followed a log-normal distribution (Eqs. (5.5) and (5.6), respectively). The normal-distribution function in Microsoft Excel was used with the logarithmic particle sizes, mean, and standard deviation as inputs to estimate the fraction of particles at specific sizes.

$$SD = \frac{\ln(p_{\max}) - \ln(p_{\min})}{6} \tag{5.5}$$

$$p_{mean} = \ln(p_{\min}) + 3 \times \ln(SD) \tag{5.6}$$

where SD is the standard deviation of the normal distribution of the logarithmic particle sizes, p_{max} is the maximum particle size (i.e. 50 μm), p_{min} is the minimum particle size (i.e. 5 μm) and p_{mean} is the mean of the normal distribution of the logarithmic particle sizes.

To simulate the airflow and aerosol transport condition, two assumptions were made to decrease computational time of the simulation. Firstly, it was assumed that the aerosols were evenly distributed in the first chamber at the start of the simulation. Secondly, particles > 10 μm were excluded from the simulation because they have little chance of entering the lower respiratory tract. Knight (1980) reported that <10% of hygroscopic particles with particle sizes of 6 μm deposited in the lower respiratory tract of humans and that an insignificant amount of deposition in the lower respiratory tract occurred for particle sizes of >20 μm. Asgharian et al. (2016) modelled the respiratory tract of a pig and reported that >80% of 10 μm particles deposited in the upper respiratory tract and that increasingly more particles were deposited inside the lower respiratory tract of pigs as the particle size decreased. Thus, particles > 10 μm in size were considered unlikely to deposit into the lower respiratory tract and therefore contribute little to the exposure dose of aerosol transmission. Aerosols with aerodynamic diameters of 0.25, 0.5, 0.75, 1, 2, 3, 4, 5, 6, 7, 8, 9, and 10 μm were generated in the simulation based on a log-normal distribution. The mass injection rate of each aerosol size per node was calculated using Eq. (5.7). The aerosols were introduced into the chamber at a single time step of 0.002 s. ANSYS Fluent requires the injection rates be inputted in units of mass per second and modifies the inputted injection rates to match the inputted time step size. To ensure that the correct aerosol injection rate was achieved, the mass rate of aerosols at each aerosol size was calculated in units of kg per 0.002 s per node, with a conversion factor added to the calculation to offset the internal calculations in ANSYS Fluent. A total of 212,888 particles were injected with a total mass of 0.112 kg during simulation. The movement of aerosols was tracked for 200 s. Although the simulation could have continued up to 6 h as per the length of aerosol exposure in the case studies, continuing the simulation would have resulted in little change in the calculated probability of infection values; thus, the simulation was terminated at 200 s. A summary of the input parameters for the discrete phase is shown in Table 5.2.

$$M_X = \frac{f_X \times V_S \times \rho_S \times cf}{N} \quad (5.7)$$

where X is the aerodynamic diameter of aerosols (μm), M_X is the mass rate of aerosols with aerodynamic diameter X that are injected into a node during the first time step (kg 0.002 s^{-1} $node^{-1}$), N is the number of nodes in the mesh, f_X is the fraction of aerosols with aerodynamic diameter X, V_s is the volume of stock solution of PRRSV aerosolised in experiment (0.001 m^3), ρ_s is the density of stock solution (998.2 kg m^{-3}) and cf is a conversion factor for initial time step size (500).

Table 5.2. CFD input parameters

Mesh	Element type	Tetrahedron
	Element size	0.075m
	No. Elements / Nodes	205,000 / 37,513
Air properties	Density	1.19 kg m^{-3}
Boundary conditions	Inlet	Velocity-inlet Velocity = 0.260 m s^{-1} Supersonic / Initial gauge pressure = 0 Pa Turbulent intensity = 5% Turbulent viscosity ratio = 10
	Outlet	Pressure-outlet Mass flow rate = 0.124 kg s^{-1} Pressure = 0 Pa Backflow turbulent intensity = 5% Backflow turbulent viscosity ratio = 10
	Wall	Enhanced wall treatment
Models	Turbulence	Standard k-ε
Discretisation Schemes	Pressure-velocity coupling	Simple C
	Gradient	Green-Gauss Node Based Gradient
	Pressure	Second order
	Momentum	Second order upwind
	Turbulent kinetic energy	Second order upwind
	Turbulent dissipation rate	Second order upwind
	Transient formulation	First order implicit
Discrete phase modelling	Interaction	Interaction with continuous phase with discrete phase model source update every flow iteration
	Time step size	0.002 s for initial injection 0.0005 s for rest of simulation
	Iterations per time step	50 for first 0.02 s of simulation 15 – 20 for rest of simulation
	Iterations between discrete phase modelling tracking	50 for first 0.02 s of simulation 15 – 20 for rest of simulation
Particle attributes	Type of injection	Custom injection (Eq. (5.7)) - Evenly distributed at node locations in chamber 1 at the beginning of simulation
	Sizes generated	0.25, 0.5, 0.75, 1, 2, 3, 4, 5, 6, 7, 8, 9, and 10 μm
	Particle type	Inert, water-liquid
	Density	998.2 kg m^{-3}
	Drag Law	Stokes-Cunningham
	Cunningham Coefficient	1
	No. particles (mass) generated	212,888 particles (0.112 kg)
	Stochastic Tracking	Discrete random walk model with time constant of 0.15

5.3.3.2. Calculation of exposure dose from CFD simulation

The average aerosol concentration in the second chamber where pigs were placed was calculated at a time interval of Δt = 0.5 s (Eq. (5.8)). The PRRSV doses inhaled by pigs were then calculated every 0.5 s of simulation time using the aerosol concentrations (Eq. (5.9)), in which the respiration rates for 12-kg and 25-kg pigs were assumed to be 3.96×10^{-5} and 8.25×10^{-5} m^3 s^{-1}, respectively (Hannon, Bossone, & Wade, 1990). The cumulative (total) PRRSV exposure dose was the sum of all 0.5-s doses over the 200 s simulation.

$$C_a = \frac{\sum_N (C_{node} \times V_{node})}{\sum_N V_{node}} \tag{5.8}$$

$$D_P = C_a \times R \times \Delta t \times \frac{C_{stock}}{\rho_S} \tag{5.9}$$

where C_a is the average aerosol concentration in the chamber at a time step (kg m^{-3}), C_{node} is the aerosol concentration at a node at a time step (kg m^{-3}), V_{node} is the volume of a cell (m^3), D_P is the PRRSV dose at a time step ($TCID_{50}$), R is the respiration rate (m^3 s^{-1}), Δt is the time step (0.5 s) and C_{stock} is the PRRSV concentration in the stock solution (1×10^{11} $TCID_{50}$ m^{-3})

5.3.3.3. Calculation of the probability of infection and comparison with case studies

To predict the probability of pigs becoming infected by being exposed to aerosols of PRRSV in the experimental chamber, the cumulative PRRSV exposure dose after 200-s aerosol exposure was inserted into the three MLE dose-response models that were developed for the Hermann et al. (2009) dataset (Eqs. (5.10-5.12)). The values of parameters are displayed in Table 5.3. The calculated probabilities were compared to the observed infection rates reported by Dee, Batista, et al. (2006) and Dee, Deen, et al. (2006) to determine how well the coupling of CFD and dose-response modelling estimated the probability of infection by aerosol exposure (Eq. (5.13)).

$$P(\sum D_p) = 1 - \exp(-r_p \sum D_p) \tag{5.10}$$

$$P(\sum D_P) = 1 - {}_1F_1(\alpha_P, \alpha_P + \beta_P, -\sum D_P) \tag{5.11}$$

$$P(\sum D_p) = 1 - \left(1 + \frac{\sum D_P}{\beta_{P,approx}}\right)^{-\alpha_{P,approx}} \tag{5.12}$$

$$P_{observed} = \frac{k_{infected}}{n_{exposed}} \tag{5.13}$$

where ΣD_p is the cumulative PRRSV exposure dose ($TCID_{50}$) over 200-s simulation, r_p is the parameter for the PRRSV exponential model for aerosol transmission, $\alpha_{P,}\beta_p$ are parameters for the PRRSV exact beta-Poisson model for aerosol transmission, $\alpha_{P,approx}$, $\beta_{P,approx}$ are parameters for the PRRSV approximate beta-Poisson model for aerosol transmission, $P_{infected}$ is the observed rate of infection in case study, $k_{infected}$ is the number of infected animals in the case study and $n_{exposed}$ is the number of exposed animals in case study.

Table 5.3. Parameter values for dose-response models developed for aerosol exposure of PRRSV

Parameter	MLE	2.5%-tile	97.5%-tile
r_p	9.282×10^{-4}	6.880×10^{-4}	1.286×10^{-3}
α_P	1.077×10^{6}	1.411×10^{-5}	7.114×10^{2}
β_P	1.159×10^{9}	3.195×10^{-6}	7.653×10^{5}
$\alpha_{P,approx.}$	2.042×10^{6}	8.253×10^{-2}	7.310×10^{2}
$\beta_{P,approx}$	2.200×10^{9}	6.868×10^{-6}	7.838×10^{5}

5.4. Results and Discussion

5.4.1. Comparison of three dose-response models

The generated EM curves for PRRSV on the aerosol, intra-nasal, and oral transmission routes are shown in Fig. 5.2a. The ability of EM to model the datasets was limited by its fixed curve shape. Specifically, the sole model parameter *r* determines the curve's placement along the x-axis (i.e. dose), but it does not significantly change the shape of the curve to allow the model to match with all datasets. Table 5.4 shows the difference between observed experimental rates of infection and predicted MLE rates of infection for PRRSV. For the EM, the difference for the aerosol dataset ranged from 5 to 38%, showing adequate agreement between observed and predicted probability of infection. For intra-nasal and oral datasets, the difference ranges were higher (0 to 92% and 0 to 99%, respectively).

Figures 5.2b and 5.2c show the dose-response curves generated by the EBPM and ABPM, respectively, for PRRSV via the aerosol, intra-nasal, and oral transmission routes. The EBPM and ABPM had equal differences between observed rates of infection and the modelled probability of infection at the dose levels used in the experiments (Table 5.4). For the aerosol dataset, the difference range was from 5 to 38%, with most values ≤ 10%. For the intra-nasal and oral datasets, the differences ranged from 1 to 31% and 3 to 100%, respectively. Despite the large range for the oral dataset, the models performed well (≤10% difference) in four out of six doses. From this analysis and the constrained shape of the EM, it was evident that the EBPM and ABPM performed better than the EM at predicting the rate of infection.

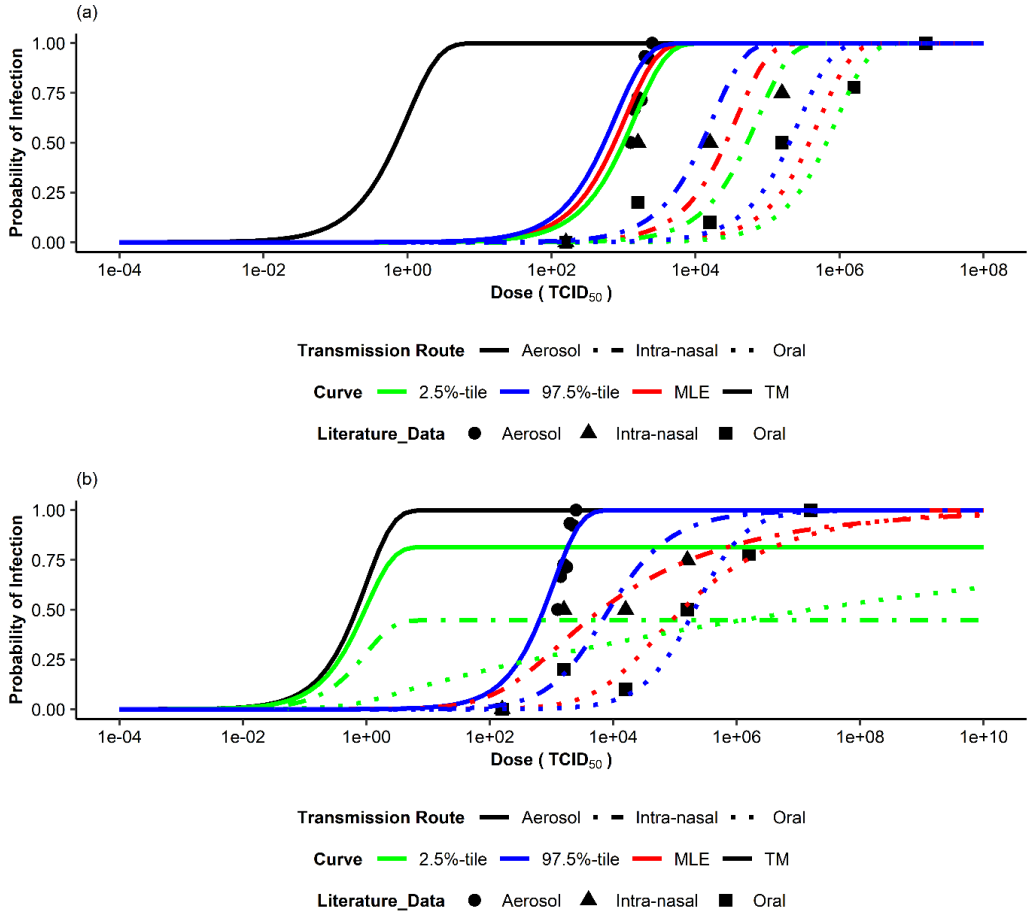

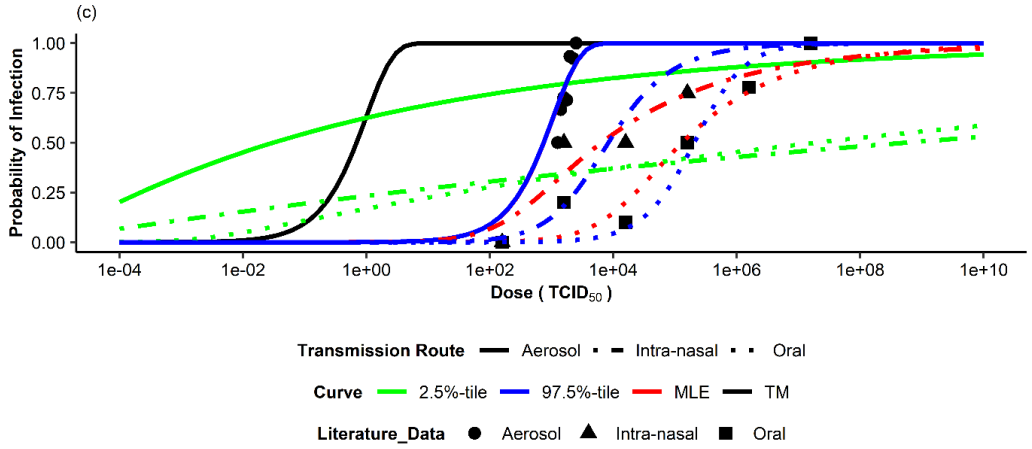

Figure 5.2. Comparison of the dose-response models of PRRSV for aerosol, intranasal, and oral transmission routes, with the theoretical maximum (TM), 2.5-percentile (2.5%-tile), 97.5-percentile (97.5%-tile), and maximum likelihood estimates (MLE): (a) exponential model, (b) exact beta-Poisson models, (c) approximate beta-Poisson models. The literature data for aerosol are from Hermann et al. (2009), while the intra-nasal and oral datasets are from Hermann et al. (2005).

Table 5.4. Comparison of the predicted probability of infection using exponential, exact beta-Poisson, and approximate beta-Poisson models (maximum likelihood estimate; MLE) to observed rates of infection for PRRSV on aerosol (dataset from Hermann et al. 2009), intra-nasal, and oral (datasets from Hermann et al. 2005) transmission routes.

		Exponential		**Exact beta-Poisson**		**Approximate beta-Poisson**	
				Aerosol			
Dose ($TCID_{50}$)	Observed Rate of Infection (%)	MLE (%)	Difference[a] (%)	MLE (%)	Difference[a] (%)	MLE (%)	Difference[a] (%)
1,259	50	69	38	69	38	69	38
1,413	67	73	10	73	10	73	10
1,585	73	77	6	77	6	77	6
1,778	71	81	13	81	13	81	13
1,995	93	84	10	84	10	84	10
2,239	92	87	5	87	5	87	5
2,512	100	90	10	90	10	90	10

		Exponential		Exact beta-Poisson		Approximate beta-Poisson	
Dose ($TCID_{50}$)	Observed Rate of Infection (%)	MLE (%)	Difference[a] (%)	MLE (%)	Difference[a] (%)	MLE (%)	Difference[a] (%)
Intranasal							
1.58×10^{2}	0%	0%	und.[b]	10%	und.[b]	10%	und.[b]
1.58×10^{3}	50%	4%	92%	34%	31%	34%	31%
1.58×10^{4}	50%	34%	32%	59%	17%	59%	17%
1.58×10^{5}	75%	98%	31%	75%	1%	75%	1%
Oral							
1.58×10^{2}	0%	0%	und.[b]	0%	und.[b]	0%	und.[b]
1.58×10^{3}	20%	0%	99%	3%	85%	3%	85%
1.58×10^{4}	10%	3%	72%	20%	100%	20%	100%
1.58×10^{5}	50%	25%	50%	53%	5%	53%	5%
1.58×10^{6}	78%	94%	21%	76%	3%	76%	3%
1.58×10^{7}	100%	100%	0%	88%	12%	88%	12%

[a] Difference was calculated using formula (MLE – Observed)/Observed, [b] 0% observed rate of infection resulted in undefined values for difference

The theoretical maximum is a curve demonstrating the maximum probability of infection values at specific exposure doses of pathogen. It is modelled by assuming that $r = 1$ in the EM (i.e., the maximum probability of a single virus particle causing an infection is 100%, with all of the virus particles having the same probability of causing an infection). When the probability of infection exceeds the theoretical maximum, it implies that an individual virus particle has more than a 100% probability of causing infection; thus, these regions of the dose-response models where the probability of infection is greater than the probability predicted by the theoretical maximum are not theoretically valid (Schmidt et al., 2013). These regions can be identified when the dose-response curves are located to the left of the theoretical maximum on the probability of infection graphs.

The theoretical maximum curve was previously used to evaluate the theoretical validity of the ABPM (Schmidt et al., 2013; Teunis & Havelaar, 2000). In Fig. 5.2c, the probability of infection estimates on the 2.5-percentile ABPM dose-response curves were greater than the theoretical maximum probabilities at low doses for all three PRRSV datasets. This indicated that the model was not theoretically valid at low doses. Teunis & Havelaar (2000) identified this problem with the ABPM, reporting that the application of the ABPM for some datasets might lead to overestimation of the probability of infection at low doses.

Comparatively, as seen in Fig. 5.2b, the probability of infection estimates of the EBPM were less than the probability of infection values on the theoretical maximum curve, indicating that the EBPM was theoretically valid. However, there is a limitation to the EBPM. Schmidt et al. (2013) reported that the EBPM can be bi-modal when both parameters are less than 1, meaning that the shape of the EBPM changes when α and β are both less than 1. A possible remedy for this issue is placing restrictions of $10^{-6} < \alpha < 10^{6}$ and $1 < \beta < 10^{6}$ during the MCMC simulations; however, the results presented in this paper did not apply these restrictions and present the EBPM as originally formulated. Specifically in this study, the 2.5-percentile curve has a different shape than the MLE and 97.5-percentile curves (Fig. 5.2b) so this should be considered when interpreting the results of this study. A recommendation for future work on dose-response models of infectious animal diseases is to perform MCMC simulations with and without restrictions on α and β and report the difference.

Overall, despite this limitation, the EBPM performed well compared to the EM and ABPM. It predicted probability of infection values relatively well compared to the EM (Table 5.4) and it did not estimate probability of infection values greater than the probability of infection values predicted by the theoretical maximum. Therefore, the EBPM results will be discussed for the remainder of the paper.

5.4.2. Dose-response modelling by exact Beta-Poisson model

The MLE values and the 2.5 and 97.5 percentile estimates for the parameters α and β in the EBPM for all the datasets are summarised in Table 5.5. It should be noted that the values of α and β individually are not necessarily an indicator of the shape of the EBPM curves as different α and β combinations can result in similar shapes. It was also interesting to note that there are some cases, as indicated in Table 5.5, where the α and β MLE values were outside the 95% confidence interval (CI) predicted by the MCMC simulations. This meant that different methods of estimating the model parameters could result in different α and β combinations that gave the best fit of model to the dataset. For example, the MLE of the α and β values for the aerosol dataset of PRRSV were outside the 95% CI (Table 5.5); however, when plotted, the MLE curve overlaps with the 97.5 percentile curve (Fig. 5.3a), while the MLE curves for the intra-nasal and oral datasets were within the 95% CI curves predicted by the MCMC simulations (Figs. 5.3b and 5.3c, respectively).

Table 5.5. Maximum likelihood estimate (MLE), 2.5-percentile estimate and 97.5-percentile estimate for parameters α and β in the exact beta-Poisson models of PRRSV, AIV, FMDV, ASFV, and PEDV on various transmission routes.

	MLE		2.5-percentile [d]		97.5-percentile	
	α	β	α	β	α	β
PRRSV						
Aerosol (Hermann et al., 2009)	1.077×10^{6} [c]	1.159×10^{9} [c]	1.411×10^{-5}	3.195×10^{-6}	7.114×10^{2}	7.653×10^{5}
Intranasal (Hermann et al., 2005)	2.130×10^{-1}	2.565×10^{2}	5.592×10^{-6}	6.921×10^{-6}	6.795×10^{-1}	4.803×10^{3}
Oral (Hermann et al., 2005)	3.003×10^{-1}	1.434×10^{4}	3.932×10^{-2}	7.259×10^{-1}	1.203	2.652×10^{5}
AIV (H9N2)						
Aerosol (Guan et al., 2013)	5.946×10^{-1}	4.996×10^{1}	1.724×10^{-1}	3.188	2.108	4.507×10^{2}
Intranasal (Guan et al., 2013)	3.920×10^{1} [c]	8.759×10^{6} [c]	3.130×10^{-1}	2.296×10^{3}	7.317	9.525×10^{5}
Oral (Guan et al., 2013)	4.855×10^{-2}	3.475×10^{4}	4.143×10^{-6}	1.505×10^{-5}	1.075×10^{-1}	7.418×10^{5}
AIV (H5N1)						
Aerosol[a] (Agranovski et al., 2010)	1.025×10^{1}	3.576×10^{2}	1.445	3.684×10^{1}	2.275×10^{4}	7.898×10^{5}
Intra-nasal/Intra-tracheal (Spekreijse, Bouma, Stegeman, et al., 2011)	7.124×10^{-1}	1.852×10^{2}	7.426×10^{-6}	2.112×10^{-6}	5.977×10^{2}	6.737×10^{5}
FMDV – Sheep						
Intranasal (Hughes et al., 2002)	1.534×10^{1}	9.543×10^{4}	7.375×10^{-1}	2.603×10^{3}	1.736×10^{2}	8.918×10^{5}
Natural Aerosol (Gibson & Donaldson, 1986)	8.879×10^{-1}	7.563	1.444×10^{-5}	4.561×10^{-6}	2.110×10^{4}	4.989×10^{5}
FMDV – Cows						
Artificial Aerosol (Donaldson et al., 1987)	5.288	9.404×10^{1}	1.366×10^{-4}	1.374×10^{-5}	3.660×10^{4}	6.986×10^{5}
Natural Aerosol (Donaldson et al., 1987)	1.025×10^{6} [c]	4.359×10^{7} [c]	5.975×10^{-6}	2.091×10^{-6}	1.318×10^{4}	5.706×10^{5}
ASFV						
Feed (Niederwerder et al., 2019)	5.352×10^{-2}	1.031×10^{2}	2.045×10^{-6}	4.374×10^{-6}	1.080×10^{-1}	3.405×10^{3}
Natural Liquid (Niederwerder et al., 2019)	1.931×10^{-1}	3.387×10^{-1}	3.997×10^{-6}	1.822×10^{-6}	4.650×10^{-1}	2.889
Nasopharyngeal (Howey et al., 2013)	5.121	6.852×10^{2}	2.398×10^{-5}	3.632×10^{-6}	5.204×10^{3}	6.879×10^{5}
Oropharyngeal (Howey et al., 2013)	9.268	1.794×10^{4}	5.746×10^{-2}	1.271×10^{-1}	1.698×10^{3}	8.244×10^{5}
PEDV						
Oral[b] (Liu et al., 2015)	1.844	7.157×10^{-8} [c]	2.727×10^{-3}	1.400×10^{-6}	7.366×10^{5}	5.952×10^{3}
Feed per gram (Schumacher et al., 2016)	6.272	1.410×10^{2}	7.285×10^{-1}	7.688	4.600×10^{4}	7.674×10^{5}
Orogastrically (Thomas et al., 2015)	1.209×10^{1}	2.602×10^{2}	1.451	2.551×10^{1}	3.752×10^{4}	7.837×10^{5}

[a] Lethal aerosol dose, [b] Measured probability of diarrhoea, [c] MLE was not within 95% confidence interval predicted by MCMC simulations, [d] 2.5-percentile predictions displayed where from MCMC simulations where no restrictions were placed on α or β.

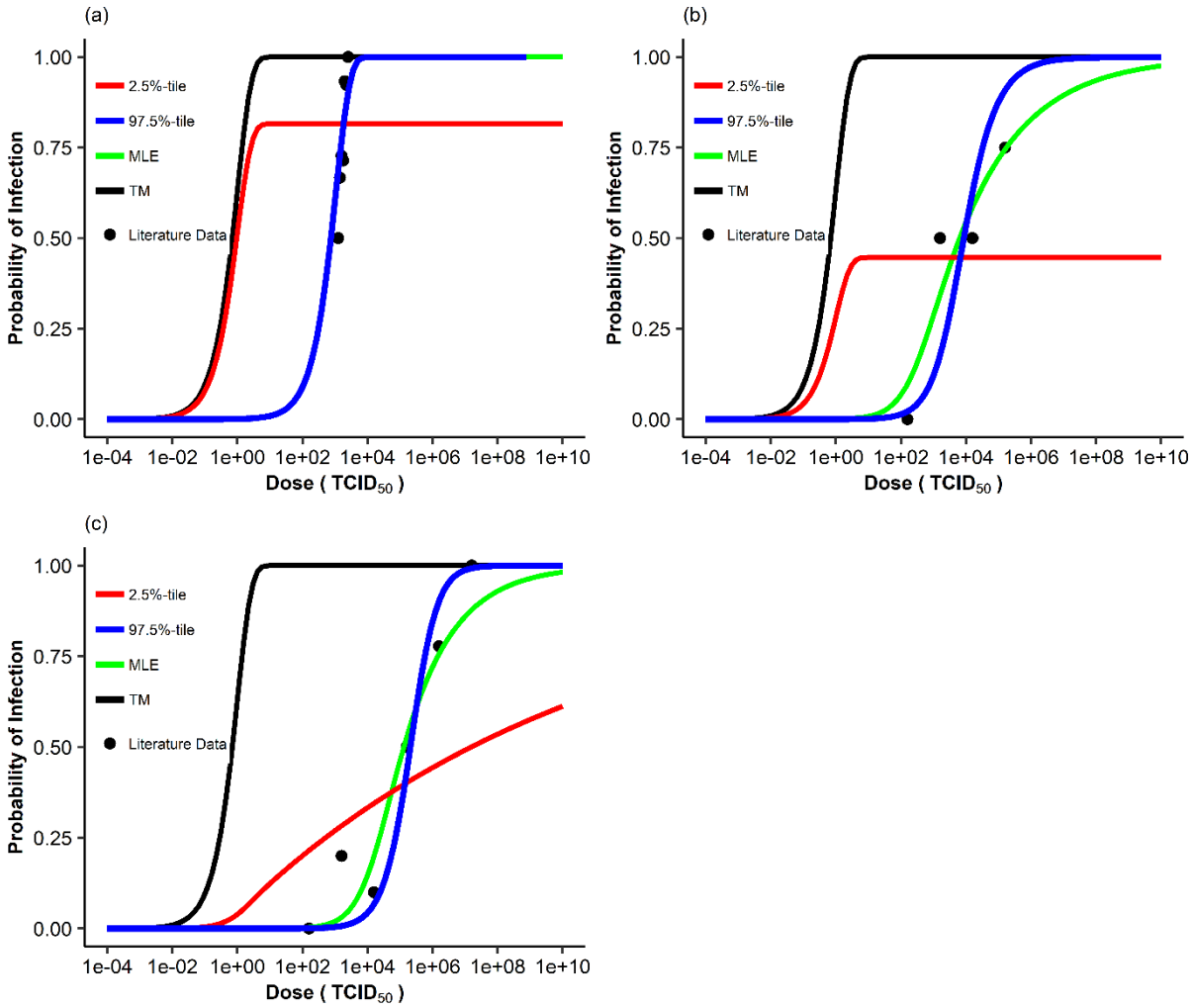

Figure 5.3. The exact beta-Poisson dose response models for PRRSV, with the theoretical maximum (TM), 2.5-percentile (2.5%-tile), 97.5-percentile (97.5%-tile), and maximum likelihood estimates (MLE): (a) aerosol transmission route (based on dataset of Hermann et al. (2009), (b) intranasal transmission route (based on dataset of Hermann et al. 2005), and (c) oral transmission route (based on dataset of Hermann et al. 2005).

5.4.2.1. PRRSV

The dose-response modelling indicated that PRRSV was most infectious on the aerosol route (Fig. 5.3a), followed by the intra-nasal route (Fig. 5.3b), and least infectious by the oral route (Fig. 5.3c). This indicates that fewer infectious PRRSV particles are required to cause an infection by the aerosol route than via the intra-nasal and oral routes.

The ID_{50} estimates for the aerosol, intra-nasal, and oral transmission routes are shown in Fig. 5.4a. The oral transmission route has two bars only because the 2.5-percentile curve did not reach 50% probability of infection. The ID_{50} for PRRSV was the lowest upon aerosol exposure and the highest upon oral exposure. This trend agreed with what has been reported in the literature. The ID_{50} estimates for PRRSV based on the logit and probit dose-response models were reported to be 1,259 $TCID_{50}$ (Hermann et al., 2009), 10,000 $TCID_{50}$, and 199,526 $TCID_{50}$ (Hermann et al., 2005) for aerosol, intra-nasal, and oral exposures, respectively. It should be noted that the logit and probit models are deterministic models, whose underlying theories for dose-response are based on individuals becoming infected after being exposed to a dose greater than the individual's tolerance dose (Sze To & Chao, 2010). Cutler et al. (2011) also performed similar experiments and dose-response modelling as Hermann et al. (2009) with a highly pathogenic strain of PRRSV (i.e. MN-184) and they reported that PRRSV MN-184 by the aerosol route had a mean ID_{50} of 0.7 to 1.8 $TCID_{50}$. This indicates that the strain type also affects the probability of infection at different exposure levels. It should be noted that the ID_{50} estimates for PRRSV in this paper were for PRRSV strain VR-2332.

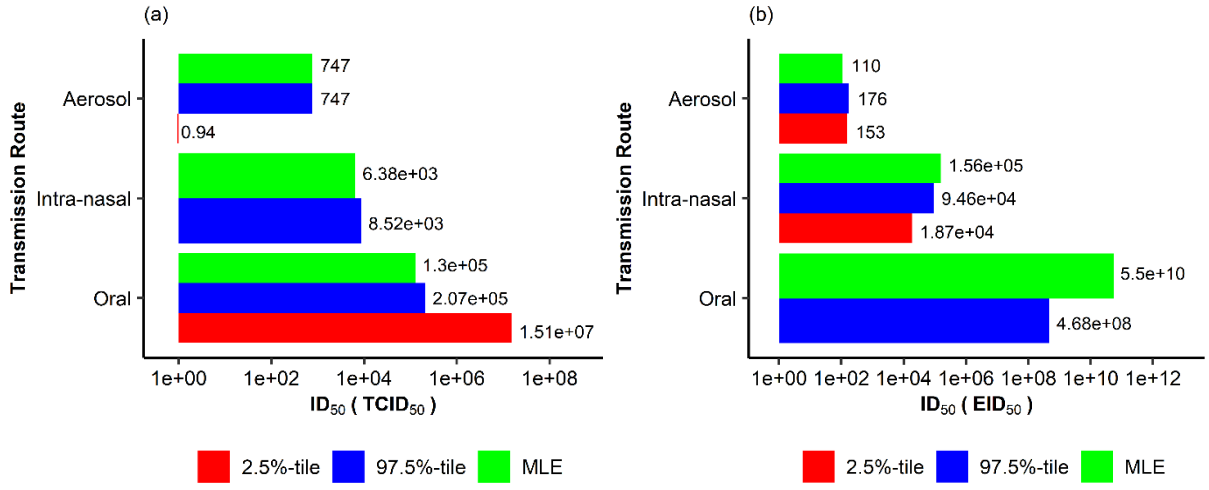

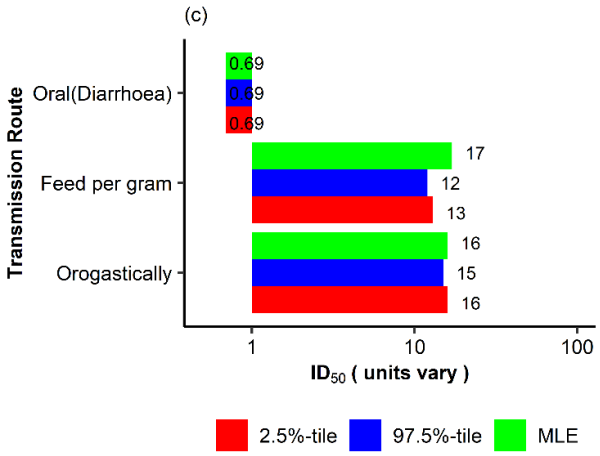

Figure 5.4. The predicted infectious dose at 50% probability of infection (maximum likelihood estimate; MLE): (a) PRRSV on aerosol, intra-nasal, and oral transmission routes; (b) AIV H9N2 on aerosol, intra-nasal, and oral transmission routes; (c) PEDV in terms of feed per gram, orogastrically, and oral (50% diarrhoea dose) transmission routes.

5.4.2.2. AIV

The MLE curve for the intra-nasal dataset was outside of the 95% CI except at higher doses, for AIV (Fig. 5.5b). The MLE estimates for α and β were also outside of the 95% CI (Table 5.5). This was likely due to the small datasets used to perform the MLE and MCMC simulations – there were only four datapoints in the intra-nasal dataset; more datapoints could allow for a better prediction of the MLE. The curves for the aerosol and oral datasets were within the 95% CI (Figs. 5.5a and 5.5c, respectively). In terms of transmission route effect on probability of infection, lower doses of H9N2 AIV were required to cause infection by the aerosol transmission route (Fig. 5.5a), followed by the intra-nasal transmission route (Fig. 5.5b) and the oral transmission route (Fig. 5.5c). The ID_{50} was also lower on the aerosol transmission route compared to the intra-nasal and oral transmission routes (Fig. 5.4b). This agreed with observations reported in the literature. The experimental data of Guan et al. (2013) showed that estimates for the ID_{50} for H9N2 AIV over aerosol, intra-nasal, and oral routes were 5.7×10^1 to 3.7×10^3 EID_{50}, 1.4×10^5 EID_{50}, and 1.4×10^8 EID_{50}, respectively. The ID_{50} estimates in this study were in good agreement with those reported in the literature. The MLE and 95% CI

estimates for the aerosol ID_{50} were within the estimated range of ID_{50} by Guan et al. (2013). The MLE for intra-nasal ID_{50} was close to the ID_{50} estimate reported by Guan et al. (2013). The MLE and 97.5-percentile estimates for oral ID_{50} were greater than the Guan et al. (2013) estimate. However, the authors had assumed that the highest used dose of 1.4×10^8 EID_{50} was the ID_{50}, although this dose had only infected 4 out of 12 chickens in their study.

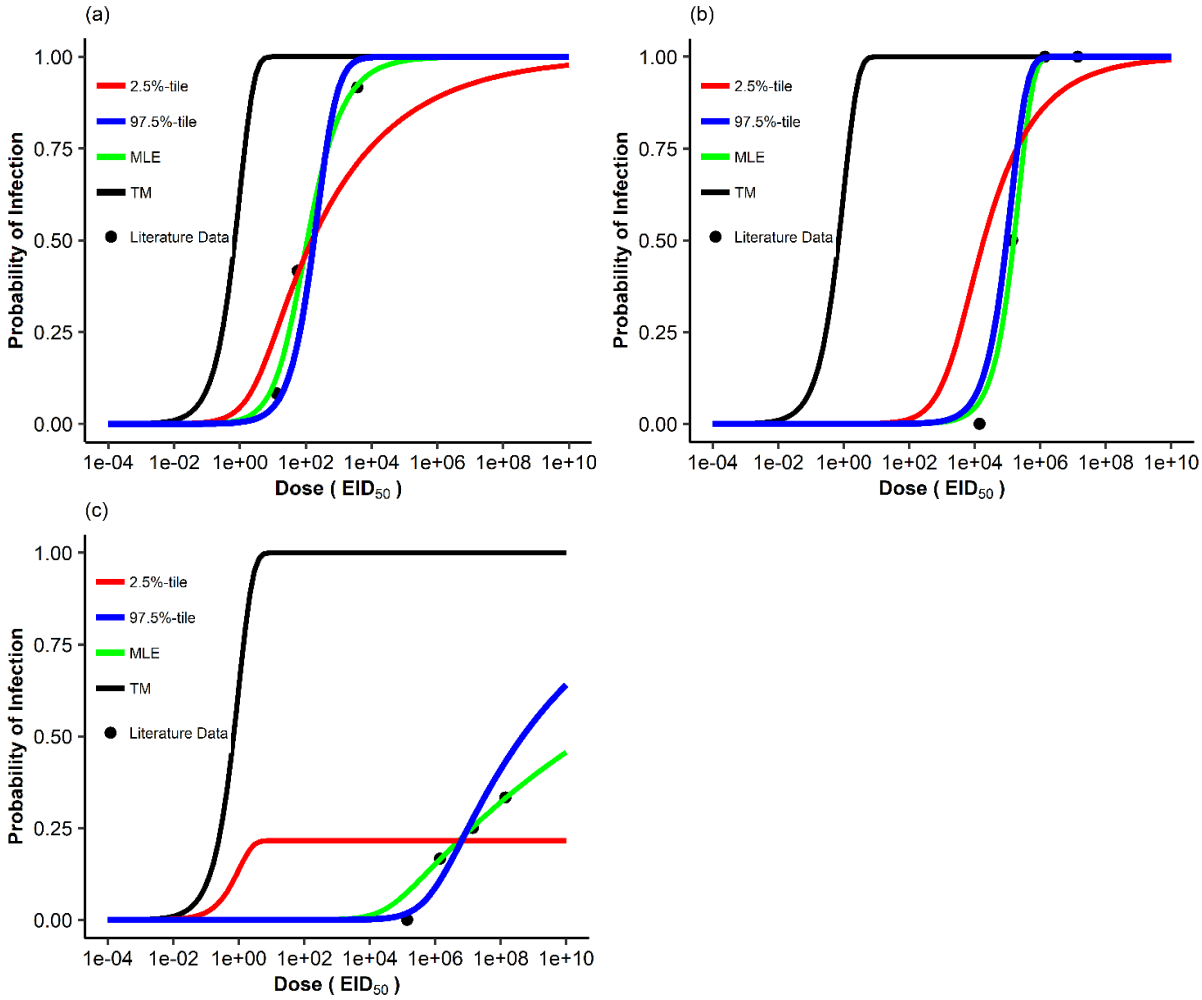

Figure 5.5. The exact beta-Poisson dose response models for AIV H9N2 (based on datasets of Guan et al. 2013), with the theoretical maximum (TM), 2.5-percentile (2.5%-tile), 97.5-percentile (97.5%-tile), and maximum likelihood estimates (MLE): (a) aerosol, (b) intra-nasal, and (c) oral transmission routes.

Figure 5.6a shows the probability of mortality from H5N1 AIV exposure on the aerosol transmission route and Fig. 5.6b shows the probability of infection upon exposure to H5N1 on the intra-nasal/intra-tracheal transmission route. The MLE curves were within the 95% CI for both cases. The lethal dose at 50% probability (LD_{50}) of H5N1 upon aerosol exposure was estimated to be between 23 to 26 FFU, which was close to the LD_{50} of 26.5 FFU estimated by Agranovski et al. (2010). The MLE for ID_{50} on the intra-nasal/intratracheal route was predicted to be 305 EID_{50}, which was close to the ID_{50} of 316 EID_{50} reported by Spekreijse et al. (2011). The two EBPM predictions for H5N1 could not be compared to each other since the virus was measured in different units (FFU and EID_{50}) and reported as different events (mortality and infection). Nevertheless, there is evidence in the literature that fewer infectious H5N1 AIV particles are required to cause infection by the aerosol route than the intra-nasal and oral routes; Sergeev et al. (2013) estimated mean ID_{50} of 16 EID_{50}, 501 EID_{50}, and 7,932 EID_{50} for the aerosol, intra-nasal, and oral transmission routes, respectively.

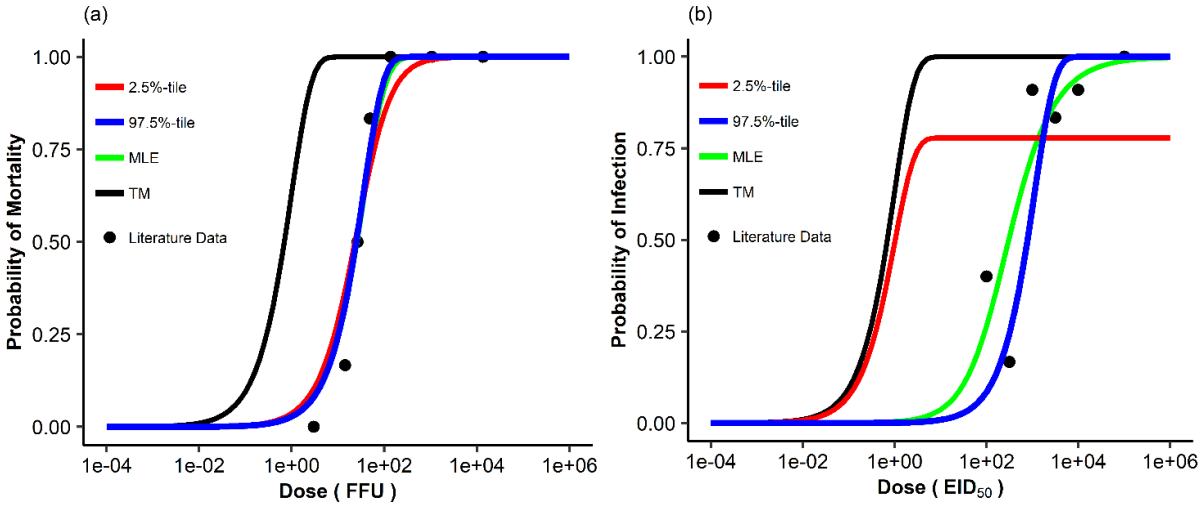

Figure 5.6. The exact Beta-poisson dose response models for AIV H5N1, with the theoretical maximum (TM), 2.5-percentile (2.5%-tile), 97.5-percentile (97.5%-tile), and maximum likelihood estimates (MLE): (a) aerosol transmission route (lethal dose; based on dataset of Agranovski et al. 2010), (b) intra-nasal and intratracheal transmission routes (based on datasets of Spekreijse et al. 2011).

5.4.2.3. FMDV

The MLE curves were within the 95% CI for all FMDV datasets (Fig. 5.7), although the MLE values for α and β for the natural aerosol dataset for cows were outside the 95% CI (Table 5.5). Dose-response modelling of FMDV indicated that the pathogen was less infectious to sheep by the intra-nasal transmission route (Fig. 5.7a) than the aerosol transmission route (Fig. 5.7b). It should be noted that the difference between the intra-nasal and aerosol infectiousness might also be due to different virus strains used in the intra-nasal experiments (Hughes et al., 2002) and the aerosol experiments (Gibson & Donaldson, 1986). The dose-response models of FMDV in cows by exposure to naturally generated (Fig. 5.7c) and artificially generated (Fig. 5.7d) aerosols were similar, with differences only in the 2.5-percentile curves, which might be due to the use of different virus strains for the natural and artificial aerosol exposures (Donaldson et al., 1987). The MLE ID_{50} for FMDV were predicted to be 4,413 $TCID_{50}$ and 9.4 $TCID_{50}$ for the intra-nasal transmission route and aerosol transmission route for sheep, respectively. The MLE ID_{50} for FMDV were predicted to be 30.2 $TCID_{50}$ and 13.9 $TCID_{50}$ on the natural aerosol transmission route and artificial aerosol transmission route for cows, respectively. These values were in good agreement with the minimum infectious doses reported in the literature. Hughes et al. (2002) ascertained from intra-nasal inoculation experiments that 10,000 $TCID_{50}$ was the minimum dose required to cause clinical infection in sheep, but that subclinical infection occurred at 3,162 $TCID_{50}$. Gibson & Donaldson (1986) estimated that a minimum dose of 10 $TCID_{50}$ of FMDV over the aerosol transmission route could cause infection in sheep. Donaldson et al. (1987) found that the minimum infectious dose for cows was 25 $TCID_{50}$ for the SAT 2 virus strain used in the natural aerosol experiments and 12.5 $TCID_{50}$ for the O_1 strain used in the artificial aerosol experiments. The low ID_{50} to which cows and sheep can become infected with FMDV by aerosol transmission contributes to the potential for FMDV to cause outbreaks in nearby facilities. For example, Sellers & Gloster (1980) estimated that 18 out of 32 outbreaks of FMDV occurred due to airborne transmission in the 1966 FMDV epidemic in the UK.

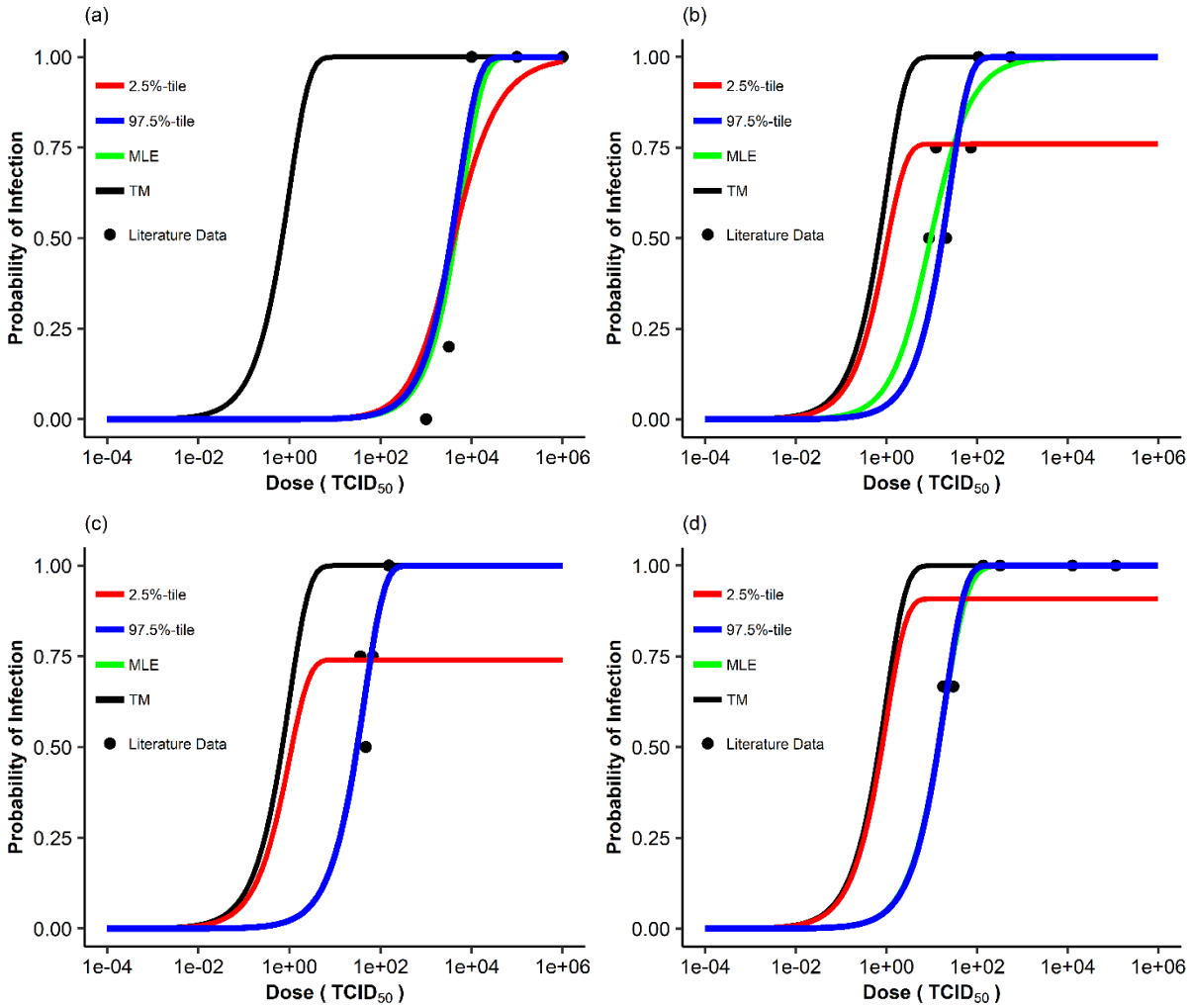

Figure 5.7. The exact beta-Poisson dose response models for FMDV, with the theoretical maximum (TM), 2.5-percentile (2.5%-tile), 97.5-percentile (97.5%-tile), and maximum likelihood estimates (MLE): (a) intra-nasal transmission route on sheep (based on dataset of Hughes et al. 2002), (b) aerosol transmission route on sheep (based on dataset of Gibson & Donaldson 1986), (c) natural aerosol transmission route on cows (based on dataset of Donaldson et al. 1987), (d) artificial aerosol transmission route on cows (based on dataset of Donaldson et al. 1987).

5.4.2.4. ASFV

The dose-response modelling of ASFV was based on the datasets reported by Niederwerder et al. (2019) for pigs consuming ASFV contaminated feed (Fig. 5.8a) and drinking liquid (Fig. 5.8b). The dose-response model for a different virus strain of ASFV, by nasopharynx and oropharynx is shown in Fig. 5.8c and 5.8d, respectively (based on datasets of Howey et al. 2013). The MLE curves for the feed, liquid, and nasopharyngeal datasets were all within the 95% CI curves, whereas the MLE curve for the oropharyngeal dataset only fit within the 95% CI curves at higher doses. This was likely to be because of the limited data points in the original dataset from Howey et al. (2013); there were only three datapoints in this dataset, with a large difference between doses. This dataset might not be sufficient for dose-response modelling.

Modelling revealed that ASFV was approximately 10 million fold more infectious when ingested as a liquid (Fig. 5.8b) than when ingested as feed (Fig. 5.8a). The MLE ID_{50} estimate for ASFV was 4.3×10^7 $TCID_{50}$ and 4.3 $TCID_{50}$ for feed and liquid, respectively. Niederwerder et al. (2019) performed dose-response modelling and predicted mean ID_{50} values of 6.3×10^6 $TCID_{50}$ and 10 $TCID_{50}$ for feed and liquid ingestion, respectively. They utilised a constrained spline regression method without assuming a functional form between dose and response to develop their dose-response model, which was the possible reason for the difference in ID_{50} values between their study and the current study. Inoculation into the nasopharynx resulted in a higher infectivity than inoculation into the oropharynx, as the MLE ID_{50} estimates were predicted to be 100 HAD_{50} and 1,394 HAD_{50}, respectively.

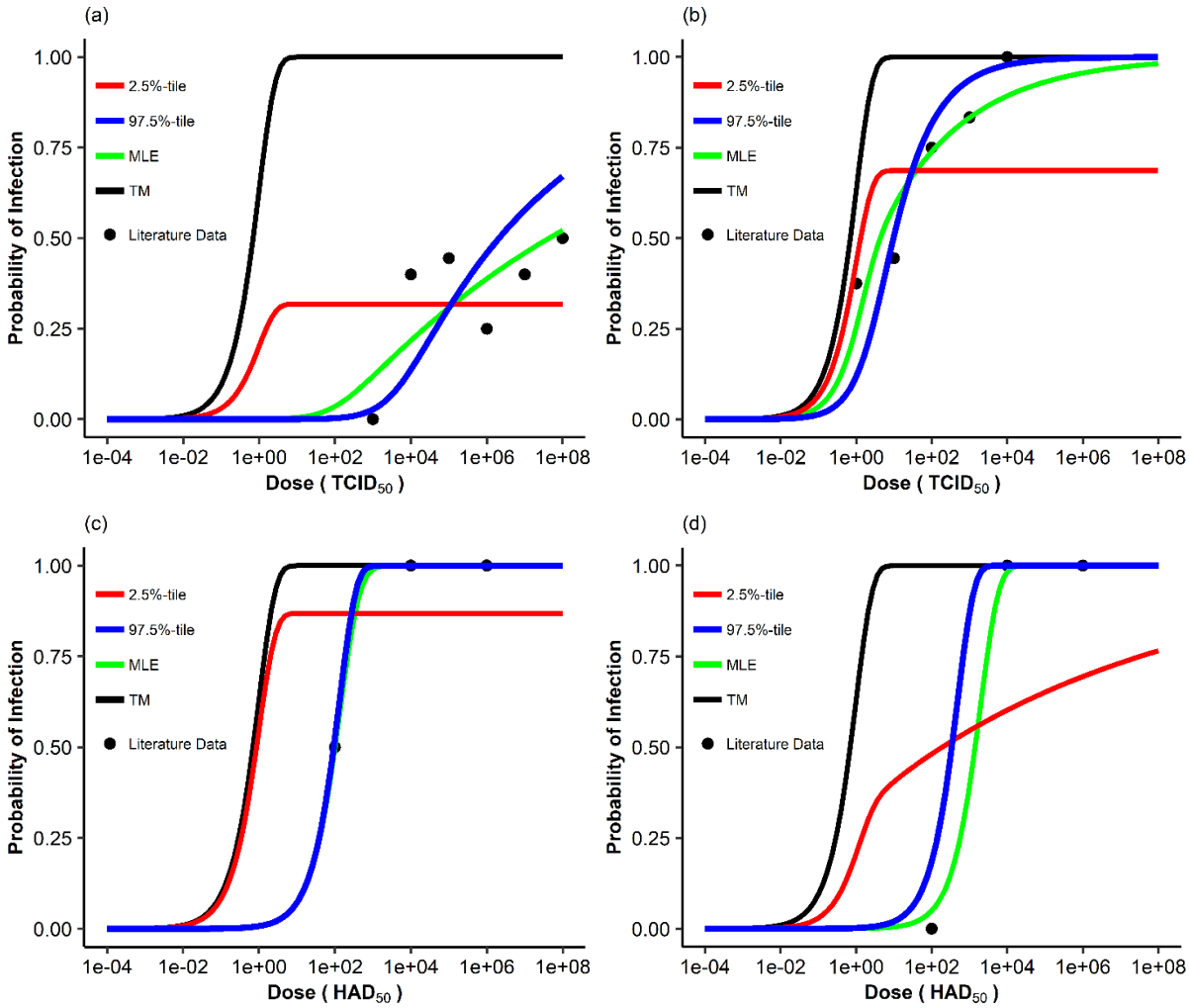

Figure 5.8. The exact beta-Poisson dose-response modelling results for ASFV, with the theoretical maximum (TM), 2.5-percentile (2.5%-tile), 97.5-percentile (97.5%-tile), and maximum likelihood estimates (MLE): (a) feed ingestion, (b) liquid ingestion (based on dataset of Niederwerder et al. 2019), (c) nasopharyngeal inoculation, and (d) oropharyngeal inoculation (based on dataset of Howey et al. 2013).

5.4.2.5. PEDV

The dose-response modelling for PEDV were based on the datasets of three different studies with oral and gastrointestinal transmission routes of exposure, including a study where the probability of diarrhoea was measured (Liu et al. 2015; Fig. 5.9a), a study where PEDV dose

was measured in terms of grams of feed (Schumacher et al. 2016; Fig. 5.9b), and a study where pigs were orogastrically inoculated with PEDV (Thomas et al., 2015; Fig. 5.9c). The MLE curves for the probability of diarrhoea dataset and orogastric dataset were within the 95% CI curves. The MLE curve for the feed per gramme dataset fit within the 95% CI curves only at higher doses, but the curve was very similar to the 97.5 percentile curve. Modelling results for all three scenarios, with some differences in virus strain, indicated that PEDV was very infectious by oral transmission route. This is further shown in Fig. 5.4c, which indicates that the ID_{50} for PEDV was less than 20 $TCID_{50}$ g^{-1} [feed] and less than 20 $TCID_{50}$ when administered orogastrically. The diarrhoea dose at 50% probability (DD_{50}) was estimated as 0.69 PFU. These ID_{50} values were congruent with the minimum infectious doses reported in the literature. Both Schumacher et al. (2016) and Thomas et al. (2015) reported that a minimum infectious dose of 56 $TCID_{50}$ infected 100% of pigs.

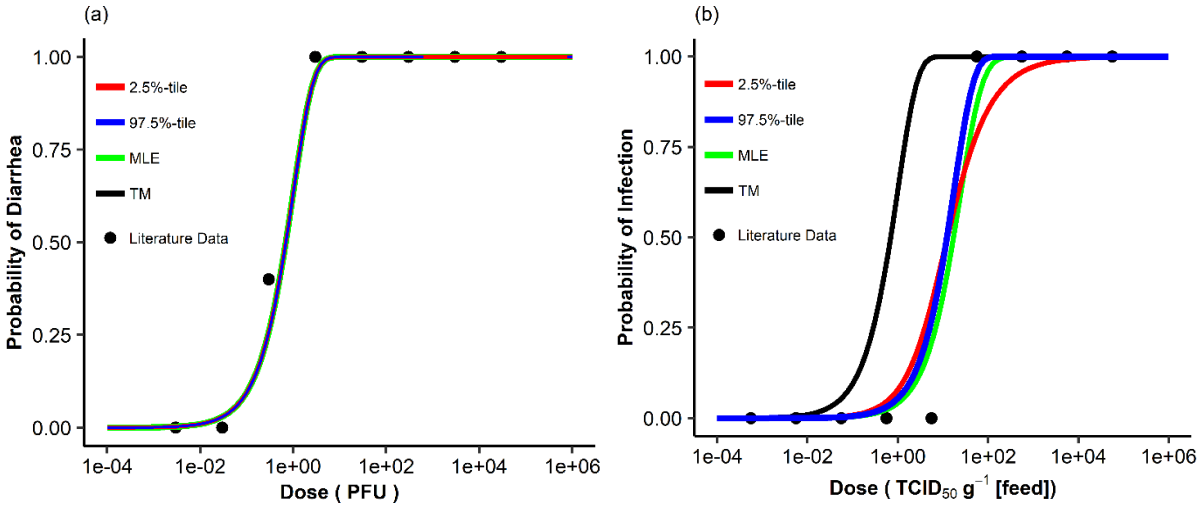

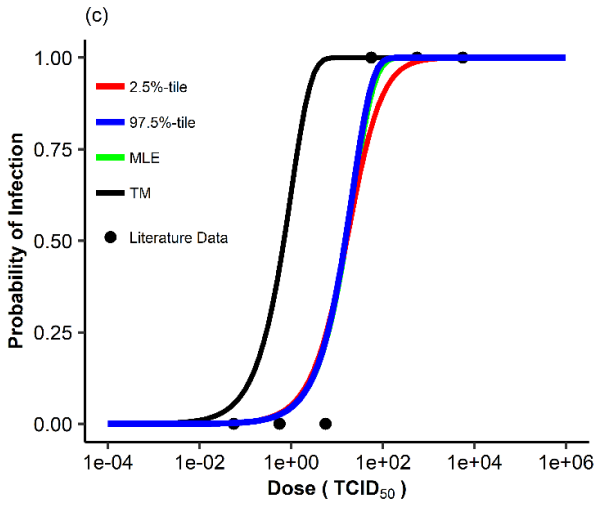

Figure 5.9. The exact beta-Poisson dose-response models for PEDV, with the theoretical maximum (TM), 2.5-percentile (2.5%-tile), 97.5-percentile (97.5%-tile), and maximum likelihood estimates (MLE): (a) oral transmission route, measuring probability of diarrhoea (based on dataset of Liu et al. 2015), (b) feed, in grams feed (based on dataset of Schumacher et al. 2016), (c) orogastric transmission route (based on dataset of Thomas et al. 2015).

5.4.2.6. Brief discussion on survival effect on transmission

Whilst the dose-response models developed in this study will enhance the understanding of infectious animal disease transmission, it is also important to understand the other components of disease transmission. The exposure dose is dependent upon the amount of infectious virus shed into the environment and the survival of the infectious virus in the environment. However, each virus survives differently in the environment and also differently depending on its form and the environmental matrix. A brief review on the survival of the five infectious animal viruses pertaining to intra-nasal, and oral transmission is presented below.

Fomite transmission occurs when an individual becomes infected with an infectious virus due to transferring of infectious virus on inanimate objects (fomites). Theoretically, fomite transmission is a potential way for intra-nasal transmission or oral transmission to occur and it is an important mode of transmission. All five viruses are shed in various secretions and excretions from infected animals, which are ways in which fomites can be contaminated with virus

(Alexandersen, Quan, et al., 2003; Germeraad et al., 2019; McVicar, 1984; Niederwerder et al., 2016; Wills, Zimmerman, Yoon, et al., 1997; Yoon et al., 1993). PRRSV did not survive past the day of inoculation on stainless steel, plastic, and boot rubber at temperatures of 25 to 27ºC (Pirtle & Beran, 1996). However, entry of PRRSV and transmission by fomites can happen quickly when a worker wears contaminated boots and clothing from an infected room to susceptible rooms (Otake et al., 2002). Primary introduction of highly pathogenic AIV into a domestic population is likely to be from direct or indirect contact with wild birds, in which indirect contact included fomite, vectors, environment, or water contaminated with faeces of infected wild birds (Alexander, 2007). In lake sediment, AIV infectivity persisted for 66 to 394 d at 0ºC and decreased at increased temperatures (Nazir, Haumacher, Ike, & Marschang, 2011). H5N1 AIV remained infectious on duck feathers up to 160 d at 4ºC and up to 15 d at 20ºC (Yamamoto, Nakamura, Yamada, & Mase, 2010). H5N1 AIV also remained infectious until the end of 13-d experiments on galvanised steel, glass, and soil when stored at low temperature and relative humidity conditions, but did not survive as long at higher temperature or relative humidity conditions (Wood, Choi, Chappie, Rogers, & Kaye, 2010). For FMDV, a literature survival analysis indicated that FMDV survival was negatively affected on inanimate objects (Mielke & Garabed, 2020). Research on survival of ASFV on fomites is required for ASFV (Mazur-Panasiuk et al., 2019). For PEDV, the virus survived up to 15 d at 4ºC and up to 2 d at 25ºC on various common pig farm items (Kim, Krishna, Torremorell, Goyal, & Cheeran, 2018). PEDV infectivity remained stable at 4ºC for 10 weeks and survived up to 5 weeks at room temperature on feed tote bags (Scott et al., 2016).

In terms of oral transmission, PRRSV remained infectious in well water and city water for up to 9 d and 11 d, respectively, when stored at 25 to 27ºC (Pirtle & Beran, 1996). In drinking water, H5N1 AIV survived up to 30 d at 4ºC (Yamamoto et al., 2010). A literature survival analysis indicated that FMDV survival was positively affected by the “microclimate conditions present” in vegetation/food (Mielke & Garabed, 2020). ASFV survival highly depended on the environmental temperature, with ASFV being very stable at low temperatures for long durations (Mazur-Panasiuk et al., 2019), including within unprocessed meats (Olesen et al., 2020). PRRSV, ASFV, and PEDV survived trans-Atlantic (37 d) and trans-Pacific (30 d) shipping environments within two, nine, and five different feed ingredients, respectively (Dee et

al., 2018); the mean half-life of ASFV in the nine ingredients during trans-Atlantic shipping ranged from 9.6 to 14.2 d (Stoian et al., 2019). PEDV also survived for 56 d within 10 feed ingredients when stored at room temperature and uncontrolled humidity conditions, with it surviving best in soybean meal (Trudeau, Verma, Sampedro, et al., 2017). Lastly, with the introduction of PEDV into Canada being linked to contaminated spray dried porcine plasma (Aubry, Thompson, Pasma, Furness, & Tataryn, 2017), several researchers have investigated the survival time of PEDV in plasma and during the production of spray dried plasma (Hulst et al., 2019; Pujols & Segalés, 2014; Quist-Rybachuk et al., 2015).

To summarise, dose-response models provide a prediction of the probability of infection upon doses of infectious virus. Some transmission routes require less virus exposure to cause infection but infectious virus may be available at greater quantities via a different transmission route due to increased shedding and ability to survive in the environment. Therefore, all transmission routes should be considered important for understanding the transmission of infectious animal diseases.

5.5. Case study of coupling CFD simulation with dose-response modelling

Coupling of CFD simulation and dose-response modelling was conducted to predict the aerosol transmission in experimental studies reported by Dee, Batista, et al. (2006) and Dee, Deen, et al. (2006). In these studies, pigs were housed in a two-chamber aerosol testing system and artificially infected by aerosolised PRRSV. Fig. 5.10a shows the aerosol concentration over the 200-second simulation in the second (recipient) chamber where pigs were housed and Fig. 5.10b shows the cumulative dose for 12-kg and 25-kg pigs. The PRRSV concentration in the second chamber ranged from 4.7×10^{1} $TCID_{50}$ m^{-3} to 1.1×10^{6} $TCID_{50}$ m^{-3} over the 200-second simulation. This range in PRRSV concentration was in the higher end of PRRSV concentrations measured at the exhaust of infected pig barns discussed in Table 3.3. This is likely because the original purpose of Dee, Batista, et al. (2006) and Dee, Deen, et al. (2006) was to test the performance of mechanical filters in between the two chambers at preventing aerosol transmission, so higher stock concentrations of PRRSV (i.e. 1×10^{8} $TCID_{50}$ l^{-1}) were utilised in the aerosolising solution.

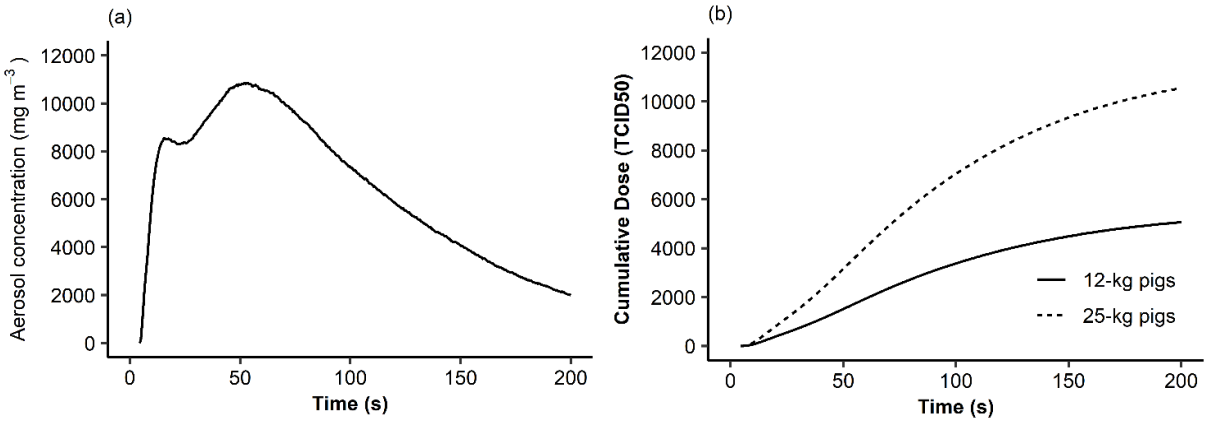

Figure 5.10. (a) Simulated aerosol concentration in second chamber over 200-second simulation, (b) cumulative aerosol dose of PRRSV for 12-kg and 25-kg pigs over the 200-second simulation.

The cumulative PRRSV aerosol doses simulated by the CFD model were introduced to the three dose-response models to predict the probabilities of infection. Dee, Batista, et al. (2006) reported infection in 9 out of 10 (90%) 12-kg pigs in the experimental chambers, while and Dee, Deen, et al. (2006) reported infection in 42 out of 50 (84%) 25-kg pigs in the experimental chambers. The predicted MLE probabilities of infection by all three models were higher than the reported experimental values (Table 5.6). However, the predicted 95% confidence intervals of infection rates did cover the experimental values. The EBPM predicted 82% to 100%, whilst the ABPM predicted 81% to 99% for 12-kg pigs and 83% to 100% for 25-kg pigs.

It was acceptable for the CFD simulation to be terminated at 200 s because it was unlikely that PRRSV would remain viable in the air for 6 h. Based on the experimental conditions in the Dee et al. (2006) studies (20ºC and 60% relative humidity), the half-life of aerosolised PRRSV was 40 min, according to Hermann et al. (2007). Ending the simulation at 200 s also provided us with an advantage of providing a more efficient simulation and reduce the computation time required to complete the simulation. Additionally, there were only 7.4% of particles remaining in the system at the end of the simulation.

Increasing the simulation time and thus the cumulative PRRSV dose would not have significantly changed the estimated probability of infection values. In Figs. 5.2a and 5.3a, the probability of infection values in the EM and EBPM, respectively, plateau when the dose

exceeds a specific amount. This also occurred for the ABPM (Fig. 5.2b), with the exception of the 2.5-percentile curve, which was due to limitations with the model that were described previously. The aerosol doses predicted by the end of the 200-s simulation were very close or had already reached the plateauing point on the dose-response models. This is evident in Table 5.6, in which doubling the dose of PRRSV by aerosol exposure from 5,064 $TCID_{50}$ to 10,550 $TCID_{50}$ minimally changed the probability of infection predicted by the three models.

Table 5.6. Predicted probabilities of infection by exponential, approximate beta-Poisson, and exact beta-Poisson models based on exposure doses from CFD simulations.

		Predicted probability of infection by aerosolised PRRSV exposure (%)	
		12-kg pigs	**25-kg pigs**
	Simulated Dose ($TCID_{50}$)	5,064	10,550
Exponential	MLE	99	100
	2.5 Percentile	97	100
	97.5 percentile	100	100
Exact beta - Poisson	MLE	99	100
	2.5 Percentile	82	82
	97.5 percentile	99	100
Approximate beta-Poisson	MLE	99	100
	2.5 Percentile	81	83
	97.5 percentile	99	100

5.6. Conclusion of journal paper

Three stochastic dose-response models were utilised to model the probability of infection of PRRSV, AIV, FMDV, ASFV, and PEDV through different routes of disease transmission. The EBPM performed better than the other two models (EM and ABPM). The combination of the two model parameters in EBPM dictated the model performance (best fit to experimental data). For PRRSV, AIV, and FMDV, aerosol transmission had the lowest predicted ID_{50}, followed by intra-nasal transmission and oral transmission. For ASFV and PEDV, low ID_{50} were identified for the liquid oral and feed route, respectively. Dose-response models were successfully coupled with CFD simulations to predict aerosol transmission of PRRSV and the estimated probability of infection values were compared to the observed rate of infection in literature. The 95% CI of the EBPM and ABPM adequately estimated the infection probabilities observed in the experimental study.

5.7. Acknowledgements

The authors acknowledge the financial support of the Natural Sciences and Engineering Research Council of Canada (NSERC).

Chapter 6. Modelling aerosol transmission of porcine reproductive and respiratory syndrome virus between buildings using computational fluid dynamics

Chapter 6 discusses the contribution of a journal paper titled "Modelling aerosol transmission of porcine reproductive and respiratory syndrome virus between buildings using computational fluid dynamics". This journal paper is formatted in the style of Biosystems Engineering Journal and is at the final stage of preparation for submission to the journal. Portions of the journal paper were removed from this chapter, specifically the literature review, to reduce repeated information.

6.1. Abstract

An integrated computational fluid dynamics (CFD) model was developed to simulate transmission of Porcine Reproductive and Respiratory Syndrome Virus (PRRSV) from a source to recipient building using an experimental study of aerosol transmission of PRRSV as a test case. The integrated model consisted of CFD simulations of PRRSV aerosols movement in the atmosphere and within the recipient building, viral infectivity decay, and infection dose-response. Specific hours with the appropriate wind direction on two days (June 6 and 7, 2006) were simulated, based on historical weather data. For a given airborne PRRSV concentration exhausted from the source building, the model predicted the PRRSV distribution at different aerosol sizes, the infectivity decay, and the probability of infection in the recipient building. The wind affected the aerosol entry into the recipient building, with more stable and continuous aerosol entry at lower wind speed conditions on June 7. Elevated aerosol and PRRSV concentrations on June 7 resulted in pigs being exposed to higher doses of PRRSV than on June 6, but this only made a difference in probability of infection when there was a moderate level of PRRSV (500 TCID m^{-3}) exhausted from the source building. At this level, there was a difference in exposure dose for pigs at different locations (pens). Overall, a positive PRRSV air sample on the morning of June 7 in the reported experimental study confirmed the adequacy of model simulations, which predicted the aerosol transmission event that infected pigs in the recipient building likely occurred on June 7, 2006.

6.2. Introduction

Aerosol transmission of Porcine Reproductive and Respiratory Syndrome Virus (PRRSV) plays an important role in the spread of PRRSV within and between pig facilities. The goal of this study is to develop an integrated CFD model to simulate aerosol transmission of PRRSV. The specific objectives are to: (1) simulate the dispersion of PRRSV aerosols from a source building to a recipient building using CFD, (2) simulate the entrance and concentration of PRRSV aerosols in the recipient building using CFD, (3) predict the exposure dose of PRRSV aerosols for exposed animals in the recipient building, taking into account the survival of infectious PRRSV during atmospheric transport in different environment conditions, and (4) estimate the probability that pigs in the recipient building would become infected with PRRSV by aerosol exposure. The study described in Pitkin et al. (2009) and Pitkin (2009), in which PRRSV aerosol transmission experiments from a source to recipient building were performed over a 1-year-period, was used as a case study to verify the CFD-based model.

6.3. Methodology

The integrated CFD model consisted of several sub-models to simulate the aerosol transmission of PRRSV from a source to recipient building (Fig. 6.1). CFD Model 1 simulated the aerosol and virus transport from the source building to the recipient building. A virus decay model was used to simulate the decay of PRRSV during transport in the field. Outputted data from CFD Model 1 was used to develop input parameters for CFD Model 2, which simulated the movement and distribution of aerosols and PRRSV in the recipient building. The decay model was also used to simulate the decay of PRRSV in the recipient building. Lastly, a dose-response model was used to estimate the probability of infection of pigs in the recipient building due to aerosol exposure to PRRSV.

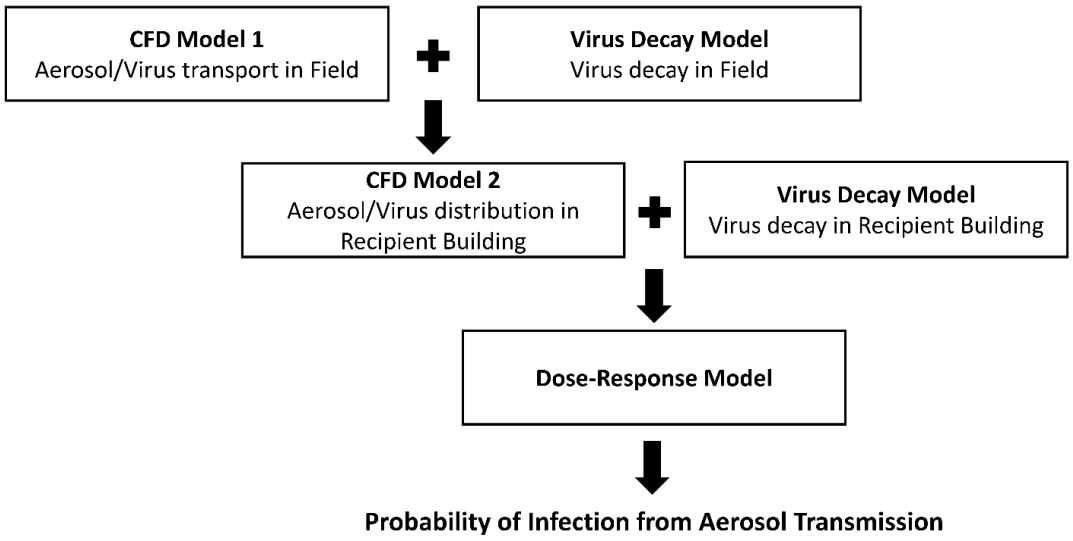

Figure 6.1. Integrated model used to simulate the aerosol transmission of PRRSV from source to recipient buildings

6.3.1. Field simulation (CFD Model 1)

CFD simulations were performed for a field study of PRRSV spread reported by Pitkin et al. (2009) and Pitkin (2009). The field study measured PRRSV spread from a source building (i.e., where infected pigs were located) to a recipient building (i.e., where non-infected pigs were placed to test for aerosol transmission from the source building). The simulation steps, as well as the inputs and outputs are summarized in Fig. 6.2 and discussed in the following subsections. To summarize, the steady-state airflow conditions in the field were calculated using the SimpleFOAM (OpenFOAM, 2018) solver and the aerosol movement within the steady-state airflow conditions were calculated using the icoUncoupledKinematicParcelFOAM solver (OpenFOAM, 2016b). The data outputted from this simulation was analyzed to generate injection files for CFD Model 2 as well as to determine the aerosol ages in the field prior to entering the building.

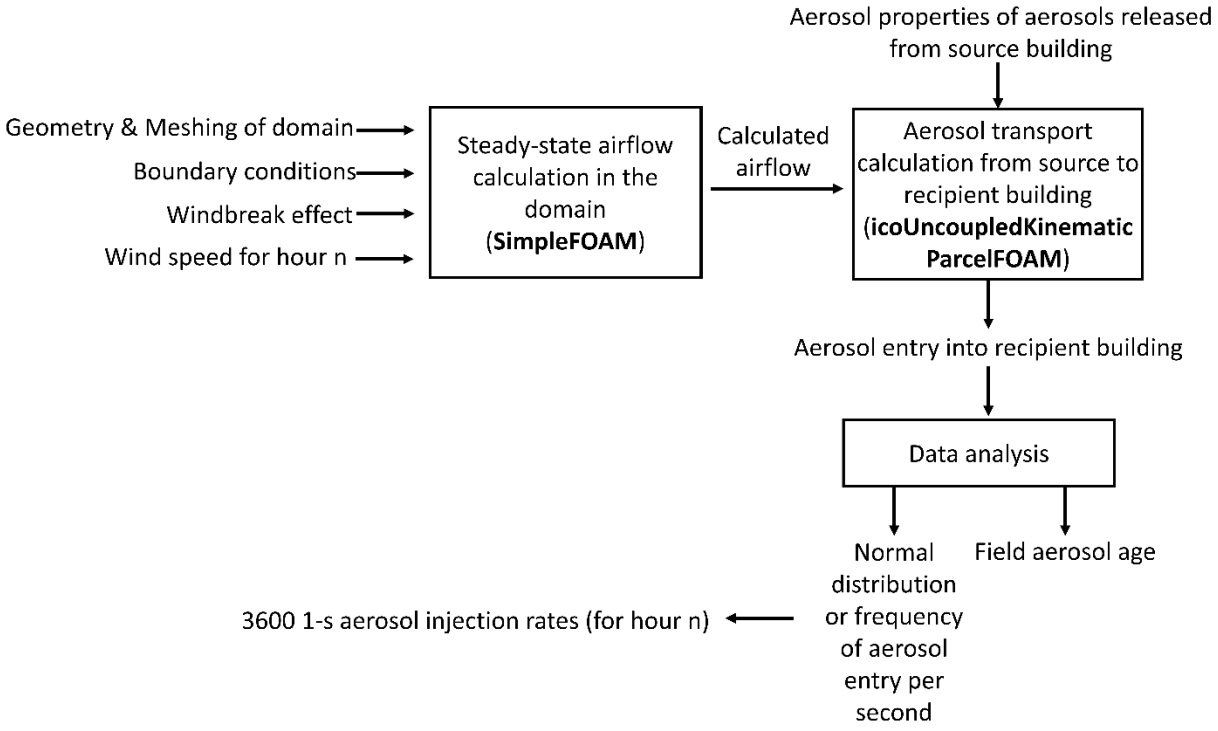

Figure 6.2. Illustration of the CFD simulation steps for the field study

6.3.1.1. Field domain and geometry

The simulation domain consisted of a source building which housed infected pigs and a recipient building with healthy pigs, as well as other buildings and features, including grain bins, windbreaks, and a manure storage facility. Google Earth Pro (Google LLC, Mountain View, California) tools were used to determine the locations of these buildings and features, and the geometry of the field site was modelled in ANSYS Workbench (2019 R2, ANSYS Inc., Canonsburg, PA; Fig. 6.3). The irregular features of the source building were considered in the modelling process. Length and width of different portions of the building (including roof) were estimated. A roof slope of 4:12 and the height of the wall (3.05 m) were assumed. There were seven exhaust fans (Pitkin, 2009) with diameter of 0.833 m (Otake et al., 2010). Their locations along the building were determined in Google Earth Pro and the fan center height was assumed to be 1.5 m above ground. The recipient building length and width were given in Pitkin, Deen, & Dee, (2009) and Pitkin (2009) as 8.5 m and 5.5 m, respectively. The building height was

assumed to be 3.05 m. There were two exhaust fans (Pitkin, 2009), with assumed fan diameters of 0.833 m, depth of 0.2 m, and center height of 2 m above ground. The fan locations on the building were estimated based on schematic diagram given in Pitkin (2009). The inlet vent was an inactive cooling pad, and the dimensions were not given. Using the minimum cooling pad area (Eq. (6.1); MWPS, 1983) and standard manufacturing sizes of cooling pads as references, the inlet vent width, depth, and height of were estimated to be 0.61 m, 0.15m, and 0.914 m, respectively; these dimensions provide a cooling pad area of 0.56 m^2, which is greater than the minimum cooling pad area of 0.39 m^2. The bottom of the inlet vent was assumed to be located 1.068 m above ground.

$$A_{cool} = 0.092903 \times \frac{Q_{n,h} \times n_n}{250} \tag{6.1}$$

where A_{cool} is the minimum cool pad area (m^2), $Q_{n,h}$ is the ventilation rate for nursery pigs per head (35 cfm $head^{-1}$; MWPS, 1983), and n_n is the number of nursery pigs (30 head).

The domain size (distances of domain boundaries from the site features) was determined according to the recommendations by Franke et al. (2006) and Tominaga et al. (2008). Specifically, the inlet, sides, and top of the domain were set 5 times the height of the windbreak (100 m) from the site, while the outlet of the domain was 15 times the height of the windbreak (300 m) from the site (Fig. 6.3). Overall, the domain was 498.25 m, 120 m, and 688 m in width, height, and depth, respectively. The domain was oriented so that the airflow would be directed from the source to recipient building, at an angle of 25° west of north. The angle was chosen from trial and error during a preliminary simulation process, to ensure that aerosols released from the source building would enter the recipient building. Fig. 6.3a shows the modelled buildings and features and Fig. 6.3b shows the full domain geometry in the CFD simulation.

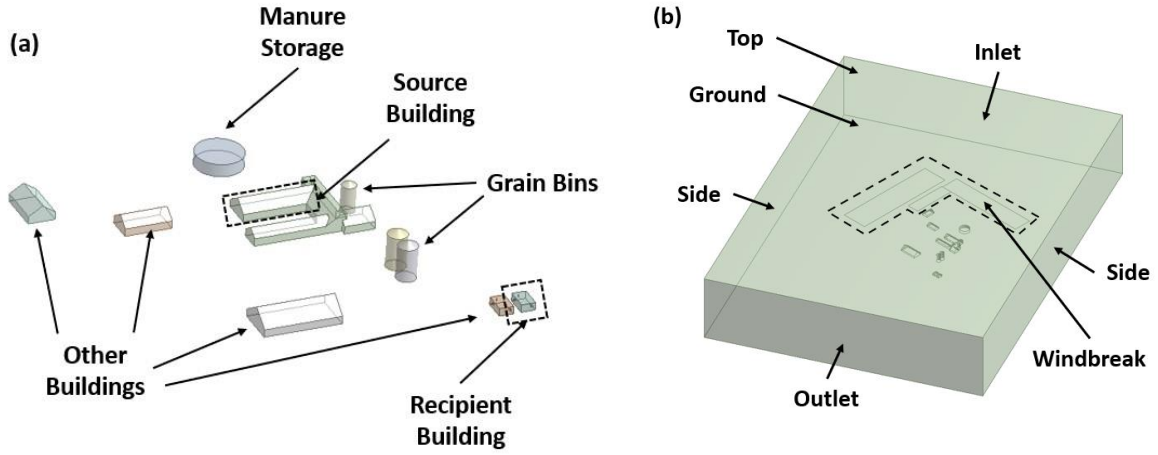

Figure 6.3. Illustration of simulation domain: (a) modelled site with source and recipient buildings identified (b) modelled site in domain with inlet, outlet, sides, top, ground, and windbreak identified

6.3.1.2. Field domain mesh refinement

The mesh for the field domain was generated in ANSYS Workbench (2019 R2, ANSYS Inc., Canonsburg, PA) and exported into OpenFOAM (Version 1806, OpenCFD Ltd., Bracknell, UK, Weller, Tabor, Jasak, & Fureby, 1998) for the simulations. The cell size at the ground was recommended to be twice the size of the surface roughness (Pontiggia, Derudi, Busini, & Rota, 2009). The local and global growth rates were less than or equal to 1.3, as recommended by (Franke et al., 2006). A mesh refinement process was performed to decide on an appropriate mesh. To summarize, three meshes were generated with the number of cells between the coarse and fine meshes increasing by a factor of 3.4 and the number of cells in the moderate mesh was $(3.4)^{0.5}$ times less than and more than the coarse and fine meshes, respectively. While it was recommended that the number of cells in consecutive meshes increase by 3.4 (Franke et al., 2006), the mesh size was limited by the computational resources in this study. A steady-state airflow simulation was performed with each mesh and the velocity along a plane from the source to recipient buildings was quantitatively compared. Based on results and the available computational resources, the fine mesh was chosen to use for all subsequent simulations in the field domain. The mesh had 15,708,582 tetrahedral cells with a global element size of 5 m. The local cell size at the ground was 1.2 m and the growth rate was 1.09.

6.3.1.3. Case study details

CFD Simulations were performed for the first replicate of the experiments performed in Pitkin et al. (2009) and Pitkin (2009), which spanned from June 1, 2006 to June 14, 2006. A positive air sample of PRRSV at the inlet of the recipient building was collected on June 7, 2006, with a titer of 4.40×10^{1} $TCID_{50}$ ml^{-1}. On June 9, 2006, PRRSV was detected in the sera of pig(s) in the recipient building, indicating aerosol transmission of PRRSV from the source building to the recipient building.

The simulations used the weather data between January 1, 2006 to December 31, 2007, collected at a weather station at the Appleton Municipal Airport located 6.8 km NW from the site of the study. Hourly weather data from June 2, 2006 to June 9, 2006 with wind directions between 303º and 348º (corresponding to the NWbw and NbW direction on a 32-point compass) were considered capable of transmitting PRRSV aerosols from the source building to the recipient building, as this range of wind directions caused the recipient building to be in the downwind plume of the source building. On June 6, 2006 and June 7, 2006, there were seven hours and five hours, respectively, in which the wind was within the wind direction range (Table 6.1). Nine CFD simulations were performed to simulate the transport of aerosols containing PRRSV from the source building to the recipient building using wind speeds measured on June 6, 2006 and June 7, 2006.

Table 6.1.Wind speeds and wind directions simulated in CFD (10 m from ground)

Date	Hour	Wind speed	Wind direction
		m s^{-1}	^{o} from true north
June 6, 2006	12	9.06	308
June 6, 2006	13	8.46	311
June 6, 2006	14	9.06	306
June 6, 2006	15	11.56	306
June 6, 2006	16	11.06	308
June 6, 2006	17	12.66	320
June 6, 2006	18	8.46	346
June 7, 2006	13	4.36	306
June 7, 2006	14	4.86	326
June 7, 2006	15	5.36	303
June 7, 2006	16	6.46	313
June 7, 2006	17	4.86	312
June 7, 2006	18	5.36	339

6.3.1.4. Steady-state airflow simulation

The CFD simulations were performed in OpenFOAM (Version 1806, OpenCFD Ltd., Bracknell, UK; Weller, Tabor, Jasak, & Fureby, 1998). A steady-state incompressible flow solver, SimpleFOAM, was used to reach a steady-state solution of the airflow pattern in the domain. The steady-state solution was considered to be achieved when the residual for pressure was below 10^{-4} and the residuals for velocity, turbulent kinetic energy, and rate of turbulent dissipation were below 10^{-5}, or if the residuals stabilized and no longer decreased with further iterations.

6.3.1.4.1. Boundary conditions

The boundary conditions for the steady-state simulation were determined according to the literature (Bonifacio, Maghirang, & Glasgow, 2015; Hargreaves & Wright, 2007; Prospathopoulos & Voutsinas, 2006; Richards & Hoxey, 1993; Tominaga et al., 2008; Versteeg & Malalasekera, 2007) and tutorial cases provided by OpenFOAM, Turbine siting and Wind Around Buildings (Weller et al., 1998). The atmBoundaryLayer boundary condition was used for the boundary conditions of velocity, turbulent kinetic energy, and rate of dissipation of turbulent energy at the inlet of the domain. This boundary condition utilizes equations developed by

(Richards & Hoxey, 1993) to calculate the velocity, turbulent kinetic energy, and rate of energy dissipation in the atmospheric boundary layers under neutral atmospheric conditions (Eqs. (6.2)-6.5)). The surface roughness z_0 of the ground was set to 0.6 m, as used by Seo et al. (2010) for agricultural and general ground.

$$U(z) = \frac{U^*}{\kappa} \ln\left(\frac{z - z_g + z_0}{z_0}\right) \tag{6.2}$$

$$k(z) = \frac{\left(U^*\right)^2}{\sqrt{C_{M\mu}}} \tag{6.3}$$

$$\varepsilon(z) = \frac{\left(U^*\right)^3}{\kappa\left(z - z_g + z_0\right)} \tag{6.4}$$

$$U^* = \kappa \times \frac{U_{ref}}{\ln\left(\frac{z_{ref} + z_0}{z_0}\right)} \tag{6.5}$$

where U(z) is the velocity profile at the inlet as a function of height z (m s^{-1}), k(z) is the turbulent kinetic energy profile at the inlet as a function of height z (m^2 s^{-2}), ε(z) is the rate of dissipation of turbulent energy profile at the inlet as a function of height z (m^2 s^{-3}), U^* is the friction velocity (m s^{-1}), κ is the von Karman's constant (0.41), z_0 is the surface roughness height (0.6 m; Seo et al., 2010), z_g is the minimum z-coordinate (0 m), $C_{M\mu}$ is the turbulence viscosity coefficient (0.09), U_{ref} is the velocity at z_{ref} (m s^{-1}), and z_{ref} is the reference height (m).

Based on guidelines for floor area of 8 to 9 ft^2 per finishing pig (MWPS, 1983) and the source building floor area of 275 m^2 (Otake, Dee, Jacobson, Torremorell, & Pijoan, 2002), it was assumed that the source building could house 350 pigs. This assumption was used to determine the ventilation rate and the velocity of the source building exhaust fans under summer conditions (Eqs. (6.6)-(6.7)), based on the recommended summer ventilation rate of 57 L s^{-1} (120 cfm) per pig for finisher pigs (MWPS, 1983). Similarly, the ventilation rate, the velocity at exhaust fans, and the velocity at the vent (Eq. (6.8)) were calculated for the recipient building by assuming it was designed for 30 nursery pigs and utilized a summer ventilation rate of 17 L s^{-1} (35 cfm) per pig (MWPS, 1983). Turbulent kinetic energy (Eq. (6.9)) and the rate of dissipation of turbulent energy at each fan (Eqs. (6.10)-(6.11)) were calculated according to methods presented in the

Wind Around Buildings tutorial provided by OpenFOAM (Weller et al., 1998). The parameters defining the boundary conditions for the steady-state simulation are summarized in Table 6.2.

$$Q_{building} = 0.0004719474 \times Q_{head} \times n_{pig} \tag{6.6}$$

$$u_{fan} = \frac{Q_{building}}{n_{fan}\left(\frac{\pi d_{fan}^{\ 2}}{4}\right)} \tag{6.7}$$

$$u_{vent} = \frac{Q_{building}}{w \times h} \tag{6.8}$$

$$k = 1.5 \times (I \times u_{fan})^2 \tag{6.9}$$

$$\varepsilon = C_{\mu}^{\ 0.75} \frac{k^{1.5}}{l} \tag{6.10}$$

$$l = 0.07 \times d_{fan} \tag{6.11}$$

where $Q_{building}$ is the ventilation rate of the building ($m^3\ s^{-1}$), Q_{head} is the summer ventilation rate per head (cfm $head^{-1}$; MWPS, 1983), n_{pig} is the number of pigs in the building, u_{fan} is the velocity of the exhaust fan of source building ($m\ s^{-1}$), u_{vent} is the velocity at the vent ($m\ s^{-1}$), w = width of vent (m), h is the height of vent (m), n_{fan} is the number of exhaust fans, d_{fan} is the diameter of the fan (m), k is the turbulent kinetic energy ($m^2\ s^{-2}$), ε is the rate of dissipation of turbulent energy at fans ($m^2\ s^{-3}$), I is the turbulence intensity of fans (5%), C_{μ} is the turbulence viscosity coefficient (0.09), and l is the length scale (m).

Table 6.2. Velocity (U), pressure (p), turbulent viscosity (μ_t), turbulent kinetic energy (k), and rate of dissipation of turbulent energy (ε) boundary conditions for field simulations

	U	**p**	**μ_t**	**k**	**ε**
Units	$m\ s^{-1}$	$m^2\ s^{-2}$	$m^2\ s^{-1}$	$m^2\ s^{-2}$	$m^2\ s^{-3}$
Inlet of domain	atmBoundary LayerInlet Velocity	zeroGradient	Calculated	atmBoundaryLayer InletK	atmBoundary LayerInletEpsilon
Outlet of domain	zeroGradient	uniform FixedValue	Calculated	zeroGradient	zeroGradient
Ground of domain	noSlip	zeroGradient	nutKAtm RoughWallFunction	kqRWallFunction Uniform	EpsilonWall Function
Top / Sides of domain	symmetry	symmetry	Symmetry	symmetry	symmetry
Exhaust fans of source buildings (inlet)	uniformFixed Value	zeroGradient	Calculated	fixedValue uniform	fixedValue uniform
Exhaust fan of recipient building (inlet)	uniformFixed Value	zeroGradient	Calculated	fixedValue uniform	fixedValue uniform
Recipient building vent (outlet)	uniformFixed Value	zeroGradient	Calculated	zeroGradient	zeroGradient
Building walls	noSlip	zeroGradient	nutKWallFunction Uniform	kqRWallFunction Uniform	epsilonWallFunction

Other important parameters in the steady state simulation are shown in Table 6.3, including numerical schemes, constants for turbulence, etc. The numerical schemes were adopted from the Wind Around Buildings tutorial, unless otherwise indicated.

Table 6.3. Air properties, k-epsilon parameters, windbreak parameters, and numerical schemes for field CFD simulations

Air properties	Density	1.20 kg m^{-3}
	Viscosity (nu)	1.50 m^2 s^{-1}
Turbulence model		Standard k-ε model (Launder & Spalding 1972)
k-ε parameters	$C_{M\mu}$	0.09
	C_1	1.44
	C_2	1.92
	σ_k	1
	σ_ε	1.11 (Hargreaves & Wright, 2007)
Windbreak parameters	Height	20 m
	Surface roughness	0.6 m (Seo et al., 2010)
	C_d	0.25 (Desmond et al., 2017; Desmond et al., 2014)
	LAD	5.75 m^{-1} (Desmond et al., 2017; Desmond et al., 2014)
	β_p	0.17 (Desmond et al., 2017; Desmond et al., 2014)
	β_d	3.37 (Desmond et al., 2017; Desmond et al., 2014)
	$C_{\varepsilon 4}$, $C_{\varepsilon 5}$	0.9 (Desmond et al., 2017; Desmond et al., 2014)
ddtSchemes[A]	default	steadyState
gradSchemes[A]	default	Gauss linear
	grad(U), grad(K), grad(epsilon)	cellLimited Gauss linear 1
divSchemes[A]	default	none
	div(phi,U)	bounded Gauss linearUpwind limited
	div(phi,k), div(phi,epsilon)	bounded Gauss limitedLinear 1
	div((nuEff*dev2(T(grad(U)))))	Gauss linear
laplacianSchemes[A]	default	Gauss linear limited corrected 0.33[B]
interpolationSchemes[A]	default	linear
snGradSchemes[A]	default	limited corrected 0.33[B]

[A] From the wind around buildings tutorial from OpenFOAM [B] From the turbine siting tutorial OpenFoam

6.3.1.4.2. Windbreak effect

Three windbreaks were present on the study site. A custom code by Segersson (2017) was utilized in OpenFOAM to simulate the windbreak effect on airflow through the addition of source terms to the momentum, turbulent kinetic energy, and rate of dissipation of turbulent energy equations. The source terms were previously used in ANSYS Fluent CFD simulations of windbreaks (Eqs. (6.12)-(6.14); Desmond, Watson, & Hancock, 2017; Desmond et al., 2014; Endalew, Hertog, Delele, et al., 2009; Endalew, Hertog, Gebrehiwot, et al., 2009). The windbreaks were assigned a surface roughness of 0.6 m (Seo et al., 2010) and a height of 20 m.

$$S_U = -\rho C_d \alpha |U| U \tag{6.12}$$

$$S_k = \rho C_d \alpha \left(\beta_p |U|^3 - \beta_d k |U| \right) \tag{6.13}$$

$$S_{\varepsilon} = \rho C_d \alpha \frac{\varepsilon}{k}\left(C_{\varepsilon 4}\beta_p |U|^3 - C_{\varepsilon 5}\beta_d k|U|\right) \quad (6.14)$$

where S_U is the source term for momentum equations (drag force in the i-direction), S_k is the source term for turbulent kinetic energy, S_ε is the source term for rate of dissipation of turbulent energy, |U| is the modulus of wind speed (m s^{-1}), U is the wind speed in the i-direction (m s^{-1}), ρ is the density of air (1.2 kg m^{-3}), C_d is the drag coefficient (0.25; (Desmond et al., 2017; Desmond et al., 2014), LAD is the leaf area density (5.75 m^{-1}; Desmond et al., 2017; Desmond et al., 2014), β_p is the constant 0.17 (Desmond et al., 2017; Desmond et al., 2014), β_d is equal to 3.37 (Desmond et al., 2017; Desmond et al., 2014), and $C_{\varepsilon 4}$ and $C_{\varepsilon 5}$ are equal to 0.9 (Desmond et al., 2017; Desmond et al., 2014).

6.3.1.5. Aerosol transport simulation

Aerosol transport simulations were performed to generate aerosols from the source building and track their movements in the atmosphere into the recipient building. The steady-state solutions for airflow were imported into the solver icoUncoupledKinematicParcelFOAM (icoUKPF) in OpenFOAM, which solves for particle movement using a pre-calculated velocity field. The icoUKPF solver tracked the location of aerosols in the domain over time after exiting the source building. The icoUKPF solver was programmed to log the entry of aerosols into the recipient building, specifically the aerosol diameters, the time that aerosols were within the field (aerosol age), and the time at which the aerosols entered the recipient building. Each simulation ran for 1500 s and aerosols were generated and tracked every 1 s.

Parameters used to calculate the aerosol size and injection rate for each aerosol size were obtained from Yang, Lee, Zhang, Wang, & Yang (2015), assuming summer conditions for a finisher pig facility. The equivalent spherical diameters (d_{eq}) of seven aerosol sizes and the mass fraction at each size were determined, assuming a log-normal distribution (Eq. (6.15)). The aerodynamic diameter (d_a) of the aerosols was calculated using Eqs. (6.16)-(6.18) (Jerez, Zhang, & Wang, 2011) to describe the aerosols in the icoUKPF simulations. The injection rates of aerosols from the north and south exhaust fans were also calculated (Table 6.4) and used as inputs in the icoUKPF simulations (Eqs. (6.19)-(6.24)).

$$d_{eq} = \begin{cases} \exp\left(\ln\left(MMD_{eq}\right) \pm 3\ln\left(GSD\right)\right) \\ \exp\left(\ln\left(MMD_{eq}\right) \pm 2\ln\left(GSD\right)\right) \\ \exp\left(\ln\left(MMD_{eq}\right) \pm \ln\left(GSD\right)\right) \\ MMD_{eq} \end{cases} \quad (6.15)$$

$$d_a = \frac{1}{2}\left[\left(6.35\lambda^2 + 4{d_{eq}}^2 C_c \frac{\rho_p}{\rho_o}\right)^{\frac{1}{2}} - 2.52\lambda\right] \quad \text{for } 0.1 \le d_{eq} < 3\ \mu\text{m} \quad (6.16)$$

$$d_a = d_{eq}\left(\frac{\rho_p}{\rho_o}\right)^{\frac{1}{2}} \quad \text{for } d_{eq} \ge 3\ \mu\text{m} \quad (6.17)$$

$$C_C = 1 + \frac{2.52\lambda}{d_{eq}} \quad \text{for } d_{eq} \ge 0.1\ \mu\text{m} \quad (6.18)$$

$$M = \frac{Q_{building} \times C_{dust}}{10^6} \quad (6.19)$$

$$M_d = M \times f_d \quad (6.20)$$

$$V_{eq} = \frac{4}{3}\pi\left(\frac{d_{eq} \times 10^{-6}}{2}\right)^3 \quad (6.21)$$

$$P_d = \frac{M_d}{n_{aerosol}\rho_p\left(V_{eq}\right)} \quad (6.22)$$

$$P_{d,north} = \frac{4P_d}{7} \quad (6.23)$$

$$P_{d,south} = \frac{3P_d}{7} \quad (6.24)$$

where d_{eq} is the seven equivalent spherical diameters of the aerosols (μm), MMD_{eq} is the equivalent spherical mass median diameter (16.6 μm; Yang et al., 2015), GSD is the geometric standard deviation (2.43; Yang et al., 2015), d_a is the aerodynamic diameter (μm), λ is the mean free path of air (0.066 μm), C_c is the slip correction factor, ρ_p is the density of aerosol (1690 kg m^{-3}; Yang et al., 2015), ρ_o is the unit density (1000 kg m^{-3}; Yang et al., 2015), M is the mass flow rate of aerosols (kg s^{-1}), C_{dust} is the concentration of particulate matter in finisher building (0.48 mg m^{-3}; Yang et al., 2015), f_d is the fraction of aerosols of diameter d_a, M_d is the fractional mass flow rate for aerosols of diameter d_a (kg s^{-1}), V_{eq} is the volume of a single aerosol of diameter d_a (m^3 $aerosol^{-1}$), P_d is the injection rate of aerosols of diameter d_a generated by source building (parcels s^{-1}), $n_{aerosol}$ is the number of aerosols per parcel (1000 aerosols $parcel^{-1}$), $P_{d,north}$ is the injection rate of aerosols of diameter d_a generated from fans on north side of source building

(parcels s^{-1}), and $P_{d,south}$ is the injection rate of aerosols of diameter d_a generated from fans on south side of source building (parcels s^{-1}).

Table 6.4. Injection rate of parcels (P_d) generated from north ($P_{d,north}$) and south ($P_{d,south}$) exhaust fans of the source building according to equivalent diameter (d_{eq}) and aerodynamic diameter (d_a).

d_{eq}	**d_a** [A]	**P_d**	**$P_{d,\ north}$**	**$P_{d,\ south}$**
µm	**µm**	Parcels s^{-1}	Parcels s^{-1}	Parcels s^{-1}
1.16	1.44	9374.15	5356.66	4017.49
2.81	3.60	10356.92	5918.24	4438.68
6.83	8.88	4583.84	2619.34	1964.50
16.60	21.58	802.36	458.49	343.87
40.34	52.44	55.92	31.95	23.96
98.02	127.43	1.55	0.89	0.66
238.19	309.65	0.02	0.01	0.01

[A] the aerodynamic diameters were used as inputs in the icoUKPF simulation

6.3.2. Recipient building simulations (CFD Model 2)

The CFD Model 2 simulated airflow and aerosol distributions in the pig pens within the recipient building. The simulation results (output) from the CFD Model 1 provided the input for performing in the simulations in the recipient building. CFD Model 2, along with the virus decay and the dose-response models calculated PRRSV exposure doses in different pens of the recipient building, as well as the subsequent probability of infection from these exposure doses. A summary of the recipient building simulations and data analysis is shown in Fig. 6.4, which shows the inputs and outputs of CFD Model 2, virus decay model, and dose-response model.

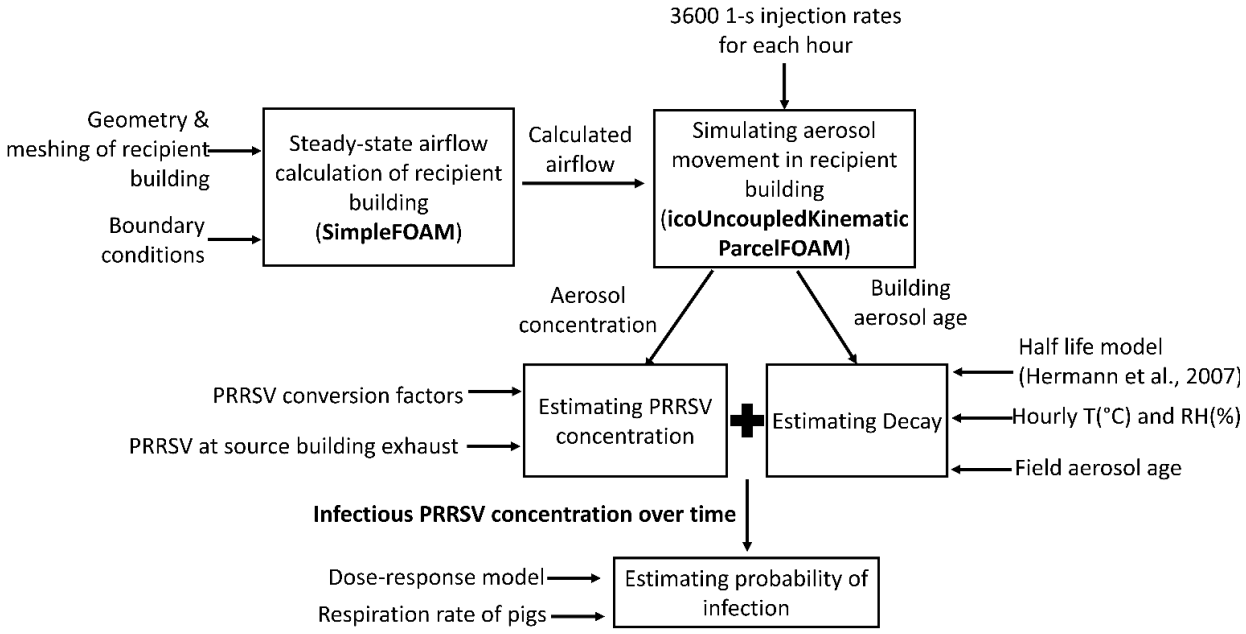

Figure 6.4. Summary of the CFD simulations and data analysis used to predict PRRSV exposure doses and probability of infection in pig pens in the recipient building

6.3.2.1. Recipient building geometry

The building dimensions were 8.5 m, 5.5 m, and 3.05 m in length, width, and height, respectively. The penning configuration was based on a schematic of the building (Pitkin, 2009). Pen walls were assumed to have a height of 1.219 m. There were six pens, each with dimensions of 1.0995 m, 1.008 m, 1.219 m in length, width, and height, respectively, and a volume of 1.351 m^3 (Fig. 6.5).

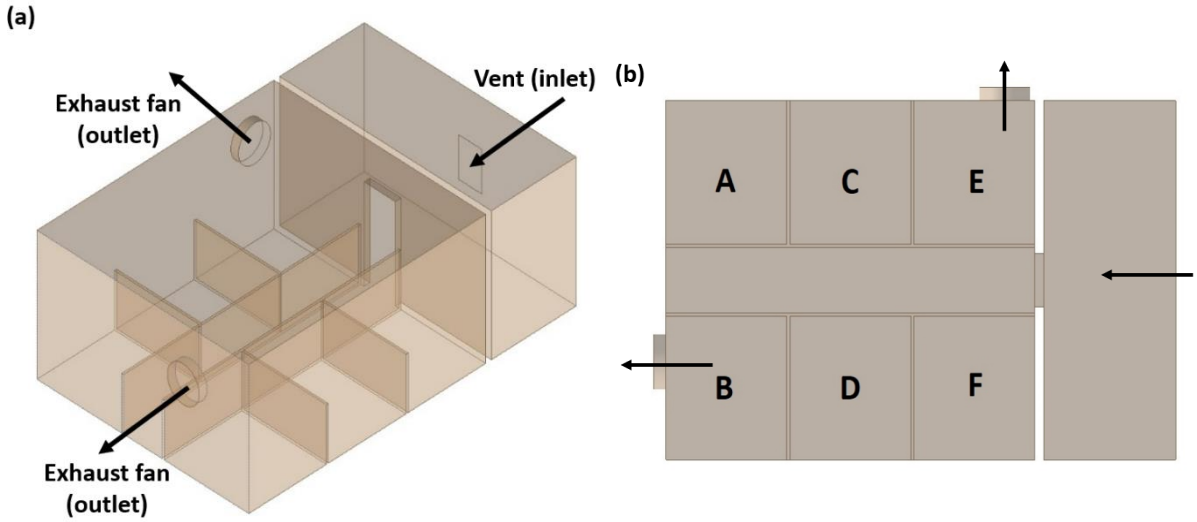

Figure 6.5. Geometry used for recipient building simulations, with arrows dictating the direction of airflow into and out of the building. (a) locations of vent (inlet) and exhaust fans, (b) top view of the geometry with location of pens A-F

6.3.2.2. Recipient building mesh refinement

Three meshes were generated for the recipient building and the mesh properties are summarized in Table 6.5. To determine the mesh that was best suited for use in subsequent simulations, a steady-state airflow simulation was performed using each mesh. The steady-state airflow solutions were exported to use with the icoUKPF solver to perform aerosol simulations. In the aerosol simulations, a constant stream of 100 parcels of 1.44 μm aerosols and 100 parcels of 3.60 μm aerosols was generated into the recipient building every second. Each parcel contained 1000 aerosols. The simulation length was 3600s. The aerosol distribution in the building was monitored every 300 s during simulations. The number of aerosols in each pen was counted during post-processing for each mesh and the average difference over the simulation period between the coarse and moderate meshes and between the moderate and fine meshes were compared. Given the results of the mesh refinement as well as the available computer resources, the finest mesh was suitable to use for subsequent simulations.

Table 6.5.Properties of three meshes generated for the recipient building

Mesh	Cell type	Cell width (m)	Number of cells
Coarse	Tetrahedral	0.1	1,192,474
Moderate	Tetrahedral	0.05	9,495,278
Fine	Tetrahedral	0.025	16,005,344

6.3.2.3. Steady-state airflow simulation

To set the velocity at the vent (inlet) and exhaust fans (outlet) of the recipient building, the boundary condition type flowRateInletVelocity (OpenFOAM, 2016a) was utilized to input the airflow rates. The airflow rate at the vent was equal to the velocity at the vent in the field simulation (CFD Model 1) u_{vent} multiplied by the area of the vent. The airflow rate at each exhaust fans was equal to half of the airflow rate at the vent, to ensure that the airflow rate into the building equaled the airflow rate out of the building and maintain conservation of mass. The pressure at the exhaust fans were calculated using Eq. (6.25) and the pressure at the vent was assumed to be 0 to create a pressure gradient from the vent to the exhaust fans. The k and ε values of the inlet vent were also calculated using Eqs. (6.26) and (6.27) using the equivalent diameter (The Engineering Toolbox, 2003). A summary of the boundary conditions for the steady-state airflow simulation are shown in Table 6.6.

$$p_{fan} = \frac{p_T - 0.5\rho {v_{fan}}^2}{\rho} \tag{6.25}$$

$$d_{vent} = 1.30 \times \frac{(w \times h)^{0.625}}{(w+h)^{0.25}} \tag{6.26}$$

$$l = 0.07 \times d_{vent} \tag{6.27}$$

where p_{fan} is the kinematic pressure at fan ($m^2 s^{-2}$), p_T is the total pressure (0 Pa), v_{fan} is the velocity at the fan ($m s^{-1}$), and d_{vent} is the equivalent diameter (m).

Table 6.6. Velocity (U), pressure (p), turbulent viscosity (μ_t), turbulent kinetic energy (k), and rate of dissipation of turbulent energy (ε) boundary conditions for recipient building simulation

	Units	Exhaust fans (outlet)	Vent (inlet)	Building wall and pens
U	$m\ s^{-1}$	flowRateInletVelocity	flowRateInletVelocity	noSlip
p	$m^2\ s^{-2}$	fixedValue uniform	fixedValue uniform	zeroGradient
μ_t	$m^2\ s^{-1}$	Calculated	Calculated	nutkWallFunction
k	$m^2\ s^{-2}$	zeroGradient	fixedValue uniform	kqRWallFunction
ε	$m^2\ s^{-3}$	zeroGradient	fixedValue uniform	epsilonWallFunction

The simulations were performed in the solver SimpleFOAM. Iterations were performed until the residuals stabilized, at 1.26×10^{-5} to 2.68×10^{-5} for velocity, 0.00145 for pressure, 0.00106 for ε, and 6.59×10^{-5} for k. The same air properties and numerical schemes were used in the recipient building CFD simulation as the field CFD simulation (Table 6.3). The k-ε parameters were also similar, and the only change was that the default σ_ε of 1.3 was used.

6.3.2.4. Aerosol movement simulation

The steady-state airflow data from the SimpleFOAM building simulation was exported to use with the solver icoUKPF. June 6 and June 7 aerosol simulations were performed separately. In each simulation, the injection rates into the building corresponded to the wind speed conditions associated with each hour, as seen in Table 6.1. During the simulations, the aerosol locations were tracked within the building and recorded every 300 s. The simulation time for both simulations was 43200 s. This accounted for the seven hours and six hours where aerosols were entering, respectively, in the June 6 and 7 simulations as well as four and five additional hours to monitor the aerosol concentration within the barn after aerosol entry ceased in the June 6 and 7 simulations, respectively.

To determine the injection rate of aerosols into the recipient building for each wind speed condition, the output data from the CFD Model 1 simulations was post-processed to count the number of aerosols per aerosol size that entered the building per second (i.e., determine the injection rate over time for each wind speed simulation). For aerosol sizes that had aerosol entry rates that varied on a normal distribution, the mean and standard deviation of the dataset of

injection rates were used to generate 3600 1-second injection rates over a 1-hour simulation. For aerosol sizes that had aerosol entry rates that did not follow a normal distribution, 3600 1-second injection rates were generated using the frequency that injection rates occurred during the field simulations. For wind speeds that occurred more than once, a different set of injection rates was generated for each hour.

6.3.3. Predicting pig infection (virus decay and dose-response models)

Data outputted from both the field and recipient building CFD simulations were used to calculate the aerosol age and PRRSV exposure doses of pigs located in different pens in the recipient building. First, literature data was used to convert aerosol concentrations to infectious PRRSV concentrations. Specifically, the amount of PRRSV exhausted from the source building, the decay of PRRSV due to exposure to different temperature and relative humidity conditions, and the effect of aerosol size on the amount of PRRSV that would be carried on an aerosol were considered in calculating the infectious PRRSV concentration in the recipient building. The respiration rate of pigs was used to determine the PRRSV exposure doses of pigs. After calculating the infectious PRRSV concentration and exposure doses, a dose-response model was used to predict that probability of infection of pigs (Fig. 6.4).

6.3.3.1. Analysis of aerosol data from CFD simulations

The aerosol data was exported from the recipient building simulations and analyzed in R Version 3.6.2 (R Core Team, 2017) in R Studio Version 1.2.5033 (RStudio Team, 2016). Filtering of data was performed using the library dplyr (Wickham, François, Henry, & Müller, 2020) to remove particles stuck on walls, pen walls, and the ground. Aerosols were also categorized by their position in the building to determine if they were located inside of a pig pen. Aerosols above the pig pens (at heights greater than 1.219 m) were not considered to be inside of the pig pens. The library ggplot2 (Wickham, 2009) was used to generate plots.

6.3.3.2. Estimating airborne PRRSV concentration

The concentration of airborne PRRSV is directly related to the concentration of aerosols in the air. Conversion factors were used to convert the number of aerosols to number of infectious PRRSV particles. The PRRSV conversion factors were determined from the data reported by Alonso et al. (2017), which provided measurements of airborne PRRSV

concentration and airborne particle (aerosol) concentrations at multiple particle size ranges. Using PlotDigitizer to determine, the measurements of aerosols (airborne particles) were reported at geometric mean diameters of 0.38, 0.70, 1.72, 3.86, 7.07, and 15.75 μm, while the airborne PRRSV concentrations were reported at geometric mean diameters of 0.06, 0.52, 0.88, 1.52, 2.65, 3.95, 5.28, 7.29, and 9.52 μm. To use the data reported in different size ranges, firstly, the cumulative aerosol fractions were calculated by dividing the aerosol concentration at each particle size by the total aerosol concentration (i.e., the sum of all individual measurements). Then, a model of the cumulative aerosol fractions was developed (Fig. 6.6; Eq. (6.28)) and was used to calculate the aerosol fraction at the aerosol size ranges that airborne PRRSV was collected in the study. These aerosols factions were used to calculate the aerosol concentration (in terms of number count) in the size ranges, using Eq. (6.29). The airborne PRRSV concentration and the newly-derived aerosol concentrations were used to calculate the conversion factor (the ratio between the number of airborne PRRSV particles and the number of airborne particles (aerosols), with Eq. (6.30). Thus, for each particle size range that airborne PRRSV was measured/reported by Alonso et al. (2017), there was an associated ratio as a PRRSV conversion factor for the aerosol sizes simulated (Table 6.7).

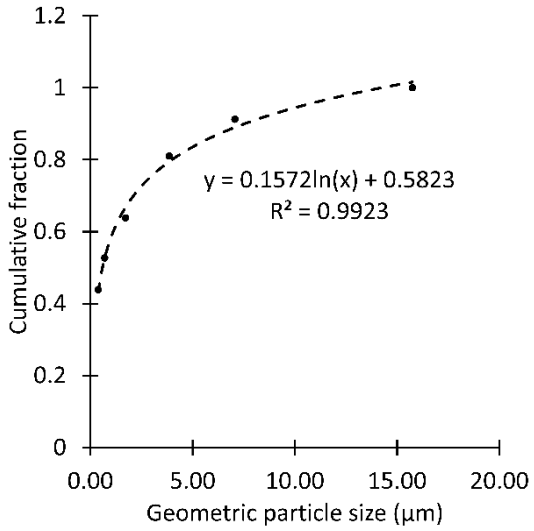

Figure 6.6. Cumulative fraction of aerosol (airborne particle) sizes measured in Alonso et al. (2017)

$$F_{N,\Delta d} = \left(\left(0.1572 \times \ln\left(d_1\right) + 0.5823\right) - \left(0.1572 \times \ln\left(d_2\right) + 0.5823\right)\right) \quad (6.28)$$

$$C_{N,\Delta d} = F_{N,\Delta d} \times \sum C_{N,m} \quad (6.29)$$

$$R_{VP} = \frac{C_{P,m\Delta d}}{C_{N,\Delta d}} \quad (6.30)$$

where $F_{N,\Delta d}$ is the fraction of particles within a size range Δd, Δd is the size range between particle diameters d_1 and d_2 (μm), $C_{N,\Delta d}$ is the aerosol (count) concentration in size range Δd (# m^{-3}), $C_{N,m}$ is the measured aerosol (count) concentrations from Alonso et al., (2017; # m^{-3}), R_{VP} is the ratio of PRRSV virus particles to aerosols (i.e., the PRRSV conversion factor) for aerosol diameter d_a, and $C_{P,m\Delta d}$ is the PRRSV RNA concentration within size range Δd measured in Alonso et al., (2017; RNA m^{-3}).

Table 6.7. The PRRSV conversion factor (R_{VP}) used to convert aerosols to infectious airborne PRRSV particles for each aerodynamic diameter (d_a) used in the CFD simulations.

d_a (μm)	**R_{VP}**
1.44	1.66×10^{-5}
3.60	6.18×10^{-5}
8.88	7.99×10^{-3}
21.6	6.22×10^{-2}

A second modification factor was required to ensure that the PRRSV concentration in the simulations matched the target minimum, mean, and maximum airborne infectious PRRSV concentrations measured at the exhaust of the source building in Pitkin et al. (2009) and Pitkin (2009). The modification factor f_{mod} was determined by trial and error using Eq. (6.31) until the $C_{P,fan}$ was within 0.5% of the measured target PRRSV concentrations. The target minimum, mean, and maximum PRRSV concentrations at the source building exhaust were 4.2, 5×10^2, and 1.25×10^5 $TCID_{50}$ m^{-3}, respectively, and the corresponding modification factors (f_{mod}) were 0.0009125, 0.10925, and 27.25.

$$C_{P,fan} = \sum_{d_a}\left(f_d C_{dust} \rho_p V_{eq} R_{VP} f_{\text{mod}}\right) \times 10^6 \quad (6.31)$$

where $C_{P,fan}$ is the concentration of PRRSV at source building exhaust ($TCID_{50}$ m^{-3}) and f_{mod} is the modification factor.

6.3.3.3. Decay of PRRSV infectivity

PRRSV infectivity decays with time (aerosol age) and the rate of decay is dependent on environmental conditions during transport in the atmosphere. The decay was modelled by a half-life equation for PRRSV that was generated by Hermann et al. (2007). The time was expressed as the aerosol age, which was calculated from the simulation results by considering two time-segments after releasing from the source building: the field segment (i.e., the time in the air before entering the recipient building, CFD Model 1) and the recipient building segment (i.e., the time in the air after entering the building, CFD Model 2). The field segment of the aerosol age for each aerosol size and wind speed was determined as the time at which more than 50% of the aerosols at that aerosol size had entered the recipient building during the simulation. The time at which more than 50% had entered was chosen as the aerosol age as it provided a good representation of the range in aerosol ages seen in the data. For example, at a wind speed of 9.06 m s^{-1}, an aerosol size of 1.44 μm had a field aerosol age of 116 s because 7541/23941 (74.6%) of 1.44-μm aerosols had entered the recipient building after 116 seconds. The building segment of the aerosol age was directly exported from the recipient building aerosol simulations.

To prepare for data analysis of CFD results, the temperature and relative humidity conditions at each hour of the June 6 and June 7 simulations were inputted into the half-life equation for PRRSV developed by Hermann et al. (2007) to calculate half-life values. The calculated half-life values were used to calculate the fraction of PRRSV remaining infectious with time; the fraction of infectivity remaining with time at different hours of the days is shown in Fig. 6.7. Exponential models were developed to describe the fraction of PRRSV infectivity at different temperature and relative humidity conditions (Table 6.8), based on the parameters θ and the field segment of aerosol age, and are described in Eq. (6.32). Exponential models for fraction of PRRSV infectivity over time in the recipient building were also developed for June 6 and June 7 using temperature and relative humidity combinations of 26˚C and 50% and 28˚C and 50%, respectively, and described by parameters θ and the building segment of aerosol age (Eq. (6.33)). These temperatures were the average of the ambient temperature in the hours simulated, while a relative humidity of 50% was chosen as MWPS (1983) recommended pig barns have a relative humidity between 50-80% and 50% was closer to the average of ambient relative humidity conditions in the hours simulated.

Eqs. (6.32)-(6.36) were used to calculate infectious PRRSV concentrations at different time points. Firstly, air parcels were individually assessed to determine their entry time into the recipient building (Eq. (6.34)), as it indicated which hour of day that the aerosol parcel was in the field and determined the value of the parameter θ (Table 6.8). The fraction of infectious PRRSV after time in the field was calculated using the field segment of aerosol age (Eq. (6.32)) and the building segment of the aerosol age was used to calculate the fraction of PRRSV infectivity remaining after entry into the building (Eq. (6.33)). The amount of infectious PRRSV within a parcel of aerosols was calculated using Eq. (6.35) and the concentration of infectious PRRSV in each pen was calculated according to Eq. (6.36).

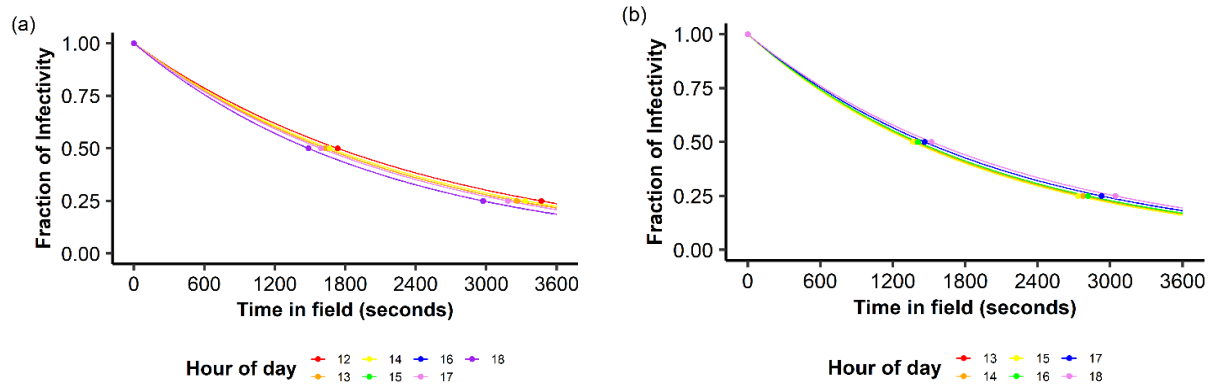

Figure 6.7. Fraction of PRRSV infectivity remaining after exposure time in field conditions in (a) the June 6 simulation and (b) the June 7 simulation. The hour of the day (time) is associated with specific temperature and relative humidity conditions indicated in Table 6.8 that affected the survival of PRRSV.

$$F_{field} = \exp\left(\theta \times T_{age,\,field}\right) \tag{6.32}$$

$$F_{building} = \exp\left(\theta \times T_{age,building}\right) \tag{6.33}$$

$$T_{enter} = t - T_{age,building} \tag{6.34}$$

$$N_{inf} = n_{aerosol} \times R_{VP} \times f_{\mathrm{mod}} \times F_{field} \times F_{building} \tag{6.35}$$

$$C_{inf}(t) = \frac{\sum_{Pen,t} N_{inf}}{V_{Pen}} \tag{6.36}$$

where T_{enter} is the time that aerosols entered building (s), θ is the parameter used to describe shape of PRRSV decay in decay model, t is the building simulation time (s), $T_{age,building}$ is the time that aerosols were inside of the building (s), F_{field} is the fraction of infectious PRRSV remaining after time in field, $T_{age,field}$ is the time that aerosols were in the field (s), $F_{building}$ is the

fraction of infectious PRRSV remaining after time in building, N_{inf} is the number of infectious PRRSV particles in an air parcel ($TCID_{50}$), $C_{inf,t}$ is the concentration of infectious PRRSV in pen at time t ($TCID_{50}$ m^{-3}), and V_{pen} is the volume of a pen (1.35 m^3).

Table 6.8. Parameter θ for calculating the fraction of infectious PRRSV remaining after field exposure (F_{field}) and building exposure ($F_{building}$) to different relative humidity (RH) and temperature (T) conditions in the simulations

Location	Hour of day	RH (%)	T (˚C)	Half-life [A] (s)	T_{enter} (s)	θ (×10^{-4})
June 6 Simulation						
Field	12	60	24	1735	0 to 3600	-3.996
Field	13	46	26	1630	3601 to 7200	-4.252
Field	14	43	26	1667	7201 to 10800	-4.157
Field	15	38	27	1592	10801 to 14400	-4.354
Field	16	36	28	1486	14401 to 18000	-4.664
Field	17	38	27	1592	18001 to 21600	-4.354
Field	18	47	27	1488	21601 to 25201	-4.659
Building	All	50	26	1575	All	-4.401
June 7 Simulation						
Field	13	36	29	1367	0 to 3600	-5.072
Field	14	34	29	1387	3601 to 7200	-4.996
Field	15	36	29	1367	7201 to 10800	-5.072
Field	16	32	29	1408	10801 to 14400	-4.921
Field	17	38	28	1464	14401 to 18000	-4.735
Field	18	44	27	1522	18001 to 21600	-4.555
Building	All	50	28	1282	All	-5.405

[A] half-life was calculated using the relative humidity and temperature values in a model developed by Hermann et al. (2007); $T_{1/2} = 339.037 \exp(-0.0839T - 0.00754RH)$, where $T_{1/2}$ is the half-life, T is the temperature (˚C), and RH is the relative humidity (%)

[B] T_{enter} is the time that aerosols entered building.

6.3.3.4. Exposure dose and probability of infection

The aerosol dose of PRRSV on 300-s intervals was calculated as a function of the mass of the pigs and their respiration rate (Eq. (6.37)). The respiration rates of pigs were obtained from Hannon, Bossone, & Wade (1990). The dose was calculated for 13.6 kg, 23.8 kg, and 34.0 kg nursery pigs, as the typical mass for nursery pigs. The probability of infection was calculated using a dose-response function (Eq. (6.38)) from Chapter 5, which describes the probability of infection upon aerosol exposure to PRRSV. The two model parameters α and β values were

determined in Chapter 5 (Table 6.9). The library gsl (Hankin, 2006) was used to call upon the Kummer confluent hypergeometric function and generate the doses according the dose-response function (Eq. (6.38)).

$$D(t) = C_{\inf}(t) \times R_{pig} \times M_{pig} \times \Delta t \tag{6.37}$$

$$P_{\inf} = 1 - {}_1F_1\left(\alpha, \alpha+\beta, -\sum_t D(t)\right) \tag{6.38}$$

where D(t) is the PRRSV aerosol dose at time t ($TCID_{50}$), R_{pig} is the respiration rate of pigs, (3.30e-6 m^3 s^{-1} kg^{-1}; (Hannon et al., 1990), M_{pig} is the mass of the pig (kg), Δt = 300 s, P_{inf} is the probability of infection, ${}_1F_1$ is the Kummer confluent hypergeometric function, and α, β are the parameters for the dose-response function.

Table 6.9. Values of parameters α and β used to calculate probability of infection due to PRRSV exposure by aerosol

	α	**β**
Maximum likelihood estimate (MLE)	1.077×10^{6}	1.159×10^{9}
2.5 percentile	1.411×10^{-5}	3.195×10^{-6}
97.5 percentile	7.114×10^{2}	7.653×10^{5}

6.4. Results and Discussion

6.4.1. Mesh refinement

6.4.1.1. Field domain mesh

The velocity magnitudes in different planes in the domain were used to determine which mesh was appropriate for field simulations (Fig. 6.8). The velocity magnitudes in the inlet of the domain in all three meshes were very similar (Fig. 6.8a). Windbreaks could have a major effect on the airflow in the atmospheric boundary layer, as windbreaks exert a drag force on the approaching airflow that slows and alters the airflow pattern (Dong et al., 2008). Simulating the effect of windbreaks on the velocity magnitudes resulted in differences in the velocity magnitudes between the three meshes. The coarse mesh predictions did not correspond well with the predictions of the moderate and fine meshes within and downwind of the windbreaks (Fig. 6.8b-d). The velocity magnitudes between the moderate and fine meshes had some differences within the windbreak (Fig. 6.8b), with the velocity at heights <20 m ≈ 0.5 m/s for the

fine mesh and ≈ 0.4 m/s for the moderate mesh. In the plane through the source building, the velocity magnitudes in the moderate mesh were generally greater than the velocity magnitude in the fine mesh, even at lower heights <20 m, but plateaued at a lower velocity magnitude at the higher heights than observed in the fine mesh (Fig. 6.8c). In the plane before the inlet of the recipient building, the velocity magnitudes at heights < 2.5 m in the three meshes were varied but were generally less than 2.5 m/s and did not have any other distinct patterns to note (Fig. 6.8d). At heights >2.5 m, the velocity magnitudes in the moderate and fine meshes followed a similar trend of velocity increase as seen in the source building plane (Fig. 6.8c). Near the outlet of the domain (Fig. 6.8e), the influence of the windbreaks on the airflow was minor as the velocity magnitudes between the meshes were approaching a trend similar to the one seen at the inlet of the domain (Fig. 6.8a). It was difficult to differentiate if the results of the mesh refinement tests were primarily affected by inadequate mesh resolution or not optimizing the simulation of the windbreak effect on airflow. Optimizing the simulation of the windbreak effect on airflow was outside of the scope of this study. Given that the inlet velocities of the three meshes were very similar, the patterns of velocity profile between the moderate and fine meshes were similar, and the difference in the average velocity magnitudes at the inlet plane being <5% between the moderate and fine meshes, the fine mesh was considered appropriate to run all subsequent simulations.

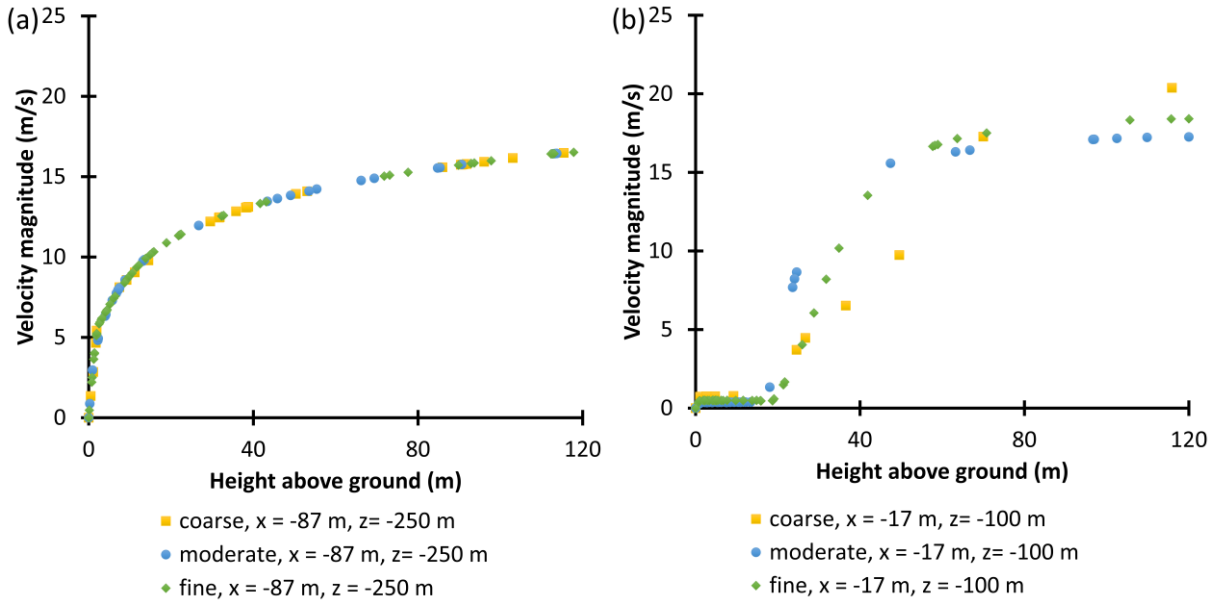

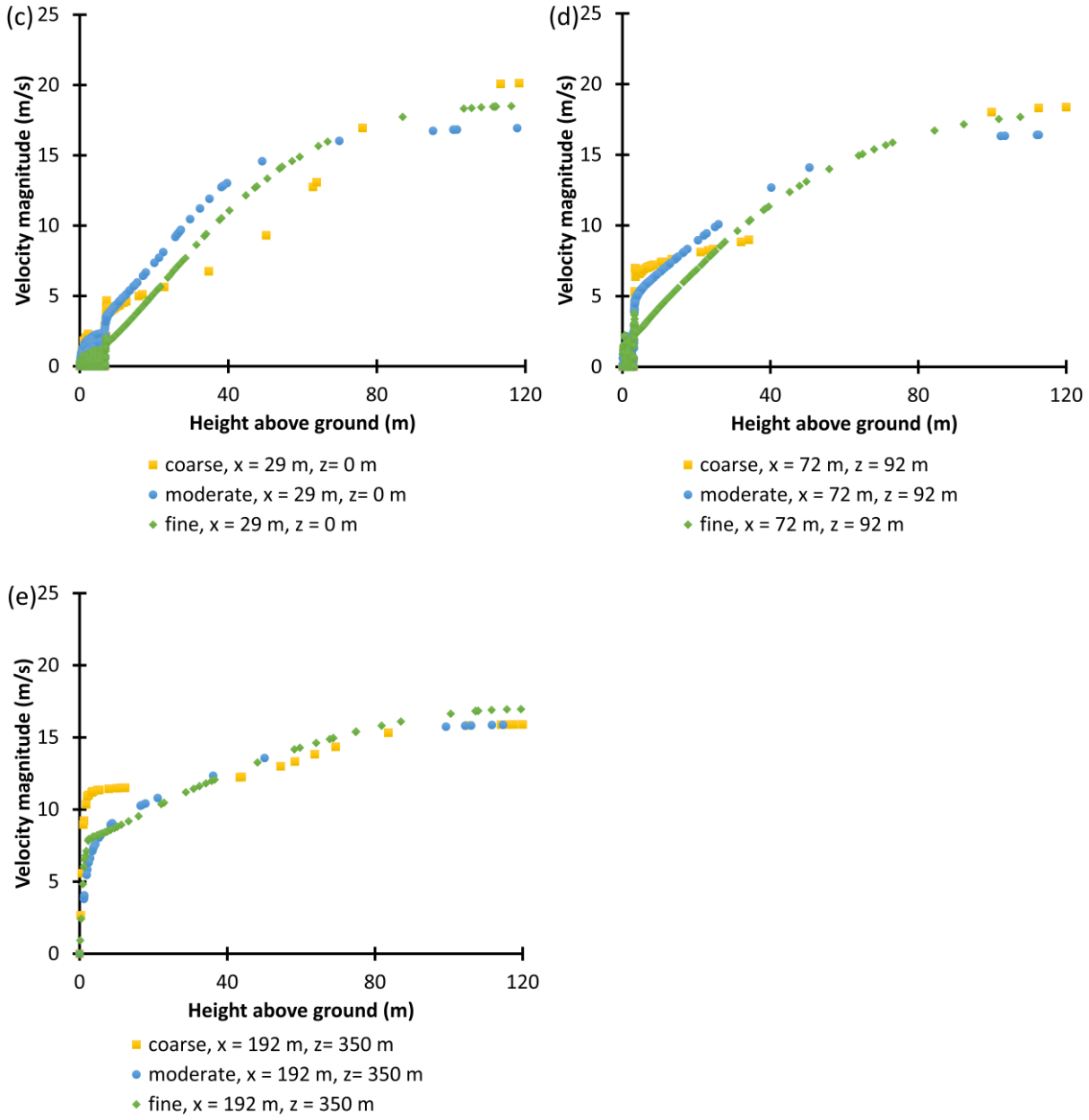

Figure 6.8. Mesh refinement results for field domain simulation, showing velocity variation between coarse, moderate, and fine meshes at (a) inlet, (b) within windbreak, (c) through source building, (d) before inlet of recipient building, (e) near outlet of the domain.

6.4.1.2. Recipient building mesh

The average difference in the number of aerosols per pen over time between different meshes are shown in Fig. 6.9. In the ideal scenario, the mesh would be chosen based on a

convergence in the difference in aerosol count between meshes. In this case, the average difference in aerosol counts between the moderate and fine meshes (Fig. 6.9b) was less than the average difference in aerosol counts between the coarse and moderate meshes (Fig. 6.9a), indicating that the difference in aerosol count was decreasing but had not yet reached convergence. In particular, the aerosol count difference in Pen E remained high, possibly due to its position relative to the entrance of the room and exhaust fan. While further mesh refinement could have been performed until the difference in results between mesh sizes was smaller, the simpleFOAM simulation with the fine mesh required two months to complete and further mesh refinement would have been impractical due to the long simulation time. Additionally, it is recommended in future work to use artificial aerosol generation, air sampling, and airflow measurements inside the enclosed space being simulated to obtain boundary conditions and data that could be used to determine the accuracy of different meshes during model development as well as optimize other features of the CFD model. In this case, there was no information on indoor virus concentrations, aerosol concentrations, or airflow patterns, so given the computational restrictions, the fine mesh (16,005,334 cells) was the best choice for subsequent building simulations.

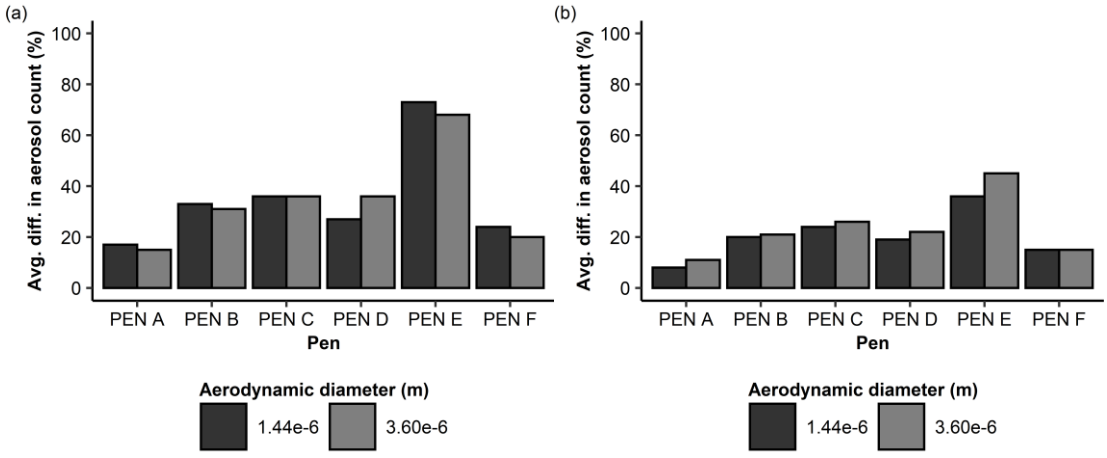

Figure 6.9. Average percent difference in the aerosol count (with aerodynamic diameters of 1.44×10^{-6} m and 3.60×10^{-6} m) in each pen (a) between the coarse and moderate meshes and (b) between the moderate and fine meshes.

6.4.2. Aerosol concentration in building

The aerosol concentration in the pens was affected by the entry rate of aerosols into the recipient building, which was dictated by the wind speed conditions in the field for a given rate of aerosol release from the source building. The distribution of aerosol entry rates for aerosols with aerodynamic diameters of 1.44 μm (Fig. 6.10a), 3.60 μm (Fig. 6.10b), and 8.88 μm (Fig. 6.10c) at wind speed conditions of 4.36 to 11.06 m s^{-1}. Note that aerosol entry rates during the 11.06 m s^{-1} simulation did not vary on a normal distribution and simulations with wind speeds of 11.56 and 12.66 m s^{-1} were not included in these figures as these simulations resulted in unstable, low aerosol entry rates of 1 parcels s^{-1} for ≤1.1% of the time.

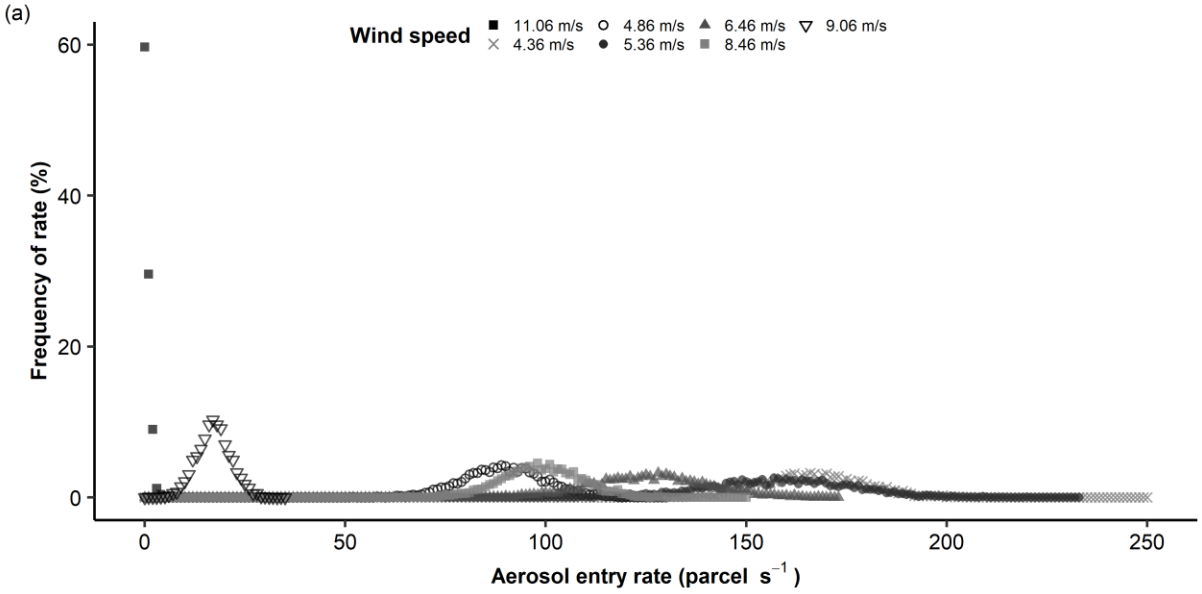

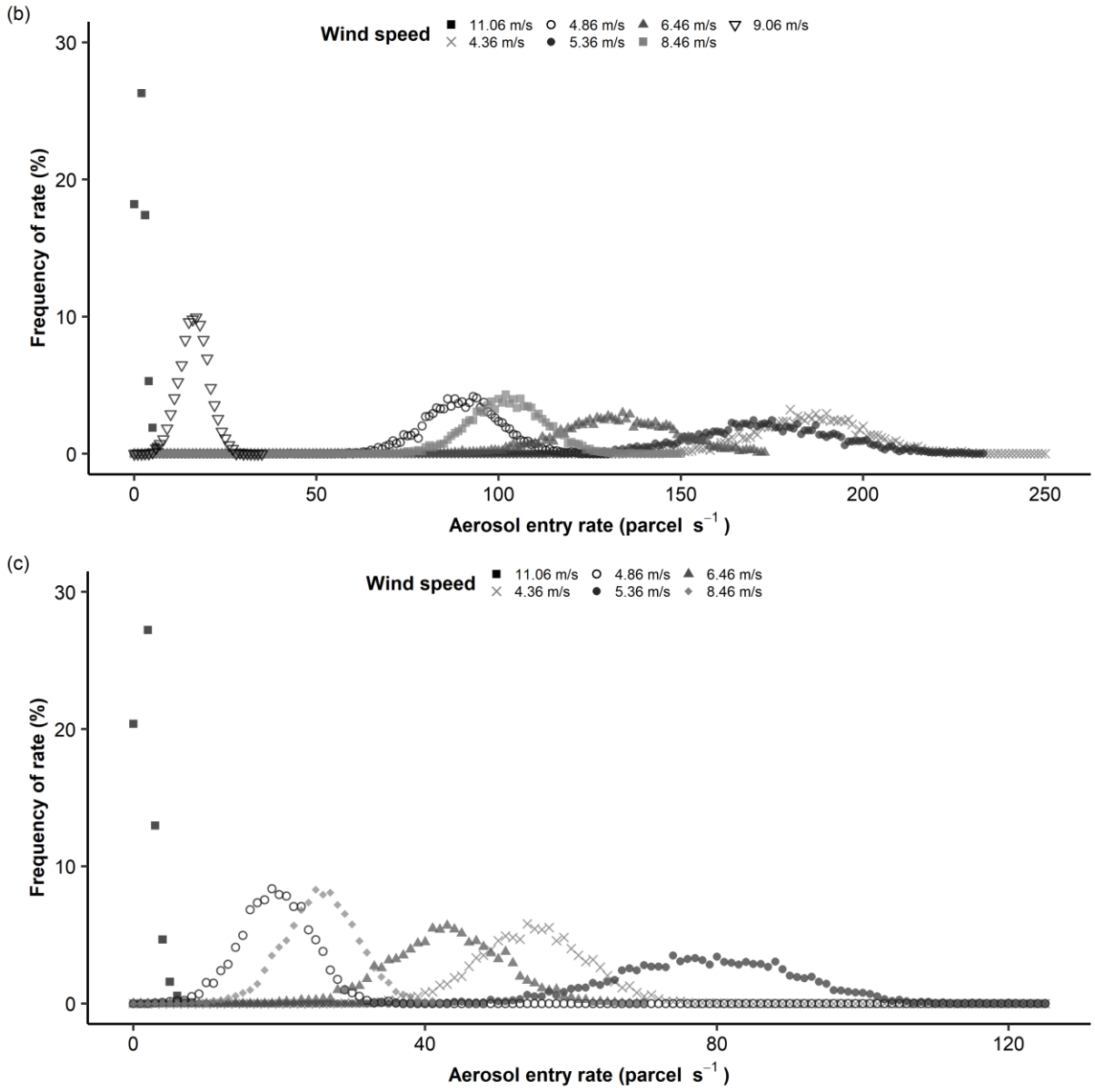

Figure 6.10. Frequency of aerosol entry rates into recipient building, according to wind speed for aerosol with aerodynamic diameters of (a) 1.44 µm, (b) 3.60 µm, and (c) 8.88 µm

The aerosol concentration over time in the June 6 simulation is shown in Fig. 6.11. The wind speeds in the field ranged from 8.46 to 12.66 m s^{-1} on June 6. The first few hours had wind speed ≤9.06 m s^{-1}, resulting in a continuous entry rate which followed a normal distribution at each wind speed. The next three hours had higher wind speeds (≥11.06 m s^{-1}) that resulted in an unstable, non-continuous entry rate of aerosols into the recipient building and a drop in the

aerosol concentration in the building as more aerosols were removed out of the building than entered. The next hour of the June 6 simulation had a lower (8.46 m s^{-1}) wind speed, resulting in an increase in the aerosol concentration over this hour. After this hour, there was no aerosol entry as the wind direction had changed, so the aerosol concentration in the building continued to decrease with time as the aerosols were ventilated out of the building. Overall, the aerosol entry rate varied in the June 6 simulation due to wind speed variations and the aerosol count per pen ranged from 4.00×10^3 to 2.41×10^6 during the seven hours of aerosol entry. It was primarily aerosols that had aerodynamic diameters of 1.44 μm (Fig. 6.11a) and 3.60 μm (Fig. 6.11b) that were present in pens, while aerosols with an aerodynamic diameter 8.88 μm were present in the pens as well (Fig. 6.11c), but less frequently than the other sizes and more often in the second, fifth, and seventh hours of the June 6 simulation. Aerosols with an aerodynamic diameter of 21.58 μm were also present within pens sporadically but were removed from the airstream quickly and did not contribute much to the aerosol concentration in the pens. Overall, the presence of more smaller aerosols in the recipient building was logical as larger aerosols were more likely to settle prior to entering the building; additionally, more aerosols with aerodynamic diameters of 1.44 μm and 3.60 μm were exhausted from the source building than aerosols with an aerodynamic diameter of 8.88 μm (Table 6.4). It was also important to distinguish between the aerosol sizes within the building, as different aerosol sizes were associated with different amounts of infectious virus. The hours with higher concentrations of 8.88-μm aerosols would have higher concentrations of infectious PRRSV as each 8.88-μm aerosol could carry 481.3 times and 129.3 times more infectious PRRSV (before decay) than a 1.44-μm and 3.60-μm aerosol, respectively.

The wind speeds on June 7 ranged from 4.36 to 6.46 m s^{-1} and the entry of aerosols into the building was continuous during the first six hours of the simulation. The entry rate of the aerosols varied with the wind speed, and the aerosol entry rates followed a normal distribution. The continuous aerosol entry in the June 7 simulation resulted in higher aerosol concentrations during the six hours of aerosol entry than June 6, ranging from 1.45×10^5 to 4.31×10^6 aerosols per pen (Fig. 6.12d). After the aerosol entry ceased due to a change in wind direction, there was a gradual decline in the aerosol concentration over time in all pens. The change in aerosol

concentration over time for aerosols with aerodynamic diameters of 1.44 μm (Fig. 6.12a), 3.60 μm (Fig. 6.12b), and 8.88 μm (Fig. 6.12c) had a similar pattern to the change in overall aerosol concentration over time for the first six hours of the simulation. In terms of magnitude, the aerosol concentrations of larger aerosols (8.88-μm) were less than that of the smaller aerosols (1.44-μm and 3.60-μm), for the same reasons mentioned for the June 6 simulation. It is important to note the higher concentration of aerosols in the pens, especially 8.88-μm aerosols, greatly increased the infectious PRRSV concentration present in the pens, compared to the June 6 simulation.

The pen location minimally affected the aerosol concentration in the pen during the first 6-7 hours of the simulations when aerosols were entering the building. A general observation was that the aerosol concentration in Pen E had a higher aerosol concentration after the aerosol entry into the building had ceased and when the aerosol entry rate was low, but Pen E also had lower aerosol concentration than other pens when aerosol entry rate was higher. Pen E is adjacent to the entrance of the room and also closest to one of the exhaust fans, so this position might have affected the airflow behavior in the pen and subsequently the aerosol concentration within this room over time.

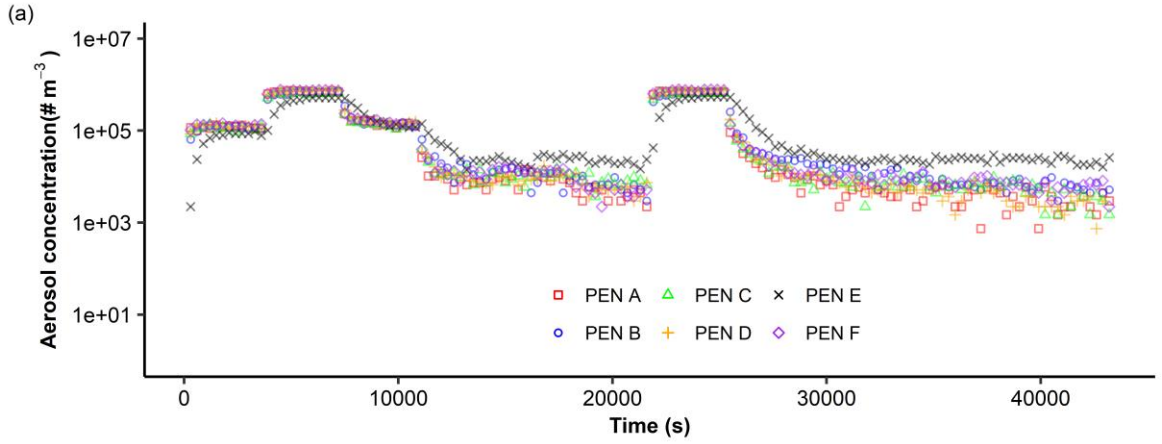

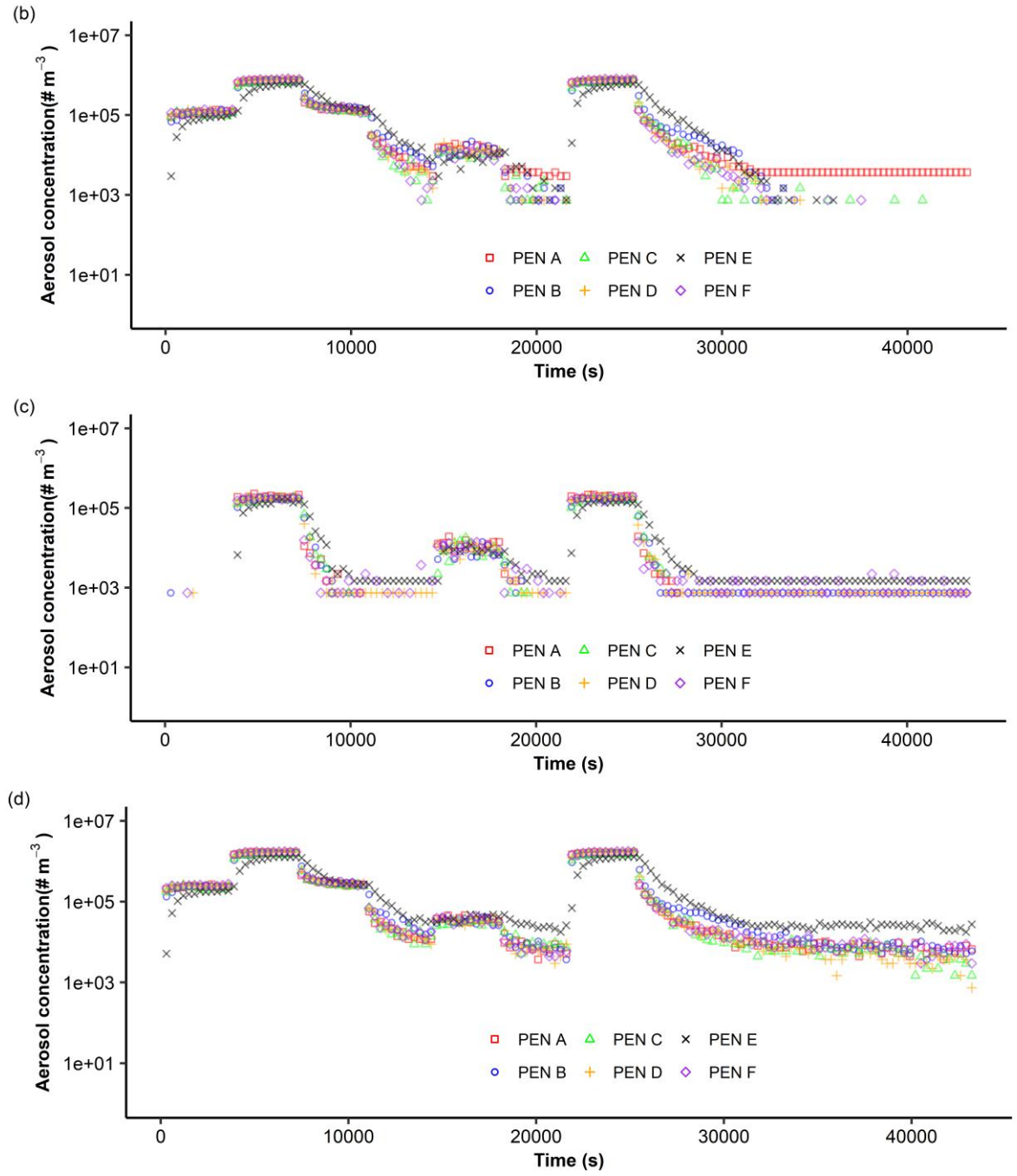

Figure 6.11. Aerosol concentration (# m^{-3}) during June 6 simulation in each pen in terms of time (s) since aerosol entry into building began, for aerodynamic diameter (a) 1.44 μm, (b) 3.60 μm, (c) 8.88 μm, (d) all particles

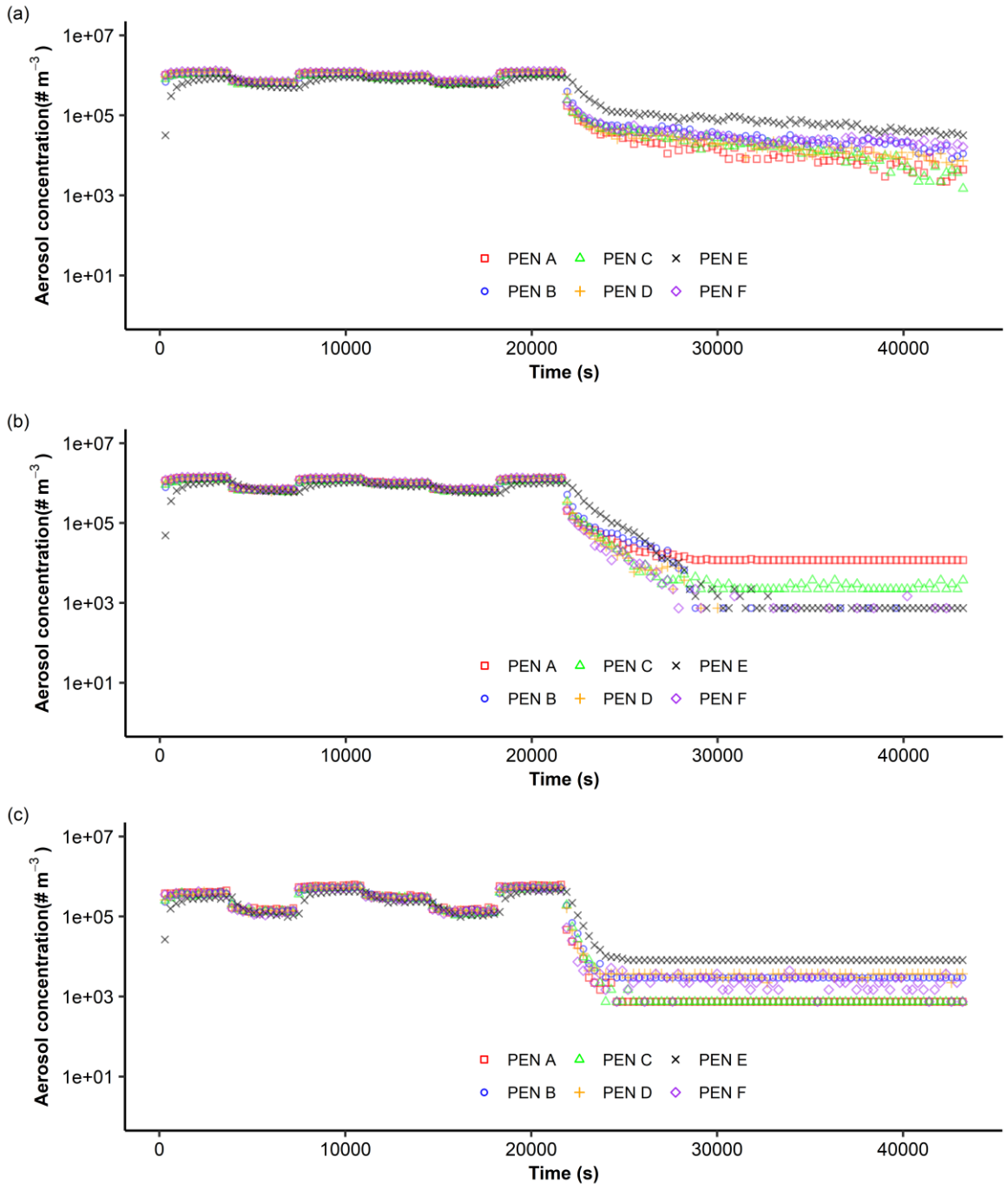
(a)
Aerosol concentration(# m^{-3})
1e+07
1e+05
1e+03
1e+01
PEN A
PEN C
PEN E
PEN B
PEN D
PEN F
0
10000
20000
30000
40000
Time (s)
(b)
Aerosol concentration(# m^{-3})
1e+07
1e+05
1e+03
1e+01
PEN A
PEN C
PEN E
PEN B
PEN D
PEN F
0
10000
20000
30000
40000
Time (s)
(c)
Aerosol concentration(# m^{-3})
1e+07
1e+05
1e+03
1e+01
PEN A
PEN C
PEN E
PEN B
PEN D
PEN F
0
10000
20000
30000
40000
Time (s)

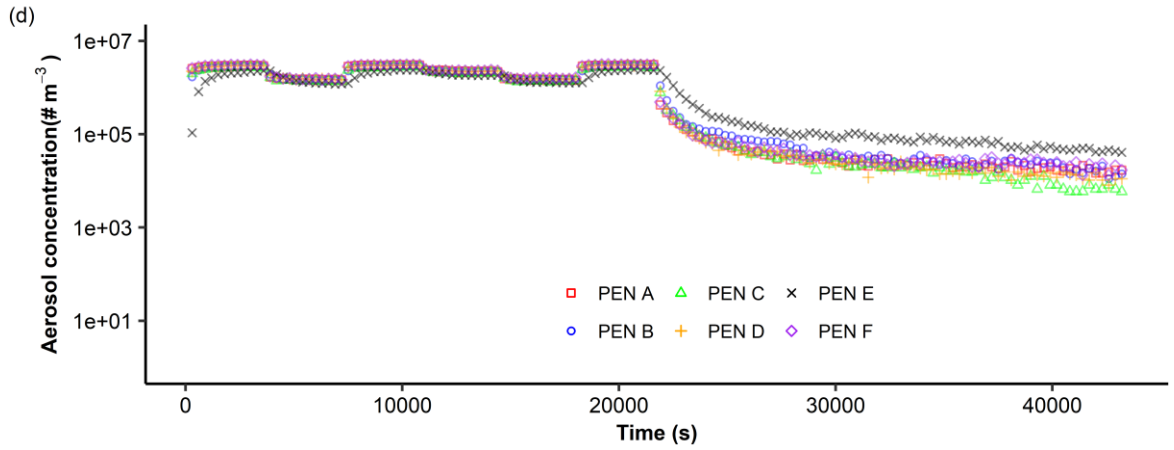

Figure 6.12. Aerosol concentration (# m^{-3}) during June 7 simulation in each pen in terms of time (s) since aerosol entry into building began, for aerodynamic diameter (a) 1.44 µm, (b) 3.60 µm, (c) 8.88 µm, (d) all particles

6.4.3. Airborne PRRSV concentration in building

After considering the loss of infectivity due to aerosol aging with time, as well as the effects of temperature and relative humidity, the infectious PRRSV concentrations within the pens of the recipient building in the June 6 simulation were predicted (Fig. 6.13 and 6.14). The PRRSV concentrations in the recipient building had the same patterns of variation with time for the minimum (Fig. 6.13a), moderate (Fig. 6.13b), and high (Fig. 6.13c) PRRSV concentrations released from source building. Over the course of the simulation, the PRRSV concentration was highest in the second and seventh hour, due to high amounts of aerosols entering the building in these two hours, and lowest during the fourth and sixth hours of the simulation, due to low amounts of aerosols entering the building. It should be noted that the fifth hour has higher PRRSV concentration than the fourth and sixth hours of the simulation, despite only having a slightly higher aerosol concentration during this hour, because of the increased amounts of 8.88-µm aerosols present in the pens during the fifth hour. Hours two and seven also had higher concentrations of 8.88-µm aerosols, and this is also reflected in the PRRSV concentration in the building. Hours eight and onward have a steady decline in PRRSV concentration because there was a decline in aerosol concentration as well as the decay in infectious PRRSV. For the June 7 simulation, since the aerosol concentrations in the pens remained high during the first six hours of the simulation, with some variations from hour to hour, the PRRSV concentrations also

remained high during this time frame (Fig. 6.14). In the seventh hour and onwards, there was a decline in the PRRSV concentration due to the aerosol concentration declining and a decay in PRRSV.

The magnitude of the PRRSV concentration in the pens was affected by the PRRSV concentration in the air exhausted from the source building. When the PRRSV concentration in the source building exhaust was minimal (4.2 $TCID_{50}$ m^3), the concentrations within the pens in both June 6 and 7 simulations were low during the hours of aerosol entry, ranging from 3.98×10^{-8} to 1.57 $TCID_{50}$ m^{-3} (Fig. 6.13a) and 1.62×10^{-1} to 4.07 $TCID_{50}$ m^{-3} (Fig. 6.14a), respectively. A moderate amount of PRRSV in the source building exhaust air (500 $TCID_{50}$ m^{-3}) resulted in pen PRRSV concentrations that ranged from 4.77×10^{-6} to 1.88×10^{2} $TCID_{50}$ m^{-3} in the June 6 simulation (Fig. 6.13b) and 1.95×10^{1} to 4.87×10^{2} $TCID_{50}$ m^{-3} in the June 7 simulation (Fig. 6.14b) during the hours of aerosol entry. A high level of PRRSV concentration in the source building exhaust air (125,000 $TCID_{50}$ m^3) resulted in pen PRRSV concentrations that ranged from 1.19×10^{-3} to 4.69×10^{4} $TCID_{50}$ m^{-3} (Fig. 6.13c) in the June 6 simulation and 4.85×10^{3} to 1.21×10^{5} $TCID_{50}$ m^{-3} in the June 7 simulation (Fig. 6.14c) during the hours of aerosol entry.

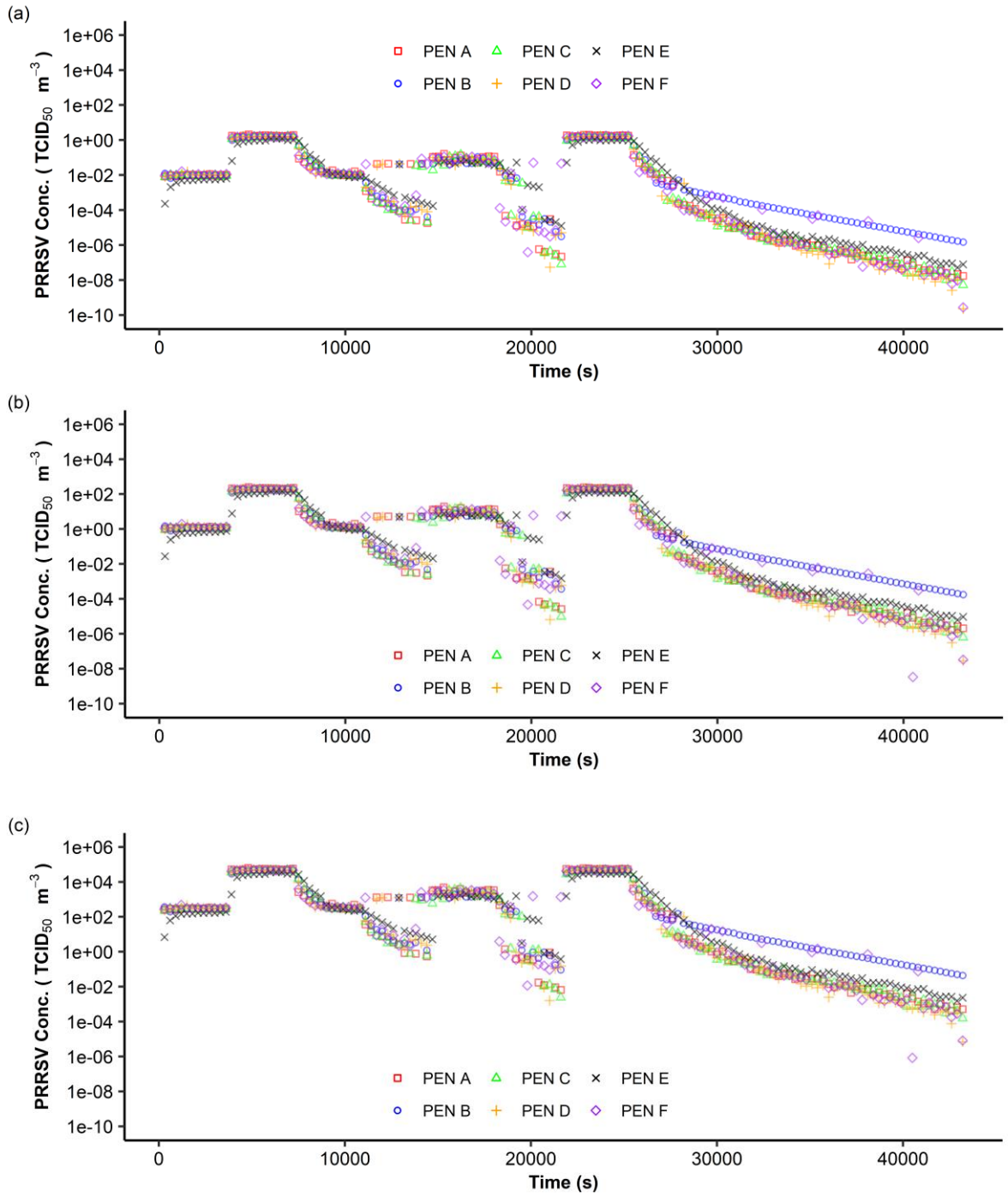

Figure 6.13. For June 6 simulation, the airborne PRRSV concentration ($TCID_{50}$ per m^3) in pens when different PRRSV concentrations were exhausted from source building, with PRRSV entry occurring during 0 to 25200s for different PRRSV concentrations released from the source building. (a) minimum release concentration of 4.2 $TCID_{50}$ m^{-3}, (b) mean release concentration of 500 $TCID_{50}$ m^{-3}, (c) maximum release concentration of 125,000 $TCID_{50}$ m^{-3}.

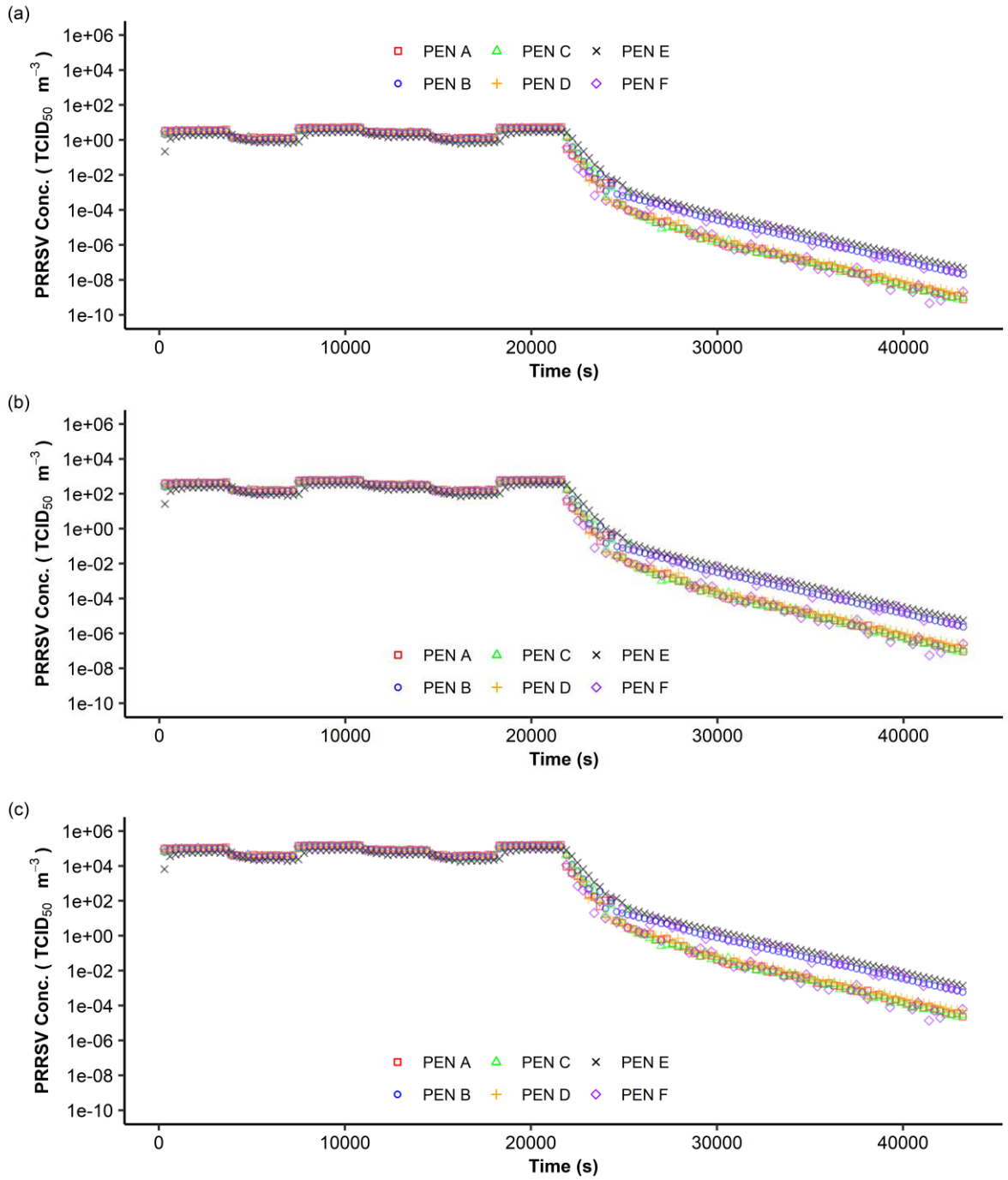

Figure 6.14. For June 7 simulation, the airborne PRRSV concentration ($TCID_{50}$ per m^3) in the pens when different PRRSV concentrations were exhausted from source building, with PRRSV entry occurring during 0 to 21600s for different PRRSV concentrations released from the source building. (a) minimum release concentration of 4.2 $TCID_{50}$ m^{-3}, (b) mean release concentration of 500 $TCID_{50}$ m^{-3}, (c) maximum release concentration of 125,000 $TCID_{50}$ m^{-3}.

6.4.4. Exposure dose and probability of infection

Based on the cumulative PRRSV exposure dose of nursery pigs, predicted probabilities of infection are summarized in Table 6.10 and Table 6.11 for the June 6 and June 7, respectively. The probability of infection was to some degree dependent upon the weight of the nursery pigs, as heavier pigs had a higher respiration rate and would acquire a larger dose of PRRSV. The pig location (pens) also had some effect on the probability of infection as well, with the lowest probability of infection occurring in Pen E and the highest probability of infection occurring in Pen A when the moderate amount of PRRSV (500 $TCID_{50}$ m^{-3}) was exhausted from the source building. For example, 13.6-kg pigs had exposure doses of 151 $TCID_{50}$ in pen E and 278 $TCID_{50}$ in pen A in the June 7 simulation, resulting in MLE probability predictions of 13% and 23%, respectively. The difference in probability of infection between pens E and A were smaller in the June 6 simulation than June 7, with 3% for pen E and 5% for pen A.

The PRRSV concentration in the air exhausted from the source building had the most effect on the probability of infection. When the source building exhausted a low PRRSV concentration (4.2 $TCID_{50}$ m^{-3}), the cumulative dose of exposure was low for both June 6 and 7, ranging from 0.3 to 1.1 $TCID_{50}$ in the June 6 simulation and 1.3 to 5.8 $TCID_{50}$ in the June 7 simulation. At these doses, the probability of infection predicted using the maximum likelihood estimates (MLE) dose-response model was between 0 to 1%. The probability of infection at these doses predicted using the 95% confidence interval predictions of α and β in the exact Beta-Poisson dose-response model varied widely, usually starting at 0% and ending in 58 to 81%.

When the source building exhausted a moderate PRRSV concentration (500 $TCID_{50}$ m^{-3}), the cumulative dose of exposure was higher for both simulations, with doses ranging from 30 to 136 $TCID_{50}$ in the June 6 simulation and 151 to 695 $TCID_{50}$ for the June 7 simulation. The higher exposure doses resulted in higher probability of infection predictions in the June 7 simulation, as the MLE predictions for probability of infection ranged from 3 to 12% for the June 6 simulation and 13 to 48% for the June 7 simulation. When a high PRRSV concentration (125,000 $TCID_{50}$ m^{-3}) was exhausted from the source building, the cumulative PRRSV exposure doses ranged from 7.57×10^3 to 3.40×10^4 $TCID_{50}$ for the June 6 simulation and 3.76×10^4 to 1.73×10^5 $TCID_{50}$ for the June 7 simulation. The corresponding MLE for probability of

infection was 100% for all June 6 and June 7 doses and the 95% confidence interval for all doses was also 82 to 100%.

In the case study simulated in this study, the authors did not specify how many pigs became infected in the recipient building on June 6 and 7, nor the location of the infected pigs. However, Pitkin (2009) specified that clinical disease was observed during the experimental replicate that included June 6 and June 7 and at least one pig tested positive for PRRSV on the 9^{th} day of the experimental replicate (~June 9). While there was no hourly data of the airborne PRRSV concentration entering or inside of the recipient building available, there was a positive PRRSV measurement that occurred the morning of June 7 at the entry of the recipient building with a titer of 4.4×10^{1} $TCID_{50}$ mL^{-1} in the air sample. This positive sample provides some verification to the CFD simulations of this study, as it indicates that: (1) infected pigs emitted infectious PRRSV aerosols on June 7; (2) the level of PRRSV concentration emitted from the source building on June 7 was high enough to be detected at the recipient building inlet; (3) the June 7 weather conditions, including wind speed, wind direction, temperature, and relative humidity, permitted the aerosol transport of infectious PRRSV from the source to recipient building, which was in agreement with the simulation result in this study. The results of this study showed that there was higher aerosol entry rate into the recipient building on June 7 due to the wind speed conditions and the probability of infection was higher in the June 7 simulation than the June 6 simulation when moderate levels of PRRSV were emitted from the source exhaust. Therefore, these results as well as the verification from Pitkin et al. (2009) and Pitkin (2009) indicate that it was likely that aerosol transmission occurred on June 7, 2006, during replicate 1 of the one-year study.

Table 6.10. Predicted probabilities of infection of pigs within recipient building according to pig weight, pen location, PRRSV concentration in source building exhaust air on June 6. MLE was the probability of infection based on the maximum likelihood estimation of parameters α and β in the exact Beta-Poisson dose-response model for aerosol transmission of PRRSV. The 95% confidence interval (CI) was the range of probability of infection values predicted with the 2.5%-percentile and 97.5-percentile estimates for α and β were used in the exact Beta-Poisson dose-response model for aerosol transmission of PRRSV.

Source Exhaust		**4.2 $TCID_{50}$ m^{-3}**			**500 $TCID_{50}$ m^{-3}**			**125,000 $TCID_{50}$ m^{-3}**		
Pig weight (kg)	Pen	Dose	MLE	95% CI	Dose	MLE	95% CI	Dose	MLE	95% CI
13.6	A	0.5	0	(0 - 30)	54	5	(5 - 82)	1.36×10^4	100	(82 - 100)
13.6	B	0.4	0	(0 - 25)	44	4	(4 - 82)	1.11×10^4	100	(82 - 100)
13.6	C	0.4	0	(0 - 25)	43	4	(4 - 82)	1.08×10^4	100	(82 - 100)
13.6	D	0.4	0	(0 - 26)	47	4	(4 - 82)	1.16×10^4	100	(82 - 100)
13.6	E	0.3	0	(0 - 18)	30	3	(3 - 82)	7.57×10^3	100	(82 - 100)
13.6	F	0.4	0	(0 - 27)	47	4	(4 - 82)	1.18×10^4	100	(82 - 100)
13.6	Avg.	0.4	0	(0 - 25)	44	4	(4 - 82)	1.11×10^4	100	(82 - 100)
23.8	A	0.8	0	(0 - 45)	95	8	(8 - 82)	2.38×10^4	100	(82 - 100)
23.8	B	0.6	0	(0 - 39)	78	7	(7 - 82)	1.94×10^4	100	(82 - 100)
23.8	C	0.6	0	(0 - 38)	76	7	(7 - 82)	1.89×10^4	100	(82 - 100)
23.8	D	0.7	0	(0 - 40)	82	7	(7 - 82)	2.04×10^4	100	(82 - 100)
23.8	E	0.4	0	(0 - 29)	53	5	(5 - 82)	1.32×10^4	100	(82 - 100)
23.8	F	0.7	0	(0 - 41)	83	7	(7 - 82)	2.07×10^4	100	(82 - 100)
23.8	Avg.	0.6	0	(0 - 39)	78	7	(7 - 82)	1.94×10^4	100	(82 - 100)
34.0	A	1.1	0	(0 - 55)	136	12	(12 - 82)	3.40×10^4	100	(82 - 100)
34.0	B	0.9	0	(0 - 49)	111	10	(10 - 82)	2.76×10^4	100	(82 - 100)
34.0	C	0.9	0	(0 - 48)	108	10	(10 - 82)	2.69×10^4	100	(82 - 100)
34.0	D	1.0	0	(0 - 51)	117	10	(10 - 82)	2.91×10^4	100	(82 - 100)
34.0	E	0.6	0	(0 - 38)	76	7	(7 - 82)	1.89×10^4	100	(82 - 100)
34.0	F	1.0	0	(0 - 51)	118	10	(10 - 82)	2.95×10^4	100	(82 - 100)
34.0	Avg.	0.9	0	(0 - 49)	111	10	(10 - 82)	2.77×10^4	100	(82 - 100)

Table 6.11. Predicted probabilities of infection of pigs within recipient building according to pig weight, pen location, PRRSV concentration in source building exhaust air on June 7. MLE was the probability of infection based on the maximum likelihood estimation of parameters α and β in the exact Beta-Poisson dose-response model for aerosol transmission of PRRSV. The 95% confidence interval (CI) was the range of probability of infection values predicted with the 2.5%-percentile and 97.5-percentile estimates for α and β were used in the exact Beta-Poisson dose-response model for aerosol transmission of PRRSV.

Source Exhaust		**4.2 $TCID_{50}$ m^{-3}**			**500 $TCID_{50}$ m^{-3}**			**125,000 $TCID_{50}$ m^{-3}**		
Pig weight (kg)	Pen	Dose	MLE	95% CI	Dose	MLE	95% CI	Dose	MLE	95% CI
13.6	A	2.3	0	(0 - 74)	278	23	(23 - 82)	6.94×10^4	100	(82 - 100)
13.6	B	1.9	0	(0 - 70)	232	19	(19 - 82)	5.79×10^4	100	(82 - 100)
13.6	C	1.9	0	(0 - 69)	229	19	(19 - 82)	5.71×10^4	100	(82 - 100)
13.6	D	2.0	0	(0 - 71)	240	20	(20 - 82)	5.98×10^4	100	(82 - 100)
13.6	E	1.3	0	(0 - 58)	151	13	(13 - 82)	3.76×10^4	100	(82 - 100)
13.6	F	2.1	0	(0 - 71)	246	20	(20 - 82)	6.14×10^4	100	(82 - 100)
13.6	Avg.	1.9	0	(0 - 69)	229	19	(19 - 82)	5.72×10^4	100	(82 - 100)
23.8	A	4.1	0	(0 - 80)	487	36	(36 - 82)	1.21×10^5	100	(82 - 100)
23.8	B	3.4	0	(0 - 79)	407	31	(31 - 82)	1.01×10^5	100	(82 - 100)
23.8	C	3.3	0	(0 - 79)	401	31	(31 - 82)	1.00×10^5	100	(82 - 100)
23.8	D	3.5	0	(0 - 79)	419	32	(32 - 82)	1.05×10^5	100	(82 - 100)
23.8	E	2.2	0	(0 - 73)	264	22	(22 - 82)	6.58×10^4	100	(82 - 100)
23.8	F	3.6	0	(0 - 79)	431	33	(33 - 82)	1.07×10^5	100	(82 - 100)
23.8	Avg.	3.4	0	(0 - 78)	401	31	(31 - 82)	1.00×10^5	100	(82 - 100)
34.0	A	5.8	1	(1 - 81)	695	48	(48 - 82)	1.73×10^5	100	(82 - 100)
34.0	B	4.9	0	(0 - 81)	581	42	(42 - 82)	1.45×10^5	100	(82 - 100)
34.0	C	4.8	0	(0 - 81)	572	41	(41 - 82)	1.43×10^5	100	(82 - 100)
34.0	D	5.0	0	(0 - 81)	599	43	(43 - 82)	1.49×10^5	100	(82 - 100)
34.0	E	3.1	0	(0 - 78)	377	30	(30 - 82)	9.40×10^4	100	(82 - 100)
34.0	F	5.1	0	(0 - 81)	615	44	(44 - 82)	1.53×10^5	100	(82 - 100)
34.0	Avg.	4.8	0	(0 - 81)	573	41	(41 - 82)	1.43×10^5	100	(82 - 100)

6.5. Conclusions

The aerosol transmission of PRRSV between a source and recipient building was successfully modelled and verified with results from a case study reported in the literature. The transport and movement of PRRSV aerosols, as well as their survival in the air, distribution amongst different aerosol sizes, and dose-response by aerosol transmission were considered during the modelling of the scenario.

The wind speed was a critical factor that affected the rate of aerosol entry (originating from the source building) into the recipient building, with lower wind speeds leading to a more consistent entry of aerosols into the recipient building. The aerosol concentration within the recipient building, in terms of both total count and differentiated by aerodynamic diameter, varied between hours based on the aerosol entry rate. Overall, after the entry of PRRSV aerosols had ceased, the infectious PRRSV concentration declined gradually due to removal of aerosols by ventilation and decay in infectivity from exposure to the environmental conditions present in the building.

The concentration of infectious PRRSV in the air exhausted from the source building was an important factor that affected the PRRSV concentration in the recipient building. Low and high PRRSV concentrations exhausted from the source building corresponded with negligible and 100% probability of infection of pigs, respectively in the recipient building. At a moderate level of PRRSV exhausted from the source building, other factors were important, such as the aerosol entry into the building at different wind speeds, aerosol concentration, PRRSV distribution at different aerosol sizes, PRRSV distribution in the recipient building, pig location in the building, and pig weight. The probability of infection predictions in this study corresponding to a positive PRRSV sample detected on the morning of June 7 in the case study provided evidence that the integrated model developed in this study could adequately predict airborne transmission of PRRS.

Acknowledgements

The authors acknowledge the financial support of the Natural Sciences and Engineering Research Council of Canada (NSERC).

Chapter 7. Overall Discussion, Conclusions and Recommendations

7.1. Knowledge gaps in modelling airborne transmission of viral pathogens

There is key knowledge provided from literature that is required to model airborne transmission of animal viral pathogens, such as: proof of short-distance airborne transmission; proof of long-distance airborne transmission; and factors affecting airborne transmission, such as shedding of virus into aerosol form, survival in environmental conditions, dose-response on aerosol transmission route, virus strain, and aerosol type. Research gaps within the field of airborne transmission of animal diseases were identified in chapter three. A summary of the research gaps is as follows:

1. Studies on airborne transmission of ASFV, PEDV, AIV, PRRSV, and FMDV have common elements but also differ in terms of the available information and research methods used. The majority of experimental research focusses on assessing short-distance (within building) airborne transmissibility, while there is some experimental research assessing long distance airborne transmissibility and factors affecting airborne transmission.
2. Many strains of AIV, PRRSV, and FMDV can transmit via short-distance airborne transmission, but there is incompleteness of information on strains of PEDV and ASFV to confirm short-distance airborne transmissibility. It should be noted that demonstrating short-distance transmissibility does not necessarily mean that pathogens can transmit over long distances.
3. The current literature is insufficient to confirm if ASFV can transmit via long distance airborne transmission. To assess if long-distance airborne transmission is possible, air samples should be collected inside, at the exhaust, and downwind of infected facilities, with lab analysis to quantify the amount of infectious virus inside air samples. Computer modelling, such as ADM, weather analysis, and epidemiological investigations, can be utilised to study past outbreaks of ASFV for long-distance airborne transmission of ASFV.
4. Air sampling PEDV downwind of, at the exhaust of, and inside of naturally infected facilities provides evidence that long-distance aerosol transmission of PEDV is possible, but there is currently not enough evidence of long-distance airborne transmission through air sampling studies or modelling studies.

5. Air sampling of AIV in multiple settings, including LPM and inside, downwind, and at the exhaust of infected poultries, provides evidence of long distance airborne transmission, but uncertainty exists as the studies reported in the literature did not quantify the amount of infectious airborne AIV. Some modelling studies (CFD, ADM, transmission network modelling) have been performed to study past outbreaks of AIV and have provided some evidence that airborne transmission contributed to spread of HPAIV in past outbreaks.
6. There is much evidence documenting that long-distance airborne transmission of PRRSV is possible, especially in areas with high farm density, but modelling of airborne transmission of PRRSV is lacking.
7. It is well recognised that FMDV can be transmitted over long distances by airborne transmission. Although there are limited air sampling studies of naturally infected FMDV farms, there are a plethora of models on airborne transmission of FMDV based on data from the past outbreaks.
8. Factors such as virus strain, aerosol type, shedding duration and concentration, environmental conditions, and aerosol infectious dose can affect airborne transmission. Many studies have quantified some of these factors for various virus strains of ASFV, PEDV, AIV, PRRSV, and FMDV, but more information on these factors is needed.

7.2. Modelling approaches to foster understanding of aerosol transmission pathway

7.2.1. CFD modelling of aerosol transport

There are a number of ways in which this thesis introduced new modelling approaches to the field of animal disease transmission, specifically aspects of the aerosol transmission pathway described by Aliabadi et al. (2011). In chapters four and five, CFD was used to simulate pathogen dispersion close to the infection source (near-field) and within a confined space. This is new to the field of animal disease transmission as CFD had not been previously used to study aerosol transmission of infectious animal diseases within a building or room. This method can be used to assess the risk of short-distance airborne transmission of animal diseases and can be customised to fit many scenarios existing in the animal industry.

In chapter six, CFD was used to simulate long-distance airborne transport. Specifically, CFD was used to simulate pathogen transport in the atmospheric boundary layer, pathogen

transport into a susceptible recipient building, and the movement and airborne pathogen concentration within the recipient building. While CFD was previously used to predict the dispersion of infectious animal diseases, such as AIV and FMDV in the atmospheric boundary layer (Seo et al., 2014; Seo et al., 2015; Wei et al., 2018), it had not been specifically used to model the entry into buildings and the concentration within buildings after entry. Thus, from applying CFD simulation in these ways, this thesis has introduced novel ways of using CFD to model the aerosol transmission process of animal diseases.

In chapter three, it was identified that there were not many studies on computer modelling of aerosol transmission of PRRSV and more work was required in this area. The work in this thesis provides three examples of CFD simulations on aerosol transmission of PRRSV. The first two are within a confined space and the third is from a source building to a recipient building. Therefore, the CFD modelling in this work has reduced the research gap for PRRSV, but continued research is required to further understand aerosol transmission of PRRSV. It is recommended that researchers continue to use CFD to study aerosol transmission of animal pathogens, such as predicting aerosol transmission events, assessing the contribution of aerosol transmission in spreading disease in past outbreaks, or assessing control measures for prevention of aerosol transmission.

7.2.2. Dose-response modelling

Dose-response modelling was used in chapter five and chapter six to simulate the probability of infection in animals upon exposure to specific amounts of aerosolised pathogens. Chapter five used a novel combination of modelling techniques, specifically CFD and dose-response modelling, to model the aerosol transmission pathway of PRRSV close to the infection source. This is not the first application of dose-response models towards modelling aerosol transmission, as dose-response models of AIV (Ssematimba et al., 2012) and FMDV (Cannon & Garner, 1999; Jones et al., 2004; Sanson et al., 2011) have been used previously with air dispersion models. However, the dose-response models for PRRSV via aerosol transmission were developed by Hermann et al. (2009) had not been combined with other computer models, including air dispersion modelling or CFD simulations, to model aerosol transmission of PRRSV.

Additionally, the combination of using CFD and dose-response modelling had not been performed to model aerosol transmission of any infectious animal disease.

It must be noted that the dose-response models developed in this thesis are virus strain specific. The ability of a virus to cause infection may differ amongst strains of the same animal virus. For example, there are different aerosol infectious doses for PRRSV VR-2332 (Hermann et al., 2009) and PRRSV MN-184 (Cutler et al., 2011) and there are different aerosol infectious doses amongst H5N1 AIV strains (Sergeev et al., 2013). The dose-response model used in chapter six was developed for PRRSV VR 2332 in chapter five. The case study used PRRSV strain MN-184, which is more infectious than VR-2332 (Cutler et al., 2011; Hermann et al., 2009). Thus, the probability values predicted in chapter six may be underpredicted; however, this was the best available data available for this study as Cutler et al. (2011), who had performed aerosol dose-response experiments on PRRSV MN-184, did not provide a dose-response equation or data to compile the dose-response equation on PRRSV MN-184.

Considering that development of dose-response models is dependent upon the research data available, it is important for researchers to continue to perform dose-response experiments on a variety of virus strains to understand how different strains affect the dose-response in exposed animals. It is recommended that the collection of dose-response experimental data and development of dose-response models continues as new strains of infectious animal viruses emerge in the future. It is also important to test perform aerosol transmission dose-response experiments and modelling on ASFV and PEDV strains, as it is currently unclear if these viruses can spread via aerosol transmission (i.e., by inhalation of the viruses) and if so, at what dose it would be possible.

7.2.3. Modelling survival of infectious animal viruses in atmosphere

A half-life model for PRRSV developed by Hermann et al. (2007) was used in chapter six to estimate the infectivity of airborne PRRSV after exposure to different temperature and relative humidity conditions. This work is the first to apply this half-life model towards modelling the aerosol transmission of PRRSV. Additionally, the CFD models, the half-life model, and a dose-response model were used combinedly to demonstrate the aerosol transmission pathway when far-field dispersion of pathogens occurred from a source building to a recipient building. The

use of this combination of modelling methods is also the first of its kind in regards to modelling aerosol transmission of any infectious animal disease. It is recommended that these modelling methods continue to be used together, with the information available at the time of modelling, to simulate the aerosol transmission pathway of animal pathogens.

Since different temperature and relative humidity conditions have different effects on the survival of airborne viruses, similar work to Hermann et al. (2007) is required for the other infectious animal viruses. Specifically, evaluating the loss of infectivity of viruses in aerosols at different room temperature and room humidity conditions is required for AIV, PEDV, FMDV, ASFV, as well as any other emerging infectious animal viruses. Removal of viruses from the air via gravity settling should also be considered in the design of future experiments, and using a temperature and relative humidity controlled rotating chamber to conduct experiments, as done by Hermann et al. (2007), can be used to minimise the settling of aerosols.

7.3. Importance of air sampling measurements in computer modelling

Air sampling was identified to be an important component of computer modelling that estimated the aerosol transport and aerosol concentration of pathogens. Literature review in chapter three showed that air sampling was pivotal in providing evidence of long distance airborne transmission of animal pathogens; specifically, collection of air samples containing virus inside, at the exhaust, and downwind of infected animal facilities provided evidence that infectious animal pathogens can travel long distances in the air. As previously stated, continued air sampling monitoring around naturally infected animal facilities is recommended to provide evidence of long distance airborne transmission.

Work in chapter four showed the importance of collecting air samples to quantify airborne pathogens and validate the CFD simulation results. Specifically, it is important to perform numerous air sample measurements over time; this was observed when the CFD simulation performed well at estimating the steady-state concentration of aerosols, but not at estimating the initial transient concentration of aerosols. Additionally, limitations of the research were the lack of air sample collection in multiple locations in the experimental chambers and the need for more experimental replicates. Therefore, it is recommended to collect multiple experimental replicates of temporally- and spatially- distributed air sample measurements within

enclosed spaces to validate the airborne concentration of pathogens or aerosol concentration predicted by CFD simulation. However, the availability of equipment used to perform air sample collection will determine the methodology, set-up, and feasibility of performing these types of measurements. For optical particle counters, the computer software of these devices usually allows for customisation of the sampling time and frequency. To allow for sampling over multiple locations, more consideration into the experimental setup and operation of the device would be required to allow for sampling of multiple locations using a single optical particle counter. Air sample collection within glass impingers or cascade impactors allows for the quantification of virus genome copies and/or infectious virus, but requires manual sample collection followed by laboratory analysis. It would be expected that quantifying virus genome copies or infectivity at multiple timepoints and in multiple locations in an enclosed space would be limited by the available samplers, equipment operators, and laboratory resources.

In chapter six, CFD was used to simulate long distance transport of airborne PRRSV from an infected facility. The amount of airborne infectious PRRSV that was transported into the recipient building was dependent upon two major input parameters used in the model development. The first important input parameter was the amount of infectious virus exhausted from the source building. The case study that was simulated did not specify the infectious PRRSV concentration at the exhaust on the specific dates of the CFD simulation, June 6 and 7, 2006 (Pitkin et al., 2009; Pitkin, 2009), but provided the minimum, maximum, and mean infectious PRRSV concentrations collected in air samples from the exhaust of the source building. These values were used in the conversion of aerosol concentration to airborne PRRSV concentrations within the recipient building and the results indicated that the probability of infection was highly variable and dependent on the concentration of infectious PRRSV exhausted from the source building. Therefore, it is important that future research using CFD for long-distance aerosol transmission to include air sampling to quantify the infectious virus released from the exhaust of the source building. The frequency of the air sample collection would depend on the design of the experiment, but long term experiments should have multiple air samples of the exhaust to provide accurate information for developing the CFD model.

The second important input parameter in model development was the ratio of virus particles per airborne particle at different aerosol sizes. Aerosols of different sizes have different aerodynamic behaviours (de Nevers, 2017). Some aerosols may settle due to gravity during the transport from a source building to a recipient building, or may settle due to gravity within the recipient building. Thus, it is important to identify the distribution of infectious virus on different aerosol sizes because it would impact the overall exposure dose of virus during aerosol transmission. The quantity of virus present in different aerosol sizes can be determined using a cascade impactor, which separates particulate matter in a sampled airstream based on aerosol size. Laboratory analysis, such as quantitative PCR or microtiter assays can be used to quantify the amount of virus within each size range. Such work was previously performed for PRRSV, from indoor air of buildings containing either naturally or artificially infected pigs (Alonso, Olson, et al., 2017; Alonso et al., 2015; Alonso, Raynor, et al., 2017). Optical particle counters can be used to quantify the aerosol size distribution (Alonso et al. 2017b, 2017a, 2015). The original case study simulated in chapter six did not perform the above measurements (Pitkin et al., 2009; Pitkin, 2009). Therefore, the ratio of PRRSV particles per airborne particle size was calculated using airborne virus concentration at different particle sizes and particulate matter concentrations at different particle sizes obtained from indoor air samples of PRRSV-infected pig farms collected in Alonso, Raynor, et al. (2017). In future research, it is recommended to use cascade impactors and optical particle counters for air sample collection of aerosol size-differentiating airborne virus concentration and particulate matter concentration. This will provide the data required to calculate the ratio of airborne virus particles per particle size that can be used to estimate airborne dose of virus.

Lastly, there is usually a difference between the amount of virus present in the air and the amount of virus quantified from air sampling, and this is affected by multiple factors. Infectious airborne virus collection consists of multiple steps: collecting the airborne virus using an air sampling device, sustaining the viral viability in a collection medium during storage, and quantifying the collected virus using laboratory techniques such as assays. In terms of air sample collection, different air sampling devices can have different collection performances. For example, a comparison of two cascade impactors at sampling artificially-generated aerosols of PRRSV and IAV showed that the Andersen cascade impactor was more effective at collecting

virus aerosols of sizes <1 μm and 1-3 μm than the Tisch cascade impactor; however, the Tisch model was more effective at collecting aerosols >3 μm for IAV (Alonso et al., 2017). Hermann et al. (2006) found that three impinger models had varying performances at collecting artificially-generated aerosols of PRRSV, and the authors also reported that collection time and the compounds added to the collection media also affected the amount of PRRSV RNA collected. The analytical sensitivity, which is the minimum amount of virus in the air required for the viruses to be detectable after air sampling and laboratory analysis, is another limiting factor to be considered in air sampling of airborne viruses. For example, the analytical sensitivity of four impingers at collecting airborne PRRSV was between $10^{1.1}$ to $10^{1.3}$ $TCID_{50}$ when PRRSV was quantified with qRT-PCR (Hermann et al., 2008). The performance of laboratory techniques may also be affected by the quantity of virus in a collected sample; for example, the qRT-PCR recovery efficiency of PRRSV and IAV from filter samples spiked with known amounts of virus ranged from 0% to 22% for PRRSV and 12 to 22% for IAV, depending on the quantity of virus spiked onto the filters (Alonso et al., 2017). Different choices during laboratory analysis can affect the amount of virus recovered from air samples. For example, Alonso et al. (2017) reported that the elution media, filter type, and active/passive virus extraction from filter media affected the amount of virus recovered from filters spiked with virus. Overall, these limitations in accurately quantifying airborne viral concentrations (infectious or genome copies) using air sampling devices and laboratory analysis should be considered in future research.

7.4. Limitations of research

7.4.1. Chapter 3

In chapter 3, the literature review focussed on five infectious animal diseases that were viral. There are also other infectious viral diseases that are important, reportable animal diseases in Canada that have the potential to transmit by airborne transmission but were not specifically addressed in chapter three (CFIA, 2021). For example, Classical Swine Fever virus is a reportable animal disease that causes severe disease leading to death (CFIA, 2014) and there is some evidence that it has short-distance airborne transmissibility (Dewulf, Laevens, Koenen, Mintiens, & De Kruif, 2000). The general recommendations provided in chapter three can also apply to other significant animal diseases in order to distinguish if the diseases are airborne transmissible. Specifically, using laboratory experiments can provide evidence that a pathogen is

short-distance airborne transmissible. Computer modelling and air sampling of infectious virus downwind of naturally-infected facilities can provide evidence of long-distance airborne transmissibility.

7.4.2. Chapter 4

There were a few limitations to the study performed in chapter 4. More experimental replicates should have been performed per treatment to improve the ability to simulate and validate the transient aerosol concentration. Additionally, because the aerosol concentration measurements were performed at one location in the chamber, the spatial distribution of aerosols determined in the CFD simulations could not be validated in this study. Based on the aerosol concentration measurements at this location, it was observed that the CFD simulation did not perform as well during the transient stage of the CFD simulation.

The standard k-ε turbulence model was used within the CFD simulations for the work described in chapters 4, 5, and 6. Using the standard k-ε turbulence model was justified as it was previously reported to be adequate for predicting turbulence in airflow. The ANSYS Fluent User Guide described the standard k-ε model as robust and economical as well as able to provide good accuracy for many types of turbulent flow (ANSYS 2013a). Seo et al. (2010) stated that the standard k-ε model provided a "realistic compromise [between] a realistic description of turbulence and computational efficiency". The standard k-ε model was also applied in previous relevant applications, such as simulating the dispersion of dust in the atmosphere (Seo et al. 2010) and the dispersion of infectious animal viruses in the atmosphere (Seo et al., 2014; Seo et al., 2015). However, it must be noted that there are flow situations where the standard k-ε turbulence model can be inaccurate, particularly when turbulence behaviour is not the same in all directions (non-isotropic; Norton et al., 2007; Versteeg & Malalasekera, 2007). Rong et al. (2016) also reported that the standard k-ε model works best in situations where turbulence is "fully developed [, which] . . . cannot be always fulfilled in the ventilated room". Li, Rong, & Zhang (2017) noted that the standard k-epsilon turbulence model performed similarly to other tested turbulence models in their study but that the turbulence model performance may be case-dependent.

Therefore, it is possible that the results of the CFD simulations during the transient phase of the simulation may have been improved by testing the performance of different turbulence models, such as the RNG k-ε model and realisable k-ε model. As shown in Rong et al. (2016), comparing the performance of different turbulence models with measured experimental results can provide information for choosing the optimal turbulence model for a CFD simulation of an indoor space in agricultural applications. It is recommended in the future that multiple turbulence models are tested in preliminary research to identify which turbulence model will best predict the airflow behaviour and aerosol concentration present in the enclosed space. Despite these limitations, the work in chapter 4 was a success. The study showed that CFD is a strong tool that can model the movement of pathogen-laden aerosols.

7.4.3. Chapter 5

In chapter 5, as previously stated, different virus strains may have different pathogenic properties than the strains used to produce the dose-response models. The case studies also did not perform aerosol concentration or infectious airborne PRRSV concentration measurements within the experimental chambers (Dee, Batista, et al., 2006; Dee, Deen, et al., 2006). Therefore, the CFD simulation results of aerosol concentration or PRRSV concentration could not be validated. Lastly, the velocity and pressure profiles of the CFD simulation were also not presented in chapter five because there was little information from the original experiments to perform validation. Thus, the velocity and pressure profiles from the CFD simulation would have provided little value to this study and distracted from the novelty of this work, which was to couple the dose-response model and CFD to predict probability of infection by aerosol. However, it is important in future research to perform experiments, collecting velocity, pressure, and airborne particle measurements throughout the experimental space, and compare the results to simulated results.

The CFD simulation and dose-response coupling was validated by comparing the calculated probability of infection values to observed rates of infection to demonstrate the process of coupling CFD with dose-response modelling. Given that a number of guesses/assumptions/estimations had to be made in simulating the cases reported in the literature,

it was reasonable to conclude both the EBPM and ABPM were able to adequately estimate the rates of infection of pigs reported by Dee, Batista, et al. (2006) and Dee, Deen, et al. (2006).

7.4.4. Chapter 6

In chapter 6, numerous assumptions were made during model development process as the data was not available in the original case study (Pitkin et al., 2009; Pitkin, 2009). Dimensions of specific building and domain features were not provided and the values of these dimensions were assumed. The ventilation rates, aerosol concentration, aerosol density, and PRRSV concentration exhausted from the source building as well as the pig weight, aerosol size distribution, and PRRSV distribution in different aerosol sizes were not provided in the case study; these values were acquired from literature and were used as assumptions. Optimally, future research in this area should quantify these measurements for use during model development.

The weather conditions, which in this case was the hourly wind speed and the atmospheric stability, affected the far-field dispersion and entry rate of contaminated aerosols into the recipient building. The wind speeds and direction simulated were hourly averages based on historical weather data. Instantaneous wind speeds and directions may have differed from the hourly average, diverting aerosols in different directions. The weather data used was also recorded at the airport of Appleton, MN, which is approximately 8.5 km away from the site of the case study; thus, there may have been some limited differences in weather between the two locations. While there was weather data recorded in the case study, limited data was provided; however, in all of the cases where PRRSV was detected in the recipient building air, the wind direction was from the NW direction, directing air from the source to recipient building (Pitkin et al., 2009).

The atmospheric boundary layer equations used in the CFD simulation assumed that there was a neutral atmospheric stability during the dates simulated (Richards & Hoxey, 1993). The atmospheric stability can be determined based on recorded hourly weather data, specifically the sensible heat flux and windspeed at 10 m height above ground (Pasquill, 1961). Based on the sensible heat flux (<300 W m^{-2}) and wind speed (>6 m s^{-1}) at 10 m height on June 6, 2006 in the hours simulated, the atmospheric stability was D (neutral). The sensible heat flux on the hours simulated on June 7, 2006 was <300 W/m^2 and the wind speed at 10 m varied between 4.36 m s^{-1}

and 6.46 m s^{-1}. This corresponds with atmospheric stability conditions of C (slightly unstable) when the wind speed was less <5 m s^{-1} and D (neutral) when the windspeed was >5 m s^{-1}. Therefore, while it was primarily reasonable to assume neutral atmospheric conditions, some select field domain CFD simulations modelling June 7 should have used equations that model slightly unstable atmospheric stability. Less aerosols may have entered the recipient building at a slightly unstable conditions compared to a neutral conditions, as slightly unstable conditions are associated with more movement of air up and down (de Nevers, 2017). However, the neutral atmospheric stability was built into OpenFOAM as a boundary condition option, while other atmospheric conditions were not available as boundary conditions in the OpenFOAM version (OpenFOAM v1806) used for model development. Additionally, using neutral weather conditions provided a worst-case scenario estimate for aerosol dispersion as it resulted in minimal dispersion from the main aerosol plume. Therefore, in future CFD simulations of aerosol movement and infectious virus movement in the atmospheric boundary layer, it is important to consider the atmospheric stability during the case study being simulated.

The velocity and pressure profiles for the CFD simulations were not presented in this study as there were no measurements of velocity and pressure given in Pitkin et al. (2009) and Pitkin (2009). Therefore, these results could not be validated and would have added little value to this study. However, in future research using CFD simulations to simulate aerosol transmission of infectious animal pathogens, it is important for researchers to validate their CFD simulations with experimental data on velocity, airflow patterns, pressure, and airborne pathogens at numerous aerosol sizes. Validation using experimental data was previously recommended in CFD guidelines for agricultural applications (Norton et al., 2007; Rong et al., 2016). Velocity and airflow pattern measurements are an important part of understanding the epidemiology of infectious diseases and were used with CFD simulations to study outbreaks of infectious human pathogens previously (Li et al., 2004). Additionally, data collection should occur at a frequency that allows for an accurate reconstruction of the aerosol transmission events.

Chapter 6 also did not investigate the fomite transmission component of airborne transmission (i.e., infection of animals via making contact with PRRSV aerosols that had settled onto surfaces). It is difficult to model the fomite transmission component because fomite transmission could have occurred due to both oral or intranasal contact with settled virus

particles; these two transmission routes require different levels of PRRSV to cause infection and have two different dose-response models. However, in chapter five, aerosol transmission was found to require the least amount of virus compared to intranasal and oral transmission to cause an infection, so it was more likely that aerosol transmission, not fomite transmission that caused PRRSV infection in the recipient building.

7.5. Conclusions

An extensive literature review of the current knowledge of airborne transmission of ASFV, PEDV, AIV, PRRSV, and FMDV indicated that there were a number of knowledge gaps existing in the field of airborne transmission of animal viruses. The majority of research focuses on short-distance airborne transmissibility via laboratory experiments, while there is some research on long-distance airborne transmissibility via air sampling studies and modelling studies. There are also many studies that have quantified factors that affect airborne transmission, including virus strain, aerosol type, shedding duration and concentration, environmental factors, and infectious dose. There is a need for more investigation of short- and long- distance airborne transmission of ASFV and PEDV, a need for more airborne transmission modelling of ASFV, PEDV, and PRRSV, and continued investigation into emerging strains of infectious animal viruses and factors affecting airborne transmission.

PRRSV movement and concentration within a confined space was successfully simulated by a CFD model and validated with experimental data of aerosol concentration from a case study which measured PRRSV aerosol movement from a source chamber to a recipient chamber. The CFD simulation performed well at simulating steady-state concentrations of PRRSV-laden aerosols (NMSE and FB within ASTM guidelines) but needed improvement at simulating the transient concentration of PRRSV-laden aerosols, as the NMSE and FB exceeded the ASTM guidelines. Mesh refinement tests were identified to be important components of CFD model development and spatially- and temporally- distributed air sampling of the confined space were identified to be important components in validating the performance of the CFD model.

Three types of stochastic dose-response models were developed for five infectious animal diseases on various transmission routes using literature data. The exact beta-Poisson model performed better than the exponential and approximate beta-Poisson models at modelling the

dose-response. Transmission route was an important factor that affected the likelihood of animals becoming infected, including PRRSV requiring less virus to cause infection by aerosol transmission than by intranasal and oral routes. A coupled CFD and dose-response model was also successfully executed to predict aerosol transmission of PRRSV. The coupled CFD and dose-response models adequately predicted the rate of infection (EBPM: 82% to 100%) observed in the exposed susceptible pigs compared to two case studies (90% and 84%).

An integrated model consisting of a series of CFD simulations of field transport of PRRSV aerosols from a source to recipient building, CFD simulations of the concentration of PRRSV aerosols within the recipient building, an infectivity decay model, and a dose-response model were successfully used to simulate aerosol transmission of PRRSV from a source to recipient building. Wind speed and wind direction affected the quantity of aerosols that entered the recipient building. However, the concentration of infectious PRRSV exhausted from the source building was the most important factor that affected probability of infection in the recipient building. Other factors, such as aerosol entry at different wind speed conditions, aerosol concentration at different aerosol sizes, pig location, and pig weight, became important when moderate levels of PRRSV (500 $TCID_{50}$ m^{-3}) were exhausted from the source building. Based on simulation results, June 7, 2006 was identified to be the likely day between June 1 and June 13 that aerosol transmission occurred, leading to infection of pigs in the recipient building. This was supported by a positive air sample of PRRSV in the inlet of the recipient building on the morning of June 7. The results of the integrated model matching with observed events shows that CFD, dose-response modelling, and infectivity decay models are powerful tools when applied to the field of airborne transmission of animal disease.

7.6. Recommendations

New infectious animal viruses and virus strains will emerge over time with different potentials to cause disease outbreaks. It is important to continue to monitor both domestic and wild animals for emerging diseases over time, as wild animals such as wild pigs (for ASFV) and birds (AIV) can often be carriers of animal diseases. Since the properties of emerging strains, such as infectivity and survivability can be different from existing virus strains, it is important to research emerging virus strains for these properties.

It is important to assess virus strains for their ability to cause infection. Thus, future research should include dose-response experiments and dose-response modelling on multiple important transmission routes, including by airborne route. It is also recommended that there is further investigation on the ability of strains, both existing and emerging strains, to transmit by air over short and long distances. As per chapter 3, short-distance airborne transmissibility can be assessed using laboratory experiments and long-distance airborne transmissibility can be assessed by performing air sampling and computer modelling of naturally infected animal facilities.

It is recommended that systematic investigation of the effects of temperature and relative humidity, as well as UV, on the survival of viruses in aerosols should be conducted for all significant infectious animal viruses. Creating half-life models based on environmental conditions can be highly useful in airborne transmission computer modelling. Virus shedding from infected animals into the air should also be researched for significant and emerging infectious animal viruses, including concentration of shedding, timeframe of shedding, and duration of shedding. This information could be used in model development of airborne transmission models. Air sampling of naturally infected animal buildings can provide information for modelling of airborne transmission of animal pathogens and also provide evidence of long-distance airborne transmissibility of animal pathogens. Specifically, field air sampling should be conducted to quantify airborne viruses inside, at the exhaust, and downwind of infected farms. For airborne transmission modelling, quantification should include the amount of infectious virus within air samples as well as the airborne infectious virus at different particle sizes. These studies should also identify meteorological conditions (temperature, relative humidity, wind conditions) at the time of sampling, as these conditions affect the viability and movement of virus aerosols.

Experiments performing measurements have error, which means that there is a difference between the experimentally measured values and the “true” values. This can be seen in the validation experiment in chapter 4 and the other measurements used in modelling that were obtained from literature throughout the text. Uncertainty analyses, such as the Taylor series method, can be used to estimate the uncertainty associated with experimentally collected data,

including systematic (bias) and random (precision) errors (Coleman & Steele, 2009). In future research, researchers should identify sources of error and perform uncertainty analysis to estimate the uncertainty of experimental measurements due to the combined effect of the errors.

It is recommended that there is further research on computer modelling of airborne transmission of animal diseases, especially for ASFV, PEDV, AIV, and PRRSV, as it can be used to better understand the significance of airborne transmission in spreading infectious disease. Modelling of indoor virus aerosol movement can improve the understanding of how building ventilation and management practices can affect spread of infectious diseases in a building by airborne transmission. Additionally, computer models should be used in future research to assess how long-distance airborne transmission contributed to building to building spread in outbreaks of animal diseases. Lastly, computer models should be used as predictive tools that provide producers with information that can reduce the spread of infectious animal diseases in cases of disease outbreaks. It is recommended that models of airborne transmission be supported with airflow or airborne virus measurements over space and time in order to validate computer models. These measurements should also be used to optimize the model development, such as to choose the optimum turbulence model and/or mesh resolution in CFD models.

The computer model utilised in this work to simulate virus aerosol transport and movement was primarily CFD; however, ADMs are also an option for simulating the transport of infectious virus aerosols in the atmosphere. ADMs estimate the movement of airborne contaminants in the atmospheric boundary layer, with inputs such as land characteristics and meteorological data. As seen in chapter 3.6, there is a large plethora of ADMs available that were previously applied to studying the airborne transmission of FMDV. ADMs were used to determine if airborne transmission contributed to FMDV outbreaks, including estimating the likelihood of rare long-distance transmission, confirming the likely source (farm or other animal processing facility) of airborne FMDV, and assessing if specific farms were infected due to airborne transmission. A comparison of six ADMs applied to the same airborne transmission scenario showed that differences in the meteorological data used for different models, the order of infection events, and assumptions related to the viral release, decay, and infectivity were

factors that affected the performance of the ADMs (Gloster et al., 2010). It is recommended that future research utilising ADMs for assessing airborne transmission of infectious animal viruses consider the impact of these factors on the simulated results.

There are some recommendations on model development and execution for CFD. There are various programs that can be used to perform CFD simulations. In this thesis, ANSYS Fluent (chapters 4 and 5) and OpenFOAM (chapter 6) were used. ANSYS Fluent was used successfully to model the airflow and aerosol movement within small geometries requiring fewer elements in the mesh in chapters 4 and 5. OpenFOAM was used in chapter 6 as the domain was large and required a greater number of elements in the mesh. OpenFOAM did not limit the number of elements in the mesh, while ANSYS Fluent had specific licensing requirements for larger mesh sizes that were not available at the time the research was performed. In terms of other differences in the two programs, ANSYS Fluent has a graphical user interface and can run in the Windows operating system, while OpenFOAM is programmed in numerous text files that are operated using terminal. OpenFOAM requires a computer with the Ubuntu operating system or a virtual machine with Ubuntu to be used. ANSYS Fluent operates within a single program, while OpenFOAM is divided into many solvers that operate different algorithms and have different applications. Both programs allow customization of simulations, such as additional models, via Fluent's user defined functions and OpenFOAM's numerous solvers and options to develop custom solvers. These options both have learning curves associated with their use, but OpenFOAM has numerous tutorial cases available for learning applications of the solvers available. Additionally, there are numerous online repositories available for OpenFOAM that can aid in model development. Both programs also allow for parallel processing, which is recommended to be used in CFD simulations to improve simulation speed.

It is recommended that users consider their computer coding proficiency when determining whether to use Fluent or OpenFOAM. Additionally, it is recommended that future researchers consider their geometry, required mesh resolution, and as available computational resources. While the element count may be limited in ANSYS Fluent depending on the software license, the element count in OpenFOAM is only limited by the computer memory required to run simulations. It is recommended that users understand options such as turbulence models,

algorithms of solving pressure-velocity coupling, and discretization schemes prior to running long-term simulations; this will reduce the time wasted on restarting simulations due to poor numerical accuracy, such as due to the use of upwind (first order) schemes. Both ANSYS and OpenFOAM can output large amounts of data and it is recommended that users learn to use either R, MatLab, or other data analysis software to process the outputted data and perform data analysis. It is also recommended that computers running CFD have a large hard drive capacity for storing the simulation results.

In regards to modelling aerosol transmission, model development is easier when there is more information on the study site. It is recommended that the following information is gathered prior to model development: dimensions of buildings, coordinates of buildings, velocity measurements at inlets and outlets, air samples of airborne viruses, aerosol size distribution, distribution of viruses amongst aerosol sizes, environmental conditions, observed rate of infection, etc. More information allows for the user to determine boundary conditions, mesh resolution, and turbulence models that are best suited for an application. Lastly, CFD models simulating aerosol movement via discrete particle models can be computationally expensive, depending on the coupling method (one-way or two-way modelling). For the aerosol sizes considered in aerosol transmission, one-way coupling is likely adequate, and these simulations would be faster than two-way coupling simulations.

Appendix A. Fundamental equations for CFD

Continuity equation (conservation of mass) for incompressible fluids (Versteeg & Malalasekera, 2007):

$$\frac{\partial u}{\partial x}+\frac{\partial v}{\partial y}+\frac{\partial w}{\partial z}=0$$

where $\frac{\partial u}{\partial x}$ =the change in the x-component of velocity in the x-direction,

$\frac{\partial v}{\partial y}$ =the change in the y-component of velocity in the y-direction,

$\frac{\partial w}{\partial z}$ =the change in the z-component of velocity in the z-direction

Reynolds-Average-Navier-Stokes equations (Versteeg & Malalasekera, 2007):

$$\frac{\partial U}{\partial t} + \text{div}(U\mathbf{U}) = -\frac{1}{\rho}\frac{\partial P}{\partial x} + \nu\text{div}(\text{grad}(U)) + \frac{1}{\rho}\left[\frac{\partial(-\rho\overline{u'^2})}{\partial x} + \frac{\partial(-\rho\overline{u'v'})}{\partial y} + \frac{\partial(-\rho\overline{u'w'})}{\partial z}\right]$$

$$\frac{\partial V}{\partial t} + \text{div}(V\mathbf{U}) = -\frac{1}{\rho}\frac{\partial P}{\partial y} + \nu\text{div}(\text{grad}(V)) + \frac{1}{\rho}\left[\frac{\partial(-\rho\overline{u'v'})}{\partial x} + \frac{\partial(-\rho\overline{v'^2})}{\partial y} + \frac{\partial(-\rho\overline{v'w'})}{\partial z}\right]$$

$$\frac{\partial W}{\partial t} + \text{div}(W\mathbf{U}) = -\frac{1}{\rho}\frac{\partial P}{\partial z} + \nu\text{div}(\text{grad}(W)) + \frac{1}{\rho}\left[\frac{\partial(-\rho\overline{u'w'})}{\partial x} + \frac{\partial(-\rho\overline{v'w'})}{\partial y} + \frac{\partial(-\rho\overline{w'^2})}{\partial z}\right]$$

where **U** = mean velocity,

U = mean velocity in the x-direction,

V = mean velocity in the y-direction,

W = mean velocity in the z-direction,

$\frac{\partial}{\partial t}$ = rate of change,

ρ = density,

P = mean Pressure,

$\frac{\partial}{\partial x}, \frac{\partial}{\partial y}, \frac{\partial}{\partial z}$ = change in x-, y-, z-direction, respectively

ν = kinematic viscosity,

$-\rho\overline{u'^2}, -\rho\overline{v'^2}, -\rho\overline{w'^2}$ = normal Reynolds stresses,

$-\rho\overline{u'v'}, -\rho\overline{u'w'}, -\rho\overline{v'w'}$ = viscous Reynolds stresses

Standard k-ε turbulence model equations (Versteeg & Malalasekera, 2007):

$$\mu_t = \rho C_\mu \frac{k^2}{\varepsilon}$$

$$\frac{\partial(\rho k)}{\partial t} + \text{div}(\rho k \mathbf{U}) = \text{div}\left[\frac{\mu_t}{\sigma_k}\text{grad}k\right] + 2\mu_t S_{ij} \cdot S_{ij} - \rho\varepsilon$$

$$\frac{\partial(\rho \varepsilon)}{\partial t} + \text{div}(\rho \varepsilon \mathbf{U}) = \text{div}\left[\frac{\mu_t}{\sigma_\varepsilon}\text{grad}\varepsilon\right] + C_{1\varepsilon}\frac{\varepsilon}{k}2\mu_t S_{ij} \cdot S_{ij} - C_{2\varepsilon}\rho\frac{\varepsilon^2}{k}$$

where k = turbulent kinetic energy,

ε = rate of dissipation of turbulent energy,

σ_t = eddy viscosity,

S_{ij} = mean rate of deformation of a fluid element due to turbulence,

$C_\mu, \sigma_k, \sigma_{\varepsilon,} C_{1\varepsilon}, C_{2\varepsilon}$ = constants

References

Aggarwal, N., Zhang, Z., Cox, S., Statham, R., Alexandersen, S., Kitching, R. P., & Barnett, P. V. (2002). Experimental studies with foot-and-mouth disease virus, strain O, responsible for the 2001 epidemic in the United Kingdom. *Vaccine*, *20*(19–20), 2508–2515. https://doi.org/10.1016/S0264-410X(02)00178-0

Agranovski, I. E., Pyankov, O. V., Pyankova, O. G., Sergeev, A. A., Sergeev, A. N., Smetannikova, M. A., & Safatov, A. S. (2010). Development of a new procedure for precise determination of viral aerosol lethal dose (ALD50) for birds. *Journal of Aerosol Science*, *41*(2), 161–169. https://doi.org/10.1016/j.jaerosci.2009.10.003

Alexander, D. J. (2000). A review of avian influenza in different bird species. *Veterinary Microbiology*, *74*(1–2), 3–13. https://doi.org/10.1016/S0378-1135(00)00160-7

Alexander, D. J. (2007). An overview of the epidemiology of avian influenza. *Vaccine*, *25*(30 SPEC. ISS.), 5637–5644. https://doi.org/10.1016/j.vaccine.2006.10.051

Alexandersen, S., & Donaldson, A. I. (2002). Further studies to quantify the dose of natural aerosols of foot-and-mouth disease virus for pigs. *Epidemiology and Infection*, *128*(2), 313–323. https://doi.org/10.1017/S0950268801006501

Alexandersen, S., Brotherhood, I., & Donaldson, A. I. (2002). Natural aerosol transmission of foot-and-mouth disease virus to pigs: Minimal infectious dose for strain O1 Lausanne. *Epidemiology and Infection*, *128*(2), 301–312. https://doi.org/10.1017/S095026880100646X

Alexandersen, S., Quan, M., Murphy, C., Knight, J., & Zhang, Z. (2003). Studies of quantitative parameters of virus excretion and transmission in pigs and cattle experimentally infected with foot-and-mouth disease virus. *Journal of Comparative Pathology*, *129*(4), 268–282. https://doi.org/10.1016/S0021-9975(03)00045-8

Alexandersen, S., Zhang, Z., Donaldson, A. I., & Garland, A. J. M. (2003). The pathogenesis and diagnosis of foot-and-mouth disease. *Journal of Comparative Pathology*, *129*(1), 1–36. https://doi.org/10.1016/S0021-9975(03)00041-0

Alexandersen, S., Zhang, Z., Reid, S. M., Hutchings, G. H., & Donaldson, A. I. (2002). Quantities of infectious virus and viral RNA recovered from sheep and cattle experimentally infected with foot-and-mouth disease virus O UK 2001. *Journal of General Virology*, *83*(8), 1915–1923. https://doi.org/10.1099/0022-1317-83-8-1915

Aliabadi, A. A., Rogak, S. N., Bartlett, K. H., & Green, S. I. (2011). Preventing airborne disease transmission: review of methods for ventilation design in health care facilities. *Advances in Preventive Medicine*, *2011*, 1–21. https://doi.org/10.4061/2011/124064

Alonso, C., Goede, D. P., Morrison, R. B., Davies, P. R., Rovira, A., Marthaler, D. G., & Torremorell, M. (2014). Evidence of infectivity of airborne porcine epidemic diarrhea virus and detection of airborne viral RNA at long distances from infected herds. *Veterinary Research*, *45*(1), 1–5. https://doi.org/10.1186/s13567-014-0073-z

Alonso, C., Olson, B. A., Goyal, S., Raynor, P. C., Davies, P. R., & Torremorell, M. (2017). Comparison of two size-differentiating air samplers for detecting airborne swine viruses under experimental conditions. *Aerosol Science and Technology*, *51*(2), 198–205. https://doi.org/10.1080/02786826.2016.1249278

Alonso, C., Raynor, P. C., Davies, P. R., & Torremorell, M. (2015). Concentration, size distribution, and infectivity of airborne particles carrying swine viruses. *PLoS ONE*, *10*(8), 1–12. https://doi.org/10.1371/journal.pone.0135675

Alonso, C., Raynor, P. C., Goyal, S., Olson, B. A., Alba, A., Davies, P. R., & Torremorell, M. (2017). Assessment of air sampling methods and size distribution of virus-laden aerosols in outbreaks in swine and poultry farms. *Journal of Veterinary Diagnostic Investigation*, *29*(3), 298–304. https://doi.org/10.1177/1040638717700221

Amaral Doel, C. M. F., Gloster, J., & Valarcher, J. F. (2009). Airborne transmission of foot-and-mouth disease in pigs: Evaluation and optimisation of instrumentation and techniques. *Veterinary Journal*, *179*(2), 219–224. https://doi.org/10.1016/j.tvjl.2007.09.010

ANSYS. (2013a). *ANSYS fluent theory guide, release 15.0*. Canonsburg, PA.

ANSYS. (2013b). *ANSYS fluent user's guide, release 15.0*. Canonsburg, PA.

Arruda, A. G., Tousignant, S., Sanhueza, J., Vilalta, C., Poljak, Z., Torremorell, M., … Corzo, C. A. (2019). Aerosol detection and transmission of porcine reproductive and respiratory syndrome virus (PRRSV): What is the evidence, and what are the knowledge gaps? *Viruses*, *11*(8). https://doi.org/https://doi.org/10.3390/v11080712

Asgharian, B., Miller, F. J., Price, O., Schroeter, J. D., Einstein, D. R., Corley, R. A., & Bentley, T. (2016). Modeling particle deposition in the pig respiratory tract. *Journal of Aerosol Science*, *99*, 107–124. https://doi.org/10.1016/j.jaerosci.2016.01.016

ASHRAE. (1987). *Standard methods for laboratory airflow measurement*. Atlanta, PA.

ASTM. (2008). *Standard guide for statistical evaluation of indoor air quality models D5157-97*. West Conshohocken, PA.

Aubry, P., Thompson, J. L., Pasma, T., Furness, M. C., & Tataryn, J. (2017). Weight of the evidence linking feed to an outbreak herds. *Journal of Swine Health and Production*, *25*(2), 69–72.

Barlow, D. F. (1972). The effects of various protecting agents on the inactivation of foot-and-mouth disease virus in aerosols and during freeze-drying. *The Journal of General Virology*, *17*(3), 281–288. https://doi.org/10.1099/0022-1317-17-3-281

Barlow, D. F., & Donaldson, A. I. (1973). Comparison of the aerosol stabilities of foot and mouth disease virus suspended in cell culture fluid or natural fluids. *Journal of General Virology*, *20*(3), 311–318. https://doi.org/10.1099/0022-1317-20-3-311

Beam, A., Goede, D., Fox, A., McCool, M. J., Wall, G., Haley, C., & Morrison, R. (2015). A porcine epidemic diarrhea virus outbreak in one geographic region of the United States: Descriptive epidemiology and investigation of the possibility of airborne virus spread. *PLoS ONE*, *10*(12). https://doi.org/10.1371/journal.pone.0144818

Belser, J. A., Pulit-Penaloza, J. A., Brock, N., Creager, H. M., Gustin, K. M., Tumpey, T. M., & Maines, T. R. (2022). Inherent heterogeneity of influenza A Virus stability following aerosolization. *Applied and Environmental Microbiology*, *88*(4). https://doi.org/10.1128/aem.02271-21

Belsham, G. J. (1993). Distinctive features of foot-and-mouth disease virus, a member of the Picornavirus family; aspects of virus protein synthesis, protein processing and structure. *Progress in Biophysics and Molecular Biology*, *60*(3), 241–260. https://doi.org/https://doi.org/10.1016/0079-6107(93)90016-d

Beltrán-Alcrudo, D., Arias, M., Gallardo, C., Kramer, S. A., & Penrith, M. L. (2017). *African swine fever detection and diagnosis - a manual for veterinarians*. Rome. Retrieved from http://www.fao.org/3/a-i7228e.pdf

Berhane, Y., Hisanaga, T., Kehler, H., Neufeld, J., Manning, L., Argue, C., … Pasick, J. (2009). Highly pathogenic avian influenza virus a (H7N3) in domestic poultry, Saskatchewan, Canada, 2007. *Emerging Infectious Diseases*, *15*(9), 1492–1495. https://doi.org/10.3201/eid1509.080231

Björnham, O., Sigg, R., & Burman, J. (2020). Multilevel model for airborne transmission of foot-and-mouth disease applied to Swedish livestock. *PLoS ONE* (Vol. 15). https://doi.org/10.1371/journal.pone.0232489

Bloemraad, M., de Kluijver, E. P., Petersen, A., Burkhardt, G. E., & Wensvoort, G. (1994). Porcine reproductive and respiratory syndrome: temperature and pH stability of Lelystad virus and its survival in tissue specimens from viraemic pigs. *Veterinary Microbiology*, *42*(4), 361–371. https://doi.org/10.1016/0378-1135(94)90067-1

Bonifacio, H. F., Maghirang, R. G., & Glasgow, L. A. (2015). Numerical simulation of transport of particles emitted from ground-level area source using aermod and CFD. *Engineering Applications of Computational Fluid Dynamics*, *8*(4), 488–502. https://doi.org/10.1080/19942060.2014.11083302

Bouma, A., Dekker, A., & De Jong, M. C. M. (2004). No foot-and-mouth disease virus transmission between individually housed calves. *Veterinary Microbiology*, *98*(1), 29–36. https://doi.org/10.1016/j.vetmic.2003.10.016

Bowes, V. A. (2007). After the outbreak: How the British Columbia commercial poultry industry recovered after H7N3 HPAI. *Avian Diseases*, *51*(s1), 313–316.

Brito, B., Dee, S., Wayne, S., Alvarez, J., & Perez, A. (2014). Genetic diversity of PRRS virus collected from air samples in four different regions of concentrated swine production during a high incidence season. *Viruses*, *6*(11), 4424–4436. https://doi.org/10.3390/v6114424

Brockmeier, S. L., & Lager, K. M. (2002). Experimental airborne transmission of porcine reproductive and respiratory syndrome virus and Bordetella bronchiseptica. *Veterinary Microbiology*, *89*(4), 267–275. https://doi.org/10.1016/S0378-1135(02)00204-3

Brookes, V. J., Hernández-Jover, M., Holyoake, P., & Ward, M. P. (2014). Import risk assessment incorporating a dose-response model: Introduction of highly pathogenic porcine reproductive and respiratory syndrome into Australia via illegally imported raw pork. *Preventive Veterinary Medicine*, *113*(4), 565–579. https://doi.org/10.1016/j.prevetmed.2014.01.016

Brouwer, A. F., Weir, M. H., Eisenberg, M. C., Meza, R., & Eisenberg, J. N. S. (2017). Dose-response relationships for environmentally mediated infectious disease transmission models. *PLoS Computational Biology*, *13*(4), 1–28. https://doi.org/10.1371/journal.pcbi.1005481

Bui, V. N., Nguyen, T. T., Nguyen-Viet, H., Bui, A. N., McCallion, K. A., Lee, H. S., … Gray, G. C. (2019). Bioaerosol sampling to detect avian influenza virus in Hanoi's largest live poultry market. *Clinical Infectious Diseases*, *68*(6), 972–975. https://doi.org/10.1093/cid/ciy583

Cambra-López, M., Aarnink, A. J. A., Zhao, Y., Calvet, S., & Torres, A. G. (2010). Airborne particulate matter from livestock production systems: A review of an air pollution problem. *Environmental Pollution*, *158*(1), 1–17. https://doi.org/10.1016/j.envpol.2009.07.011

Camfil. (2017). XS Absolute standard capacity HEPA filter. Retrieved May 2, 2017, from http://www.camfil.us/FileArchive/_30_Product_Support_Material_CamTab/Product Literature/Absolute HEPA and ULPA Filters/Absolute XS Standard Capacity HEPA Filter Product Sheet.pdf

Cannon, R. M., & Garner, M. G. (1999). Assessing the risk of wind-borne spread of foot-and-mouth disease in australia. *Environment International*, *25*(6–7), 713–723.

https://doi.org/10.1016/S0160-4120(99)00049-5

Casal, J., Moreso, J. M., Planas-Cuchí, E., & Casal, J. (1997). Simulated airborne spread of Aujeszky's disease and foot-and-mouth disease. *Veterinary Record*, *140*(26), 672–676. https://doi.org/10.1136/vr.140.26.672

Casal, J., Planas-Cuchí, E., Moreso, J. M., & Casal, J. (1995). Forecasting virus atmospherical dispersion. Studies with foot-and-mouth disease. *Journal of Hazardous Materials*, *43*(3), 229–244. https://doi.org/10.1016/0304-3894(95)00040-2

CFIA. (2013). Foot and mouth disease overview. Retrieved December 10, 2020, from https://www.inspection.gc.ca/animal-health/terrestrial-animals/diseases/reportable/foot-and-mouth-disease/plan/eng/1332174353793/1332174430101?chap=2

CFIA. (2014). Classical swine fever - fact sheet. Retrieved from https://inspection.canada.ca/animal-health/terrestrial-animals/diseases/reportable/classical-swine-fever/fact-sheet/eng/1330139051721/1330139178061

CFIA. (2021). Reportable diseases: Terrestrial animals. Retrieved from https://inspection.canada.ca/animal-health/terrestrial-animals/diseases/reportable/eng/1303768471142/1303768544412

Chasey, D., & Cartwright, S. F. (1978). Virus-like particles associated with porcine epidemic diarrhoea. *Research in Veterinary Science*, *25*(2), 255–256. https://doi.org/https://doi.org/10.1016/s0034-5288(18)32994-1

Chen, P. S., Lin, C. K., Tsai, F. T., Yang, C. Y., Lee, C. H., Liao, Y. S., … Lin, K. H. (2009). Quantification of airborne influenza and avian influenza virus in a wet poultry market using a filter/real-time qPCR method. *Aerosol Science and Technology*, *43*(4), 290–297. https://doi.org/10.1080/02786820802621232

Chen, P.-S., Tsai, F. T., Lin, C. K., Yang, C.-Y., Chan, C.-C., Young, C.-Y., & Lee, C.-H. (2010). Ambient influenza and avian influenza virus during dust storm days and background days. *Environmental Health Perspectives*, *118*(9), 1211–1216. https://doi.org/10.1289/ehp.0901782

Cho, J. G., & Dee, S. A. (2006). Porcine reproductive and respiratory syndrome virus. *Theriogenology*, *66*(3), 655–662. https://doi.org/10.1016/j.theriogenology.2006.04.024

Cho, J. G., Dee, S. A., Deen, J., Trincado, C., Fano, E., Jiang, Y., … Joo, H. S. (2006). The impact of animal age, bacterial coinfection, and isolate pathogenicity on the shedding of Porcine reproductive and respiratory syndrome virus in aerosols from experimentally infected pigs. *Canadian Journal of Veterinary Research*, *70*(4), 297–301.

Cho, J. G., Deen, J., & Dee, S. A. (2007). Influence of isolate pathogenicity on the aerosol transmission of Porcine reproductive and respiratory syndrome virus. *Canadian Journal of Veterinary Research*, *71*(1), 23–27.

Christensen, L. S., Normann, P., Thykier-Nielsen, S., Sørensen, J. H., de Stricker, K., & Rosenørn, S. (2005). Analysis of the epidemiological dynamics during the 1982-1983 epidemic of foot-and-mouth disease in Denmark based on molecular high-resolution strain identification. *Journal of General Virology*, *86*(9), 2577–2584. https://doi.org/10.1099/vir.0.80878-0

Christensen, L. S., Brehm, K. E., Skov, J., Harlow, K. W., Christensen, J., & Haas, B. (2011). Detection of foot-and-mouth disease virus in the breath of infected cattle using a hand-held device to collect aerosols. *Journal of Virological Methods*, *177*(1), 44–48. https://doi.org/10.1016/j.jviromet.2011.06.011

Coffman, M. S., Sanderson, M. W., Dodd, C. C., Arzt, J., & Renter, D. G. (2021). Estimation of foot-and-mouth disease windborne transmission risk from USA beef feedlots. *Preventive Veterinary Medicine*, *195*(January), 105453. https://doi.org/10.1016/j.prevetmed.2021.105453

Coleman, H. W., & Steele, W. G. (2009). Taylor Series Method (TSM) for Uncertainty Propagation. In *Experimentation, Validation, and Uncertainty Analysis for Engineers* (3rd ed., pp. 257–269). John Wiley & Sons, Ltd. https://doi.org/10.1002/9781119417989.app2

Colenutt, C., Gonzales, J. L., Paton, D. J., Gloster, J., Nelson, N., & Sanders, C. (2016). Aerosol transmission of foot-and-mouth disease virus Asia-1 under experimental conditions. *Veterinary Microbiology*, *189*, 39–45. https://doi.org/10.1016/j.vetmic.2016.04.024

Colenutt, C., Brown, E., Nelson, N., Paton, D. J., Eblé, P., Dekker, A., … Gubbins, S. (2020). Quantifying the transmission of foot-and-mouth disease virus in cattle via a contaminated environment. *MBio*, *11*(4), 1–13. https://doi.org/10.1128/mBio.00381-20

Colenutt, C., Brown, E., Nelson, N., Wadsworth, J., Maud, J., Adhikari, B., … Gubbins, S. (2018). Environmental sampling as a low-technology method for surveillance of foot-and-mouth disease virus in an area of endemicity. *Applied and Environmental Microbiology*, *84*(16), 1–11. https://doi.org/10.1128/aem.00686-18

Continental Fans. (2012). *IRIS damper product specification guide*. Mississauga, ON.

Cutler, T. D., Wang, C., Hoff, S. J., & Zimmerman, J. J. (2012). Effect of temperature and relative humidity on ultraviolet (UV 254) inactivation of airborne porcine respiratory and reproductive syndrome virus. *Veterinary Microbiology*, *159*(1–2), 47–52. https://doi.org/10.1016/j.vetmic.2012.03.044

Cutler, T. D., Wang, C., Hoff, S. J., Kittawornrat, A., & Zimmerman, J. J. (2011). Median infectious dose (ID50) of porcine reproductive and respiratory syndrome virus isolate MN-184 via aerosol exposure. *Veterinary Microbiology*, *151*(3–4), 229–237. https://doi.org/10.1016/j.vetmic.2011.03.003

Daggupaty, S. M., & Sellers, R. F. (1990). Airborne spread of foot-and-mouth disease in Saskatchewan, Canada, 1951-1952. *Canadian Journal of Veterinary Research / Revue Canadienne de Recherche Vétérinaire*, *54*(4), 465–468.

Dalpé, B., & Masson, C. (2009). Numerical simulation of wind flow near a forest edge. *Journal of Wind Engineering and Industrial Aerodynamics*, *97*(5–6), 228–241. https://doi.org/10.1016/j.jweia.2009.06.008

de Carvalho F., H. C., Weesendorp, E., Quak, S., Stegeman, J. A., & Loeffen, W. L. A. (2013). Quantification of airborne African swine fever virus after experimental infection.

Veterinary Microbiology, *165*(3–4), 243–251. https://doi.org/10.1016/j.vetmic.2013.03.007

de Nevers, N. (2017). *Air pollution control engineering* (3rd ed.). Long Grove, IL: Waveland Press Inc.

Dee, S. A., Batista, L., Deen, J., & Pijoan, C. (2006). Evaluation of systems for reducing the transmission of porcine reproductive and respiratory syndrome virus by aerosol. *Canadian Journal Veterinary Research*, *70*(1), 28–33.

Dee, S. A., Deen, J., Cano, J. P., Batista, L., & Pijoan, C. (2006). Further evaluation of alternative air-filtration systems for reducing the transmission of Porcine reproductive and respiratory syndrome virus by aerosol. *Canadian Journal of Veterinary Research*, *70*(3), 168–175.

Dee, S., Batista, L., Deen, J., & Pijoan, C. (2005). Evaluation of an air-filtration system for preventing aerosol transmission of porcine reproductive and respiratory syndrome virus. *Canadian Journal of Veterinary Research*, *69*(4), 293–298.

Dee, S., Deen, J., Rossow, K. D., Mahlum, C., & Pijian, C. (2005). Laboratory model to evaluate the role of aerosols in the transport of porcine reproductive and respiratory syndrome virus. *Veterinary Record*, *156*(16), 501–504. https://doi.org/https://doi.org/10.1136/vr.156.16.501

Dee, S., Otake, S., & Deen, J. (2010). Use of a production region model to assess the efficacy of various air filtration systems for preventing airborne transmission of porcine reproductive and respiratory syndrome virus and Mycoplasma hyopneumoniae : Results from a 2-year study. *Virus Research*, *154*(1–2), 177–184. https://doi.org/10.1016/j.virusres.2010.07.022

Dee, S. A., Bauermann, F. V., Niederwerder, M. C., Singrey, A., Clement, T., De Lima, M., … Diel, D. G. (2018). Survival of viral pathogens in animal feed ingredients under transboundary shipping models. *PLoS ONE*, *13*(3), 1–18. https://doi.org/10.1371/journal.pone.0194509

Dee, S., Neill, C., Singrey, A., Clement, T., Cochrane, R., Jones, C., … Nelson, E. (2016). Modeling the transboundary risk of feed ingredients contaminated with porcine epidemic diarrhea virus. *BMC Veterinary Research*, *12*(1), 1–12. https://doi.org/10.1186/s12917-016-

0674-z

Dee, S., Otake, S., Oliveira, S., & Deen, J. (2009). Evidence of long distance airborne transport of porcine reproductive and respiratory syndrome virus and Mycoplasma hyopneumoniae. *Veterinary Research*, *40*(4). https://doi.org/10.1051/vetres/2009022

Desmond, C. J., Watson, S. J., & Hancock, P. E. (2017). Modelling the wind energy resources in complex terrain and atmospheres. Numerical simulation and wind tunnel investigation of non-neutral forest canopy flows. *Journal of Wind Engineering and Industrial Aerodynamics*, *166*(March), 48–60. https://doi.org/10.1016/j.jweia.2017.03.014

Desmond, C. J., Watson, S. J., Aubrun, S., Ávila, S., Hancock, P., & Sayer, A. (2014). A study on the inclusion of forest canopy morphology data in numerical simulations for the purpose of wind resource assessment. *Journal of Wind Engineering and Industrial Aerodynamics*, *126*, 24–37. https://doi.org/10.1016/j.jweia.2013.12.011

Dewulf, J., Laevens, H., Koenen, F., Mintiens, K., & De Kruif, A. (2000). Airborne transmission of classical swine fever virus under experimental conditions. *Veterinary Record*, *147*(26), 735–738. https://doi.org/10.1136/vr.147.26.735

Dillon, M. B. (2011). Skin as a potential source of infectious foot and mouth disease aerosols. *Proceedings of the Royal Society B: Biological Sciences*, *278*(1713), 1761–1769. https://doi.org/10.1098/rspb.2010.2430

Donaldson, A. I. (1972). The influence of relative humidity on the aerosol stability of different strains of foot-and-mouth disease virus suspended in saliva. *Journal of General Virology*, *15*(1), 25–33. https://doi.org/10.1099/0022-1317-15-1-25

Donaldson, A. I., & Alexandersen, S. (2002). Predicting the spread of foot and mouth disease by airborne virus. *OIE Revue Scientifique et Technique*, *21*(3), 569–575. https://doi.org/10.20506/rst.21.3.1362

Donaldson, A. I., & Ferris, N. P. (1976). The survival of some air-borne animal viruses in relation to relative humidity. *Veterinary Microbiology*, *1*(4), 413–420. https://doi.org/10.1016/0378-1135(76)90056-0

Donaldson, A. I., Alexandersen, S., Sørensen, J. H., & Mikkelsen, T. (2001a). Relative risks of the uncontrollable (airborne) spread of FMD by different species. *Veterinary Record*, *148*(19), 602–604. https://doi.org/10.1136/vr.148.19.602

Donaldson, A. I., Alexandersen, S., Sørensen, J. H., & Mikkelsen, T. (2001b). Relative risks of the uncontrollable (airborne) spread of FMD by different species. *Veterinary Record*, *148*, 602–604. https://doi.org/10.1136/vr.148.19.602

Donaldson, A. I., Gibson, C. F., & Oliver, R. (1987). Infection of cattle by airborne foot-and-mouth disease virus: minimal doses with O1 and SAT 2 strains. *Research in Veterinary Science*, *43*, 339–346.

Donaldson, A. I., Gloster, J., Harvey, L. D., & Deans, D. H. (1982). Use of prediction models to forecast and analyse airborne spread during the foot-and-mouth disease outbreaks in Brittany, Jersey and the Isle of Wight in 1981. *Veterinary Record*, *110*(3), 53–57. https://doi.org/10.1136/vr.110.3.53

Donaldson, A. I., Herniman, K. A. J., Parker, J., & Sellers, R. F. (1970). Further investigations on the airborne excretion of foot-and-mouth disease. *Journal of Hygiene (London)*, *68*, 557–564. https://doi.org/https://doi.org/10.1017/s0022172400042480

Dong, Z., Mu, Q., Luo, W., Qinan, G., Lu, P., & Wang, H. (2008). An analysis of drag force and moment for upright porous wind fences. *Journal of Geophysical Research Atmospheres*, *113*(4), 1–8. https://doi.org/10.1029/2007JD009138

Duguid, J. P. (1946). The size and the duration of air-carriage of respiratory droplets and droplet-nuclei. *Journal of Hygiene*, *44*(6), 471–479. https://doi.org/10.1017/S0022172400019288

Eblé, P., De Koeijer, A., Bouma, A., Stegeman, A., & Dekker, A. (2006). Quantification of within- and between-pen transmission of foot-and-mouth disease virus in pigs. *Veterinary Research*, *37*(5), 647–654. https://doi.org/10.1051/vetres:2006026

Egli, C., Thür, B., Liu, L., & Hofmann, M. A. (2001). Quantitative TaqMan® RT-PCR for the detection and differentiation of European and North American strains of porcine reproductive and respiratory syndrome virus. *Journal of Virological Methods*, *98*(1), 63–75.

https://doi.org/10.1016/S0166-0934(01)00358-5

Endalew, A. M., Hertog, M., Delele, M. A., Baetens, K., Persoons, T., Baelmans, M., … Verboven, P. (2009). CFD modelling and wind tunnel validation of airflow through plant canopies using 3D canopy architecture. *International Journal of Heat and Fluid Flow*, *30*(2), 356–368. https://doi.org/10.1016/j.ijheatfluidflow.2008.12.007

Endalew, A. M., Hertog, M., Gebrehiwot, M. G., Baelmans, M., Ramon, H., Nicolaï, B. M., & Verboven, P. (2009). Modelling airflow within model plant canopies using an integrated approach. *Computers and Electronics in Agriculture*, *66*(1), 9–24. https://doi.org/10.1016/j.compag.2008.11.002

Esteves, I., Gloster, J., Ryan, E., Durand, S., & Alexandersen, S. (2004). *Appendix 35-Natural aerosol transmission of foot-and-mouth disease in sheep*. Retrieved from http://www.fao.org/ag/againfo/commissions/docs/research_group/greece04/App35.pdf

Fano, E., Pijoan, C., & Dee, S. (2005). Evaluation of the aerosol transmission of a mixed infection of Mycoplasma hyopneumoniae and porcine reproductive and respiratory syndrome virus. *Veterinary Record*, *157*(4), 105–108. https://doi.org/10.1136/vr.157.4.105

Franke, J., Hirsch, C., Jensen, A. G., Krüs, H. W., Schatzmann, M., Westbury, P. S., … Wright, N. G. (2006). Recommendations on the use of CFD in wind engineering. In *International Conference on Urban Wind Engineering and Building Aerodynamics: COST action C14 - impact of wind and storm on city life and built environment* (p. C1.1-C1.11).

Furumoto, W. A., & Mickey, R. (1967). A mathematical model for the infectivity-dilution curve of tobacco mosaic virus: Experimental tests. *Virology*, *32*(2), 224–233. https://doi.org/10.1016/0042-6822(67)90272-3

Galindo, I., & Alonso, C. (2017). African swine fever virus: A review. *Viruses*, *9*(5). https://doi.org/10.3390/v9050103

Gallien, S., Andraud, M., Moro, A., Lediguerher, G., Morin, N., Gauger, P. C., … Grasland, B. (2018). Better horizontal transmission of a US non-InDel strain compared with a French InDel strain of porcine epidemic diarrhoea virus. *Transboundary and Emerging Diseases*,

65(6), 1720–1732. https://doi.org/10.1111/tbed.12945

Garner, M. G., Hess, G. D., & Yang, X. (2006). An integrated modelling approach to assess the risk of wind-borne spread of foot-and-mouth disease virus from infected premises. *Environmental Modeling and Assessment*, *11*(3), 195–207. https://doi.org/10.1007/s10666-005-9023-5

Germeraad, E. A., Sanders, P., Hagenaars, T. J., de Jong, M. C. M., & Gonzales, J. L. (2019). Virus shedding of avian influenza in poultry: A systematic review and meta-analysis. *Viruses*, *11*(9), 812. https://doi.org/https://doi.org/10.3390/v11090812

Gibson, C. F., & Donaldson, A. I. (1986). Exposure of sheep to natural aerosols of foot-and-mouth disease virus. *Research in Veterinary Science*, *41*, 45–49.

Gloster, J., Blackall, R. M., Sellers, R. F., & Donaldson, A. I. (1981). Forecasting the airborne spread of foot-and-mouth disease. *Veterinary Record*, *108*(17), 370–374. https://doi.org/https://doi.org/10.1136/vr.108.17.370

Gloster, J., Champion, H. J., Mansley, L. M., Romero, P., Brough, T., & Ramirez, A. (2005). The 2001 epidemic of foot-and-mouth disease in the United Kingdom: Epidemiological and meteorological case studies. *Veterinary Record*, *156*(25), 793–803. https://doi.org/10.1136/vr.156.25.793

Gloster, J., Champion, H. J., Sørensen, J. H., Mikkelsen, T., Ryall, D. B., Astrup, P., … Donaldson, A. I. (2003). Airborne transmission of foot-and-mouth disease virus from Burnside Farm, Heddon-on-the-Wall, Northumberland, during the 2001 epidemic in the United Kingdom. *Veterinary Record*, *152*(17), 525–533. https://doi.org/10.1136/vr.152.17.525

Gloster, J., Freshwater, A., Sellers, R. F., & Alexandersen, S. (2005). Re-assessing the likelihood of airborne spread of foot-and-mouth disease at the start of the 1967-1968 UK foot-and-mouth disease epidemic. *Epidemiology and Infection*, *133*(5), 767–783. https://doi.org/10.1017/S0950268805004073

Gloster, J., Doel, C., Gubbins, S., & Paton, D. J. (2008). Foot-and-mouth disease: Measurements

of aerosol emission from pigs as a function of virus strain and initial dose. *Veterinary Journal*, *177*(3), 374–380. https://doi.org/10.1016/j.tvjl.2007.06.014

Gloster, J., Jones, A., Redington, A., Burgin, L., Sørensen, J. H., Turner, R., … Paton, D. (2010). Airborne spread of foot-and-mouth disease - Model intercomparison. *Veterinary Journal*, *183*(3), 278–286. https://doi.org/10.1016/j.tvjl.2008.11.011

Gloster, J., Williams, P., Doel, C., Esteves, I., Coe, H., & Valarcher, J. F. (2007). Foot-and-mouth disease - Quantification and size distribution of airborne particles emitted by healthy and infected pigs. *Veterinary Journal*, *174*(1), 42–53. https://doi.org/10.1016/j.tvjl.2006.05.020

Guan, J., Fu, Q., & Shayan, S. (2015). Replication of an H9N2 avian influenza virus and cytokine gene expression in chickens exposed by berosol or intranasal routes, *59*(2), 263–268. https://doi.org/10.1128/AEM.02227-09

Guan, J., Fu, Q., Chan, M., & Spencer, J. L. (2013). Aerosol transmission of an avian influenza H9N2 virus with a tropism for the respiratory tract of chickens. *Avian Diseases*, *57*(3), 645–649. https://doi.org/10.1637/10486-010913-Reg.1

Haas, C. N. (1983). Estimation of risk due to low doses of microorganisms: a comparison of alternative methodologies. *American Journal of Epidemiology*, *118*(4), 573–582. https://doi.org/10.1093/oxfordjournals.aje.a113662

Hagerman, A. D., South, D. D., Sondgerath, T. C., Patyk, K. A., Sanson, R. L., Schumacher, R. S., … Magzamen, S. (2018). Temporal and geographic distribution of weather conditions favorable to airborne spread of foot-and-mouth disease in the coterminous United States. *Preventive Veterinary Medicine*, *161*(October), 41–49. https://doi.org/10.1016/j.prevetmed.2018.10.016

Hankin, R. K. S. (2006). Special functions in R: introducing the gsl package. *R News*, *6*(4).

Hannon, J. P., Bossone, C. A., & Wade, C. (1990). Normal physiological values for conscious pigs used in biomedical research. *Laboratory Animal Science*, *40*(3), 293-298.

Hargreaves, D. M., & Wright, N. G. (2007). On the use of the k-ε model in commercial CFD

software to model the neutral atmospheric boundary layer. *Journal of Wind Engineering and Industrial Aerodynamics*, *95*(5), 355–369. https://doi.org/10.1016/j.jweia.2006.08.002

Hendersen, R. J. (1969). The outbreak of foot-and-mouth disease in Worcestershire: An epidemiological study: with special reference to spread of the disease by wind-carriage of the virus. *Journal of Hygiene*, *67*(1), 21–33. https://doi.org/https://doi.org/10.1017/s0022172400041383

Hermann, J. R., Muñoz-Zanzi, C. A., & Zimmerman, J. J. (2009). A method to provide improved dose-response estimates for airborne pathogens in animals: An example using porcine reproductive and respiratory syndrome virus. *Veterinary Microbiology*, *133*(3), 297–302. https://doi.org/10.1016/j.vetmic.2008.07.002

Hermann, J. R., Hoff, S. J., Yoon, K. J., Burkhardt, A. C., Evans, R. B., & Zimmerman, J. J. (2006). Optimization of a sampling system for recovery and detection of airborne porcine reproductive and respiratory syndrome virus and swine influenza virus. *Applied and Environmental Microbiology*, *72*(7), 4811–4818. https://doi.org/10.1128/AEM.00472-06

Hermann, J. R., & Zimmerman, J. J. (2008). Analytical sensitivity of air samplers based on uniform point-source exposure to airborne Porcine reproductive and respiratory syndrome virus and swine influenza virus. *Canadian Journal of Veterinary Research*, *72*(5), 440–443.

Hermann, J. R., Muñoz-Zanzi, C. A., Roof, M. B., Burkhart, K., & Zimmerman, J. J. (2005). Probability of porcine reproductive and respiratory syndrome (PRRS) virus infection as a function of exposure route and dose. *Veterinary Microbiology*, *110*(1–2), 7–16. https://doi.org/10.1016/j.vetmic.2005.06.012

Hermann, J., Hoff, S., Muñoz-Zanzi, C., Yoon, K.-J., Roof, M., Burkhardt, A., & Zimmerman, J. (2007). Effect of temperature and relative humidity on the stability of infectious porcine reproductive and respiratory syndrome virus in aerosols. *Veterinary Research*, *38*(1), 81–93. https://doi.org/https://dx.doi.org/10.1051/vetres:2006044

Ho, C. K. (2021). Modelling airborne transmission and ventilation impacts of a COVID-19 outbreak in a restaurant in Guangzhou, China. *International Journal of Computational*

Fluid Dynamics. https://doi.org/10.1080/10618562.2021.1910678

Holcomb, D. L., Smith, M. A., Ware, G. O., Hung, Y. C., Brackett, R. E., & Doyle, M. P. (1999). Comparison of six dose-response models for use with food-borne pathogens. *Risk Analysis*, *19*(6), 1091–1100. https://doi.org/10.1023/A:1007078527037

Holtkamp, D. J., Kliebenstein, J. B., Neumann, E. J., Zimmerman, J. J., Rotto, H. F., Yoder, T. K., … Haley, C. A. (2013). Assessment of the economic impact of porcine reproductive and respiratory syndrome virus on United States pork producers. *Journal of Swine Health and Production*, *21*(2), 72–84.

Hong, S., Lee, I., Hwang, H., Seo, I., Bitog, J., Kwon, K., … Ko, H. (2011). CFD modelling of livestock odour dispersion over complex terrain, part I : Topographical modelling. *Biosystems Engineering*, *108*, 253–264. https://doi.org/10.1016/j.biosystemseng.2010.12.009

Howey, E. B., Donnell, V. O., Carvalho, H. C. De, Borca, M. V, & Arzt, J. (2013). Pathogenesis of highly virulent African swine fever virus in domestic pigs exposed via intraoropharyngeal, intranasopharyngeal, and intramuscular inoculation, and by direct contact with infected pigs. *Virus Research*, *178*(2), 328–339. https://doi.org/https://doi.org/10.1016/j.vetmic.2008.07.002

Hughes, G. J., Kitching, R. P., & Woolhouse, M. E. J. (2002). Dose-dependent responses of sheep inoculated intranasally with a type O foot-and-mouth disease virus. *Journal of Comparative Pathology*, *127*(1), 22–29. https://doi.org/10.1053/jcpa.2002.0560

Hugh-Jones, M. E., & Wright, P. B. (1970). Studies on the 1967-8 foot-and-mouth disease epidemic: The relation of weather to the spread of disease. *Journal of Hygiene*, *68*, 253–271. https://doi.org/https://doi.org/10.1017/S0022172400028722

Hulst, M. M., Heres, L., Hakze-van der Honing, R. W., Pelser, M., Fox, M., & van der Poel, W. H. M. (2019). Study on inactivation of porcine epidemic diarrhoea virus, porcine sapelovirus 1 and adenovirus in the production and storage of laboratory spray-dried porcine plasma. *Journal of Applied Microbiology*, *126*(6), 1931–1943.

https://doi.org/10.1111/jam.14235

Jacobs, A. C., Hermann, J. R., Muñoz-Zanzi, C., Prickett, J. R., Roof, M. B., Yoon, K. J., & Zimmerman, J. J. (2010). Stability of porcine reproductive and respiratory syndrome virus at ambient temperatures. *Journal of Veterinary Diagnostic Investigation, 22*(2), 257–260. https://doi.org/10.1177/104063871002200216

Jennings, S. (1988). The mean free path in air. *Journal of Aerosol Science, 19*(2), 159–166. https://doi.org/10.1016/0021-8502(88)90219-4

Jerez, S. B., Zhang, Y., & Wang, X. (2011). Measurement of particle size distribution in a swine building. *Transactions of the ASABE*, *54*(3), 1103–1117.

Jones, R., Kelly, L., French, N., England, T., Livesey, C., & Wooldridge, M. (2004). Quantitative estimates of the risk of new outbreaks of foot-and-mouth disease as a result of burning pyres. *Veterinary Record*, *154*(6), 161–165. https://doi.org/10.1136/vr.154.6.161

Jonges, M., Leuken, J. Van, Wouters, I., Koch, G., & Meijer, A. (2015). Wind-mediated spread of low-pathogenic avian influenza virus into the environment during outbreaks at commercial poultry farms. *PLoS ONE*, *10*(5). https://doi.org/10.1371/journal.pone.0125401

Kauffold, J., Beckjunker, J., Scheller, R., Schwarz, B. A., Beynon, N., & Sobiraj, A. (2005). Effects of type of machine and covering on viruses and microorganisms recovered from dust in ultrasound machines used in German swine production operations. *Journal of Swine Health and Production, 13*(2), 72–80.

Kim, Y., Krishna, V. D., Torremorell, M., Goyal, S. M., & Cheeran, M. C. J. (2018). Stability of porcine epidemic diarrhea virus on fomite materials at different temperatures. *Veterinary Sciences*, *5*(21). https://doi.org/10.3390/vetsci5010021

Klausner, Z., Klement, E., & Fattal, E. (2015). Modeling long distance dispersal of airborne foot-and-mouth disease virus as a polydisperse aerosol - Application to the emergence of a new strain from Egypt to Israel. *Atmospheric Environment, 122*, 332–342. https://doi.org/10.1016/j.atmosenv.2015.09.067

Knight, V. (1980). Viruses as agents of airborne contagion. *Annals of the New York Academy of*

Sciences, *353*(1), 147–156. https://doi.org/10.1111/j.1749-6632.1980.tb18917.x

Kocherhans, R., Bridgen, A., Ackermann, M., & Tobler, K. (2001). Completion of the porcine epidemic diarrhoea coronavirus (PEDV) genome sequence. *Virus Genes*, *23*(2), 137–144. https://doi.org/10.1023/A:1011831902219

Kochhar, H. S. (2017). Porcine epidemic diarrhea in Canada: An emerging disease case study. *Canadian Veterinary Journal*, *58*(8), 802–804.

Kristensen, C. S., Bøtner, A., Takai, H., Nielsen, J. P., & Jorsal, S. E. (2004). Experimental airborne transmission of PRRS virus. *Veterinary Microbiology*, *99*(3–4), 197–202. https://doi.org/10.1016/j.vetmic.2004.01.005

Kritana, P., Taehyeung, K., Hyeontae, K., Ki Youn, K., & Wongeun, S. (2014). Atmospheric pathway: A possibility of continuous outbreaks of foot-and-mouth disease in South Korea in 2010-2011. *Computers and Electronics in Agriculture*, *108*, 95–104. https://doi.org/10.1016/j.compag.2014.07.007

Kuchipudi, S. V., Tellabati, M., Nelli, R. K., White, G. A., Perez, B. B., Sebastian, S., … Chang, K. C. (2012). 18S rRNA is a reliable normalisation gene for real time PCR based on influenza virus infected cells. *Virology Journal*, *9*, 1–7. https://doi.org/10.1186/1743-422X-9-230

Kurmi, B., Murugkar, H. V., Nagarajan, S., Tosh, C., Dubey, S. C., & Kumar, M. (2013). Survivability of highly pathogenic avian influenza H5N1 virus in poultry faeces at different temperatures. *Indian Journal of Virology*, *24*(2), 272–277. https://doi.org/10.1007/s13337-013-0135-2

La, A. (2015). *Effectiveness of negative air ionization in reducing airborne porcine reproductive and respiratory syndrome virus (PRRSV) and aerosols*. University of Manitoba.

La, A., & Zhang, Q. (2019). Experimental validation of CFD simulations of bioaerosol movement in a mechanically ventilated airspace. *Canadian Biosystems Engineering / Le Genie Des Biosystems Au Canada*, *61*(1), 1–14. https://doi.org/10.7451/CBE.2019.61.5.01

La, A., Zhang, Q., Cicek, N., Levin, D. B., & Coombs, K. M. (2021). Dose–response modelling

of infectious animal diseases coupled with computational fluid dynamics: A simulation of airborne porcine reproductive and respiratory syndrome virus. *Biosystems Engineering*, *208*, 58–78. https://doi.org/10.1016/j.biosystemseng.2021.05.005

Lambkin, K., Hamilton, J., McGrath, G., Dando, P., & Draxler, R. (2019). Foot and mouth disease atmospheric dispersion system. *Advances in Science and Research*, *16*, 113–117. https://doi.org/10.5194/asr-16-113-2019

Launder, B. E., & Spalding, D. B. (1972). *Lectures in Mathematical Models of Turbulence*. London, England: Academic Press.

Lee, H. S., Bui, V. N., Dao, D. T., Bui, N. A., Le, T. D., Kieu, M. A., … Oh, S. I. (2021). Pathogenicity of an African swine fever virus strain isolated in Vietnam and alternative diagnostic specimens for early detection of viral infection. *Porcine Health Management*, *7*(1), 1–11. https://doi.org/10.1186/s40813-021-00215-0

Lee, H., Suh, K., Jung, N., Lee, I., Seo, I., Moon, O., & Lee, J. (2014). Prediction of the spread of highly pathogenic avian influenza using a multifactor network : Part 2 - Comprehensive network analysis with direct / indirect infection route. *Biosystems Engineering*, *118*, 115–127. https://doi.org/10.1016/j.biosystemseng.2013.11.009

Li, H., Rong, L., & Zhang, G. (2017). Reliability of turbulence models and mesh types for CFD simulations of a mechanically ventilated pig house containing animals. *Biosystems Engineering*, *161*, 37–52. https://doi.org/10.1016/j.biosystemseng.2017.06.012

Li, S., Zhou, Y., Gao, S., Pang, Q., & Miao, Z. (2017). A small-scale study on airborne transmission of H9N2 avian influenza virus under field conditions. *Journal of Infection in Developing Countries*, *11*(12), 962–966. https://doi.org/10.3855/jidc.9013

Li, Y., Huang, X., Yu, I. T. S., Wong, T. W., & Qian, H. (2004). Role of air distribution in SARS transmission during the largest nosocomial outbreak in Hong Kong. *Indoor Air*, *15*(2), 83–95. https://doi.org/10.1111/j.1600-0668.2004.00317.x

Lin, C. M., Saif, L. J., Marthaler, D., & Wang, Q. (2016). Evolution, antigenicity and pathogenicity of global porcine epidemic diarrhea virus strains. *Virus Research*, *226*, 20–39.

https://doi.org/10.1016/j.virusres.2016.05.023

Liu, X., Lin, C. M., Annamalai, T., Gao, X., Lu, Z., Esseili, M. A., … Wang, Q. (2015). Determination of the infectious titer and virulence of an original US porcine epidemic diarrhea virus PC22A strain. *Veterinary Research*, *46*(1), 1–6. https://doi.org/10.1186/s13567-015-0249-1

Lycett, S. J., Duchatel, F., & Digard, P. (2019). A brief history of bird flu. *Philosophical Transactions of the Royal Society B: Biological Sciences*, *374*(1775), 0–3. https://doi.org/10.1098/rstb.2018.0257

Malik, N., Kotecha, A., Gold, S., Asfor, A., Ren, J., Huiskonen, J. T., … Stuart, D. I. (2017). Structures of foot and mouth disease virus pentamers: Insight into capsid dissociation and unexpected pentamer reassociation. *PLoS Pathogens*, *13*(9), 1–15. https://doi.org/10.1371/journal.ppat.1006607

Manitoba Agriculture. (2020). Porcine epidemic diarrhea (PED) virus. Retrieved January 20, 2021, from https://www.gov.mb.ca/agriculture/animal-health-and-welfare/animal-health/porcine-epidemic-diarrhea.html

Maragon, S., Facchin, E., Moutou, F., Massirio, I., Vincenzi, G., & Davies, G. (1994). The 1993 Italian foot-and-mouth disease epidemic: epidemiological features of the four outbreaks identified in Verona province (Veneto). *Veterinary Record*, *135*, 53–57. https://doi.org/https://doi.org/10.1136/vr.135.3.53

Mason-D'Croz, D., Bogard, J. R., Herrero, M., Robinson, S., Sulser, T. B., Wiebe, K., … Godfray, H. C. J. (2020). Modelling the global economic consequences of a major African swine fever outbreak in China. *Nature Food*, *1*(4), 221–228. https://doi.org/10.1038/s43016-020-0057-2

Mayer, D., Reiczigel, J., & Rubel, F. (2008). A lagrangian particle model to predict the airborne spread of foot-and-mouth disease virus, *42*, 466–479. https://doi.org/10.1016/j.atmosenv.2007.09.069

Mazur-Panasiuk, N., Żmudzki, J., & Woźniakowski, G. (2019). African swine fever virus -

persistence in different environmental conditions and the possibility of its indirect transmission. *Journal of Veterinary Research (Poland)*, *63*(3), 303–310. https://doi.org/10.2478/jvetres-2019-0058

McVicar, J. W. (1984). Quantitative aspects of the transmission of African swine fever. *American Journal of Veterinary Research*, *45*(8), 1535–1541.

McVicar, J. W., & Eisner, R. J. (1983). Aerosol exposure of cattle to foot-and-mouth disease virus. *Journal of Hygiene*, *91*(2), 319–328. https://doi.org/10.1017/S0022172400060332

Mielke, S. R., & Garabed, R. (2020). Environmental persistence of foot-and-mouth disease virus applied to endemic regions. *Transboundary and Emerging Diseases*, *67*(2), 543–554. https://doi.org/10.1111/tbed.13383

Mikkelsen, T., Alexandersen, S., Astrup, P., Champion, H. J., Donaldson, A. I., Dunkerley, F. N., … Thykier-Nielsen, S. (2003). Investigation of airborne foot-and-mouth disease virus transmission during low-wind conditions in the early phase of the UK 2001 epidemic. *Atmospheric Chemistry and Physics*, *3*(6), 2101–2110. https://doi.org/10.5194/acp-3-2101-2003

Montgomery, R. E. (1921). On a form of swine fever occurring in British East Africa (Kenya Colony). *Journal of Comparative Pathology and Therapeutics*, *34*, 159–191. https://doi.org/10.1016/s0368-1742(21)80031-4

Morris, R. S., Wilesmith, J. W., Stern, M. W., Sanson, R. L., & Stevenson, M. A. (2001). Predictive spatial modelling of alternative control strategies for the foot-and-mouth disease epidemic in Great Britain, 2001. *Veterinary Record*, *149*(5), 137–144. https://doi.org/10.1136/vr.149.5.137

Mortensen, S., Stryhn, H., Sogaard, R., Boklund, A., Stärk, K. D. C., Christensen, J., & Willeberg, P. (2002). Risk factors for infection of sow herds with porcine reproductive and respiratory syndrome (PRRS) virus. *Preventive Veterinary Medicine*, *53*(1–2), 83–101. https://doi.org/10.1016/S0167-5877(01)00260-4

Moutou, F., & Durand, B. (1994). Modelling the spread of foot-and-mouth disease virus.

Veterinary Research, *25*(2–3), 279–285.

MWPS. (1983). *Swine Housing and Equipment Handbook*. Ames, Iowa: Midwest Plan Service.

Nazir, J., Haumacher, R., Ike, A. C., & Marschang, R. E. (2011). Persistence of avian influenza viruses in lake sediment, duck feces, and duck meat. *Applied and Environmental Microbiology*, *77*(14), 4981–4985. https://doi.org/10.1128/AEM.00415-11

Nelson, N., Paton, D. J., Gubbins, S., Colenutt, C., Brown, E., Hodgson, S., & Gonzales, J. L. (2017). Predicting the ability of preclinical diagnosis to improve control of farm-to-farm foot-and-mouth disease transmission in cattle. *Journal of Clinical Microbiology*, *55*(6), 1671–1682. https://doi.org//10.1128/jcm.00179-17

Niederwerder, M. C., Nietfeld, J. C., Bai, J., Peddireddi, L., Breazeale, B., Anderson, J., … Hesse, R. A. (2016). Tissue localization, shedding, virus carriage, antibody response, and aerosol transmission of porcine epidemic diarrhea virus following inoculation of 4-week-old feeder pigs. *Journal of Veterinary Diagnostic Investigation*, *28*(6), 671–678. https://doi.org/10.1177/1040638716663251

Niederwerder, M. C., Stoian, A. M. M., Rowland, R. R. R., Dritz, S. S., Petrovan, V., Constance, L. A., … Hefley, T. J. (2019). Infectious dose of African swine fever virus when consumed naturally in liquid or feed, *25*(5).

Norton, T., Sun, D. W., Grant, J., Fallon, R., & Dodd, V. (2007). Applications of computational fluid dynamics (CFD) in the modelling and design of ventilation systems in the agricultural industry: A review. *Bioresource Technology*, *98*(12), 2386–2414. https://doi.org/10.1016/j.biortech.2006.11.025

Olesen, A. S., Belsham, G. J., Bruun Rasmussen, T., Lohse, L., Bødker, R., Halasa, T., … Bøtner, A. (2020). Potential routes for indirect transmission of African swine fever virus into domestic pig herds. *Transboundary and Emerging Diseases*, *67*(4), 1472–1484. https://doi.org/10.1111/tbed.13538

Olesen, A. S., Lohse, L., Boklund, A., Halasa, T., Gallardo, C., Pejsak, Z., … Bøtner, A. (2017). Transmission of African swine fever virus from infected pigs by direct contact and aerosol

routes. *Veterinary Microbiology*, *211*(October), 92–102. https://doi.org/10.1016/j.vetmic.2017.10.004

OpenFOAM. (2016a). Flow rate. Retrieved November 27, 2019, from https://www.openfoam.com/documentation/guides/latest/doc/guide-bcs-inlet-flow-rate-inlet.html

OpenFOAM. (2016b). icoUncoupledKinematicParcelFoam.C file reference. Retrieved August 2, 2022, from https://www.openfoam.com/documentation/guides/latest/api/icoUncoupledKinematicParcelFoam_8C.html

OpenFOAM. (2018). simpleFoam. Retrieved August 2, 2022, from https://www.openfoam.com/documentation/guides/latest/doc/guide-applications-solvers-incompressible-simpleFoam.html

Otake, S., Dee, S. A., Jacobson, L., Torremorell, M., & Pijoan, C. (2002). Evaluation of aerosol transmission of porcine reproductive and respiratory syndrome virus under controlled field conditions. *Veterinary Record*, *150*(26), 804–808. https://doi.org/https://doi.org/10.1136/vr.150.26.804

Otake, S., Dee, S., Corzo, C., Oliveira, S., & Deen, J. (2010). Long-distance airborne transport of infectious PRRSV and Mycoplasma hyopneumoniae from a swine population infected with multiple viral variants. *Veterinary Microbiology*, *145*(3–4), 198–208. https://doi.org/10.1016/j.vetmic.2010.03.028

Otake, S., Dee, S. A., Acvm, D., Rossow, K. D., Deen, J., Bvp, D. A., … Pijoan, C. (2002). Original research syndrome virus by fomites (boots and coveralls). *Journal of Swine Health and Production*, *10*(2), 59–65.

Pacheco, J. M., Brito, B., Hartwig, E., Smoliga, G. R., Perez, A., Arzt, J., & Rodriguez, L. L. (2017). Early detection of foot-and-mouth disease virus from infected cattle using a dry filter air sampling system. *Transboundary and Emerging Diseases*, *64*(2), 564–573. https://doi.org/10.1111/tbed.12404

Pasick, J., Berhane, Y., Ojkic, D., Maxie, G., Embury-Hyatt, C., Swekla, K., … Alexandersen, S. (2014). Investigation into the role of potentially contaminated feed as a source of the first-detected outbreaks of porcine epidemic diarrhea in Canada. *Transboundary and Emerging Diseases*, *61*(5), 397–410. https://doi.org/10.1111/tbed.12269

Pasick, J., Handel, K., Robinson, J., Copps, J., Ridd, D., Hills, K., … Czub, S. (2005). Intersegmental recombination between the haemagglutinin and matrix genes was responsible for the emergence of a highly pathogenic H7N3 avian influenza virus in British Columbia. *Journal of General Virology*, *86*(3), 727–731. https://doi.org/10.1099/vir.0.80478-0

Pasquill, F. (1961). The estimation of the dispersion of windborne material. *The Meteorological Magazine*, *90*(1063), 33–49.

Pikalo, J., Zani, L., Hühr, J., Beer, M., & Blome, S. (2019). Pathogenesis of African swine fever in domestic pigs and European wild boar – Lessons learned from recent animal trials. *Virus Research*, *271*(February), 197614. https://doi.org/10.1016/j.virusres.2019.04.001

Pirtle, E. C., & Beran, G. W. (1996). Stability of porcine reproductive and respiratory syndrome virus in the presence of fomites commonly found on farms. *Journal of the American Veterinary Medical Association*, *208*(3), 390–392.

Pitkin, A. N. (2009). *The production region model: a new approach to evaluate routes of transmission and protocols of biosecurity for PRRS virus*. University of Minnesota.

Pitkin, A., Deen, J., & Dee, S. (2009). Use of a production region model to assess the airborne spread of porcine reproductive and respiratory syndrome virus. *Veterinary Microbiology*, *136*(1–2), 1–7. https://doi.org/10.1016/j.vetmic.2008.10.013

Plummer, M., Best, N., Cowles, K., & Vines, K. (2006). CODA: Convergence diagnosis and output analysis for mcmc. *R News*, *6*(1), 7-11.

Pontiggia, M., Derudi, M., Busini, V., & Rota, R. (2009). Hazardous gas dispersion: A CFD model accounting for atmospheric stability classes. *Journal of Hazardous Materials*, *171*(1–3), 739–747. https://doi.org/10.1016/j.jhazmat.2009.06.064

Power, C. A. (2005). An investigation into the potential role of aerosol dispersion of dust from poutlry barns during an outbreak of avian influenza (H7:N3) in Abbotsford, BC in 2004. In *Proceedings of the Fourth St. Andrews Aquaculture Workshop: Water Movement and Aquatic Animal Health* (pp. 7–14). St. Andrews, NB: Aquaculture Association Canada.

Prospathopoulos, J., & Voutsinas, S. G. (2006). Implementation issues in 3D wind flow predictions over complex terrain. *Journal of Solar Energy Engineering, 128*, 539–553. https://doi.org/10.1115/1.2346702

Pujols, J., & Segalés, J. (2014). Survivability of porcine epidemic diarrhea virus (PEDV) in bovine plasma submitted to spray drying processing and held at different time by temperature storage conditions. *Veterinary Microbiology, 174*(3–4), 427–432. https://doi.org/10.1016/j.vetmic.2014.10.021

Pyankov, O. V., Pyankova, O. G., & Agranovski, I. E. (2012). Inactivation of airborne influenza virus in the ambient air. *Journal of Aerosol Science, 53*, 21–28. https://doi.org/10.1016/j.jaerosci.2012.05.011

Quist-Rybachuk, G. V., Nauwynck, H. J., & Kalmar, I. D. (2015). Sensitivity of porcine epidemic diarrhea virus (PEDV) to pH and heat treatment in the presence or absence of porcine plasma. *Veterinary Microbiology, 181*(3–4), 283–288. https://doi.org/10.1016/j.vetmic.2015.10.010

RCoreTeam. (2017). R: A language and environment for statistical computing. Ver. 3.6.2. Retrieved from https://www.r-project.org/

Richards, P. J., & Hoxey, R. P. (1993). Appropriate boundary conditions for computational wind engineering models using the k-ϵ turbulence model. *Journal of Wind Engineering and Industrial Aerodynamics*, *46&47*, 145–153.

Rong, L., Nielsen, P. V, Bjerg, B., & Zhang, G. (2016). Summary of best guidelines and validation of CFD modeling in livestock buildings to ensure prediction quality. *Computers and Electronics in Agriculture, 121*, 180–190. https://doi.org/10.1016/j.compag.2015.12.005

Rosendal, T., Dewey, C., Friendship, R., Wootton, S., Young, B., & Poljak, Z. (2014). Spatial and temporal patterns of porcine reproductive and respiratory syndrome virus (PRRSV) genotypes in Ontario, Canada, 2004-2007. *BMC Veterinary Research*, *10*. https://doi.org/10.1186/1746-6148-10-83

RStudioTeam. (2016). RStudio: Integrated development for R. Ver. 1.1.423. Retrieved from http://www.rstudio.com/.

Rushton, J., & Knight-Jones, T. (2012). The impact of foot and mouth disease. In *FAO and OIE. Proceedings of the FAO/OIE Global Conference on Foot and Mouth Disease Control* (pp. 205–209). Bangkok, Thailand: FAO/OIE. Retrieved from https://hdl.handle.net/10568/76285

Sanson, R. L., Gloster, J., & Burgin, L. (2011). Reanalysis of the start of the UK 1967 to 1968 foot-and-mouth disease epidemic to calculate airborne transmission probabilities. *Veterinary Record*, *169*(13), 336. https://doi.org/10.1136/vr.d4401

Sanson, R. L., Rawdon, T., Owen, K., Hickey, K., van Andel, M., & Yu, Z. D. (2017). Evaluating the benefits of vaccination when used in combination with stamping-out measures against hypothetical introductions of foot-and-mouth disease into New Zealand: a simulation study. *New Zealand Veterinary Journal*, *65*(3), 124–133. https://doi.org/10.1080/00480169.2016.1263165

Schmidt, P. J., Pintar, K. D. M., Fazil, A. M., & Topp, E. (2013). Harnessing the theoretical foundations of the exponential and beta-poisson dose-response models to quantify parameter uncertainty using markov chain monte carlo. *Risk Analysis*, *33*(9), 1677–1693. https://doi.org/10.1111/risa.12006

Schofield, L., Ho, J., Kournikakis, B., & Booth, T. (2005). *Avian influenza aerosol sampling campaign in the British Columbia Fraser Valley, 9-19 April 2004: Sampling of rare biological events*. Suffield, Alberta.

Schumacher, L. L., Woodworth, J. C., Jones, C. K., Chen, Q., Zhang, J., Gauger, P. C., … Dritz, S. S. (2016). Evaluation of the minimum infectious dose of porcine epidemic diarrhea virus

in virus-inoculated feed. *American Journal of Veterinary Research*, *77*(10), 1108–1113. https://doi.org/10.2460/ajvr.77.10.1108

Scoizec, A., Niqueux, E., Thomas, R., Daniel, P., Schmitz, A., & Le Bouquin, S. (2018). Airborne detection of H5N8 highly pathogenic avian influenza virus genome in poultry farms, France. *Frontiers in Veterinary Science*, *5*(FEB). https://doi.org/10.3389/fvets.2018.00015

Scott, A., McCluskey, B., Brown-Reid, M., Grear, D., Pitcher, P., Ramos, G., … Singrey, A. (2016). Porcine epidemic diarrhea virus introduction into the United States: Root cause investigation. *Preventive Veterinary Medicine*, *123*, 192–201. https://doi.org/10.1016/j.prevetmed.2015.11.013

Sedlmaier, N., Hoppenheidt, K., Krist, H., Lehmann, S., Lang, H., & Büttner, M. (2009). Generation of avian influenza virus (AIV) contaminated fecal fine particulate matter (PM2.5): Genome and infectivity detection and calculation of immission. *Veterinary Microbiology*, *139*(1–2), 156–164. https://doi.org/10.1016/j.vetmic.2009.05.005

Segersson, D. (2017). A tutorial to urban wind flow using OpenFOAM. In *Proceedings of CFD with OpenSource Software* (pp. 1–35).

Seiler, P., Kercher, L., Feeroz, M. M., Shanmuganatham, K., Jones-Engel, L., Turner, J., … Webster, R. G. (2018). H9N2 influenza viruses from Bangladesh: Transmission in chicken and new world quail. *Influenza and Other Respiratory Viruses*, *12*(6), 814–817. https://doi.org/10.1111/irv.12589

Sellers, R. F., & Daggupaty, S. M. (1990). The epidemic of foot-and-mouth disease in Saskatchewan, Canada, 1951-1952. *Canadian Journal of Veterinary Research/Revue Canadienne de Recherche Vétérinaire*, *54*(4), 457–464.

Sellers, R. F., & Forman, A. J. (1973). The Hampshire epidemic of foot-and-mouth disease, 1967. *Journal of Hygiene*, *71*(1), 15–34. https://doi.org//10.1017%2Fs0022172400046179

Sellers, R. F., & Gloster, J. (1980). The Northumberland epidemic of foot-and-mouth disease, 1966. *Journal of Hygiene*, *85*(1), 129–140.

https://doi.org//10.1017%2Fs0022172400027145

Sellers, R. F., & Parker, J. (1969). Airborne excretion of foot-and-mouth disease virus. *Journal of Hygiene*, *67*, 671–677. https://doi.org/10.1017%2Fs0022172400042121

Seo, I.-H., Lee, I.-B., Shin, M.-H., Lee, G.-Y., Hwang, H.-S., Hong, S.-W., … Bartzanas, T. (2010). Numerical prediction of fugitive dust dispersion on reclaimed land in Korea. *Transactions of the ASABE*, *53*(3), 891–901.

Seo, I.-H., Lee, I.-B., Hong, S.-W., Noh, H.-S., & Park, J.-H. (2015). Web-based forecasting system for the airborne spread of livestock infectious disease using computational fluid dynamics. *Biosystems Engineering*, 129, 169–184. https://doi.org/10.1016/j.biosystemseng.2014.10.004

Seo, I.-H., Lee, I.-B., Moon, O.-K., Jung, N.-S., Lee, H.-J., Hong, S.-W., … Bitog, J. P. (2014). Prediction of the spread of highly pathogenic avian influenza using a multifactor network : Part 1 - Development and application of computational fluid dynamics simulations of airborne dispersion. *Biosystems Engineering*, 121, 160–176. https://doi.org/10.1016/j.biosystemseng.2014.02.013

Sergeev, A. A., Demina, O. K., Pyankov, O. V., Pyankova, O. G., Agafonov, A. P., Kiselev, S. A., … Sergeev, A. N. (2013). Infection of chickens caused by avian influenza virus A/H5N1 delivered by aerosol and other routes. *Transboundary and Emerging Diseases*, *60*(2), 159–165. https://doi.org/10.1111/j.1865-1682.2012.01329.x

Shi, H., Ashraf, S., Gao, S., Lu, J., & Liu, X. (2010). Evaluation of transmission route and replication efficiency of H9N2 avian influenza virus. *Avian Diseases*, *54*(1), 22–27. https://doi.org/10.1637/9210.1

Smith, L. P., & Hugh-Jones, M. E. (1969). The weather factor in foot and mouth disease epidemics. *Nature*, *223*, 712–715. https://doi.org/10.1038/223712a0

Sobsey, M. D., & Meschke, J. S. (2003). *Virus survival in the environment with special attention to survival in sewage droplets and other environmental media of fecal or respiratory origin*. *Report for the World Health Organization. Geneva, Switzerland*.

Sørensen, J. H., Jensen, C., Mikkelsen, T., Mackay, D. K. J., & Donaldson, A. I. (2001). Modelling the atmospheric dispersion of foot-and-mouth disease virus for emergency preparedness. *Physics and Chemistry of the Earth, Part B: Hydrology, Oceans and Atmosphere*, *26*(2), 93–97. https://doi.org/10.1016/S1464-1909(00)00223-9

Sørensen, J. H., Mackay, D. K. J., Jensen, C. Ø., & Donaldson, A. I. (2000). An integrated model to predict the atmospheric spread of foot-and-mouth disease virus. *Epidemiology and Infection*, *124*(3), 577–590. https://doi.org/10.1017/S095026889900401X

Spekreijse, D., Bouma, A., Koch, G., & Stegeman, A. (2013). Quantification of dust-borne transmission of highly pathogenic avian influenza virus between chickens. *Influenza and Other Respiratory Viruses*, *7*(2), 132–138. https://doi.org/10.1111/j.1750-2659.2012.00362.x

Spekreijse, D., Bouma, A., Koch, G., & Stegeman, J. A. (2011). Airborne transmission of a highly pathogenic avian influenza virus strain H5N1 between groups of chickens quantified in an experimental setting. *Veterinary Microbiology*, *152*(1–2), 88–95. https://doi.org/10.1016/j.vetmic.2011.04.024

Spekreijse, D., Bouma, A., Stegeman, J. A., Koch, G., & de Jong, M. C. M. (2011). The effect of inoculation dose of a highly pathogenic avian influenza virus strain H5N1 on the infectiousness of chickens. *Veterinary Microbiology*, *147*(1–2), 59–66. https://doi.org/10.1016/j.vetmic.2010.06.012

Spronk, G., Otake, S., & Dee, S. (2010). Prevention of PRRSV infection in large breeding herds using air filtrations. *Veterinary Record*, *166*(24), 758–759. https://doi.org/10.1136/vr.b4848

Ssematimba, A., Hagenaars, T. J., & de Jong, M. C. M. (2012). Modelling the wind-borne spread of highly pathogenic avian influenza virus between farms. *PLoS ONE*, *7*(2), 1–9. https://doi.org/10.1371/journal.pone.0031114

Stein, H., Schulz, J., Morgenstern, R., Voglmayr, T., Freymüller, G., Sinn, L., … Ladinig, A. (2018). Use of three air samplers for the detection of PRRSV-1 under experimental and field conditions. *Animals*, *8*(12), 4–9. https://doi.org/10.3390/ani8120233

Stenfeldt, C., Bertram, M. R., Smoliga, G. R., Hartwig, E. J., Delgado, A. H., & Arzt, J. (2020). Duration of contagion of foot-and-mouth disease virus in infected live pigs and carcasses. *Frontiers in Veterinary Science*, *7*(June), 1–12. https://doi.org/10.3389/fvets.2020.00334

Stenfeldt, C., Hartwig, E. J., Smoliga, G. R., Palinski, R., Silva, E. B., Bertram, M. R., … Arzt, J. (2018). Contact challenge of cattle with foot-and-mouth disease virus validates the role of the nasopharyngeal epithelium as the site of primary and persistent infection. *MSphere*, *3*(6), 1–18. https://doi.org/10.1128/msphere.00493-18

Stoian, A. M. M., Zimmerman, J., Ji, J., Hefley, T. J., Dee, S., Diel, D. G., … Niederwerder, M. C. (2019). Half-life of African swine fever virus in shipped feed. *Emerging Infectious Diseases*, *25*(12), 2261–2263. https://doi.org/10.3201/eid2512.191002

Sturtz, S., Ligges, U., & Gelman, A. (2005). R2WinBUGS: A package for running winbugs from r. *Journal of Statistical Software*, *12*(3), 1-16.

Su, Y.-S., & Yajima, M. (2015). *R2jags: Using r to run 'JAGS'*. R Package Version 0.5-7. Retrieved from https://cran.r-project.org/web/packages/R2jags/

Sze To, G. N., & Chao, C. Y. H. (2010). Review and comparison between the Wells-Riley and dose-response approaches to risk assessment of infectious respiratory diseases. *Indoor Air*, *20*(1), 2–16. https://doi.org/10.1111/j.1600-0668.2009.00621.x

Teunis, P. F. M, Nagelkerke, N. J. D., & Haas, C. N. (1999). Dose response for infectious gastroenteritis. *Risk Analysis*, *19*(6), 1251–1260.

Teunis, P. F. M., Brienen, N., & Kretzschmar, M. E. E. (2010). High infectivity and pathogenicity of influenza A virus via aerosol and droplet transmission. *Epidemics*, *2*(4), 215–222. https://doi.org/10.1016/j.epidem.2010.10.001

Teunis, P. F. M., Moe, C. L., Liu, P., Miller, S. E., Lindesmith, L., Baric, R. S., … Calderon, R. L. (2008). Norwalk virus: How infectious is it ? *Journal of Medical Virology*, *80*, 1468–1476. https://doi.org/10.1002/jmv

Teunis, P. F. M., & Havelaar, A. H. (2000). The beta Poisson dose-response model is not a single-hit model. *Risk Analysis*, *20*(4), 513–520. https://doi.org/10.1111/0272-4332.204048

Thomas, J. T., Chen, Q., Gauger, P. C., Giménez-Lirola, L. G., Sinha, A., Harmon, K. M., … Zhang, J. (2015). Effect of porcine epidemic diarrhea virus infectious doses on infection outcomes in naïve conventional neonatal and weaned pigs. *PLoS ONE*, *10*(10), 1–18. https://doi.org/10.1371/journal.pone.0139266

Tominaga, Y., Mochida, A., Yoshie, R., Kataoka, H., Nozu, T., Yoshikawa, M., & Shirasawa, T. (2008). AIJ guidelines for practical applications of CFD to pedestrian wind environment around buildings. *Journal of Wind Engineering*, *96*, 1749–1761. https://doi.org/10.1016/j.jweia.2008.02.058

Toolbox, T. E. (2003). Equivalent diameter. Retrieved November 1, 2019, from https://www.engineeringtoolbox.com/equivalent-diameter-d_205.html

Torremorell, M., Alonso, C., Davies, P. R., Raynor, P. C., Patnayak, D., Torchetti, M., & McCluskey, B. (2016). Investigation into the airborne dissemination of H5N2 highly pathogenic avian influenza virus during the 2015 spring outbreaks in the Midwestern United States. *Avian Diseases*, *60*(3), 637–643. https://doi.org/10.1637/11395-021816-Reg.1

Torremorell, M., Pijoan, C., Janni, K., Walker, R., & Joo, H. S. (1997). Airborne transmission of Actinobacillus pleuropneumoniae and PRRSV in nursery pigs. *American Journal of Veterinary Research*, *58*(8), 828–832.

Tousignant, S., & Morrison, B. (2012). PRRS incidence / prevalence pilot study. In *2012 Allen D. Leman Swine Conference* (Vol. 39, pp. 93–94). St. Paul.. MN.

Traulsen, I., Rave, G., & Krieter, J. (2010). Sensitivity analysis of a stochastic simulation model for foot and mouth disease. *Archives Animal Breeding*, *53*(5), 529–544. https://doi.org/10.5194/aab-53-529-2010

Traulsen, I., & Krieter, J. (2012). Assessing airborne transmission of foot and mouth disease using fuzzy logic. *Expert Systems with Applications*, *39*(5), 5071–5077. https://doi.org/10.1016/j.eswa.2011.11.032

Trincado, C., Dee, S., Otake, S., Pijoan, C., Jacobson, L., & Rossow, K. (2004). Attempts to transmit porcine reproductive and respiratory syndrome virus under controlled field

conditions. *Veterinary Record*, *154*(10), 294–297. https://doi.org/10.1136/vr.154.10.294

Trudeau, M. P., Verma, H., Sampedro, F., Urriola, P. E., Shurson, G. C., & Goyal, S. M. (2017). Environmental persistence of porcine coronaviruses in feed and feed ingredients. *PLoS ONE*, *12*(5), 1–12. https://doi.org/10.1371/journal.pone.0178094

Trudeau, M. P., Verma, H., Urriola, P. E., Sampedro, F., Shurson, G. C., & Goyal, S. M. (2017). Survival of porcine epidemic diarrhea virus (PEDV) in thermally treated feed ingredients and on surfaces. *Porcine Health Management*, *3*, 1–7. https://doi.org/10.1186/s40813-017-0064-3

Tsukamoto, K., Imada, T., Tanimura, N., Okamatsu, M., Mase, M., Mizuhara, T., … Yamaguchi, S. (2007). Impact of different husbandry conditions on contact and airborne transmission of H5N1 highly pathogenic avian influenza virus to chickens. *Avian Diseases*, *51*(1), 129–132. https://doi.org/10.1637/0005-2086(2007)051[0129:iodhco]2.0.co;2

USDA. (2018). *Swine enteric coronavirus disease (SECD) situation report – Feb 22, 2018*. Retrieved from https://www.aphis.usda.gov/animal_health/animal_dis_spec/swine/downloads/secd_sit_rep_02_22_18.pdf

Valarcher, J. F., Gloster, J., Doel, C. A., Bankowski, B., & Gibson, D. (2008). Foot-and-mouth disease virus (O/UKG/2001) is poorly transmitted between sheep by the airborne route. *Veterinary Journal*, *177*(3), 425–428. https://doi.org/10.1016/j.tvjl.2007.05.023

Versteeg, H. K., & Malalasekera, W. (2007). *An Introduction to Computational Fluid Dynamics* (2nd ed.). Essex: Pearson Education Limited.

Vlasova, A. N., Marthaler, D., Wang, Q., Culhane, M. R., Rossow, K. D., Rovira, A., … Saif, L. J. (2014). Distinct characteristics and complex evolution of pedv strains, North America, May 2013-February 2014. *Emerging Infectious Diseases*, *20*(10), 1620–1628. https://doi.org/10.3201/eid2010.140491

Watanabe, T., Bartrand, T. A., Weir, M. H., Omura, T., & Haas, C. N. (2010). Development of a dose-response model for SARS coronavirus. *Risk Analysis*, *30*(7), 1129–1138.

https://doi.org/10.1111/j.1539-6924.2010.01427.x

Webster, R. G., Bean, W. J., Gorman, O. T., Chambers, T. M., & Kawaoka, Y. (1992). Evolution and ecology of influenza A viruses. *Microbiological Reviews*, *56*(1), 152–179.

Wei, J., Zhou, J., Cheng, K., Wu, J., Zhong, Z., Song, Y., … Li, Y. (2018). Assessing the risk of downwind spread of avian influenza virus via airborne particles from an urban wholesale poultry market. *Building and Environment*, *127*(October 2017), 120–126. https://doi.org/10.1016/j.buildenv.2017.10.037

Weller, H. G., Tabor, G., Jasak, H., & Fureby, C. (1998). A tensorial approach to computational continuum mechanics using object-oriented techniques. *Computers in Physics*, *12*(6), 620. https://doi.org/10.1063/1.168744

Wickham, H. (2009). *ggplot2: Elegant Graphics for Data Analysis*. New York: Springer-Verlag.

Wickham, H., François, R., Henry, L., & Müller, K. (2020). dplyr: A grammar of data manipulation. Retrieved from https://cran.r-project.org/package=dplyr

Wilkinson, P. J., & Donaldson, A. I. (1977). Transmission studies with African swine fever virus. The early distribution of virus in pigs infected by airborne virus. *Journal of Comparative Pathology*, *87*(3), 497–501. https://doi.org/10.1016/0021-9975(77)90038-X

Wilkinson, P. J., Donaldson, A. I., Greig, A., & Bruce, W. (1977). Transmission studies with African swine fever virus. Infections of pigs by airborne virus. *Journal of Comparative Pathology*, *87*(3), 487–495. https://doi.org/10.1016/0021-9975(77)90037-8

Wills, R. W., Zimmerman, J. J., Swenson, S. L., Yoon, K. J., Hill, H. T., Bundy, D. S., & McGinley, M. J. (1997). Transmission of PRRSV by direct, close, or indirect contact. *Journal of Swine Health and Production*, *5*(6), 213–218.

Wills, R. W., Zimmerman, J. J., Yoon, K. J., Swenson, S. L., Huffman, L. J., McGinley, M. J., … Platt, K. B. (1997). Porcine reproductive and respiratory syndrome virus: Routes of excretion. *Veterinary Microbiology*, *57*(1), 69–81. https://doi.org/10.1016/S0378-1135(97)00079-5

Wong, B. C. K., Lee, N., Li, Y., Chan, P. K. S., Qiu, H., Luo, Z., … Yu, I. T. S. (2010). Possible role of aerosol transmission in a hospital outbreak of Influenza. *Clinical Infectious Diseases*, *51*(10), 1176–1183. https://doi.org/10.1086/656743

Wong, T. W., Lee, C. K., Tam, W., Lau, J. T. F., Yu, T. S., Lui, S. F., … Parashar, U. D. (2004). Cluster of SARS among medical Sstudents exposed to single patient, Hong Kong. *Emerging Infectious Diseases*, *10*(2), 269–276. https://doi.org/10.3201/eid1002.030452

Wood, J. P., Choi, Y. W., Chappie, D. J., Rogers, J. V., & Kaye, J. Z. (2010). Environmental persistence of a highly pathogenic Avian Influenza (H5N1) virus. *Environmental Science and Technology*, *44*(19), 7515–7520. https://doi.org/10.1021/es1016153

Woonwong, Y., Tien, D. Do, & Thanawongnuwech, R. (2020). The future of the pig industry after the introduction of African swine fever into Asia. *Animal Frontiers*, *10*(4), 30–37. https://doi.org/10.1093/af/vfaa037

Wu, Y., Shi, W., Lin, J., Wang, M., Chen, X., Liu, K., … Wang, T. (2017). Aerosolized avian influenza A (H5N6) virus isolated from a live poultry market, China. *Journal of Infection*, *74*(1), 89–91. https://doi.org/10.1016/j.jinf.2016.08.002

Xu, W., Berhane, Y., Dubé, C., Liang, B., Pasick, J., VanDomselaar, G., … Muhire, B. (2016). Epidemiological and evolutionary inference of the transmission network of the 2014 highly pathogenic avian influenza H5N2 outbreak in British Columbia, Canada. *Scientific Reports*, *6*(August), 30858. https://doi.org/10.1038/srep30858

Yamamoto, Y., Nakamura, K., Yamada, M., & Mase, M. (2010). Persistence of avian influenza virus (H5N1) in feathers detached from bodies of infected domestic ducks. *Applied and Environmental Microbiology*, *76*(16), 5496–5499. https://doi.org/10.1128/AEM.00563-10

Yang, S., Lee, G. W. M., Chen, C.-M., Wu, C.-C., & Yu, K.-P. (2007). The size and concentration of droplets generated by coughing in human subjects. *Journal of Aerosol Medicine*, *20*(4), 484–494. https://doi.org/http:/doi.org/10.1089/jam.2007.0610

Yang, X., Lee, J., Zhang, Y., Wang, X., & Yang, L. (2015). Concentration, size, and density of total suspended particulates at the air exhaust of concentrated animal feeding operations.

Journal of the Air and Waste Management Association, *65*(8), 903–911. https://doi.org/10.1080/10962247.2015.1032446

Yao, M., Lv, J., Huang, R., Yang, Y., & Chai, T. (2014). Determination of infective dose of H9N2 avian influenza virus in different routes: Aerosol, intranasal, and gastrointestinal. *Intervirology*, *57*(6), 369–374. https://doi.org/10.1159/000365925

Yao, M., Zhang, X., Gao, J., Chai, T., Miao, Z., Ma, W., … Zhang, H. (2011). The occurrence and transmission characteristics of airborne H9N2 avian influenza virus. *Berliner Und Merliner Und Tierarztliche Wochenschrift*, *124*, 136–141.

Yoon, I. J., Joo, H. S., Christianson, W. T., Morrison, R. B., & Dial, G. D. (1993). Persistent and contact infection in nursery pigs experimentally infected with porcine reproductive and respiratory syndrome (PRRS) virus. *Swine Health and Production*, *1*(4), 5–8.

Ypma, R. J. F., Bataille, a. M. a., Stegeman, a., Koch, G., Wallinga, J., & van Ballegooijen, W. M. (2012). Unravelling transmission trees of infectious diseases by combining genetic and epidemiological data. *Proceedings of the Royal Society B: Biological Sciences*, *279*(1728), 444–450. https://doi.org/10.1098/rspb.2011.0913

Ypma, R. J. F., Jonges, M., Bataille, A., Stegeman, A., Koch, G., Van Boven, M., … Wallinga, J. (2013). Genetic data provide evidence for wind-mediated transmission of highly pathogenic avian influenza. *Journal of Infectious Diseases*, *207*(5), 730–735. https://doi.org/10.1093/infdis/jis757

Yu, I. T. S., Li, Y., Wong, T. W., Tam, W., Chan, A. T., Lee, J. H. W., … Ho, T. (2004). Evidence of airborne transmission of the severe acute respiratory syndrome virus. *The New England Journal of Medicine*, *350*(17), 1731–1739. https://doi.org/10.1056/NEJMoa032867

Zeng, X., Liu, M., Zhang, H., Wu, J., Zhao, X., Chen, W., … Shu, Y. (2017). Avian influenza H9N2 virus isolated from air samples in LPMs in Jiangxi, China. *Virology Journal*, *14*(1), 1–6. https://doi.org/10.1186/s12985-017-0800-y

Zhao, Y., Richardson, B., Takle, E., Chai, L., Schmitt, D., & Xin, H. (2019). Airborne transmission may have played a role in the spread of 2015 highly pathogenic avian

influenza outbreaks in the United States. *Scientific Reports*, *9*(1), 1–10. https://doi.org/10.1038/s41598-019-47788-z

Zhou, J., Wu, J., Zeng, X., Huang, G., Zou, L., Song, Y., … Yen, H. L. (2016). Isolation of H5N6, H7N9 and H9N2 avian influenza A viruses from air sampled at live poultry markets in China, 2014 and 2015. *Eurosurveillance*, *21*(35), 1–14. https://doi.org/10.2807/1560-7917.ES.2016.21.35.30331

Zhou, X., Li, N., Luo, Y., Liu, Y., Miao, F., Chen, T., … Hu, R. (2018). Emergence of African swine fever in China, 2018. *Transboundary and Emerging Diseases*, *65*(6), 1482–1484. https://doi.org/10.1111/tbed.12989

Zhu, R., Xu, D., Yang, X., Zhang, J., Wang, S., Shi, H., & Liu, X. (2018). Genetic and biological characterization of h9n2 avian influenza viruses isolated in china from 2011 to 2014. *PLoS ONE*, *13*(7), 1–19. https://doi.org/10.1371/journal.pone.0199260